

043
CHD
13747

**SPECTROSCOPIC STUDY OF COMETS
WITH SPECIAL REFERENCE TO HALLEY'S COMET**

BY

**DEBI PRASAD CHOUDHARY
PHYSICAL RESEARCH LABORATORY
AHMEDABAD - 380 009,INDIA**

**A THESIS SUBMITTED TO GUJARAT UNIVERSITY
FOR THE DEGREE OF DOCTOR OF PHILOSOPHY
SEPTEMBER 1988**

043



B13747

*TO
MY PARENTS*

THE ENCOUNTER

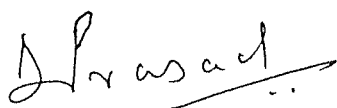
The distant mountains seem easy of access and climbing the top beckons but, as one approaches, difficulties appear, and the higher one goes the more laborious becomes the journey and the summit recedes into the clouds. Yet the climbing is worth the effort and has its joy and satisfaction. Perhaps it is the struggle that gives value to life, not so much the ultimate results. Often it is difficult to know which is the right path ; it is easier some times to know what is not right , and to avoid that is something after all.

Jawahar Lal Nehru.
(1936 , AN AUTOBIOGRAPHY)

CERTIFICATE

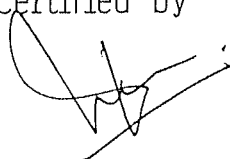
I hereby declare that the work presented in this thesis is original and has not formed the basis for the award of any degree or diploma by any University or Institute.

AUTHOR



Debi Prasad Choudhary
Physical Research Laboratory
AHMEDABAD 380 009, India

Certified by



J.N. Desai
Professor-in-charge
Physical Research Laboratory
AHMEDABAD 380 009, India

ABSTRACT

This thesis details the high-resolution spectroscopic and imaging observations, their analysis and the derived results on Comet P/Halley (1982i).

In particular the thesis focusses on some poorly understood short lived plasma events in the coma tail region and on those aspects of cometary physics which benefit from the methods of imaging spectroscopy. The study draws upon a large data base accumulated during a 8 month period of observation from Oct 1985 upto May 1986 spanning almost the entire activity zone of the comet.

The thesis also discusses some aspects of the study of neutral species in comets. The neutral Oxygen atom is now identified as one of the important water group species. High resolution techniques like the one discussed in the thesis are needed to isolate its emission at 6300 Å from other emissions. Even though the intense C₂ Swan band emission is one of the oldest identified spectral features, the understanding of the band spectrum is far from complete. High resolution imaging spectroscopy is needed to identify the dynamics of C₂ molecule at various distances from the coma.

Two sophisticated Fabry-Perot spectrometers were specially designed in order to observe Comet P/Halley in various emission lines and bands. One of the instruments is an Imaging

Fabry-Perot spectrometer with Generation II image intensifier camera as detector. It could take interferograms when used with narrow band filters (isolating line emissions) or could take photographs with relatively broad band filters. This instrument was used with a 35 cm aperture f/11 telescope with a specially developed drive corrector at Gurushikhar ($+24^{\circ} 39'N$, $72^{\circ} 43' E$, 1700 m altitude) Mt. Abu, India. Comet Halley was first observed on 16 October 1985 ($r = 2.14$ AU); observations were continued upto 15 Jan 1986 ($r = 0.8$ AU) in the pre perihelion period and from 8 March 1986 ($r = 0.82$ AU) till 7 May 1986 ($r = 1.72$ AU) in the post perihelion period. Over 200 frames of good quality including 100 frames of white light images of the inner coma have been obtained. Six interferograms three in C_2 , one each in H_{α} , [OI] and Na have been recorded.

The second instrument is a piezo-electrically controlled and central aperture scanned Fabry-Perot interferometric system with resolving power 4×10^4 at H_{α} . This instrument was used with a 1 meter f/13 telescope at Kavalur ($+12^{\circ} 34' 35''$, $78^{\circ} 49' 45'' E$, 725 m altitude) and line profiles of cometary [OI] 6300 Å emission, well separated from its neighbouring NH_2 feature were obtained. Cometary H_{α} emission was however below the detection limit of the instrument at the time of our observation in April 1986. The data has been analysed and important results which have emerged are presented in the thesis.

Two transient events occurring in the coma have been

studied in detail. The filter photographic observations carried out at 0^h UT on 13 March 1986 show a transient ionic event (lasting less than one hour) in the form of a blob of H_2O^+ emission. A Fabry-Perot interferogram in $\text{H}\alpha$ taken a few minutes later at the same location reveals strong hydrogen emission associated with the blob. The velocity field in the blob is structured with relative velocities upto ~ 35 km/s. The blob has a recession radial velocity of $\sim 30 \pm 10$ km/s relative to the comet (as seen from the earth). At this time the comet was crossing the interplanetary sector boundary. Therefore an attempt has been made to explain the event in terms of magnetic field reconnection mechanism in the inner coma region.

The imagery data of the Halley's Comet obtained on 8th January 1986 shows a condensation region in the inner coma at a distance of 2.3×10^5 km from the nucleus moving at velocity of ~ 35 km/s in the anti-solar direction. It was rich in CO^+ emission. Its confined nature implies that the condensation region is the result of a rapid ionization process lasting for $\sim 10^3$ - 10^4 seconds. Possible mechanism of its formation and acceleration have been investigated. The inter connection of this observed feature with ionic tail activities is explored in detail.

The scanning Fabry-Perot observations at Kavalur provided the $[\text{OI}]$ 6300 Å line profiles spectrally separated from nearby NH_2 feature. The line profiles were found to be symmetrical with Gaussian widths of 3 to 3.5 km/s. The ratio NH_2 6298.62/

[OI] 6300.303 is ~ 0.5 . The Fabry-Perot interferogram in [OI] 6300 Å obtained from Gurushikhar, Mt. Abu shows that the outflow differential velocity in the coma of size 10^5 km does not exceed ~ 5 km/s. Some correlation studies of [OI] production rate with the evolutionary parameters of comets such as inverse of semi-major axis and absolute brightness have been carried out. [OI] production rate normalized to the absolute brightness does not show any correlation with the inverse of semi-major axis, whereas it is very well directly correlated with absolute brightness. Comet Halley was found to have lower [OI] production rate by a factor of ~ 15 compared to the general trend. A possible explanation in terms of cometary chemical composition has also been described.

The interferograms in C_2 (0-0) Swan band obtained in the pre and post perihelion period have been analysed to obtain the differential outflow velocity of C_2 molecules. It was found that there does not exist any differential motion of C_2 molecules above 7 km/s within 10^6 km from the nucleus. The implication of this result in constraining the identification of C_2 parent molecules has been discussed.

The thesis concludes with some final remarks and suggestions for future studies in cometary science.

LIST OF PUBLICATIONS

Scientific Publications

1. "High resolution imaging interferometer for Halley's Comet - Concepts and performance",
Debi Prasad, J.N.Desai, T.Chandrasekhar and N.M.Ashok,
1985, 'Opto-electronic Imaging' Tata-McGraw Hill Pvt.Ltd.,
New Delhi, p.101.
2. "Study of the ionic and neutral species in the coma of Comet Halley with an Image Intensifier Camera",
T.Chandrasekhar, C.Debi Prasad, J.N.Desai, N.M.Ashok and
Ranjan Gupta,
1987, ESA, SP-278, "Diversity and Similarity of Comets",
p.567.
3. "A compact image intensifier coupled Fabry-Perot interferometer for Comet Halley and other extended astronomical sources",
Chandrasekhar T., Ashok N.M., Debi Prasad C and Desai J.N.,
1988, Opt. Engg. Jan, 27, 67.
4. "A digital filter for optimal enhancement for faint Fabry-Perot Interferograms",
Debi Prasad and J.N.Desai,
1988, Astrophys and Space Sciences (In press).
5. "Piezo-electrically controlled scanned Fabry-Perot Spectrometer for emission line studies of extended astronomical objects",
T.Chandrasekhar, C.Debi Prasad, J.N.Desai and N.M.Ashok,
1988, Opt. Engg. (In press).
6. "High resolution spectroscopic observations of Comet Halley in [OI]",
C.Debi Prasad, T.Chandrasekhar, J.N.Desai and N.M.Ashok,
1988, Pub.Astr. Soc.Paci., (In press).
7. "Optical interferometric observations of a transient event of March 13, 1986 in the coma of Comet Halley",
1988, J.Astr. Astrophys (submitted).
8. "The plasma condensation region in the coma of Halley's Comet",
C.Debi Prasad and J.N.Desai,
1988, Mon.Not.Roy.Astr.Soc. (submitted).
9. "Comparative study of [OI] 6300 A° emission among comets",
(In preparation).
10. "The interferometric study of Comet Halley in C₂ Swan band"
(In preparation).
11. "Observations on near nucleus activities of Comet Halley during Jan. 1986",
C.Debi Prasad, T.Chandrasekhar, J.N.Desai, and N.M.Ashok,
1988, Adv.Space. Research (In press).

Papers presented at Symposia/Conferences

1. "Digital Image Processing of Comet Halley images and interferograms",
C.Debi Prasad, T.Chandrasekhar, Ranjan Gupta, N.M.Ashok, J.N.Desai, K.N.Padia, B.Gopalkrishnan, K.L.Majumdar and A.K.S.Gopalan,
Proceedings of workshop on Image processing in Astronomy Ooty, March 23-27, 1987.
2. "Interferometric observations of Comet Halley",
C.Debi Prasad, T.Chandrasekhar, J.N.Desai, N.M.Ashok and Ranjan Gupta,
Proc. National Symposium on Comet Halley, Oct.27-29, 1987, Bangalore.
3. "High-resolution spectroscopy of Halley's Comet with scanning Fabry-Perot spectrometer",
C.Debi Prasad, T.Chandrasekhar, J.N.Desai, N.M.Ashok, K.R.Sivaraman, and R.Rajamohan,
Proc. National Symposium on Comet Halley, Oct.27-29, 1987, Bangalore.
4. "High-resolution study of 6300 Å [OI] in Comet Halley"
C.Debi Prasad, T.Chandrasekhar, J.N.Desai and N.M.Ashok,
13th meeting of the Astronomical Society of India, 11-15 Oct. 1988, Srinagar, (to be presented).
5. "The plasma condensation region in the coma of Halley's Comet",
C.Debi Prasad and J.N.Desai,
13th ASI Meeting of the Astronomical Society of India, 11-15 Oct. 1988, Srinagar, (to be presented).
6. "The Near Nuclear Jet activity of Comet P/Halley in November 1985",
Pradeep Gothaskar, Debi Prasad and J.N.Desai,
13th ASI Meeting of the Astronomical Society of India, 11-15 Oct. 1988, Srinagar (to be presented).

ACKNOWLEDGEMENTS

The work of this thesis has been carried out under the kind supervision of Professor J.N. Desai. It was a great privilege for me to work under his guidance. I was greatly benefited from his keen insight and critical assessment of the current views. His unflinching ability for taking the "On the spot" decision during the field experiments made this work easy. I enjoyed my studentship for his imaginative approach to science, inspiring guidance coupled with his kind attitude and the freedom of work and thought. Indeed it is a great experience to work under him. No word is sufficient to express my gratitude to him. I treasure these experiences.

I am fortunate to have the fruitful association of my senior colleague Dr.T.Chandrasekhar. I was greatly benefited by his unfailing inspiration, his friendly attention and the quality of his labour. To me, he is a gracious friend with good counsel. His ever willingness for discussing any topic earthly or heavenly made my work attractive. I am immensely grateful to him for the unrecountable help that I have received on many occasions.

I am profoundly grateful to Professor D.Lal, FRS and Prof. S.P.Pandya for their ardent interest and encouragements during my Ph.D tenure. I am thankful to our Director Prof.R.K.Varma for his constant encouragement throughout my study.

My sincere gratitudes to Prof.P.V.Kulkarni, the Chairman

of our group, for his constant encouragement and valuable critical assessment of my work. His timely help on many occasions were extremely useful.

I am highly indebted to Prof. Klaus Jockers of Max-Planck-Institute für Aeronomie, FRG for providing me the current information on cometary science. His critical comments and encouragements on my work at several occasions were indeed helpful. I specially thank him for providing the few illustrations used in this thesis (prior to the publication). I am also grateful to Prof. Micheal A' Hearn of University of Maryland U.S.A. for his kind encouragement. Prof. A'Hearn has kindly provided some of the unpublished wide field Comet photographs and IHW CN filter at a short notice. The help rendered by Prof. David Rees, for identifying the filed stars in our 13 March 1986 comet frame, is gratefully acknowledged. I acknowledge Dr. F. Sabbadin of Asiago Observatory, Italy for providing me a beautiful spectra of Comet Halley. I also thank Prof. T. Gehrels of University of Arizona, U.S.A. for some interesting and useful discussions.

I appreciate greatly Prof. J.C. Bhattacharyya, Director, Indian Institute of Astrophysics, Bangalore for being enthusiastic about our efforts, to take observations on Comet Halley at Kavalur 1 meter telescope. I wish to thank him for his generous allocations of telescope time. My sincere thanks to Prof. K.R. Sivaraman, for his kind help during our observations at Kavalur. My special thanks to Dr. Ram Sagar and Mr. Jayarajan of IIA, Bangalore who helped me during the digitization of the Comet imageries.

Mr. Jayarajan's enthusiastic willingness for working till late night made it possible to digitize a large number of Comet photographs within a short time. It is a pleasure to thank my friend Mr. Partha Dhurandhar of IIA, and my senior colleague Dr. Harish Bhatt whose company I enjoyed during my stay at Bangalore.

I wish to express my sincere gratitude to Dr. T. Velusamy for his warm hospitality and kind support during the image processing work at the National Imaging Processing facility, Ooty. I also thank Dr. A. Patnayak and Miss P. Latha for their help during my stay at Ooty.

I must express my heartily thanks to Dr. N. M. Ashok, Dr. B. G. Anandarao and Dr. U. C. Joshi for their extremely helpful nature. Various kinds of help that I received from them on numerous occasions are valuable. Special mention must be made for the help and enjoyable company provided by Dr. N. M. Ashok during the observational period of this work and useful suggestions during the data analysis, without fail. I also greatly enjoyed the company of Dr. P. D. Angreji during and after the observation of Comet Halley. I am very grateful to Prof. M. R. Deshpande for constant encouragement. Dr. D. B. Vaidya's help during observations at Kavalur and digitization work at IIA, Bangalore is gratefully acknowledged.

I would like to express my gratitude to Prof. A. C. Das and Dr. N. N. Rao. I had useful discussion on several aspects of plasma physics, which helped me in understanding the cometary

plasma processes. The useful discussions with Prof. B. Buti on the acceleration mechanism of cometary ions is gratefully acknowledged. My special thanks to Dr. J. N. Goswami for encouragement and useful suggestions and for giving me his personal copy of the "Comet" book edited by Wilkening. I thank Prof. Krishnaswami for kindly providing me the useful papers on the formation of ocean. My grateful thanks to Prof. B. H. Subbaraya for providing the spectrometer to calibrate the IHW filters. I thank Dr. R. Sridharan for many discussions regarding the airglow 6300 Å emission lines. Dr. P. N. Shukla has kindly provided the latest literatures on "mass extinction", which is duly acknowledged. My sincere thanks to Dr. Kailash Sahu of European Southern Observatory, La Silla, for his help during my initial days at PRL. I was greatly benefitted by his brotherly guidance and scholarly discussions. The leisurely discussions with Mrs. Meenakshi Sahu was extremely informative and educative which are duly acknowledged.

I wish to express my sincere thanks to my friend late Anjani Kulshrestha. On enumerable occasions we had discussion on topics covering every aspect of the nature. His philosophical attitude towards the creation, urge for getting a meaning to everything made this mortal world uninterestly for him. He decided to quit this place in search of a better one! I admire you my friend, I hope you found one!

It is my pleasant duty to record my thanks to my colleagues of our group, namely Asoke Sen, Rekha, Raju, Seema and

Banerjee. The help rendered by them, whenever it was needed, is acknowledged. I had fruitful discussions with Dr. Ranjan Gupta of Indian Institute of Geomagnetism, Bombay for which I am grateful to him. The modern cartoon of Comet given at the end of thesis was drawn by my artist friend Shishir Deshpande of Institute for Plasma Research, Ahmedabad. I thank him for this.

I am immensely grateful to Dr. K. P. Subramanian for painstaking job of going through the manuscript of some sections of this thesis and making many constructive suggestions. During my last five year's association he has been always very affectionate towards me.

The engineering help by Mr. N. S. Jog with the able assistance of Messrs. F. M. Pathan, P. K. Kikani and R. T. Patel made it possible to construct the instrumentation in a short time. It is a pleasure to acknowledge their help. I am extremely grateful to Mr. H. I. Pandya for his unhesitant and efficient assistance in computational work during the data analysis. I also thank Mrs. S. K. Jani for her help through the course of the present work. I am grateful to Mr. K. S. B. Manian for his enthusiastic help during several critical occasions. I am also very thankful to other group members namely Messrs. R. K. Mahadkar, N. C. Shah, Mrs. Mary Thomas and Mr. R. M. Parmar who have helped me in various ways.

It is a pleasure to acknowledge the help received from the personnel at our workshop, particularly Messrs. P. S. Panchal,

Atmaram Panchal and Jadhavbhai Panchal. Their efficient workmanship made it possible to construct the instruments within a short time, which was critical for Comet Halley observations.

I owe my sincere thanks to all my batchmates namely, Vinod, Sunil, Bhaskaran and Ashok Sharma. I enjoyed their company during all these years in particular the useful discussions with Vinod. I am very much indebted to my friends at hostel namely, Krishnakumar, Sarkar, Bhusan, Anjan, Pandey, Sushanta, Subrat, Mathew, Guru, Krishanan, Vijaya Kumar, Janardhan, Abhijit Ganguli, Gufran, Maqbool, Manoharlal, Supriya, Durga, Swataketu who made the life joyful. Post dinner discussions with Sarkar which invariably ended with no conclusion, are really memorable. Krishnakumar's nice company and unhasitant help of any kind at any time needs special mention. My special thanks to Navin Jual for providing me a homely atmosphere. I am also thankful to my senior friends Amrendra, Vijayashankar, Nikam and Ajayakumar. I would specially thank Sushanta, Raju, Guru and Manoharlal for helping me during the preparation of this thesis.

I am extremely grateful to Mrs.R.Bharucha, Mrs.Ghia and other members of the library staff for their ready help and co-operation throughout the work. Special thanks to Mrs.Kokilaben for xeroxing the many diagrams and papers at a very short notice.

Mr.A.M.Kolge's help during the observation at Mt.Abu

is gratefully acknowledged.

Dr.A.Bhatnagar provided the special Kodak film 2415 for the present work. I sincerely acknowledge for his kind help.

The help received from documentation section of the laboratory is gratefully acknowledged. I offer a special word of thanks to Mr.D.R.Ranpura for making the illustrations of this thesis and also for his help during the observations.

I gratefully appreciate Mrs.Mira Karanjgaokar for carefully and diligently typing the thesis. I also thank Mr.V.C.Mathew for active help rendered during the typing work.

Finally I am extremely grateful to my parents for providing me the constant encouragement throughout my career and in particular my father's keen interest in my present work.

***SPECTROSCOPIC STUDY OF COMETS
WITH SPECIAL REFERENCE TO HALLEY'S COMET***

CONTENTS

Page No

ABSTRACT	i to iv
LIST OF PUBLICATIONS	v to vi
ACKNOWLEDGEMENTS	vii to xiii
CHAPTER 1	<u>INTRODUCTION</u>
1.1	The Cometary Science : The State of art 1
1.2	A Historical Account of Cometary Research 3
1.2.1	The dark age 4
1.2.2	The dawn of the cometary science 5
1.2.3	Post Newtonian era 6
1.3	The Modern Concepts in Cometary Science 9
1.3.1	The origin of Comets 10
1.3.2	The structure of Cometary Nucleus 13
1.3.3	The Nature of the Coma 20
1.3.4	The physical processes in the Cometary tail 24
1.4	The Comet Halley 34
1.5	The relevance of cometary research with other fields 36
1.5.1	The evolution of solar system 36
1.5.2	The earth related phenomena 37
1.5.3	Astrophysical related studies 41
1.5.4	The plasma physics related studies 43
1.6	High-resolution spectroscopic studies in comets 46
1.6.1	Studies with grating spectrometers 46
1.6.2	Interference spectroscopy 48
1.7	The Motivation for the present work 50

CHAPTER 2 INSTRUMENTATION AND OBSERVATIONS

2.1	Selection of Parameters	54
2.1.1	Flux collecting power (L)	55
2.1.2	Choice of the emission lines	55
2.1.3	The exposure time	57
2.2	Fabry-Perot Spectrometer	58
2.2.1	The basic equations	58
2.2.2	Instrumental broadening	60
2.3	Imaging Fabry-Perot Spectrometer	60
2.3.1	Mode selection	61
2.3.2	The Etalon	62
2.3.3	The image intensifier	63
2.3.4	Optical layout	65
2.3.5	The camera and data recording	65
2.3.6	The film and calibration	66
2.3.7	Interferometric and Imaging mode of operation	67
2.3.8	Performance of the instrument	68
2.4	Servo Controlled Piezo-electrically scanning Fabry-Perot Spectrometer	70
2.4.1	Choice of the device	70
2.4.2	Optical system	73
2.4.3	Mechanical system	74
2.4.4	Electronics	75
2.4.5	Performance	80
2.5	Telescope at Gurushikhar	81
2.6	The observing site	83
2.7	Observation and Data	84
	Appendix 2.1	84

CHAPTER 3 THE TIME VARYING PLASMA PROCESSES IN THE COMA

3.1	An Overview of the Near Nucleus Plasma Activity of Comet P/Halley in 1985-86	86
3.2	The Optical Interferometric Observation of a Transient Plasma Structure in the Coma of Comet Halley - The 1986 March 13 event	90
3.2.1	Introduction	90
3.2.2	Transient events	92
3.2.3	Methods of observation and analysis	94
	(A) Observations	94
	A.1 Association of blob with comet	95
	A.2 Digitization and image analysis	98
	(B) Velocity determination	
	B.1 Radial scan analysis and determination of differential velocity map	100
3.2.4	Discussion	
	(A) State of the coma activity on 13th March 1986 from other observations	105
	(B) State of the Inter-Planetary magnetic field	109
	(C) Kinematics of the blob	111
3.2.5	A Theoretical model for the event	112
3.2.6	Summary and Conclusion	115
3.3.1	Introduction	117
3.3.2	Method of observation and analysis	119
	(A) Observations	120
	(B) Identification of the condensation	121
	(C) The velocity determination	122
	(D) Determination of the size of the condensation	123
	(E) The emission from the condensation	123
	(F) Ionization time scale	125

3.3.3	Discussion	126
(A)	The nuclear activity of Comet Halley in early January 1986	126
(B)	Ionization source	128
(C)	Acceleration of the condensation	135
3.3.4	The relation of the condensation with the tail activities	138
3.3.5	Summary and Conclusion	140

CHAPTER 4 STUDY OF THE NEUTRALS

4.1	Introduction	142
4.2	[OI] 6300 Emission Line Study	146
4.2.1	Observation of [OI] 6300 emission of Comet Halley with Scanning Fabry-Perot Spectrometer	149
(A)	Observations	149
(B)	[OI] results	150
(C)	Study of NH ₂ emission	152
4.2.2	Observation of [OI] 6300 emission of Comet Halley with Imaging Fabry-Perot Spectrometer	154
(A)	Observations	154
(B)	Analysis and results	156
4.2.3	Comparative study of 6300 emission among Comets	158
(A)	Source of Data	161
(B)	Results and discussion	162
4.2.4	Conclusions	
4.3	Study of C ₂ Interferograms	166
(1)	Aim	166
(2)	The observations	167
(3)	The dispersion velocity measurements	168
(4)	Conclusions	171

CHAPTER 5 SUMMARY

CHAPTER 1

INTRODUCTION

1.1 The Cometary Science The State of Art.

Since the dawn of civilization man has looked at the heavens and across its canopy, observed with dread and foreboding, the slow, majestic march of the comets. The thinkers, at the same time, were stimulated to probe more deeply.

Though cometary science is an old subject, significant advances have been made only in the last few decades. The extensive co-ordinated ground based observations with modern instrumentation, space observations in the new windows of the electro-magnetic spectrum and the spacecraft in-situ probing of comets have increased our understanding by leaps and bounds in this branch of science.

Today we definitely know that most if not all of these objects belong to our solar system. Our present understanding is that cometary nuclei are fragile entities containing mainly water ice and also porous refractory boulders cemented together with an ice-dust grain mixture

(Houppis and Gambosi 1986). A panorama of activities and spectacular structures of the ion tail resulting from solar wind interaction with the plasma components of the cometary atmosphere have been extensively studied from the ground and from space. The existence of vast Ly α cloud around comets and its breathing nature has been recently recognized from rocket experiments. Molecules like S₂ and HCN which dissociate easily, have been identified. The recent ground based imaging observations subjected to sophisticated image processing techniques have revealed the additional sources of a few molecules like C₂, CN etc. In summary, the data that has piled up from observations of several comets during the last few decades, enriched several folds during the apparition of Comet P/Halley in 1985-86, has unveiled several secrets of these mysterious objects, opening at the same time new horizons in diverse fields such as chemistry of ion-molecular reactions, turbulence studies etc.

Some results relate to the origin of these objects and the nature of various physical processes observed in the coma and the tail. High-resolution Spectroscopy has already contributed a great deal to the study of comets viz. unambiguous detection of water as the dominant constituent in comets from near IR spectroscopy. (Mumma et al., 1986, Weaver et al., 1986). However, the technique has not been used to its fullest capability and is bound to play an important role in the understanding of comets in the coming years. The

estimation of the abundance of hydrogen, oxygen and several other chemical species in faint comets of short periodicity using sensitive detectors would help in determining the relationship between the various groups of comets. The measurement of isotopic ratios of several elements of cosmogonic importance such as $^{12}\text{C}/^{13}\text{C}$, $^{16}\text{O}/^{18}\text{O}$, D/H etc. in comets with high resolution spectroscopy, is essential in understanding the location of their origin. Whether comets are from the outer solar system or have an interstellar origin. The velocities and accelerations in the ion tails deduced from the study of proper motions of fine features are not yet definitely known to be due to either the actual motion of particles or the hydromagnetic waves in cometary plasma. The mapping of velocity field over large portion of the tail by measuring the Doppler shifts of emission lines with high resolution spectrometers of large throughput such as Fabry-Perot spectrometers would conclusively settle these questions.

The ambitious space craft missions of the future ("The comet Nucleus sample return mission" Ed. Melita, 1986, ESA SP - 249) specially the "comet sample return mission" by ESA and "Comet Rendezvous and Asteroid flyby" (CRAF) by NASA are definitely going to enrich this ancient field of human endeavour particularly to settle the still vexing question 'What are comets really made of?'

1.2 A Historical Account of Cometary Research ;

1.2.1 The dark age

The systematic scientific research in cometary astronomy can be said to have started with the measurements of their positions in the sky around 1337 AD. In the words of Edmund Halley (1705), "Upon turning over very many Histories of Comets, I find nothing at all that can be of service in this affair, before A.D. 1337 at which time Nicephorus Gregoras, a Constantinopolitan, Historian and Astronomer pretty accurately described the path of a comet among the fixed stars, but was too less as to the account of the time; so that this most doubtful and uncertain comet only deserves to be inserted in our catalogue for the sake of appearing near 400 years ago".

Earlier the understanding of the nature and origin of comets was mostly based on speculations under two themes "the celestial hypothesis" in which it was thought that the comets are celestial bodies similar to stars and planets and "atmospheric theory" which argued the comets as manifestations of some atmospheric phenomena. Aristotle was one of the main proponents of atmospheric theory. Following the general acceptance of the Ptolemaic universe cometary astronomy entered a dark age from which it did not emerge till the era of renaissance. However the recorded observations of bright comets were made in 684 AD in

Nuremberg Chronicle and in 1066 AD the Bayeux a Tapestry depicts Comet Halley overseeing the Battle of Hastings.

1.2.2 The Dawn of Cometary Science:

Following positional observations of several comets by Toscanelli (1397-1482), attempted distance measurements by Peurbach (1423-61) and the observation that the tail always points anti-sunward by Fracastoro (1483-1553) serious scientific study of these objects began. A major breakthrough came when Tycho Brahe measured the distance to the famous comet in the period 1577 Nov.13 to 1578 Jan 26. Comparing the positional measurements from the island of Hven (near Copenhagen) with those of Hagecius at Prague separated by ~ 600 km, he showed the difference in its position relative to the stellar background to be 1 or 2 arc minutes. This angle amounts to distance to the comet of over ~ 1 million km (i.e) the cometary orbit lies beyond the orbit of the Moon which is 400,000 km away. Another development in cometary science around this time was due to Johannes Kepler (1571-1630) who considered that comets were numerous. He described the comets as the gross matter in the form of a sphere. The material from the sphere is sputtered due to sun rays. He described the tail to be due to reflected sun light from the sputtered material of the sphere. Note the close resemblance with the present concepts.

The orbital determination of these objects was the point of attention for two hundred years following Tycho Brahe. Kepler believed comets to move in straight lines with irregular speed, whereas Giovanni Borelli (1608-79) and J. Hevelius (1611-87) suggested parabolic orbits. Hevelius also hypothesized that comets are the ejected vapours from planetary atmosphere. Curiously Galileo Galilei (1564-1642) still believed in atmospheric theory. It is also interesting to note that Newton who later was convinced by Halley, did not initially agree with the discovery of the parabolic orbit for the comet of 1681 by Flamsteed, resulting in their subsequent unpleasant relations.

Finally the dispute whether cometary orbits can be parabolic was settled, when Halley published in 1705 his table listing the orbital parameters of as many as twenty four comets reproduced in Fig. 1.1 and table 1.1. This work can be considered another milestone in cometary astronomy. However, due to the inaccuracies in the available data, Halley could predict the periodicity of only one comet correctly. He identified the comets of 1456, 1531 and 1607 as one and the same comet, which later was named after him. It is also important to note Halley employed considerable diplomatic skills on Sir Isaac Newton in a bid to change his mind and succeeded in July 1687. Newton's great work, the "Philosophiae Naturalis Principia", which included important studies on comets, planets and tides. The teleological dogma at this time revolved around percepts such as the creation

TABLE 1.1

A rewritten version of Halley's original Table,

Comet year	T_0	q	e	ω	Ω	i
1337	June 2.2674	0.40666	1.0	46.367	84.350	147.817
1472	Feb 28.9326	0.54273	1.0	236.214	281.772	174.667
1531	Aug 24.8878	0.56700	1.0	107.768	49.417	162.067
1532	Oct 19.9250	0.50910	1.0	30.667	80.450	32.600
1556	Apr 21.8354	0.46390	1.0	103.133	175.700	32.108
1577	Oct 26.7813	0.18342	1.0	256.500	25.867	105.454
1580	Nov 28.6250	0.59628	1.0	90.142	18.956	64.667
1585	Sept 27.8056	1.09358	1.0	331.142	37.708	6.067
1590	Jan 29.1563	0.57661	1.0	308.603	165.511	150.322
1596	July 31.8299	0.51293	1.0	83.942	312.208	124.80
1607	Oct 16.1597	0.58680	1.0	108.083	50.350	162.967
1618	Oct 29.5160	0.37975	1.0	286.217	76.017	37.567
1652	Nov 2.6528	0.84750	1.0	300.14	88.167	79.467
1661	Jun 16.9868	0.44851	1.0	33.469	83.008	32.597
1664	Nov 24.4944	1.025755	1.0	310.543	81.233	158.692
1665	Apr 14.2191	0.10649	1.0	156.125	228.033	103.917
1672	Feb 20.3590	0.69739	1.0	109.483	297.508	83.369
1677	Apr 26.0260	0.28059	1.0	99.201	236.819	100.946
1680	Dec 8.0000	0.006125	1.0	350.625	272.033	60.933
1682	Sept 4.3188	0.58328	1.0	108.396	51.275	162.067
1683	July 3.1181	0.56020	1.0	87.892	173.838	96.817
1684	May 29.4278	0.96015	1.0	330.617	268.250	65.801
1686	Sept 6.6063	0.32500	1.0	86.425	350.578	31.361
1698	Oct 8.7063	0.69129	1.0	3.118	267.738	168.233

The orbital parameters are, time of perihelion passage, T_0 , perihelion distance q AU, eccentricity e , argument of perihelion ω , longitude of ascending node Ω , and inclination i .

of planetary system by collision of Comets and Sun (Buffon, 1745) and comets as the carriers of the water and air between stars harbouring life.

1.2.3 Post Newtonian Era:

The eighteenth century witnessed a major triumph of the theory of gravitation in the first predicted return of Comet Halley. Based on the periodic nature of Comets Kant (1755) in "Universal natural history and theory of the Heavens" proposed that the comets originated from an extended diffuse proto-solar nebula. The idea that "Comets are the solar system objects" is based on the ellipticity of their orbits. However, at this time, from the measurements, it was not possible to distinguish between the parabolic and highly eccentric elliptical orbits. Moreover though the analysis of orbital elements of the Lexell's Comet showed a periodicity of 6 years, it did not return. (later it was shown to be ejected to a much longer orbit by Jupiter's perturbation).

The physical appearance and orbital characteristics of different comets were found to differ. Based on these observations Cole (1823) and others ruled out the periodicity in the cometary orbits and attributed the observations to mere coincidences or exceptions. It was therefore thought that comets might come from interstellar medium. Hence in the beginning of 19th century, the two

thousand year old "Atmospheric versus celestial" debate on the nature of comets was replaced by the "Solar system versus interstellar" debate. Incidentally due to the close approach of Lexell's Comet, it was possible to derive a limit of its mass. Since the earth's orbit was not perturbed Laplace (1805) estimated its mass to be less than $1/5000^{\text{th}}$ earth mass or $< 10^{21}$ kg.

The random distribution of the orbital inclination to the ecliptic, contradicted the model for the solar-system formation proposed by Laplace (1805). He argued that the proto-solar nebula was a rotationally flattened system which contracted quasi-statistically to throw off successive rings of materials to form planets. Showing the inconsistency of the observed cometary orbits he argued that most of the comets captured from interstellar medium would have parabolic or hyperbolic orbits, whereas a few can have elliptic orbits which are perturbed by Jupiter. However, he ignored the motion of solar system inferred from the proper-motion studies by Herschel (1783). It was also difficult to explain many telescopic comets mainly due to Jupiter's perturbations. At this time Lagrange (1814) initiated the link between comets and solar system by calculating the energy needed to put a planetary fragment, produced by an explosion, in the cometary orbit.

Johan Encke (1791-1864) discovered the non-gravitational force by studying the cometary orbit of

the famous comet (later named after him) in Jan 1786, Nov 1795, Oct 1805 and Nov 1818 with the mathematical technique developed by Gauss. He found that every 3.3 years, the comet returns 0.1 day earlier. It is now known that there are some periodic comets which return later than predicted. This acceleration or deceleration of the cometary motion is due to its rotation combined with the outgassing from the afternoon side (Fig.1.2). If the spin of the comet is in the same sense as revolution around the sun, the recoil force due to degassing from the afternoon side adds vectorially with the orbital force and accelerates the comet. In the reverse case the deceleration is caused.

The connection between the comet and meteors were established by Giovanni Schiaparelli in 1866. The Biela's Comet of 6.75 year periodicity was not observed in 1858, instead a tremendous meteor shower was experienced, which weakened in its successive returns of 1872, 1885, 1892 and 1899. In the return previous to 1858 Bielas' comet was seen split which was a single entity before. Meteors were thus observationally established to result from the distintegration of comets.

1.3 The Modern Concepts in Cometary Science

Since the turn of this century with the advent of large telescopes and improved spectrometric techniques a rapid progress in understanding the nature and origin of comets

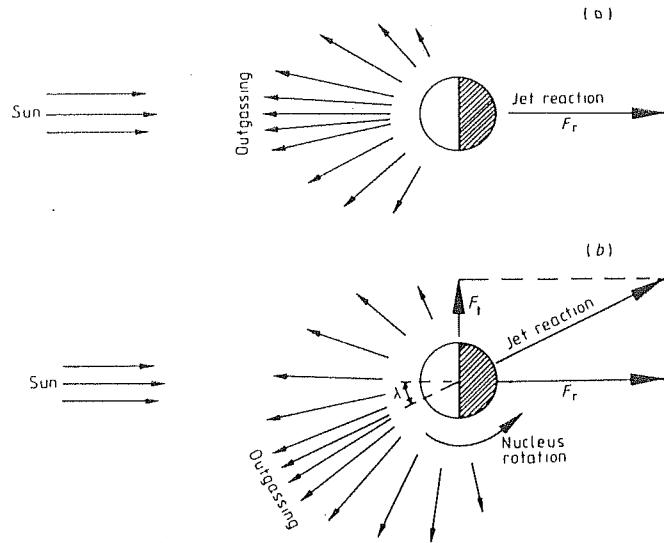


Figure 1.2. The action of non-gravitational forces on comets. The subliming gases from the nucleus give rise to a jet force in opposite direction to that of maximum outgassing. A non-rotating nucleus will experience a radial non-gravitational force (a), on a rotating nucleus the zone of the maximum outgassing will lag with respect to the subsolar point, giving rise to a transverse component of the non-gravitational force (b).

F_r = radial component of the non-gravitational force

F_t = transverse component of the non-gravitational force

λ = lag angle between the radial and transverse component of the non-gravitational force.

has been made. In this section a brief account of the modern theories explaining several of these aspects are discussed.

1.3.1 Origin of Comets:

Comets could have formed either along with the planets during the formation of solar system from the primordial solar nebula or independently in the interstellar medium and captured by the solar system as a consequence of some cataclysmic or repeatable events. However any scenario describing the origin of comets must explain their dynamical properties as well as the chemical composition.

Plotting the inverse semi major axes $1/a_0$ (a measure of orbital energy $E = -GM/2a_0$ where GM is the gravitational mass of solar system) versus the number of dynamically new comets (not perturbed by planets) as shown in Fig. 1.3 (Marsden et al. 1978), it is possible to study their dynamical properties. From the distribution, the prominent peak of orbits between 0 and 0.1×10^{-3} AU is evident. According to the Oort theory (1950) these comets are making their first passage through the planetary region from a vast reservoir of comets now called Oort's cloud located at a distance of $\sim 5 \times 10^4$ AU from sun. They become short period comets or are ejected from the solar system by subsequent planetary perturbations. The weakly hyperbolic orbits ($1/a_0 < 0$) in Fig. 1.3 are thought to be due to the error in calculation of the orbital elements compounded by

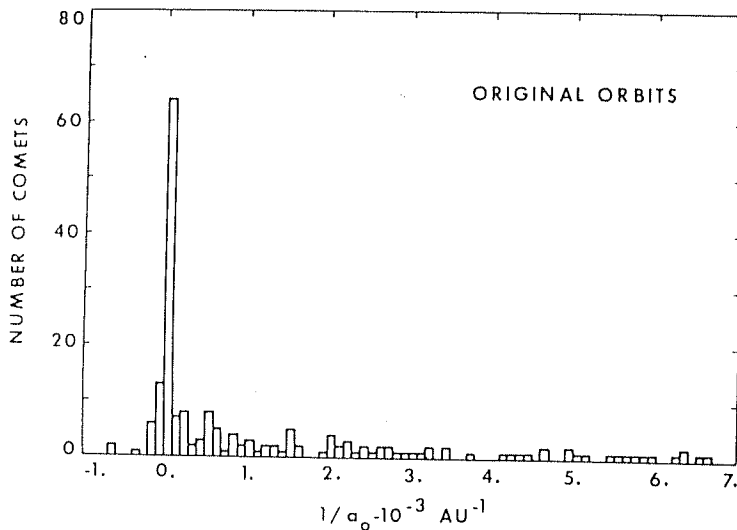


Figure 1.3. The distribution of original inverse semimajor axes for 190 long-period comets as found by Marsden et al (1978). The large spike at near-zero energy represents the dynamically new comets from the Oort cloud. The low continuous distribution is composed of returning comets which have already been perturbed in orbital energy by the planets.

non-gravitational forces on the comet. However, since the most negative value observed is $\sim 7.27 \times 10^{-4}$, this corresponds to the hyperbolic velocity ~ 0.8 Km/s. The extra solar system comets would have an excess hyperbolic velocity of 20 km/s due to the motion of the solar system in the interstellar medium. This corresponds to $1/a_0 \sim -0.45$ AU $^{-1}$ which is much larger than the observed value. Based on the average number of new comets observed, estimates of stellar encounters with the solar system, the population of Oort cloud can be estimated to be $\sim 10^{11}$ - 10^{12} comets. The concept of inner Oort cloud can however increase the number of comets around the solar system. Essentially this concept is based on the following evidence.

The comets between the outer planet and the Oort cloud are unaffected by the perturbations by planets or stars or interstellar clouds because they are deeper in the sun's gravitational potential well. The existence of such a cloud at 40-50 AU with 10-20 M would explain the perturbation of Neptune's orbit (Whipple, 1964). The evolution of short period comets is shown to be more favoured from such a source by Monte-Carlo simulation Club and Napier (1982, 84) showed that the comets with semimajor axis $> 10^4$ AU would be stripped off due to the encounter of a Giant Molecular Cloud (GMC). The outer Oort cloud can be replenished more efficiently from inner Oort cloud than from GMC. Moreover the theories of solar system formation suggest that the formation of comets was at 35 AU from sun before sun's T

Tauri phase (Cameron,1962,73).Bailey (1983) have suggested that the IR background at $100\ \mu\text{m}$ measured by the IRAS satellite could be atleast partly attributed to the inner Oort cloud.

The studies of dynamical evolution of short period comets (comets with periods < 200 years,mostly < 20 years) as a group have been attempted (Fernandez and Ip 1983, Everhart 1972). These comets have semimajor axes < 34.2 AU and inclination $< 30^\circ$. This group of comets crosses the orbit of Jupiter,and hence is called the "Jupiter family". They are believed to have evolved by the influence of Jupiter's mass and higher encounter probability (Russel 1920). The "Kreutz group" of comets having similar inclination and very low perihelion values of ~ 0.002 to 0.008 AU are also called sungrazing comets. They are considered to be the fragments of a large comet split during a previous perihelion passage. Examining 472 such comets Opik (1971) could derive 97 groups whereas Whipple (1977) showed them as a result of random chance,except the Kreutz group.

The formation zone of comets can be studied on the basis of observed chemical compositions and their isotopic ratios. The presence of the volatile moleclues and gases would indicate their formation within a temperature zone corresponding to their sublimation. Hence knowing the presence of volatile constituent,their place of formation

can be identified. For example the observation of S_2 molecule in comet IRAS-Araki-Alcock (1983d) (A'Hearn et al. 1983, Feldman et al. 1984) definitely show their formation beyond 100 AU, as it would dissociate within this zone (dissociation temperature ~ 20 K). Observations of resonance lines of Ne and Ar (736 \AA^0 and 1048 \AA^0 respectively) would show their formation in still cooler regions. The observed proto-planetary disk with $25\text{-}60 \text{ \mu m}$ IR excess in β pictoris by IRAS, indicates that the formation of cometary bodies is possible upto a distance of 400 AU from the central star (Smith & Terrile 1984, Weissmann 1986). The isotopic ratio in table 1.2 show that the observed values in comets are close to the solar system values indicating the formation of comets in solar system. However, more refined observations are needed for drawing definitive conclusions regarding cometary origins.

1.3.2 Structure of cometary nucleus:

Before 1950, the nucleus of a comet was thought to be a collection of interstellar dust grains, attracted and captured by the sun's gravity, when solar system passes through the galactic clouds in course of its way around the galaxy. This theory known as "Flying sand bank model" proposed by Lyttleton (1953) could not explain the following observations.

1. The large ratio of volatile to non-volatile

TABLE 1.2

	D/H $\times 10^5$	$^{12}C/^{13}C$
Interstellar medium	0.5-2	80 \pm 7
Galactic centre		93 \pm 8
		25
Protostellar Nebula	2 \pm 1	
Earth (S MOW)	15.3	89 \pm 4
Venus	1600 \pm 200	89.3 \pm 1.6
Jupiter	3.6 \pm 1.2	89 \pm 12
		-10
Saturn	2.0 \pm 1.5	160 \pm 35
		-53
Uranus	9 \pm 9	89-18
	-4.5	
Titan	16.5 \pm 16.5	
	-8.8	
Meteorites		
Carbonaceous Chondrites	8-60	89 \pm 2
Ordinary chondrites		
Interplanetary Dust	8-105	
	12-160	
Comets		100 \pm 20
		115 \pm 30
		-20
		135 \pm 65
		-45
		110 \pm 30
		-20
Comet Halley	0.06-0.48	

material observed in comets and in particular in same proportions on each return of a periodic comet could not be accounted for by a sand bank model. This is because of the fact that in a single perihelion passage the volatile content in a grain will be evaporated which cannot be replenished effectively before its next return.

2. The non-gravitational effects observed in comets needs the nucleus to be a single solid body for the rocket effects to work.

3. The similarity of pre and post perihelion appearance of comets are hardly expected for sand bank comets as they would loose the gas component during perihelion passage.

4. At times multiple nuclei are observed with a single comet. These are the result of the splitting of single nuclei. Such splitting of cometary nuclei are not conceivable for a sand bank comet.

5. In any case the dust grains of a sand bank comet would fall into the sun due to Poynting-Robertson force leading to instability of such a system.

These difficulties could be elegantly explained by Whipple (1950) with his "dirty ice" model, which describes the nucleus as a single aggregate of ice and meteoritic

matter. Following Whipple's classic paper, a number of important improvements have been made on his model to understand 1)size of the nucleus 2)its rotation period and 3)its internal structure.

The "bare-nucleus" of comets are not generally observable. Halley's comet is the only comet whose nucleus has been imaged by spacecraft (Fig.1.4).In a crude estimate A'Hearn (1988) finds that only about half the periodic comets have nuclei that would be detectable at aphelion even with the Hubble Space telescope. The size of the nucleus is derived from the brightness observations with the albedo-area relation given by (Spinrad et al. 1979),

$$R_e^2 P_v \phi(\alpha) = \frac{F_o}{F_\theta} r^2 \Delta^2$$

where F_o = Flux reflected from the comet

F_θ = Flux emitted by the sun

r and Δ = heliocentric and geocentric distances respectively.

R_e and P_v = radius and Albedo of the comet

$\phi(\alpha)$ = phase function of the cometary light scattering at phase angle α .

Cometary albedo which plays an important role was directly measured for Comet Halley as 0.04 (Sagdeev, et al.,

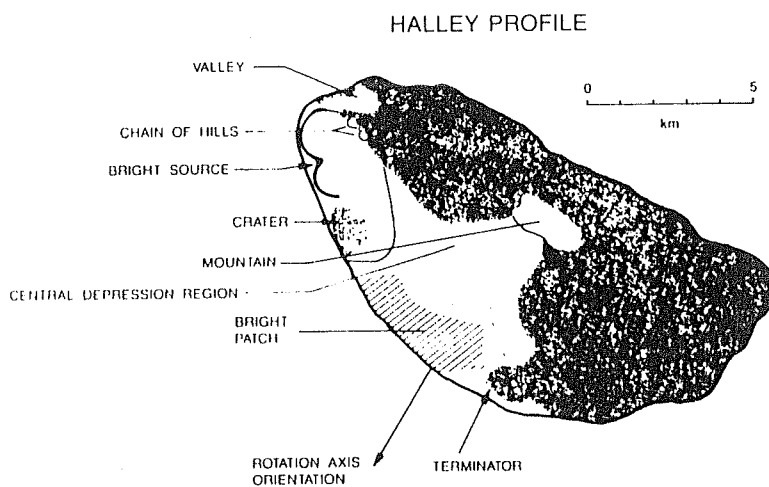


Figure 1.4. Composite image of the nucleus of Halley's comet. The picture is a composite of four images taken by the Halley Multicolour Camera (HMC) on board Giotto at 19947, 9847, 4947 and 2490 km from the nucleus.

1986) an unexpectedly low value. If albedo is taken as a typical value the sizes of few comets can be calculated. These values are given in table 3. Comets at large heliocentric distances, vary in the brightness of their reflected nuclear light because of changing the geometrical crosssection (owing to their irregular size) to sun and the earth. The rotation of such an object would result in periodic light curve. Using these ground based data rotation periods are estimated as given in table 1.3 which agrees with the in-situ measurements of P/Halley.

The internal structure of cometary nucleus is modelled by estimating the size of the nucleus along with the mass loss, derived from the gas and dust production rates. The expected total icy mass to be lost by P/Halley in its entire apparition centered on 1986 was $\sim 2.2 \times 10^{11}$ kg or 7×10^{10} kg on inward lag and 1.5×10^{11} kg after perihelion of which the ratio of the total number of molecules compared to that of H_2O was 1.2 and the mean molecular weight of all was 22.3. (Devine et al., 1985). Though the actual mass loss is not definitely known, the IUE measurements show the loss of 2.4×10^{11} kg of H_2O . The value increased has to be by a factor $(1.2 \times 22.3 / 18) = 1.49$ to account for other gaseous components total ice mass loss which gives a value $\sim 3.5 \times 10^{11}$ kg - 1.5×10^{11} kg inbound and 2.0×10^{11} kg outbound. For a complete estimate the gas/dust ratio is required. The spacecraft results show a value of < 1 , and as IR observations give $1/4.5$ to $1/2.2$. Adopting a value of 0.3

TABLE 1.3

Rotational dichotomy table for P/Halley

Set	Reference	Technique	P_{mod}^a (day)	Comment
1	Kaneda et al. 1986	L α "breathing"	2.2	Conflict with Set 7
2	Sekanina & Larson 1986a,b	Dust envelope shapes	2.2	Assumes $v_{ej} \approx 1 \text{ km s}^{-1}$
3	Belton et al. 1986	Fourier analysis of photometry	2.2	Also some 7 ^d 4 amplitude
4	Schlosser et al. 1986	CN shells	2.2	Recurrent shell expansions; imprecise
5	Sagdeev et al. 1986a,b	Vega nuclear orientation	2.2	Comparison, Vegas 1 and 2
6	Keller et al. 1986	Vega plus Giotto orientation	2.2	Comparison of Giotto and Vegas
7	Stewart 1986	L α photometry	7.4	Conflict with Set 1
8	Festou et al. 1986	Analysis of distant photometry	7.4	May allow 2 ^d 2 also
9	Schleicher et al. 1986	Photometry at encounters	7.4	Production rates modulated
10	Millis et al. 1986	Photometry after perihelion	7.4	Production rates modulated

^a P_{mod} is the modulation period; it may or may not be the true axial rotation P of the cometary nucleus.

Cometary nuclear rotation

Comet	Observers	Technique	Period (days)
P/Neujmin 1	Wisniewski & Fay 1985	Photometry with photomultipliers	1.05
P/D'Arrest	Fay & Wisniewski 1978	Photometry with photomultipliers	0.215
P/Arend-Rigaux	Jewitt & Meech 1985	CCD photometry	0.28
P/Arend-Rigaux	Wisniewski et al. 1986	Photometry with photomultipliers	0.57
P/Arend-Rigaux	Wisniewski et al. 1986	Photometry with photomultipliers	or 1.13
P/Arend-Rigaux	A'Hearn 1986	Photometry with photomultipliers	0.56

for this ratio the total mass loss of Comet Halley is estimated as 5×10^{11} kg. Slightly higher mass loss is also suggested for other considerations (Whipple 1986), depending on the assumptions concerning lag angle and gas production asymmetry before and after perihelion and with the nuclear size of $\sim 5 \times 10^{11} \text{ cm}^3$ from space mission. Rickman (1986) finds the mass of the nucleus in the range 5 to 13×10^{13} kg or mean density in the range of 0.08 to 0.24 g cm^3 and adopts a mean value of $\sim 0.15 \text{ g/cm}^3$. This low density implies too low a thermal conductivity for any appreciable radioactive heating, particularly by ^{26}Al . However the density derived for Comet Halley may not be the same for all comets and may also vary with depth inside each comet. The lifetime of a comet can also be derived from size and mass loss data. For Comet Halley the adopted mass loss of 5×10^{11} kg per revolution of P/Halley over an area of $\sim 320/\text{cm}^2$ corresponds to a surface loss of $1.6/\mathcal{J} \text{ m}$, where \mathcal{J} is the density in g cm^{-3} . This suggests a life expectancy of fewer than 1000 revolution for P/Halley in its present orbit. The nuclear splitting and outbursts can arise due to the cracking of the mantle by thermal stress. Such mantles are expected to cover $\sim 85\%$ of nuclear surface as Comet Halley jet activities were confined to only 15% of its surface. The low albedo; low density, variable jet activity from relatively small area on the surface and chemistry of dust and gas observed from the nucleus of Comet Halley provide strong constraints to the theories of Cometary structure and origin. There are however several puzzling

aspects as to the exact formation region of Comet Halley. The observation of ortho and para H_2 (Mumma et al., 1986) and S_2 (A'Hearn 1985,86) implies their formation at large heliocentric distances whereas the isotopic ratio $^{34}S/^{32}S$ from Giotto ($\sim 0.45 \pm 0.010$) compared to terrestrial ratio of 0.44 suggests source material in the inner solar system. A direct linkage between asteroids and comets has become difficult to propound because of low albedo and mean density estimations. However, a point to note is the peculiar green ($4600 \text{ \AA} < \lambda < 7000 \text{ \AA}$) enhancement of Comet Halley seen at resembles 2201 oljato asteroid (McFadden et al., 1984). Post perihelion confirmation of this enhancement is awaited.

Any model describing the cometary nucleus must account for the low density and albedo. To achieve such characteristics several modified "dirty ice" models have been proposed. They are, (1) The "Fractal model" (Donn, 1985) describing nucleus as low density porous object formed from interstellar medium (2) "The primordial rubble pile" model (Weissman 1980). (3) "ice glue" model (Hopkins et al., 1986) suggesting the porous boulders to be glued together by an accumulated matrix of ice-dust grains. However, a true cometary nucleus may or may not resemble any of these models or their combinations. The true nature can only be known by studying the sample from these objects. The present observational status of the cometary nucleus is summarized in a brief and excellent manner by A'Hearn (1988). The

summary of the present knowledge of cometary nuclei after Halley encounter, is reproduced below:

(1) Cometary nuclei, atleast of periodic comets, are bigger and blacker than usually thought as recently as five years ago. Geometric albedos may be typically 3, almost unbelievable dark and typical radii are probably of the order of 5 km. For only a very few comets are these independent determination of albedo and size done.

(2) Nuclei of the periodic comets are probably highly prolate unless they are both oblate and rotating about one of the major axes, which is unlikely.

(3) There are significant discrepancies among the various methods for determining the rotational vector of nuclei. The motions are probably much more complex for most comets than is assumed in models.

(4) The images of P/Halley provide convincing evidence for the existence of mantles discussed in many models. Data for nearly "extinct" comets suggest that those comets are almost totally covered with refractory mantles, as predicted by models.

(5) There are numerous pieces of evidences suggesting a connection between cometary nuclei and A-A asteroids of types D and C, but there are still a number of differences

that must be understood before the connection is definite.

(6) Further attempts to study cometary nuclei must be encouraged, since it is likely to be many years before another spacecraft views a cometary nucleus at short range.

Therefore it is clear that our knowledge of cometary nucleus is far from complete even in the post Halley encounter era. However based on the valuable results from the Halley encounter experiments, the future ground based observations can be properly designed to study some particular aspects of the nucleus.

1.3.3 The nature of the coma:

The onset of the activity and development of a large coma of a comet depends on the composition of volatiles in the outer layer of its nucleus. It also depends to a lesser extent on its rotation rate and polar inclination. On solar heating, the volatiles sublime and drag with them the dust, flowing radially outward forming the large coma. The gaseous component emits the characteristic radiation in visible, U V and IR wavelengths due to several emission mechanisms. Figure 1.5 show a typical spectra taken with Halley's Comet in mid January 1986. After the collision zone is passed the dust is decoupled from gas, attaining a terminal velocity ~ 1 km/s. It is acted upon by the effective solar gravitational force i.e. gravitational force diluted by

radiation pressure effects and follow spiral trajectories. Recent image enhancements of photographs of P/Halley taken in 1910 and 1986 (Fig.1.6) (Larson et al.,1986) have shown that the tracing of such jets backward in time is feasible. The comet has retained its active zones in the nucleus throughout its passage in the outer solar system.

The simplest model for interpreting the gas emission from comets is due to Haser (1957), assuming that the molecule evaporating from a cometary nucleus lead to a coma density given by,

$$n(r) = \frac{Q}{4 \pi r^2 v} \exp\left(-\frac{r}{vT}\right) \dots\dots(1)$$

where $n(r)$ number density at distance r from the nucleus, Q = production rate, v = outflow velocity of the molecule and T = mean lifetime of the molecule. The daughter molecule distribution produced from the parent depicted in (1) is given by,

$$n_d(r) = \frac{Q_p \gamma_d}{4 \pi r^2 v_d (\gamma_p - \gamma_d)} \left[\exp\left(-\frac{r}{\gamma_p}\right) - \exp\left(-\frac{r}{\gamma_d}\right) \right] \dots(2)$$

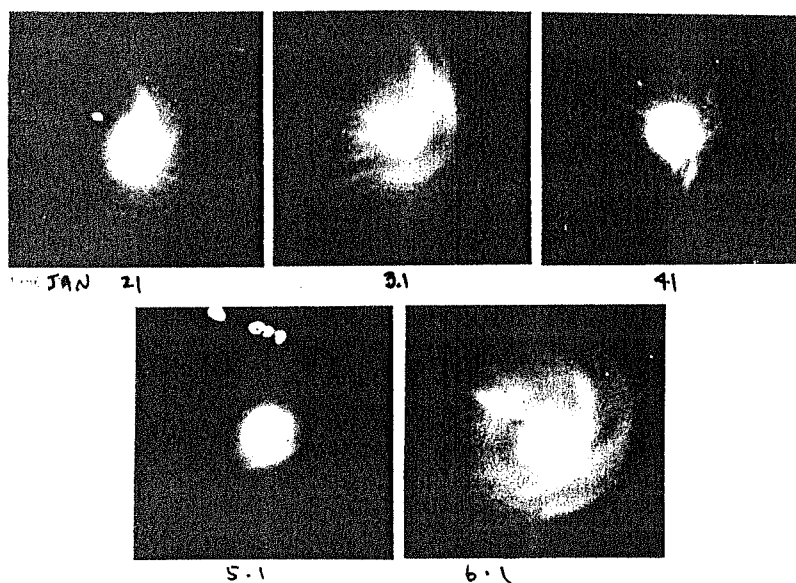


Figure 1.6. Enhanced broad band red CCD images showing daily changes in the perihelion dust jet distribution for 1986 January 2-6 UT. Orientation in north up and east to the left and each edge is 150,000 km at the comet. The direction to the sun is towards the lower right.

where $\gamma = VT$, the scale length, subscripts P and d refer to the parent and daughter respectively. This simple model has explained the observed gross distribution in the coma for many species. However, the recent observations with high spatial resolution in the optical band of comet IRAS-Araki-Alcock (Oliveresen, 1985) showed that the distribution of these molecules are concentrated in clumps instead of decreasing smoothly as given by eqn. (2). A possible explanation is that large fragments of ice broke off from nucleus and began to sublime as they separated. It is also observed that the dust to gas ratio derived from C_2 measurements as a function of cometocentric or heliocentric distances does not remain the same. In many instances a simple two component Haser model does not suffice.

The photoionization of neutral coma by solar UV radiation mass loads and thus slows down the solar wind. Since the cometary atmosphere is freely expanding, these interactions take place at a distance of \sim a million kms from the tiny cometary nucleus (Biermann et al., 1967). This was indeed observed by the instrument "Energy spectrum of particles" on board Suisei at a distance of 9.7×10^6 km (for Protons) and 4×10^6 km (for water group ions). (Terasawa T et al., 1986). The theoretical studies of solar wind flow near comet were carried mainly in the frame work of

hydro-dynamical description of plasma (Wallis 1973, Schmidt and Wegman, 1982). The main results are the existence of some boundaries in the coma which separate different zones of interaction between the solar wind and cometary plasma. (Galeev 1987). As a consequence of mass loading in the solar wind a standing bow shock is formed at a distance of R_L ahead of the comet. The magnetic field builds up in the mass loading region situated at a distance of $\sim 0.1 R_L$. The magnetic field continues to build up as the velocity decreases upto region called stagnation region, where the magnetic pressure becomes comparable to the material pressure called "Stagnation Pressure". Considering the collision between the neutral particles with the plasma, collision pause and contact surface are expected. At the collision pause the plasma density suddenly drops to a minimum value due to the continuous inflow of cometary ions with the solar wind into the plasma pile up region and the recombination of the stagnant plasma. This effect can also result due to faster recombination of cooler electrons of this region. The contact surface separates the solar wind flow from a purely cometary flow. By equating the dynamic pressure of the solar wind to the dynamic pressure of the ion outflow from the cometary nucleus, the distance of the contact surface is estimated. Fig. 1.7 shows these boundaries schematically. The insitu measurements with space crafts detected these boundaries alongwith several unpredicted dramatic features. It was found that mass loading of the solar wind by a small number of cometary ions makes it

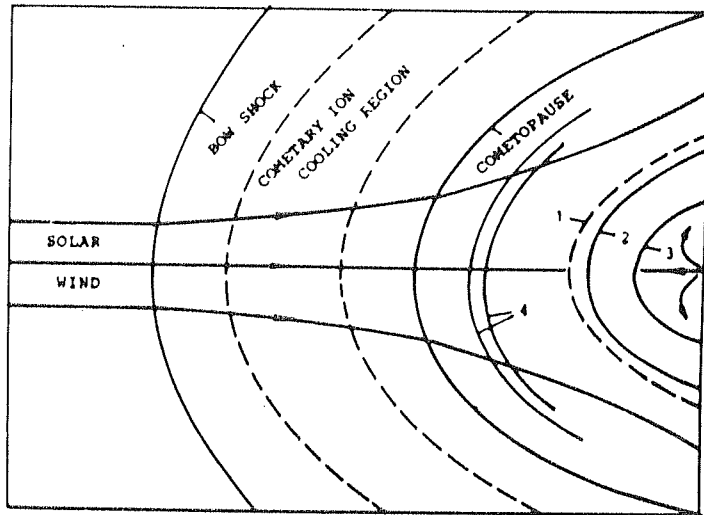


Figure 1.7. A schematic view of plasma structures in a cometary coma. The structure in the inner coma are: 1. the collision pause, 2. the plasma pile up region, 3. the contact surface, 4. the receding plasma envelope. The direction of solar wind flow and cometary plasma expansion are indicated by arrows on flow lines.

turbulent over a huge area around the comet, indicating thereby violation of adiabatic approximation (Wallis and Ong, 1976). Usually these approximations are used to describe the pitch angle scattering of cometary ions picked up by solar wind. The extremely small thickness of the boundaries shown in Fig.1.7 compared to the collision lengths indicate the importance of collisionless interaction of different components of plasma. A revised theory of such processes is described by Galeev (1987).

The transient plasma processes observed in Comet P/Halley (Ip et al., 1986, Debiprasad et al., 1988), in comet IRAS-Araki-Alcock in several emission bands (Lutz et al., 1986) and Comet G-Z in IR (Telesco et al., 1986) need a detailed investigation. The origin of plasma features of the ionic tail is well within the coma as conjectured by Jockers (1985) and can be observed with narrow band short exposure images (Debiprasad and J.N.Desai 1988). These aspects of studying the coma will be discussed at length in chapter 3.

1.3.4 The physical processes in the cometary tail

In general there are two types of tails seen in comets. The Blue type I tails are due to the ionic emission mainly CO^+ at 4260 \AA and morphologically highly structured, long, straight, pointing in the anti-sun direction. The red type II tails are due to the reflected solar radiation by dust

particles and are morphologically featureless, diffuse and curved so as to lag behind sun-comet line, opposite to the direction of cometary orbital motion. Under favourable projection conditions when the comet is close to the ecliptic plane the heavy dust particles, in the sunward direction of the comet appear as the tail pointing towards the sun, called "anti-tail". The detailed statistics of tail observations is given in table 1.4. Fig. 1.8 shows type I & II tails in Comet Halley (1982i).

Plasma tail: It is evident from table 1.4 that not all comets possess a plasma tail. From the same study Antrack et al (1964) showed that type I tail appears at heliocentric distance < 2 AU having no significant dependence on heliographic latitude. With a homogeneous set of data on Comet Kohoutek, Jockers (1985) showed that discrete tail disturbance events ("Comet tail substorms") are related to solar wind disturbances. He also showed that the change in solar wind induces the kinks in the plasma tail. The formation of the plasma tail and its structure is dependent on the nuclear composition. This aspect was clearly shown from the strong correlation seen between tail length with nuclear rotation period in CO^+ images (Celnik. W., 1987). Celnik et al also showed that the change in aberration angle (the angle between the sun-comet radius vector and plasma tail measured in the sense opposite to the comet orbital velocity) does not depend on the solar wind velocity, density or temperature but may have a weak

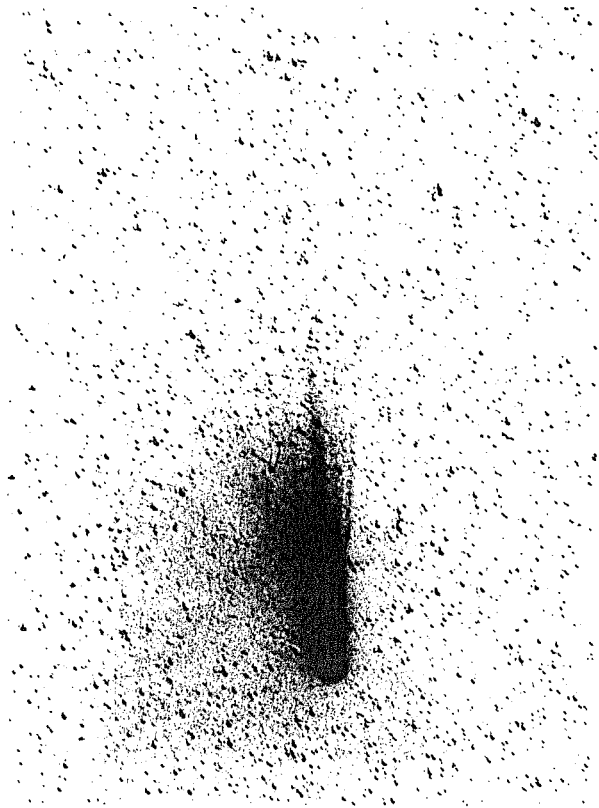


Figure 1.8. The wide angle photograph of comet Halley taken on 12.3.1986 at 0754-0934 UT without any filter. The straight plasma tail, side rays and the diffused dust tail are easily noticeable. (Courtesy : Dr.Klaus Jockers, MPAE Lindau, FRG).

TABLE 1.4

a.

DIVERSITY OF COMETARY TAILS.				
TYPE :	I	II	III	ANTITAIL
NATURE :	PLASMA	DUST	DUST	DUST
CURVATURE :	STRAIGHT	SMALL	STRONG	-
ACCELERATION: (solar units)	30 - 300	0.3 - 3	0.03-0.3	0
GRAINS SIZES : (micrometers)	-	3 - 30	30 - 300	1000

b.

ONSET OF PLASMA TAILS			
COMET SIZE	FAINT	BRIGHT	GIANT
ABS. MAGNIT.	9	4	1.5
PREDICTED	0.16 AU	1.6 AU	5.0 AU
OBSERVED	NONE AT MORE THAN 0.4 AU (a)	1 TO 2 AU FOR MOST BRIGHT COMETS	>2 AU MOREHOUSE 5 AU HUMASON 6 AU SCH-WACH-I

(a) exceptions : p/Encke has a faint transient plasma tail close to 0.4 AU; the faint plasma tail of Giacobini-Zinner has been crossed by spacecraft near 1 AU.

c.

NATURE OF LONG-PERIOD COMETS' TAILS				
PERIHELION DISTANCE	PLASMA TAIL	DUST TAIL	NO TAIL	TOTALS
0 - 2 AU	41	62	41	144
2 - 3 AU	0	12	6	18
3 - 5 AU	0	10	2	12
> 5 AU	0	0	0	0
TOTALS	41	84	49	174

(simplified from Antrack, Biermann and Lüst 1964)

dependence on crossing of sector boundary of interplanetary magnetic field. From this analysis it was also found that such crossings are responsible for dramatic disconnection events (DE).

The observed acceleration in cometary plasmas are $\sim 20-200 \text{ cm/s}^2$, whereas the solar radiation pressure could produce only $\sim .02$ to 2 cm/s^2 and long range Coulomb interactions could produce $\sim 0.2 \text{ cm/s}^2$. This indicates a strong interaction between cometary plasma and solar wind. Alfven (1957) developed a "magneto-hydrodynamic model" in which the solar-wind with its "frozen-in" magnetic fields "hit" the cometary plasma and "hung-up". The field lines are dragged into the tail as shown in Fig. 1.9 which strongly resembles the observed tail morphology. The interaction between the solar wind and cometary ionosphere would excite the plasma instabilities. In a detailed account Chernikov (1975) showed that ion acoustic instability has the largest growth rate. With typical plasma parameters these instabilities can give rise to an acceleration ($2-200 \text{ cm/sec}^2$). In presence of magnetic field several other instabilities such as ion-cyclotron, magneto-acoustic and Alfven oscillations are possible. Rao et al (1988) have shown that the magneto-sonic modes in the cometary plasma can be driven unstable by electron and ion-drift waves. They have explained the low frequency fluctuations found in the hydromagnetic turbulence of G-Z comet using such instabilities. Krishan (1980) showed that the freely

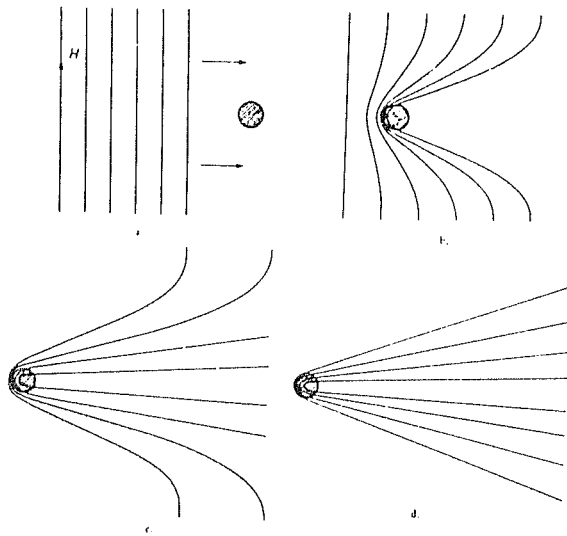


Figure 1.9. The "piling up" of the interplanetary magnetic field convected by the solar wind against the cometary ionosphere (Alfven, 1957).

interpenetrating solar wind and cometary plasma can produce ion-acoustic turbulence resulting in very high accelerations of $\sim 500-2.5 \times 10^4 \text{ cm/s}^2$. These instabilities can occur only in the transition layer of both the components of interacting plasma with wave number $\sim 10^3 \text{ cm}^{-1}$. However, the hydromagnetic Kelvin-Helmholtz instability can occur inside and outside the transition layer with wave number $K \sim 10^{-8} \text{ cm}^{-1}$ (Lee & Wu 1979). These instabilities can produce accelerations upto $\sim 30-300 \text{ cm/s}^2$ due to the pitch-angle scattering the fluctuating magnetic field. This mechanism also predicts fluctuations in number density of the plasma, which would produce observable scintillations of compact radio sources occulted by them. Though observations of such effects are claimed (Anantakrishnan et al., 1975, Alurkar et al., 1986, Slee et al., 1987) a conclusive observation is still awaited (Anantkrishnan et al., 1987, Hajivassilliua et al., 1987). Since the interplanetary medium is found to be more active than expected (Steven. J. et al., Intriligator, 1985) due to the presence of active current sheets and transient ionic enhancements, such experiments must be performed with utmost care. Buti et al (1987) have shown that only a fraction of turbulent electric field produced by the lower hybrid waves during the interaction of solar wind and cometary pick up ions can account for the stochastic ion accelerations and their heating. The results are compatible with observations in comet G-Z and Halley. Buti (1988) has discussed extensively the role of various stochastic and coherent processes in cometary plasma. Based

on the unipolar generation of current by a conductor in a magnetic field Verigin et al (1987) has proposed a basic acceleration mechanism in cometary plasma, which apparently reproduces the observed accelerations in comet Bennett and Halley (Minami et al., 1986). $\vec{J} \times \vec{B}$ force due to the reconnected magnetic field could produce the accelerations of about $10-20 \text{ km/s}^2$ or more (Ip 1980). The magnetic pressure gradient in the ionic tail can also accelerate the cometary plasma at a rate of $\sim 200 \text{ cm/s}^2$.

However, the observed accelerations in cometary plasma tail are not universally agreed upon as the motion of particles in cometary plasma. Mendis (1978) described them as the dissipation of large amplitude Alfvén waves propagating down the cometary magnetotail with accelerations ranging $10-100 \text{ cm/s}^2$. Stressing upon the same point Nees and Donn (1966) remarked that the observed accelerations of condensations may be due to the increase in the Alfvén velocity as a result of decrease in the plasma density down the tail, while the magnetic field remains almost constant. Hyder et al (1974) described the "helical" features observed in the tail of Comet Kohoutek 1973p as the wave motion with velocity $\sim 200 \text{ km/s}$. However the observed velocities in terms of Doppler shifts of several plasma components such as H_2O^+ , are claimed to be $\sim 20-30 \text{ km/s}$ (Huppler et al., 1975), indicating the particle acceleration in plasma tail. For a conclusive distinction of these mechanisms, a systematic study with high-resolution

spectroscopic observations at various points of plasma tail is essential which has still not been done satisfactorily!

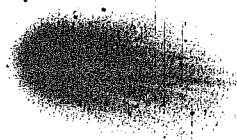
Fine structures: The type I tails are rich in time varying fine structures like Kinks, condensations, envelopes and helical waves. Large dynamical structures are the rays and disconnection events.

The narrow rays shown in fig.1.10 emerging within 10^3 km of the nucleus, curved in the sun-side are observed at an angle of $> 60^\circ$ (Wurm et al., 1967). Within ~ 10 -15 hours they merge on to the central main tail moving a rate of $\sim 3^\circ$ /hours. These are widely believed to be current carrying magnetic flux tubes (Ip and Mendis, 1976). Jockers (1981) pointed out that the kinks can be produced in the rays when solar wind intersects them. The "helical waves" in the plasma tails, carrying axial current are believed to be triggered by the kink instability (Hyder et al., 1974). They can also be described as the large-scale wave phenomena due to the Kelvin-Helmholtz instability as there exists a velocity shear at the boundary of solar wind and cometary plasma. However, the existence of finite boundary ($> 10^4$ km), the effect of compressibility, Landau damping and finite Larmor radius ($\sim 10^2$ - 10^3) would question the existence of such instabilities. Buti (1982, 83) argued that high-frequency electrostatic turbulence observed in the solar wind would stabilize all hydromagnetic waves up to a critical distance governed by the production rate of the

R 38

1986-03-15 0809-0819 UT
 λ 367.4 \pm 0.5 nm

CO_2^+



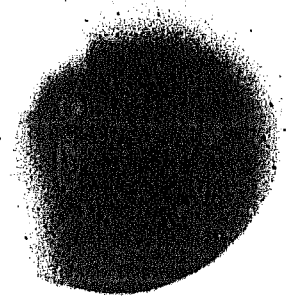
F 39

1986-03-15

0851-0856 UT

λ 401.9 \pm 0.5 nm

CO^+



scale ca 25"/mm on the print

scale ca. 25"/mm on the print

Figure 1.10. The comet Halley images taken in ionic emission bands in CO^+ & CO_2^+ . The narrow ray structures are clearly seen. The details of the photographs are mentioned in the figure. (Courtesy: Dr. Klaus Jockers, MPAE, Lindau, FRG).

comet.

The most dramatic events are the disconnection events having strong correlation with interplanetary sector boundary crossing (Niedner & Brandt 1978, 79). Using the basic equations of reconnection theory and criteria for current sheet instability Niedner et al (1978) explained such events. However Ip and Mendis (1978) pointed out that high-speed stream associated with magnetic sector boundaries could result in flute instability leading to tail disruption. Jockers (1983) believes that observed morphologies of DE are not consistent with reconnection processes. He proposes that ion tails can be torn apart due to differential accelerations between more and less dense parts along different segments. This explanation has a close resemblance with observed morphology. In an alternative view (Fernandez et al., 1983), DEs are also believed to be caused due to anomalous ionization and irregular degassing of nucleus causing an enhanced ionic region followed by a depleted density region.

Not much detailed study is available on the chemical abundance in type I tail. Following the flow of ions Ip (1979) showed that there is a rapid depletion of H_2O^+ ion via dissociative recombination resulting in a decrease of $n(\text{H}_2\text{O}^+)/n(\text{CO}^+)$. Hence CO^+ , CO_2^+ & N_2^+ can be traced to a longer distance compared to H_2O^+ even in water rich comets. Beyond 10^7 kms only atomic species H^+ , O^+ , and C^+ are

abundant. He also showed that molecular ions are more concentrated towards the axes whereas atomic ions are spread out further. In this context Jocker's (1987) efforts for obtaining tail images in CO_2^+ , CO^+ , N_2^+ and CH^+ with a Fabry-Perot spectrometer based focal reducer imaging system needs special mention as a pioneering work. David Rees has also obtained narrow band images of ionic emission using an imaging photoncounting system. The wide field CCD photographs obtained through IHW comet filters by M. A'Hearn are also useful in this respect. The detailed study of such images will be useful in understanding the physicochemical processes in the ionic tail.

It is clear from this discussion that several alternative complicated plasma processes exist to give rise to an observed phenomena in a comet tail. It is very difficult to point out the right one or a right group of mechanisms. The author feels that it could be worth while to investigate the individual events in depth with maximum available observations for a satisfactory understanding.

Dust tail: In contrast to the plasma tails, dust tails of the comet are seen at a heliocentric distance of > 3 AU, some even at 4-5 AU. Dust tails at 5-15 AU from sun are also observed (Sekanina, 1973). The dynamics of the dust tails are governed by the solar radiation pressure and gravitational force, both of which vary as r^{-2} . Hence the particles move with an effective gravity βF_{grav} , where β is expressed as,

$$1 - \beta = \frac{1.19 \times 10^{-4} Q_{\text{rad. press.}}}{\rho_d d}$$

Here $Q_{\text{rad. press.}}$ depends on size & optical property of dust grains and ρ_d is the bulk density. The dust grains attain their terminal velocity within 10-20 nuclear radius, where they decouple from gas component and move freely. There are three possibilities for the resulting orbit. If $1 - \beta < 1$, the grains move under a "diminished" solar gravitational force and so the orbit will be a branch of a hyperbola concave to the sun. If $1 - \beta = 1$, the repulsive radiation pressure exactly balances the solar gravity and consequently the grain will describe a straight line. Finally if $1 - \beta > 1$, radiation pressure over compensates solar gravitation, and so the grain will move in a hyperbola convex to the sun. The locus of the particles of same size (same β) emitted at a certain observation time t_c , emitted from the nucleus with zero relative velocity at different times $t_c - \tau$ is called the "Syndynes", whereas the loci for the particles of different size released from the nucleus at the same time is called "synchrons". In practise one gets a convolution of many syndynes of different particle sizes. The situation becomes complicated due to the outbursts of short duration (Guigay, 1960). Unlike syndynes, synchrons are not radial anywhere including near the nucleus. Thus the observed non-radial tail orientations are anticipated in purely

kinematic manner if they were identified as synchrons. Finson and Probststein (1968) showed that taking into account three parametric functions of size, velocity and time the brightness distribution of the cometary dust tail can be calculated by a "synthetic" approach.

Wallis and Hassan (1982) have pointed out that in addition to the solar gravity and radiation pressure, the electromagnetic forces also play an important role in dynamics of small dust grains, since they get charged in a plasma and radiative environment. These charged dust grains experience shocked and undisturbed solar wind electric field. Haranyi and Mendis (1985) have pointed out that the effect of electromagnetic force for typical Olivine and magnetic grains are negligible when ' a ' $> 1 \mu\text{m}$ (where ' a ' is radius of the particle) and it becomes important for ' a ' $< 0.1 \mu\text{m}$. For the grains $a = 0.03 \mu\text{m}$ electromagnetic effect dominates over radiation pressure. Using such effects Hill and Mendis (1980) explained striae band in several comets and Haranyi and Mendis (1985) in comet Donati. The interaction of dust and solar wind giving rise to the streaming instability is invoked for the explanation of the dust jets, expanding halos and stria (Havnes, 1988).

The so called "Anti-tails" are essentially due to geometrical perspective, best seen in comet Arend-Roland 1957 III. As the radiation pressure pushes radially outward, for the conservation of angular momentum the larger

particles are required to fall behind the nucleus in its orbital motion around the sun. As a result the 'older' synchrones are crowded in the apparent sunward direction, consequently the lag angle between the particle and the extended radius vector from the sun to the comet steadily increases and may exceed 90° after perihelion. When the line of sight to the nucleus from the earth splits the synchrons, both a normal tail and antitail would be observed.

1.4 Comet Halley

The Comet P/Halley is an historic object that has had an enormous impact on men's minds through the centuries for the last 2225 years atleast. This was the great comet which Edmond Halley reported to the Royal Society in June and July 1696. He suggested that the comets of 1607 and 1682 had similar orbits and were probably of the same, if so the comet would return in 1758. And the comet was indeed recovered on christmas day 1758 by George Palitsch. The first well documented sighting of Comet Halley was in 240 BC in China. At the time of Jain Saint Mahavira's death the appearance of a bright comet in the morning sky was recorded in Indian chronides. A preliminary work by Chopra (1983) shows that the comet appeared in the constellation, where Halley's Comet was expected. However the year of Mahavira's death i.e 526 BC does not coincide with the expected date of appearance of Comet Halley from its periodicity. Again in 526 BC no bright comet was recorded in

China or Japan Hasegawa (1980). Hence there exists a lot of uncertainty in the mentioned date which needs further work. If it really was Comet Halley then the most ancient sighting of this historical comet is going to be in India. With a period of 76.1y nearly equalling the human life span, it has been by every generation. The recovery of the comet in 1758 by an amateur astronomer a farmer living near Dresden was specially significant as it was vindication of prediction based on celestial mechanics governed by Newton's law of gravitation. Whereas 30 firmly documented passages Comet Halley exist in recorded history, only five appearances have occurred since the invention of the telescope; only three since the availability of photography in astronomy and at only one - the last apparition of 1985-86 with space borne instrumentation.

Apart from its historical importance Comet Halley's appearance in 1985-86 was scientifically significant because of the following reasons:

(1) The predicted orbital parameters were highly accurate, thanks to the work of Yeomans and Kiang (1981). This made it possible for conducting the well planned experiments including the space-missions.

(2) In terms of the absolute magnitude (defined as the magnitude when the comet is at distance of 1 AU from both sun and earth and at a phase angle of 90°) Comet Halley is

the brightest among the comets with periods upto 1000 years, which have returned atleast twice to the inner solar system (Fig.1.11). Its absolute magnitude has not changed recognisably during last 2000 years and has an average value of 5.5 (Hughes 1987,83).

(3) Though the observation of dynamical parameters of Comet Halley shows that it is not a typical comet, the physical properties indicates its similarity with many of other short period comets (Weissman,1987). Hence until the future spacecraft data on comets indicate differently, the wealth of information gathered from Comet Halley can be used for understanding other comets.

1.5 Relevance of Cometary Research to other Fields:

Today Comets are no longer seen as the mysterious fearsome entities they were once thought to be. Rather they seem to bear the key to several vital questions in many diverse fields. In this section a brief account of the importance of cometary research to other fields is discussed.

1.5.1 Evolution of Solar System:

Available evidences show that the sun, terrestrial planets along with the moon were formed ~ 4.6 billion years ago from the primordial solar nebula. The knowledge of the

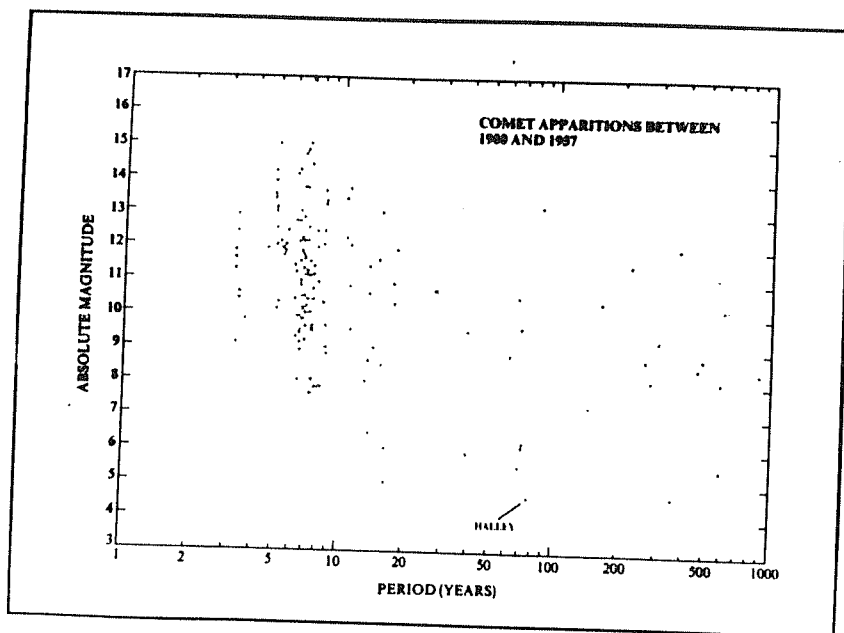


Figure 1.11. Absolute magnitude of comets with periods upto 1000 years. Of all the comets that have returned atleast twice to the inner solar system, Halley is the brightest (R.Reinhard, 1986 ESA Bull. 46, 15).

constituents of the primordial solar nebula today would help in a better understanding of the formation of process of the Solar System. Whereas nuclear fusion has altered the primordial material in the interior of the Sun the material has undergone differentiation by physical and chemical processes in planets. Smaller bodies, like small satellites, asteroids, meteorites may also be made from differentiated material. But the comets seem to have formed under a very slow process in a cool environment ($\sim 100^{\circ}\text{K}$) which is evident from the presence of primeval molecules like S_2 , HCN , CH_3CN and CO_2 . These constituents have been hardly altered because they have been subjected to low gravitational field and have remained in a deep freeze environment most of the time. Hence, undisputably comets contain very primitive and undifferentiated material or at least much less differentiated than carbonaceous chondrites, which seem to have conserved their CNO in solar proportion (Delsemme, 1977). Hence if the paradigm, in which comets are coeval with the planetary system and have since remained cold for ever, is indeed correct, then the molecular composition and the micro - macroscopic physical characteristics of the cometary nuclei will provide a wealth of information about the conditions under which the solar system formed.

1.5.2 Earth related phenomena:

(i) Origin of life: Thirty five years ago Miller had shown that the amino acids can be formed in the laboratory

by circulating water vapour, methane (CH_4) ammonia (NH_3) and hydrogen in an electric discharge for a week (Miller, 1953). Such signatures are also found in carbonaceous chondrites (Shimoyama et al., 1979, Kotra 1981). Large quantities of complex organic molecules with as many as 11 atoms (HC_9N) are found in interstellar clouds (Hoyle 1980). Presence of HCO , H_2CO , H_2S , NH_4 and S_2 (Cosmovici 1984 a,b) in comet Halley suggests the rich abundance of organic molecules in comets. Irvine (1980) has discussed the role of the presence of radioactive ^{26}Al in early solar nebula, inferred from the anomalous ^{26}Mg content in meteorites (Lee. T et al., 1970, 1977) in the chemistry of comet. ^{26}Al if trapped in comets, would serve as a radioactive heat source and the energetic radiation could produce biologically significant molecules in them. These molecules can be encapsulated within the dust grains which would enable them to withstand the hazards encountered during their transfer to the earth. Under special conditions such molecules can be transferred to earth (Weber et al., 1985). Time and again Hoyle (1986) has propounded the idea that certain absorption lines seen in the interstellar medium are due to dead bacterial shells, an interpretation, which is not entirely unambiguous (J. Maddox, 1986). For example the recent observation of such a feature at $3-4 \mu\text{m}$ in comet Halley by Wikrama Singhe and Allen can be explained by (i) bacterial model (Hoyle et al 1987) (ii) irradiated ice model (Chyba et al 1987) and (iii) interstellar dust model (Greenberg et al., 1988). However the concept of extraterrestrial origin of life needs a serious

study owing to the discovery of the existence of self-replicating life at an early stage of earth $\sim 4.2 \times 10^9$ years ago (Kevin A, 1988). One asks the questions Could primitive earth have evolved such a complex life form? or did that life originate elsewhere? With the present uncertainties in understanding the composition of the cometary nucleus, the author strongly feels that study of the deep core sample from a "comet nucleus sample return" mission would be crucial in answering decisively the question of extraterrestrial origin of life.

(ii) Mass extinction: Short and long term periodicities of terrestrial phenomena are being found in the geological data base as given in table 1.5. The cyclic nature of the biological mass extinction with dominant periodicity of ~ 30 Myr is given in Fig. 1.12. (Raup et al., 1984). The periodicity of impact craters are now found to be ~ 28.4 Myr, in phase with the periodicity of mass extinction, with the probability of accidental coincidence of 0.1% well within the measurement errors (W. Alvarez et al., 1984). The time sequence of terrestrial catastrophes and other solar system phenomena are found to be apparently stochastic, but for an underlying galactic modulation (Napier et al., 1979). Studying the track density as a function of depth in lunar sample Goswami and Lal (1978) have found the galactic modulation of impact cratering having periodicity of ~ 250 Myr. The solar system also make vertical oscillation about the plane of galaxy. During this

TABLE 1.5

Phenomenon	'Period' (Myr)
Climatic (?) and sea level variations	≈ 30 ≈ 32 ≈ 30
Tectonic cycles	≈ 30
Mass extinctions	≈ 32 26-30
Geomagnetically disturbed epochs	32-34
Ages of Craters	≈ 27 31 ± 1 ≈ 28
Ice ages	≈ 250 ≈ 200
Major tectonic events	≈ 200 ≈ 230
Climatic cycle	≈ 300
Mixed magnetic intervals	≈ 285

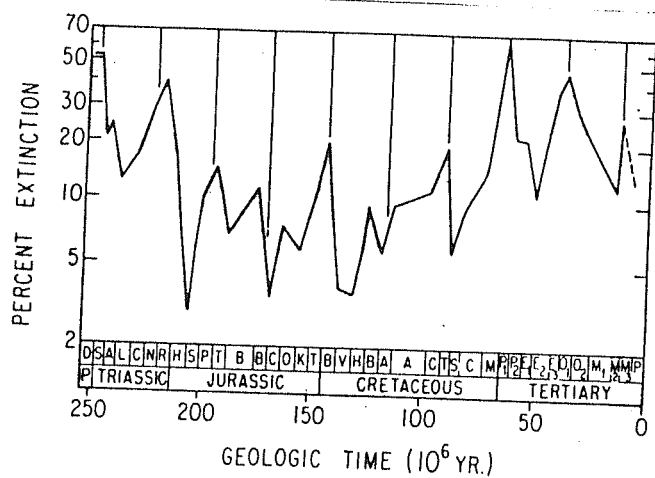


Figure 1.12. Extinction record for the past 250 ma. Letter codes (bottom) identify stratigraphic stages. The best-fit 26-ma cycle is shown along the top.

course it encounters the galactic plane (which is a denser medium having large number of molecular clouds of various size) once every ~ 30 million years. Such galactic modulation show that as the solar system moves in the galaxy, periodically it encounters denser regions causing enhanced impacting. The large impacts of a comet of mass 10^{18} gm on earth can create a number of atmospheric effects such as inverse Greenhouse effect (Hoyle et al., 1978) leading to an ice age, change of boundary conditions at earth's core and mantle leading to magnetic field reversal and principal plate movement. Table 1.6 illustrates the mean estimate of energy compared to several terrestrial effects. Tunguska event at 1908 is a most probable example of such an event due to collision of a 10^{17} g body. Out of major extinctions, atleast two events at the end of Cretaceous and Eocene are known to be associated with the impact of a comet or asteroid of few km in diameter (Davis et al., 1984) as the deep sea sediments corresponding to these periods show significant amounts of enhanced of iridium. Attempts have been made on the basis of sea level and/or climatic changes to explain these observations (Hallam 1979, Sarkar 1986). It seems the strong point about the comet impact theory is the noble gas anomaly, whereas the weak point is its unsound statistical base. However a few extinction must have been due to the comet impact. Since a large amount of energy is released during the impacts of sizable comets. Hut (1987) have discussed this topic in an unified way.

TABLE 1.6

Energetic Effects a Cometary Collision with Earth Could Produce	
Energy to the Earth from Sun in 1 yr	3.48×10^{31} erg
Earthquake of ninth magnitude	2×10^{25} erg
Energy of comet of 10^{18} g and velocity 45 km s^{-1}	10^{31} erg
Fraction of yearly solar energy	0.29
Energy required to remove atmosphere and scatter australites ⁷	4.4×10^{30}
If all energy absorbed by	
(1) atmosphere, elevation of temperature	190° C
or (2) ocean water, elevation of temperature	0.175° C
or (3) 100 m of ocean water, elevation of temperature	5° C
or (4) water volatilized at 100° C	4×10^{20} g
Edge of cube to contain this water	74 km
Area of ocean 3 km deep to contain water	$1.33 \times 10^5 \text{ km}^2$
or (5) mass which could be thrown in circle about Earth	3.24×10^{19} g
or (6) earthquakes of ninth magnitude	5×10^5

(iii) The contribution of comets to oceans of primitive earth : On the basis of recent compilation of lunar impact records, combined with the mass scaling law for crater diameter in the large body regime, an estimation of the total mass incident on the moon during the period of heavy bombardment can be made. Extrapolating lunar impact frequency, with comets having water ice composition of about 50%, Chyba (1987) has shown that earth would have acquired an exogenous ocean of water between ~ 4.5 and 3.8 billion years ago, even if only $\sim 10\%$ of the impacting objects were comets. This hypothesis is further supported by the fact that the Juvenile water from earth's interior contains 15% less deuterium than the ocean (Kokuba et al., 1961) suggesting the extraterrestrial source of oceanic H_2O (Anders .E et al., 1977). Further the oceanic D/H ratio (1.6×10^{-4}) and that of Comet Halley ($0.6-4.8 \times 10^{-4}$) are both an order of magnitude above cosmic abundance (Eberhardt. et al., 1986). This implies that comets can serve as a complementary source of ocean water to the usual account of terrestrial volatile origin through outgassing.

1.5.3 Astrophysical related studies:

(1) Extra solar system comets: Far IR excess has been detected around α -Lyrae (Aumann et al., 1984), ϵ Eridani, α Piscis Austrini and β -Pictoris and atleast 20 other stars within 25 pc of the sun. These observations suggest that a large fraction of the F, G and K main

sequence stars with longer life time than 'A' stars may be surrounded by protoplanetary disks (Aumann, 1985, Sadakane, 1984). It has been conjectured that the occasional sudden outbursts observed in Vega in $H\alpha$ (Barker et al., 1978, Griffin and Griffin, 1978, Goraya and Singh 1983) could be due to close encounters with cometary bodies (Bhatt, 1985). Similarly isotropic distribution of γ -ray bursters give the energy output at 0.2-1.5 Mev within a few seconds (Klebesadel et al., 1973). Their frequency is around 5 bursts per year with integrated flux $\sim 10^{-5}$ esgs cm^{-2} . The disintegration of a comet and the nuclear collision of oxygen nuclei due to the heating of standing shock front at a speed of $1/3$ C would account for such observations (Harwit and Salpeter, 1973). Suklovskii (1974) have also worked out a scenario of observational consequences of collision between a comet and neutron star or a white dwarf. Whipple (1975) has ruled out the encounter with interstellar comets for such event on the basis of extremely small probability. Cometary phenomena may be more common around sunlike stars. If it is indeed so, there are several consequences for the evolution of galaxy and other cosmological problems.

(2) Chemical evolution of galaxy: If the formation of the comet cloud of the Oort type is a general feature of star formation, then they can act as significant sinks for elements heavier than 'He'. This could provide a plausible explanation for the slow rate at which the metal abundance

of disk stars has increased during the life time of the galaxy. It is observed that metal abundance of the oldest stars in the disk population of the solar neighbourhood is about half that of the youngest stars (Hearnshaw, 1973). Yet, it is expected that the abundance of the heavy element of the interstellar gas should be doubling on a time scale of about $\sim 3 \times 10^9$ yr. Hence the abundance (Mass Fraction) of heavy element increases by about 0.008 per 10^9 yr, which is a significant fraction of its present value (~ 0.025).

The theoretical attempts for explaining this inconsistency are mainly based on the argument that not all the mass in a galaxy take part in nucleosynthesis; and not all the elements synthesized in a star are returned to the interstellar medium. Several hypothesis have been proposed to explain this effect, such as locking up a large chunk of material in brown dwarfs, blackholes (Truran and Cameron, 1971), infall of metal poor gas diluting the stellar enrichment (Larson 1972, Quirk et al., 1973, Biermann 1974) and enhancement of star formation region in chemically inhomogeneous interstellar medium (Talbot et al., 1973). It has been calculated by Tinsley (1974) that if a mass equal to that of a star is condensed into comets then the heavy element anomaly can be explained.

1.5.4 Plasma physics related studies:

(1) Interplanetary medium:

Observing the persistence of ionized tail of comets and their consistent antisunward direction Biermann(1951) argued that the solar wind in the interplanetary medium exists at all times and all solar latitudes. Since then a number of advances have been made in this field. By far the largest volume in the interplanetary space and largest span of time are covered by comets with plasma tails. More than 150 comets with plasma tails are known (see table 1.4) with the frequency, of new discoveries of one or even two per year. Comets are thus excellent probes for the study of the interplanetary medium. However, there are a number of other techniques to probe the interplanetary medium (IPM). For example the interplanetary scintillation method (measures the fluctuation of the radio sources due to the variation of electron density in the line-of-sight) can be used to infer the electron density of IPM. Such data from three different places is used to determine the velocity of plasma in IPM. Using this method it is possible to derive the parameters of IPM only upto ~ 0.3 AU from sun and the parameters are integrated over line-of-sight. Study of geometric disturbances due to energetic particles in IPM and spacecraft based insitu measurements sample the IPM mainly in the ecliptic plane. It is in this regard that comets are very useful tools, because they can 'appear' at any heliographic latitude and any heliocentric distance. For example comet Humason 1961e, showed plasma activity at 5 AU

at a solar latitude of 25° (Greenstein, 1962). Hence comets can still be used as probes of the interplanetary medium with valuable scientific returns. Fig. 1.3 illustrates the range upto which these techniques can be used. There is no way to study the phenomena at solar latitudes outside the active zone which could be entirely different from the ones observed at low solar latitudes.

(2) Studying the basic plasma processes:

Cometary plasma provides an ideal laboratory with extreme conditions of vacuum, and magnetic field conditions. Here plasma is free of boundary effects and surface contaminations. It is possible to achieve large number of gyro-radii and Coloumb mean free paths in cometary plasma as compared to the laboratory conditions. Cometary plasma is not disturbed by probing.

In the history of plasma physics we know that several important concepts like double layer (Wescott et al., 1976, Alfven et al 1967), collisionless shock (Paul, 1971), critical ionization phenomena (Alfven, 1954) have emerged from the study of space plasmas. The active probing of Comet Halley has provided a large amount of valuable previously unknown information about the plasma processes in cometary ionosphere (Galeev, 1987) such as magnetic free cavity in the nuclear region upto 4000 km, contact surface locations in the coma, excess turbulence in the tail region etc.

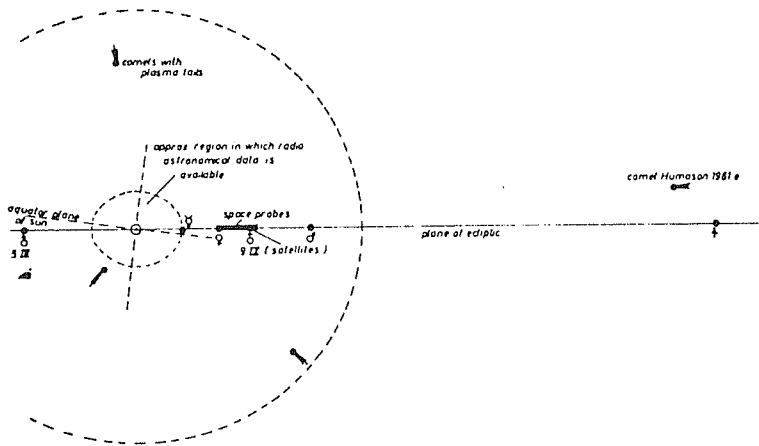


Figure 1.13. Range of different probes for studying the interplanetary medium. Comets are the cost-free probes, which can be used at any distance from sun and at any heliographic latitude.

1.6 High-Resolution Spectroscopic Study in Comets

Several of the problems listed in earlier sections can be dealt with, using high-resolution spectroscopic technique. Few of them are listed below:

1.6.1 Studies with grating spectrometers.

The main questions pertaining to the excitation mechanisms of spectral lines in comets to which high resolution spectroscopic study can be applied are 1) Are collisional processes significant for Comets? 2) Is the cometary cloud truly optically thin to emission line radiations? 3) Is statistical equilibrium rapidly achieved? Various attempts with high resolution techniques in Comets have been made since decades with partial success. Using a 120-inch coude spectrograph with dispersion in ultraviolet, visual and IR regions of 2.0, 4.1 and 4.1 $\text{\AA}/\text{mm}$ respectively and a slit of 1' in length, Preston (1967) had obtained a high-resolution spectra of comet Ikeya-seki 1965f. He had shown that the intensity distribution in P - and R - branches of CN(0-0) band show the mutilating effects due to fluorescence excited by solar radiation. It was also found that the apparent abundance ratio KI/NaI was low and the ratio CuI/FeI was unaccountably high in the comet relative to the sun, meteorites and Earth's crust. The high-resolution

visual spectrum of comet Mrkos 1957d by Greenstein et al (1962) showed that NaI lines are asymmetric with respect to the nucleus. A 0.3 \AA^0 resolution spectrum of the $V=+1$ sequence in the C_2 swan system from comet West 1976 VI at a heliocentric distance of $\sim 0.78 \text{ AU}$ was found to correspond to G vibrational and rotational temperature of $\sim 3500+400 \text{ K}$ for the upper $d^3 \pi_g$ state (Lambert et al., 1983). If intercombination transitions are neglected the predicted temperature for C_2 excited by fluorescence in sunlight is considerably hotter than the observed temperature. Their study suggests that intercombination transitions involving excited states may be important in the singlet-triplet conversions and influence the vibrational temperature achieved in the $a_3 \pi_u$ state. Using the spectrometers of resolving power of $\sim 10^4$ the importance of collision in exciting the lower rotational levels of CH has been studied quantitatively (Arpigny, 1987).

As discussed earlier in section 1.2.1 the measurement of isotopic ratios of carbon, oxygen and Hydrogen are of vital importance for understanding the origin of comets. The first ever attempted observation in this direction with low resolution spectrograph was by Stawikowski et al., (1964) following by Owen (1973). These measurements indicate that the ratios of $^{12}\text{C}/^{13}\text{C}$ to be $\sim 70 \pm 15$ and 100 ± 20 respectively for Comet Ikeya 1963I and Tago-Sato-Kosaka. Danks et al (1974) found the same ratio $115 (+30, -20)$ and $135 (+65, -45)$ for Comet Kohoutek. Clearly these measurements have the

errors of +30% - 50%, too poor for warranting any hypothesis. Arpigny et al (1986) have made a great improvement in this direction. They have obtained a high S/N ratio spectra with high resolution (0.05 \AA) and with calibration in C_2 (0,0) band, the analysis of which is awaited.

High-resolution spectroscopy is quite useful in estimating the true line strengths, uncontaminated with the nearby emission bands. Recently Arpigny (et al., 1987) has pointed out that contamination of NH_2 in estimating the oxygen abundance from $[OI]6300 \text{ \AA}$ line measurements introduce an error of ~ 50 to 100%.

1.6.2 Interference Spectroscopy

Jacquinet (1954) has shown that for a fixed resolution, the light gathering power for interferometric devices like Fabry-Perot and Fourier Transform Spectrometers is much higher compared to grating and prism based devices. Such spectrometers of higher throughput have been applied to cometary study only since the last decade. High Resolution studies of Comets by Fabry-Perot interferometric techniques by Huppler et al (1975) and P. Shih et al (1984) in H_α of comets Kohoutek and Austin respectively have shown the existence of hydrogen atoms of various velocity groups. This result indicates there are different sources for hydrogen in comets. Huppler et al (1975) have studied H_2O^+ line profiles in the coma and in the tailward

direction and have concluded that the Doppler velocities to be $\sim 20-40$ km/s. However, a detailed study covering a large portion of the tail, is yet to be done to distinguish between the particle versus wave motion in the cometary plasma tail. Kerr et al (1987) have inferred collimated atomic hydrogen flow in the inner hydrogen coma of Halley's comet. One of the most important achievements of recent times by these devices is the detection of water with a Fourier Transform Spectrometer (FTS). Using a high resolution FTS with a resolving power $\sim 3 \times 10^5$ (NASA Kuiper Airborne Observatory) in the near infrared ($2-3 \mu\text{m}$) observations Larson et al (1986, 87) have convincingly established that H_2O is a major volatile component of the cometary material. Further their results show that H_2O outflows from the entire Sun-lit hemisphere of the nucleus and not from a single, narrow jet emanating from the nucleus. They also measured the pre and post perihelion outflow velocities as 0.9 ± 0.2 and 1.4 ± 0.2 km/s respectively.

The application of FPS and FTS techniques in cometary science is a recent development. There is ample scope for the full utilisation of these techniques in future comets particularly in imaging spectroscopy with the development of 2-dimensional detector arrays. Studying the high-resolution imaging spectrum of the comet, it would be possible to deduce the velocity of ionic and neutral species in the coma or tail. As discussed earlier the ion velocity information as a function of cometocentric

distance in the type I tail would resolve the wave versus mass motion controversy. Study of the transient outbursts is another new area which can greatly benefit from spectral imaging

1.7 Motivation for the Present Work

As described in section 1.2.3 the interaction of solar wind with cometary ionosphere produces a variety of phenomena in the coma, which manifest themselves in the form of various large and small scale features. Some of the structures observed in the ionic tail are the consequences of such processes occurring in the coma. For example the narrow rays could be traced into the coma region within $\sim 10^3$ km of the nucleus (Wurm et al., 1967). The condensation regions seen in the tail are expected to have originated from well within the coma (Jockers, 1985). Various transient features in the coma have been reported (Telesco et al., 1986, Roosen et al., 1976 and Ip et al., 1986) on several comets. For understanding the nature of such features it is essential to know the velocity field in them.

The measurement of forbidden oxygen line [OI] at 6300 \AA is an important method for determining the production rate of neutral oxygen. Oxygen atom is now recognized as an important species belonging to the water group. Unfortunately NH_2 emission blends 6300 \AA oxygen line. Arpigny (1987) have shown that 30-50% error can be

introduced in the estimation of [OI] intensity from the blended spectra. In this case however, high resolution Fabry-Perot spectroscopy could play an important role in obtaining unblended [OI] line profiles.

Even though the chemical models of the coma suggest that C_2 is formed primarily by chemical reactions, its density distribution deviates considerably from a Haser model (Heubner 1981, Wyckoff, 1988). A multiple parent source, for C_2 is indicated with the CHON particle and/or some ionic complex molecules being some of the parents. Hence the high-resolution spectroscopic study would be helpful in understanding some aspects of C_2 emission.

The above considerations make it clear that there is a strong case for making observations for,

- (i) Obtaining the velocity structure of the regions in the cometary ionosphere where the transient plasma features are present.
- (ii) Obtaining series of short exposure images of coma, at selected wavelengths with a view to record the plasma features for studying their origin and dynamics.
- (iii) Obtaining the unblended line profiles of [OI].
- (iv) Obtaining the two dimensional spectroscopic data

of the coma in various emission lines and bands.

(v) Studying the shift of wavelength of a particular emission line of a neutral or plasma component for determining the acceleration as a function of cometocentric distance.

This thesis addresses itself to some of the above stated problems of cometary physics employing the technique of Fabry-Perot interferometric spectroscopy. Short exposure images of the coma have been obtained in various filter bands. Interferograms in C_2 (5165 \AA^0), $H \alpha$ and [OI] giving two-dimensional spectral information have been recorded and sophisticated piezo Fabry-Perot used to secure unblended [OI] and NH_2 line profiles.

Chapter 2 deals with the conceptual development, design, fabrication and testing of the image intensifier coupled photographic (imaging) Fabry-Perot Spectrometer, and central aperture scanning servo controlled Fabry-Perot Spectrometer alongwith the site selection and details of the observations.

Chapter 3 describes the method of analysis used in reducing the data of two plasma events observed on 8th January and 13 March 1986. The results and their implications to cometary science is discussed.

Chapter 4 deals with the high-resolution line profile data in [OI] 6300 \AA emission obtained with piezo-electrically scanning spectrometer. The analysis of [OI] 6300 \AA interferogram obtained from Mt. Abu is also discussed. A correlation study of 6300 \AA emission with other characteristics cometary parameters is presented. The studies of C_2 interferogram to obtain the different outflow velocities is also presented.

Chapter 5 summarizes the present study. A few important suggestions have been made for the future studies.

CHAPTER 2

INSTRUMENTATION AND OBSERVATION

This chapter describes the instrumentation used for the observations in the present work. The Instrumentation involved a) installing a 14 inch telescope and setting up a mini-observatory at Gurushikhar Mt. Abu, India and b) designing, fabricating and testing of the two high resolution Fabry-Perot Spectrometers (FPS) used respectively in imaging and scanning modes. Most of the observation were carried out from Gurushikhar using the imaging Fabry-Perot system. The 1 meter telescope of Vainu Bappu Observatory, Kavalur, S. India was used with the piezo-electrically scanning FPS to obtain the line profiles of certain cometary emissions during the few nights of allotted telescope time in April 1986.

2.1 Selection of the parameters of Fabry-Perot Spectrometers

A Comet is an extended object with the emission lines and bands embedded in a strong continuum. A particular advantage of the Fabry-Perot system is its ability to discriminate the line and continuum sharply. Combined with its high light gathering power or etendue, it is thus a very

useful and powerful instrument for studying comets. The present instrumentation is optimized for both imaging in the cometary emissions with an intensifier camera.

2.1.1 Flux collecting power(L)

The flux collecting power, light gathering power or luminosity or etendue "L" of a spectrometer is defined as

$$L = \epsilon A \Omega$$

where ϵ = transmission factor, A = area of the dispersing element, Ω = acceptance solid angle of the spectrometer. Since comet is an extended object, increasing Ω would result in higher L upto the angular extent of the comet. Jacquinot (1954, 1960) showed that for each class of spectrometers the product $L \times R$ is a constant, where R is the resolving power of the spectrometer. For an interferometric device like a Fabry-Perot which works on the principle of division of amplitude, possessing a circular symmetry, L is higher by a factor of 30 to 100 compared to grating spectrometer and 300 to 1500 compared to prism devices (Meaburn 1976). Since A is nearly the same for different types of spectrometers, for a given resolving power an F.P. can collect light over a wider solid angle; and hence it is advantageous to use for observing an extended object.

2.1.2 Choice of emission lines

The choice of emission lines for the present study and

suitable filters are based on two criteria.

(a) One of the major aims was to study the kinematics of the plasma and neutrals in the Coma and tail by measuring the doppler shifts. Guided by the previous work of Huppler et al (1975) one of the lines selected was at $H\alpha$ 6563 \AA in the wings of which H_2O^+ rotational line feature (0, 7, 0) is present. The [OI] line at 6300 \AA was also selected to study the neutrals, since oxygen is one of the important water group atom in the coma. These lines have less crowded spectrum in comparison to other emission lines of H and O and are suitable for a study with a Fabry-Perot. They were also the emissions for which narrow band filters were readily available. Study of these lines would also help to understand the nature of the parents of H & O.

The C_2 (0-0) Swan band at 5165 \AA is uncontaminated by the emission from NH_2 unlike at other visible wavebands. Hence it was decided to use this band to obtain the FP interferogram for C_2 .

Since the cometary spectra is rich in emission lines and bands all over the visible spectrum, it is necessary to use narrow band pre-filters to avoid the inter order overlapping. Proper choice of free spectral range (FSR) is also a crucial aspect, which will be discussed in chapter 4. Table 2.1a gives the details of the narrow band filters used for the interferometric work.

TABLE 2.1a

Characteristics of Narrow Band Interference Filters

Emission	λ Å	$\Delta \lambda$ Å	Peak Trans (%)	Size (dia-meter)	Temperature coefficient
H α	6563 at 20°C	5	40	50 mm	0.15 Å/°C size towards red
[OI]	6300 at 20°C	3	40	50 mm	"
Na	5890	30	40	50 mm	"

(b) For obtaining the cometary images in several emission and continuum wave bands a number of interference filters were selected to isolate the spectral features. These relatively broad band filters were procured from the International Halley Watch (IHW). Table 2.1b gives the detailed characteristics of these filters.

Figure 2.1 gives a typical cometary spectrum and the filter bandwidths used in the present work.

2.1.3 The exposure time:

The near nucleus images of Comet Halley in white light, Kodak Wratten filters and IHW filters were obtained with short exposures of $< 1^s - 3^m$. The short exposures of this type have the advantage of removing the smear due to the internal motion of cometary material. Typical exposures were

White light $< 10^s$

Wratten filters $< 30^s$

IHW filters 2^m

It is to be noted that the relatively small exposure times on the comet was made possible mainly due to the use of an image intensifier with a quoted gain $\sim 30,000$.

TABLE 2.1 b
Characteristics of IHW filters

Emission	λ \AA	$\Delta\lambda$ \AA	Peak Trans (%)	size (diameter)
CN	3874	50	25	25
C ₃	4060	73	44.5	25
CO ⁺	4260	70	42	25
Cont.	4850	65	70	25
C ₂	5135	90	61	25
Cont.	6840	98	74	25
H ₂ O ⁺	7000	175	77	25

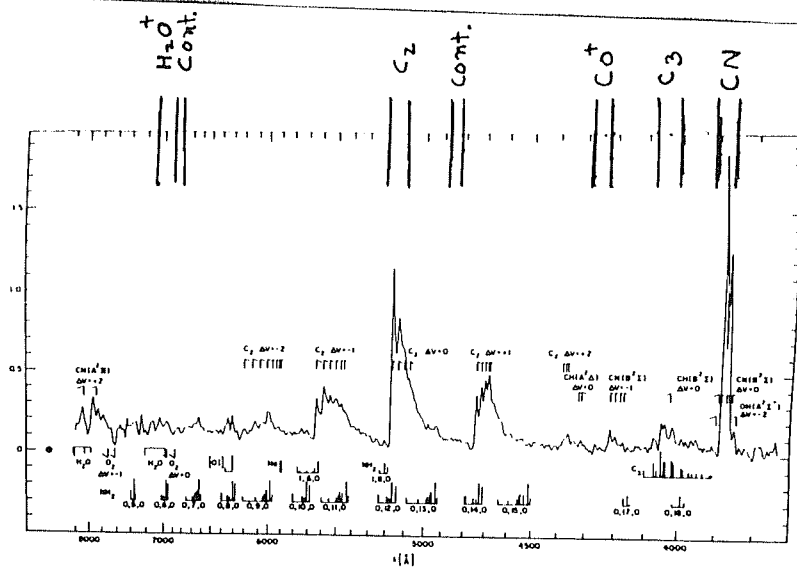


Figure 2.1 A typical cometary spectrum. On the top, indicated the band widths of the filters used.

2.2 Fabry-Perot Spectrometers

A number of good books and reviews are available on Fabry-Perot spectrometers, the most recent being by G Hernandez (1986). The practical use of the device in interferogram mode and scanning mode are nicely described by T. Chandrasekhar (1982) and K.C.Sahu (1985). Apart from several other reviews by Vaughan (1967), Meaburn (1970) and others J.N.Desai (1984) summarizes the use of F.P. Spectroscopy in studying various aspects of space science. Here a few basic equations, useful for the present discussion will be given.

2.2.1 The basic equations:

A F-P etalon is essentially a pair of optical flat $\lambda/200$ fused silica plates, held parallelly ($\sim \lambda/100$) at a distance t . To avoid the absorption loss, the facing surfaces of the plates are coated with high reflectivity ($\sim 95\%$) multilayer dielectric coating. The transmission profile of an ideal F-P is described by Airy function (a function of transmission light of wavelength λ , through a F-P etalon).

$$I = I_0 \left(\frac{T}{I-R} \right)^2 \left(1 + \frac{4 \pi}{(I-R)^2} \sin^2 \delta/2 \right)^{-1} \quad \dots 2.2$$

$$\text{where } \delta = \frac{2\pi}{\lambda} \left[2 \mu t \cos \theta - 2r/\lambda \right] \quad \dots 2.3$$

T and R = Transmission and Reflectivities of etalon flats.

r = Phase change on reflection.

μ = Refractive index of the medium between the plates.

θ = Angle of incidence.

λ = Wavelength of incident light.

Since r is negligible for visual wavelengths, it follows from above equations that the Airy function peaks when,

$$2 \mu t \cos \theta = n \lambda$$

...2.4

where n is an integer called the order number. This shows that the wavelength separation between the two successive orders of a given line can be expressed as

$$\Delta \lambda = \frac{\lambda^2}{2 \mu t}$$

...2.5

$\Delta \lambda$ is called free spectral range (FSR). The full width at half maximum of the Airy function (2.2) is known as the resolution limit and given as,

$$\delta \lambda = \frac{\lambda^2 (1 - R)}{2 \mu t \pi \sqrt{R}}$$

...2.6

Where $\frac{\pi \sqrt{R}}{1 - R}$ ($= N_R$) is called the reflective finesse.

Hence for the higher finesse higher the resolution of the instrument. In actual practice, however, the effective finesse is decided not only by the reflectivity of the plates but

also from several other sources as described in the next section.

2.2.2 Instrumental broadening:

The instrumental profile is the convolution of five basic functions i.e. Airy (AI), spherical plate defect (PD), Misalignment (MI), Microsmoothness (MS) and aperture (AP) and expressed as,

$$I = AI * PD * MI * MS * AP$$

(* symbol for convolution)

The resultant width becomes more than expected from eqn. (2.6) due to the deterioration of finesse by several factors listed above. The nature of these functions are described in detail by Hernandez (1986). The detailed derivation of these functions and in particular the misalignment function is summarized by Ranjan Gupta (1985). A brief summary of constructing the synthetic line profile is given in the appendix 2.1. Table 2.2 summarizes the contribution of different functions towards the finesse of the instrument. The synthetic profiles by convolving these functions were carried out by the author with the parameters of the spectrometer and given in section 3 and 4.

2.3 Imaging Fabry-Perot Spectrometer

TABLE 2.2

Five Basic Functions Contributing to the
Instrumental Broadening

Source	Function	Width	Finesse	Note
Microscopic flatness imperfection	Gaussian	$\Delta\lambda/M / 4.7$	$MG/4.7$	λ/MG =surface defect
Spherical plate defect	rectangular	$\frac{\Delta\lambda}{Ms/2}$	$MS/2$	λ/Ms =Plate defect
Misalignment	Inverted parabola	$\frac{\Delta\lambda}{MP/\sqrt{3}}$	$MP/\sqrt{3}$	λ/Mp =departure from parallelism
Aperture	rectangular	$\frac{\lambda \Omega}{2 \pi}$	$\frac{2 \pi}{n \Omega}$	Ω =Solid angle subtended by the aperture at the etalon
Airy	Airy	$\frac{\Delta\lambda}{N_R}$	$N_R = \frac{R\sqrt{R}}{1-R}$	R =Reflectivity of the etalon plates

Each point on the FP fringe corresponds to a definite direction of incident flux and hence to a definite location on the object under study. Hence a interferogram is an imaging spectra of the source. This property of the FP has been extensively used in various fields such as for studying the dynamics of Solar Corona (T.Chandrasekhar et al., 1981), determination of the velocity field and turbulent structure of gaseous nebula (Deharveng 1973) and gas dynamics in galaxies (Vaucouleurs et al., 1980).

2.3.1 Mode selection:

The basic principle involved in this method is the "Spatial Scanning" consisting of varying the order number (n) of eq. 2.4 by changing the value of the angle θ for a given wavelength λ . On each fringe of a given order, θ can be varied in small increments to scan in λ , thereby constructing the line profile.

In general there are two ways of accomplishing i.e. (1) varying the effective radius of an angular aperture and its width in a controlled manner in the image plane of the etalon fringe or (2) using a 2 dimensional detector array for recording the fringe pattern. A detailed account of the various modes of operation is described by Hernandez (1986). The advent of two dimensional imaging solidstate detector arrays have made it possible to use the later method widely. In practice this is realised in two modes, namely

telecentric or non-classical and classical. The telecentric mode has the advantages of perfect smearing over a selected area of the source, thereby removing the contribution due to sharp intensity gradients. Telecentric mode however sacrifices spatial resolution, which can be retrieved to a limited extent by using insect eye camera lens. The other advantage of this method is the improvement of finesse, because of using a small area of FP, which may not be so effective due to the availability of high quality etalons. However, it can be seen from eqn 2.1 that the disadvantage of this method is the low effective etendue (because of using smaller part of the etalon). The spatial resolution is also sacrificed.

In the present case the intensity gradient in the coma is not a serious problem. The more important problem is correctly assessing the contribution of the continuum and correcting for it. The columnar intensity due to neutral species such as C_2 is expected to follow a power law i.e. r^{-1} . $H\alpha$ or [OI] emissions also do not have sharp gradients in the coma. Hence the spatial smearing has no advantage in this case. It would be advantageous to obtain spatially resolved information. The available finesse of the etalon was sufficient for the present work. Therefore it was decided to use the classical mode of obtaining the interferograms.

2.3.2 The Etalon

The alignment and the spacing control between the two plates of the etalon are achieved by the optical contacting technique. This method has the advantage of stability (required under exacting field conditions) over several other methods employing the mechanical stress as described by Hernandez (1986). Though this is a passive method of control, usually very high stability is achieved throughout the operation.

For the present work the entire visible range from 4500 \AA to 6700 \AA was covered by using two airspaced optically controlled etalons. The etalon parameters are given in table 2.3. Each of the two etalons is mounted in a ring that can be rotated to offset the fringe centre from the optic axis of the system. The off-axis mode is useful in varying the spectro-spatial resolution across the extended source. For instance, in this mode a single fringe can be positioned over most of a comet tail to provide spatially continuous line profiles.

2.3.3 The image intensifier:

Since exposures as short as possible were derived to avoid the smearing due the internal motion of cometary material, the problems of telescope drive and rapidly varying sky conditions (while working at the zenith angles

TABLE 2.3

Etalon parameters.		
Parameter	Green etalon	Red etalon
Spectral coverage	4500 Å to 5500 Å	5700 Å to 6700 Å
Spacer value	300 μm	1000 μm
Usable aperture	40 mm	24 mm
Free spectral range	4.17 Å (at $\lambda = 5000$ Å)	2.15 Å (at $\lambda = 6563$ Å)
Effective finesse	14	20
Effective instrumental width	0.30 Å	0.11 Å
Plate flatness	$\lambda/100$	$\lambda/100$

close to 90°), a high gain second generation (Gen II) image intensifier was used. The working principle of this device is simple. The optical image is converted into a electron image using a S-20 type photocathode, which is then passed through a micro-channel plate producing an intensified electron image. This electron image falls on a phosphor screen of p39 type (having long time constant, advantages for longer integration) to produce an optical image with again of $\sim 3 \times 10^4$. A "zero-thickness" optical fibre glass plate is used to transfer the image from phosphor screen to any detector (a photographic film in the present case). The Gen II image intensifiers have the economic advantage over earlier generations, due to the use of microchannel plates and the built in power supply, which is desirable for the field experiments.

The scale size at the phosphor end of the intensifier was determined by measuring the separation of a binary system of stars ("Mizar" in Ursa Major in the present case) with known angular separation. The calibration interferograms were also used to determine the magnification. It was established that the magnification of the image intensifier was 1.2. The phosphor background was seen to be uniform over more than 95% of the area in the image plane. The essential parameters of the image intensifier used are listed in table 2.4.

The image intensifier was found to perform

TABLE 2.4

Image intensifier parameters.	
Effective diameter of multialkali photocathode	25 mm
Spectral range	3500 Å to 9100 Å
Wavelength of peak response	6000 Å
Limiting spatial resolution at center at 5% MTF level	30 line pairs/mm
Maximum image distortion near edge compared to center	5%
Equivalent background input minimum detectable flux	2×10^{-17} lx
Gain (variable by potentiometric control)	20,000 to 40,000
Weight	300 g
External power supply	3 V dc

satisfactorily under field conditions. It was however found to exhibit small spots distributed over the image plane, which can be readily recognized. At times flashes of light were also noticed near the edges, which did not significantly impair the observations.

2.3.4 The optical layout:

Figure 2.2 is a schematic of the interferometer. The light from the comet was collected by the telescope mirror P and S. The collimation of the image formed at the Cassegrain focus of the telescope was accomplished by an 80 mm focal length $f/1.2$ special camera lens L. It is convenient and accurate to carry out the collimation adjustment with just the front end of the instrument coupled to the telescope and with a bright star, e.g. Sirius as the source. The adjustment was found to be stable over a period of several weeks with the instrument coupled to the telescope. The collimated light passed through the FP etalon E and filter F (several filters as given in table 2.1a) focussed by a 50 mm focal length $f/1.2$ Nikkor camera lens O onto the photocathode of the image intensifier.

2.3.5 The camera and data recording:

To record the image, the film plane has to be flush with the fiber optic output plate. This arrangement poses a few problems since commercially available 35 mm cameras are

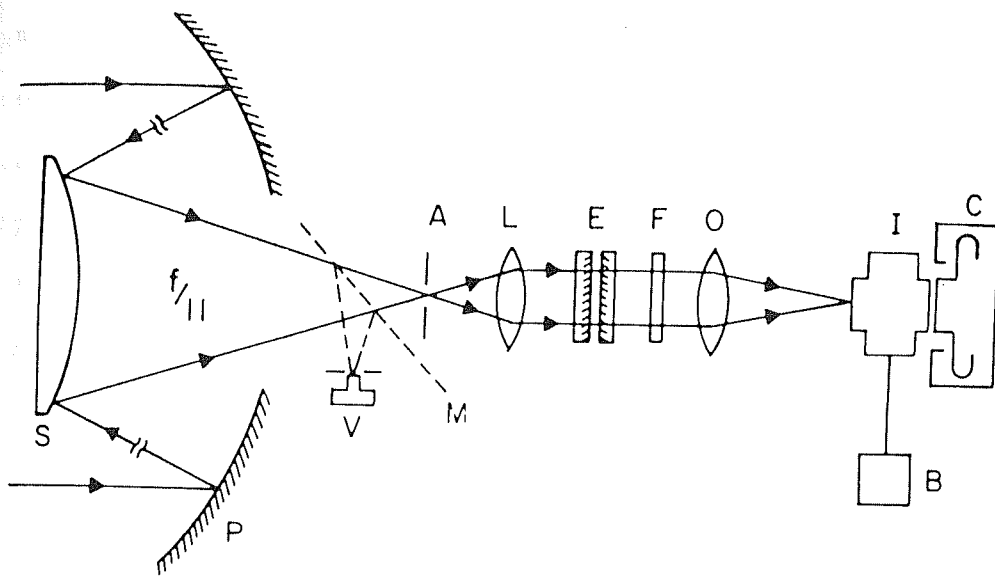


Figure 2.2. Schematic of the imaging Fabry-Perot interferometer optics.

S = Secondary mirror of the telescope

P = Primary mirror of the telescope

V = Visual port

M = Flip mirror assembly

A = Entrance aperture

L = Collimator lens

E = Fabry-Perot etalon

F = Narrow band filter

O = Camera lens

I = Image intensifier

B = Battery supply

C = Camera.

usually single lens reflex (SLR), in which the film plane is inaccessible from the front end. Reimaging the phosphor output onto the film by a short focus lens is difficult and involves loss of light. This problem was overcome by modifying an old 35 mm non-SLR camera. Two slots were made on the front side of the camera body to bring out the film and make it slide smoothly over a velvet-lined metallic projection. Thus when fitted to the image intensifier, the film remains in contact with the fiber optic window, being pressed by the projection. A pin and slot arrangement made for attaching the camera to the intensifier ensures easy coupling in the dark. In operation, the phosphor screen is viewed by a high power eye-piece and the star field is focussed. The eye-piece is then removed and the camera is coupled to the intensifier. The film movement is reasonably smooth, and no serious problem of film scratch was encountered.

2.3.6 The film and calibration:

A high contrast, microscopic grain (~ 320 lines/mm with D 19 developer) Kodak's technical pan 2415 film in 35 mm format, with extended red sensitivity was used in proximity contact with the phosphor screen of intensifier to record the comet images and interferograms. We have obtained the image of Crab nebula (M1) which is of 8.6 magnitude with the exposure of 30^s .

However, feeble night airglow feature at 6300[OI] could be recorded only on a faster emulsion Kodak 2485. For comet work 2415 emulsion was found to be satisfactory.

For converting the photographic densities to relative intensity, a step wedge (with 7 steps) impression was invariably taken on each film using a wedge sensitometer shown in figure 2.3. The calibration curve was constructed by measuring the photographic density steps in the wedge impressed on the film and ($D = -\log_{10} T$) and the corresponding diffuse densities ($\log_{10} E$), both measured in the laboratory with a microdensitometer. The typical characteristics curves are given in the following chapters. The film is subject to low intensity reciprocity failure. This effect was not serious, wherever the morphological structures were considered. However for intensity estimation and profile width measurements, proper care has been taken as will be discussed in later chapters.

For the spectroscopic calibrations the He-Ne (6328 \AA^0) Na (5890 and 5896 \AA^0) and Hg (5461 \AA^0) interferograms were taken on each observing session. Fig.8 gives a typical laser interferogram. The analysis and results of the calibration interferogram is given in sec 3.8.

2.3.7 Interferometric and imaging mode of operation:

This instrument was used both in interferometric and

SCHEMATIC DIAGRAM OF WEDGE SENSITOMETER

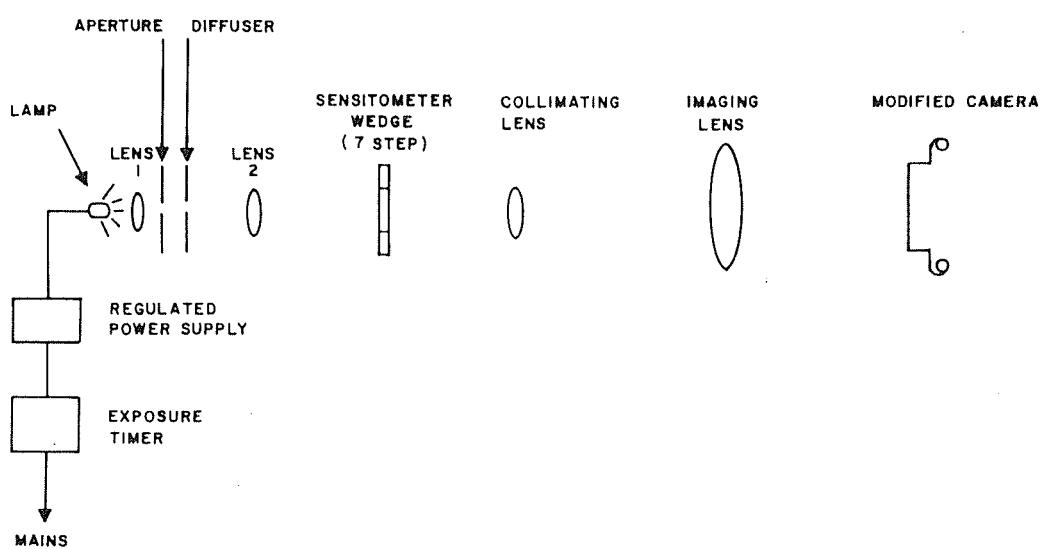


Figure 2.3. Schematic diagram of the wedge sensitometer.

imaging mode. The interferometric mode was realised with the optical scheme shown in Fig. 2.2. By removing the narrow band filter F, the same instrument could be used in imaging mode. On removing the narrow band filter, the interferometer samples the spectrum every free spectral range, $\sim 2 \text{ \AA}^0$ for red etalon and $\sim 4 \text{ \AA}^0$ for the green etalon, at each point of the extended object, within the spectral range of the etalon. It then acts as a comb filter, and the net effect is a nearly white light image. There is of course large flux loss due to etalon reflection [$\sim 90\%$] but with the intensifier this did not pose a problem with broad band filters. The interferometric optics results in an effective f/no of $f/7$, hence reducing the exposure time by a factor of ~ 2.5 compared to the $f/11$ system. The image scale size and the field of view on the film were 67 arc sec/mm and 21 arc min. in the plane of sky respectively.

At times, the image intensifier camera system was attached with a commercial telecompressor and filter slide assembly to obtain the comet images at higher f/Nos. In this case the image scale size and field of view were 83 arc sec/mm and 28 arcmin respectively.

2.3.8 Performance of the instrument:

Fig. 2.4 show the laboratory assembly of the interferometer. The instrument weighs $\sim 6 \text{ kg}$ and is $\sim 66 \text{ cm}$ long. Fig 2.5 show the field assembly of the instrument with

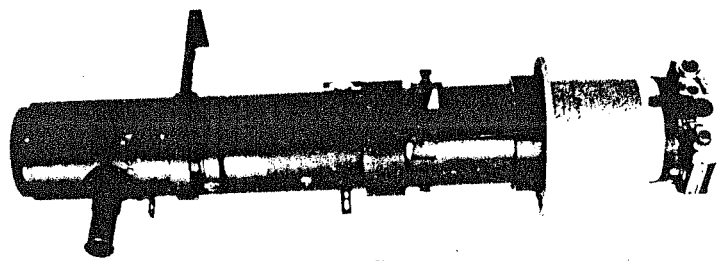


Figure 2.4. The laboratory assembly of the imaging Fabry-Perot interferometer.

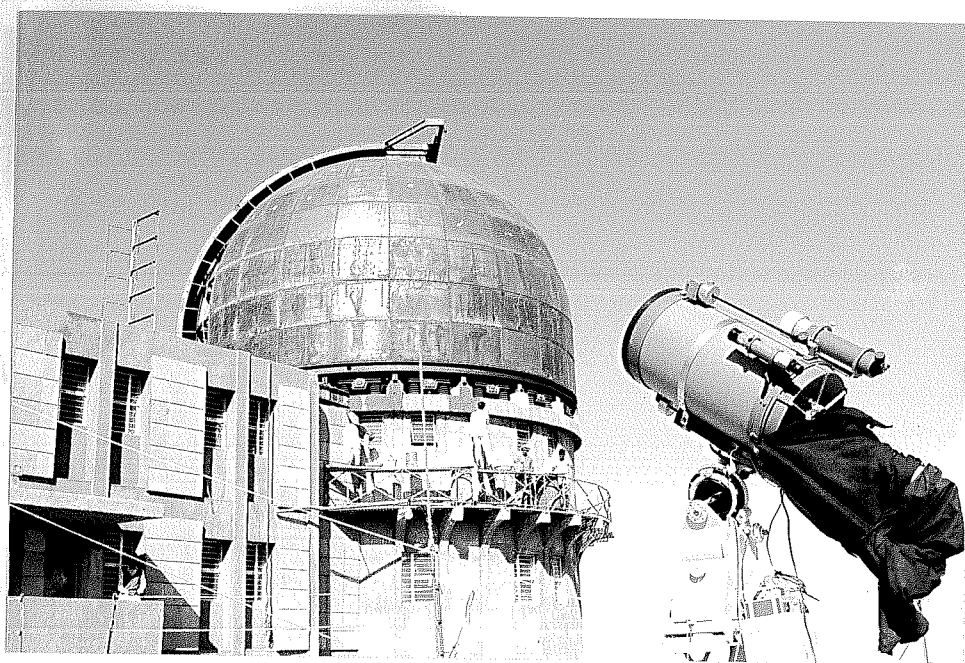


Figure 2.5: The imaging interferometer coupled to C-14 telescope at Gurushikhar, Mt.Abu.

the C-14 telescope. The off centered laser/spectral lamp fringe system were routinely taken (at times with superimposed comet images) for locating the fringe centre and defining the instrumental profile. Fig 2.6 a,b show the laser and Na lamp interferogram. The observed instrumental profile was obtained by scanning a typical region of the calibration interferogram and constructing a wavelength λ vs relative intensity plot.

The stability of the instrument was determined in the following way. Three laser fringes, the second in the beginning, one at the middle and the third at the end of the observing session, were selected (observation lasted for 8 months from October 1985 to May 1986). The difference between the radii of successive orders i.e.

$$(R_{n2}^2 - R_{n1}^2) = 2F\lambda/2\mu t$$

was found to be constant over this long period with a maximum variation of $+ 5 \mu m$ from the quoted value, within the measurement errors. This implies μt was stable upto 2% all through the observations. The slight variation can be expected due to the change in μ and t . However for each night of observation μt was determined to use for analysing the data of that night, reducing further the error due to this source.

The test results for the instrument were obtained on

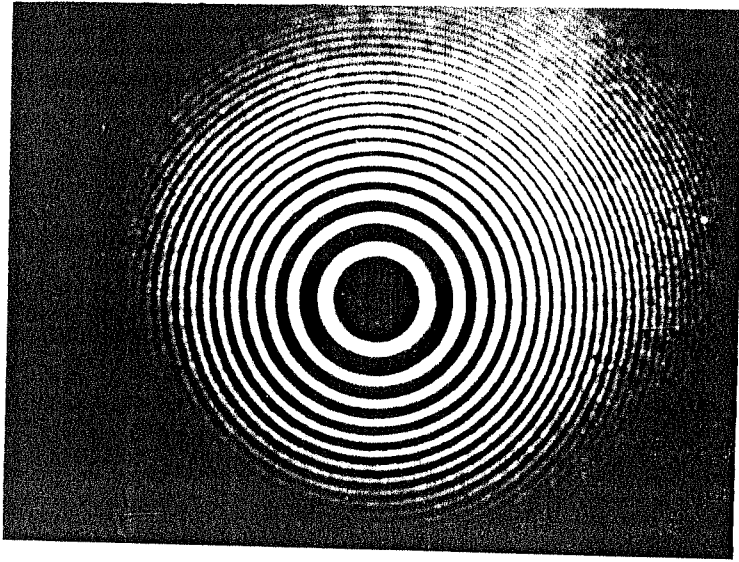


Figure 2.6a. A typical He-Ne (6328 \AA) laser interferogram taken with the imaging Fabry-Perot interferometer.

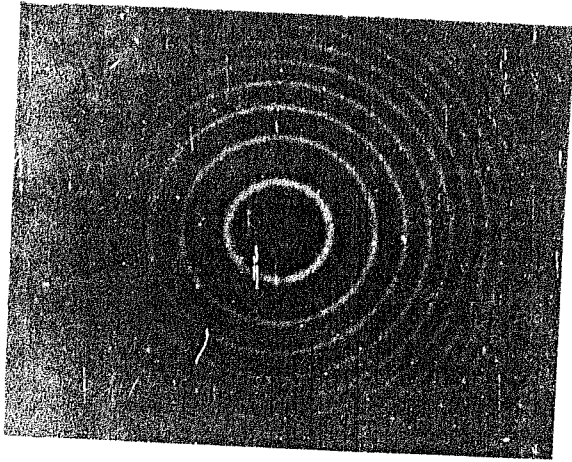


Figure 2.6b. A typical Na (5890 \AA) interferogram taken with the imaging Fabry-Perot interferometer.

the Orion nebula. Fig 2.7 and 2.8 show the interferogram taken in the [OIII] line ($5007/10 \text{ \AA}$) and $H\alpha$ ($6563/5 \text{ \AA}$). The line profile analysis from these interferograms give

the internal velocities, consistent with the results obtained by earlier observations. An important point to note here is the ease of operation and short exposure times needed for obtaining spatially resolved observations from a relatively faint nebulosity.

2.4. Servo Controlled Piezo-Electric Scanning Fabry-Perot Interferometer

In order to obtain the photoelectric line profiles of [OI], $H\alpha$ and H_2O^+ emissions, a central aperture scanning Fabry-Perot spectrometer with higher finesse and stability was developed. Unlike the instrument described in the earlier section, this instrument has active control of the gap and parallelism and the scanning is achieved at the etalon proper. Unlike the interferometer described above which was a light weight device specially designed to go with C 14 telescope the scanning F.P was designed to operate on a 1 meter Cassegrain telescope and was a much more sophisticated instrument.

2.4.1 Choice of the device

Cometary spectra is rich in closely spaced emission bands and lines throughout the visible spectrum. Moreover

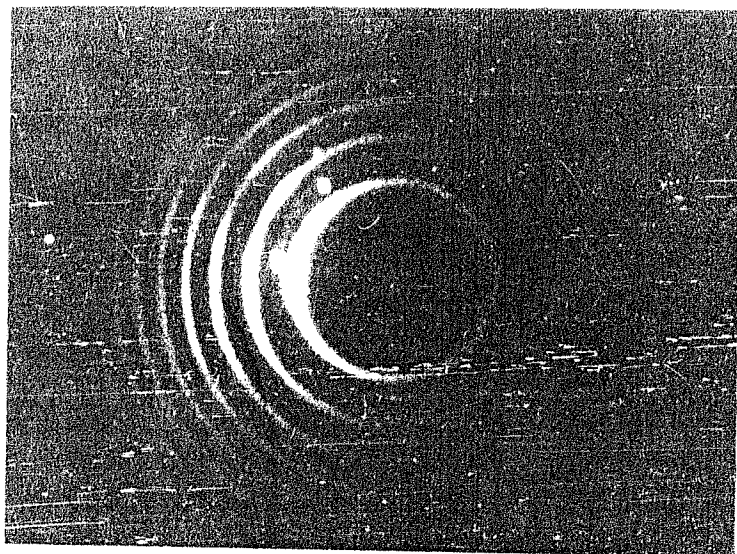


Figure 2.7 . Interferogram of Orion Nebula taken in [OIII] ($5007/10 \text{ \AA}$).

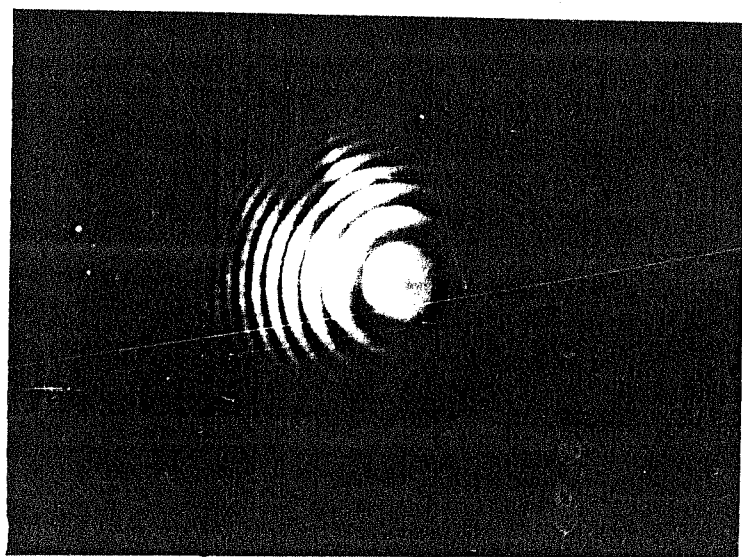


Figure 2.8 . Interferogram of Orion Nebula taken in H-alpha
(6563/5 Å).

the feeble emissions are embedded in a strong continuum background. In the coma the continuum brightness varies as $1/\vartheta$, where ϑ is the projected distance from the nucleus. The emission lines such as [OI], NH_2 etc. are confined very strongly towards the nuclear region. Therefore the noise introduced due to the tracking error or atmospheric scintillation is considerable in this case.

To obtain the line profiles under the conditions described above, it is essential to design a spectrometer with a large free spectral range, so that the two orders of a given line are well separated in wavelength and the filter band width need not be too narrow. Care also must be taken so that other orders of a different emission line do not overlap. To obtain a large spectral resolution with a wide free spectral range, it is necessary to have as high finesse as possible. Coadding several scans of the same spectral region can improve the S/N, which needs a highly stable system.

Since the optical finesse of the plates presently available are high ($\sim \lambda / 200$), the overall finesse of an etalon is limited by the control of alignment and spacing. Essentially there are two ways of achieving the alignment and spacing control i.e. passive and active. In the passive method, after the alignment is reached, the etalon spacer and support combination are supposed to remain stable while the observations are on. In the optically contacted etalon used

in the previous instrument the passive alignment is maintained to a high degree of accuracy by the optical banding the FP plates at the time of manufacture. In optically contacted system at best parallelism upto $\lambda/20$ may be achieved. In the present case however an active method was employed. The active method can be realized in many ways. One way is to monitor of Brewster white light or monochromatic light fringes formed by double passing the etalon at opposite ends of two perpendicular diameters from an auxiliary source. (Ramsey, 1962, 66). The fall in intensity level in the resulting fringe pattern in the measure of the degradation of the parallelism, which is restored by using the piezo-electric transducers. However this method has two drawbacks of introducing the light. The break through in FP servo control came about with the development of capacitance micrometry by Hicks et al (1974) and Jones and Richards (1973) Piezo-electric transducers and capacitance micrometry have been used in the present instrument, which will be discussed in the section 4.4.

As it can be seen from equation 2.4 wavelength scanning is achieved by changing the optical spacing μt of the etalon.

This can be realised by changing μ or t . Changing μ is achieved by changing the pressure of the chamber or using the electro-optic materials. The range of scanning is also limited in pressure scanned devices. For e.g. a spectral

range of $\sim 4 \text{ \AA}^0$ at H_{α} would require a pressure variation of over 2 atmospheres in air. Hence a more stable method of "mechanical scanning" was employed in the present case. Again mechanical scanning can be accomplished by several techniques as described by Hernandez (1986). The most successful method to attain mechanical scanning has been associated with the use of the piezo-electric materials which is used in this device. In section 4.4, this will be discussed in detail.

2.4.2 Optical system:

The optical layout and the electronics of the piezo-electrically controlled central aperture scanning Fabry-Perot Spectrometer is shown schematically in Fig. 2.9. The $f/13$ Cassegrain beam from the telescope is focussed on to an aperture wheel has different entrance apertures ranging from 8" to 160" in the sky. A fixed aperture of ~ 50 " was used during the observations. A flip mirror system is provided for viewing the star field to ensure that the object of interest is properly centred on the cross wire. A post focal plane flip mirror-eye piece system is also provided to actually verify that the object is on the optic axis and is properly focused. The same flip mirror arrangement also permits light from a He-Ne laser or a suitable calibration source like a low pressure, spectral lamp to be diverted into the system for evaluating the instrumental profile. The light from the telescope is

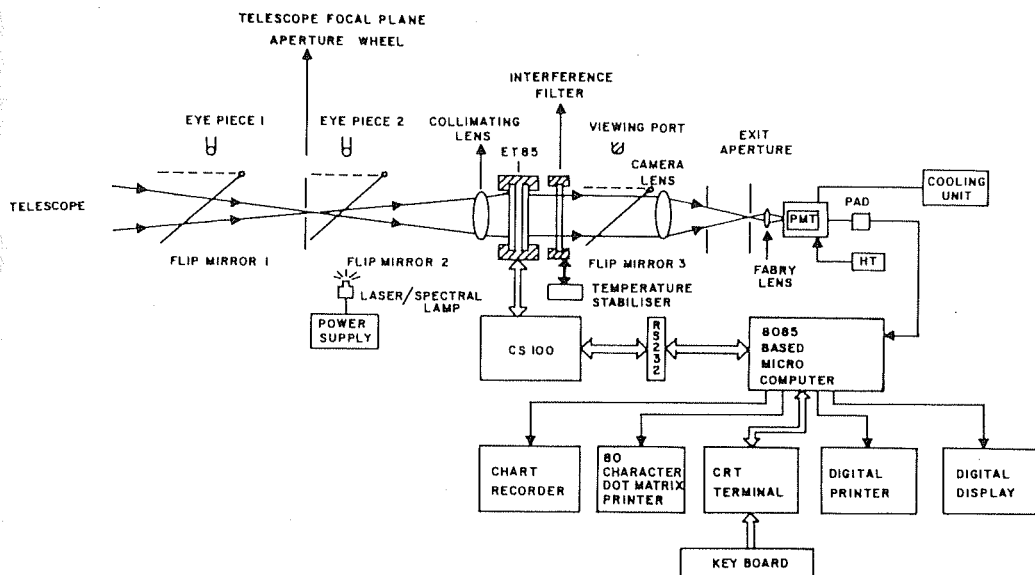


Figure 2.9. The optical layout and electronics of the piezo-electrically central aperture scanning Fabry-Perot spectrometer.

collimated, passed through the ET 85 etalon and focussed by the camera lens onto the exit aperture. A Fabry lens then images the telescope primary onto the photomultiplier cathode and prevents small seeing effects or photocathode sensitivity variations from effecting the line profile. Just in front of the camera lens another flip mirror is provided to view the fringe system from a calibration source like the laser. This visual check on the alignment of the etalon was found to be very useful in the initial adjustments when the exact setting of electronic control were not known. The optical parameters are summarized in table 2.5.

2.4.3 Mechanical system:

The mechanical system consists of several Aluminium tubes which are all threaded on the inside. The optical elements enclosed in Brass or Aluminium casings are mounted inside these tubes and can be moved along the threads for fine adjustment.

The etalon is housed in a thermocol padded enclosure so that it is not subject to rapid temperature variations. There is a provision for enclosing the interference filters in metallic rings and heating them by passing a current through a coil embedded in the rings. A well calibrated thermister serves as a temperature sensor which can be adjusted to a value to tune the filter for the peak of the spectral line under investigation. The temperature

TABLE 2.5

Optical parameters

Entrance apertures available : 8, 16 32, 48, 64, 80 and 160.
 arc. sec. in the sky with
 f/13 beam and 1 m telescope.

	<u>Focal length(mm)</u>	<u>Diameter (mm)</u>
Collimating lens	290	50
Camera lens	180	57.5
Fabry lens	10	10

Interference filter

Size	: 50 mm diameter
Peak wavelength	: 6563 Å at 20°C
Bandwidth (FWHM)	: 5 Å
Temperature coefficient	: 0.15 Å/o _C rise towards red.
Peak transmission	: 40%

coefficient of a multilayer dielectric filter is typically $\sim 0.15 \text{ \AA}^\circ$ shift towards red per degree centigrade rise of temperature. A typical 10°C range of the temperature control unit, employed in the present instrument, provides a wavelength tuning range of $\sim 1.5 \text{ \AA}^\circ$ which is generally adequate.

There is a special provision for permanently mounting and aligning a He-Ne laser through the first flip mirror for monitoring the performance of the piezo-electric system at any position of the telescope. In actual operation this arrangement was found to be very convenient in deriving the instrumental function.

The photomultiplier with its thermo-electric cooling unit and the preamplifier circuit is also attached to the main system. Four thick Aluminium rods (12 mm thick) run through the entire system providing the necessary structural strength at all orientations. The FP spectrometer system including the optics, coupling Cassegrain plate, PMT housing and connecting cables weighs 72 kg and is a little more than 1 metre in length. The laboratory assembly of the instrument along with the associated electronics is shown in Fig. 2.10. Fig. 2.11 show the instrument attached to 1 m telescope.

2.4.4 Electronics:

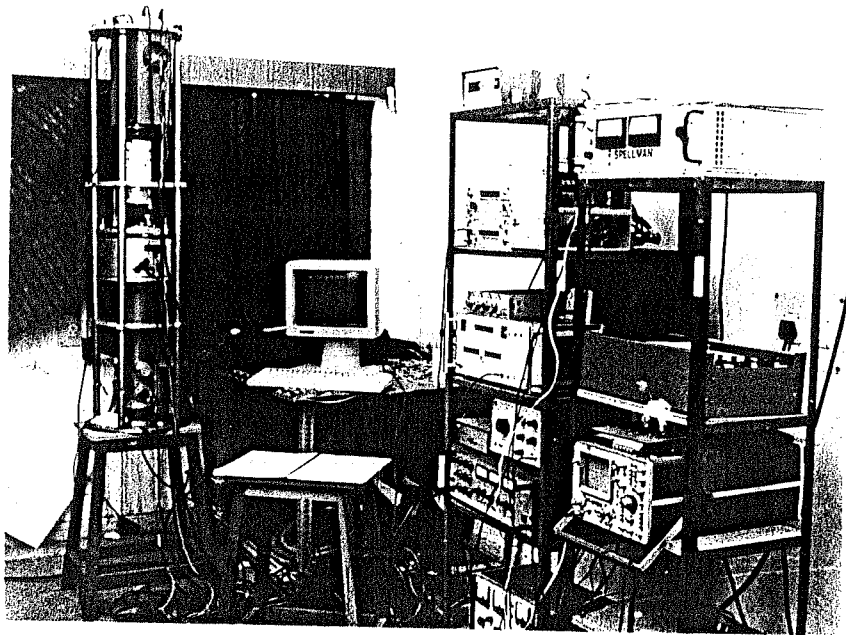


Figure 210. The Laboratory assembly of the scanning Fabry-Perot spectrometer alongwith the electronics.

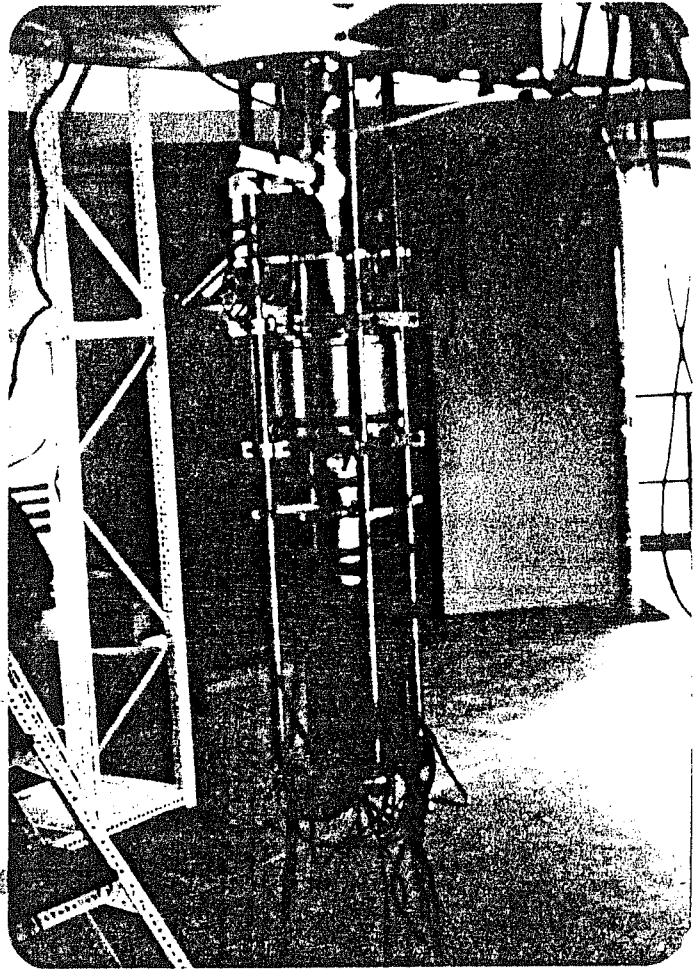


Figure 2.11. The piezo-electrically central aperture scanning Fabry-Perot spectrometer coupled to 1 meter $f/13$ telescope.

The electronics associated with the instrumentation consists of three parts, namely (1) Servo control of the etalon (2) wavelength scanning (3) control and the data acquisition system.

(1) Servo control of the etalon:

The servo system for maintaining the parallelism between the plates of the etalon consists of the sensors which are capacitance micrometers and piezo-electric transducers. The deviation from parallelism detected by micrometers are compensated by giving appropriate voltages to the piezo-transducers.

A. The Sensor:

In order to sense the deviation from the parallelism or the prescribed inter plate gap, very small displacements are to be detected. For example, in an FP system of finesse ~ 50 , a scan over one FWHM of instrumental profile would require a plate movement of,

$$t \sim \frac{\lambda}{100}$$

If the tolerance in this movement is taken at 1% level then sensor should be able to detect changes $\sim \lambda/10^4 \sim 0.5 \text{ \AA}$

(at 5000 Å⁰). The capacitance micrometers can detect length variations down to $\sim 10^{-12}$ m. Further in this method, no optical beam is needed and hence the problem of scattered light does not arise. (The rapid response of the sensor (~ 0.03 ms) and the fast loop response permits a fast servo-control of plate parallelism to be developed).

Although ET 85 system (which was used in the present device) is a commercial equipment supplied by Queensgate Inc. a brief description of the system here would not be out of place.

B. The piezo-electric etalon:

The characteristics of a piezo-electric etalon ET85 (Queensgate Instruments Inc) used by us is shown in table 2.6. The etalon has five capacitors CX_1, CX_2, CY_1, CY_2 and CZ formed by evaporating gold pads on to one of the interferometer plates and fused silica pillars optically contacted to the etalon base plate. Parallelism information along X axis is obtained by comparing CX_1 with CX_2 and similarity along Y axis by comparing CY_1 with CY_2 . CZ measures the actual spacing of the etalon in comparison with a fixed reference capacitor. The error signal derived from the capacitor is fed to three piezo-electric transducer elements (PZt-5 H vernitron) with a net coefficient of 2.6 m/750 V for maintaining parallelism. The details of etalon mounting, derivation of the error signal

TABLE 2.6

Piezo-electric etalon

Type	:	ET 85 (Queensgate Instruments Inc).
Spectral range	:	5500 - 6700 Å.
Usable Aperture	:	85 mm
Plate flatness	:	$\sim \lambda / 100$
Plate separation	:	$496 \pm 3 \mu\text{m}$
Peak Reflectivity	:	95% at 6000 Å
	:	93% at 6560 Å
Reflective finesse	:	43 at 6563 Å
Material	:	Spectrosil B
Free spectral range (F.S.R).	:	4.0 Å (6300 Å)

and the control system (i.e. CS100) electronics are discussed by Hicks et al (1984).

(2) Scanning

The scanning of the ET-85 piezo-electric etalon is also governed by CS100 system. Scanning is achieved by applying the same step voltages to all the piezo stacks through the Z offset input of the CS100 unit. Z offset is a 12 bit binary number giving a range -2048 to + 2047 units corresponding to the maximum separation of the etalon plates of $\pm 1 \mu\text{m}$. The smallest increment in the spacing is thus $\sim 5 \text{ \AA}$ which results in a wavelength sampling interval of $\delta\lambda = (\delta t/t)\lambda \sim \lambda/10^6$. An eight step increment would result in a sampling interval of $\sim 0.053 \text{ \AA}$ giving for one free spectral range at 6328 \AA 76.1 increments. The full range of $\pm 1 \mu\text{m}$ of the plate separation would result in a scan range spanning 6 orders at $H\alpha$. The Z input voltage and piezo expansion are not in general linearly related because of hysteresis and thermal drifts. The closed loop nature of the control system, however takes care of the above effects to give a scan wherein the CS100 step is linear to better than 0.1% with the scan wavelength.

(3) Control

A 8085 based microcomputer was employed for controlling the scan and recording the data. Through an RS-232 interface

it transmits the sequence of numbers to CS100 unit for varying the plate separation. For a scan (at laser wavelength of 6328 \AA) of one order, the etalon the plate gap should change by $\lambda/2 \sim 3164 \text{ \AA} \sim 76.1$ increments of 8 steps each - each wavelength increment corresponding to 0.053 \AA . In order to analyze a profile, a scan range of 2 FSR locating two adjacent order peaks distinctly in the scan is necessary. At each increment the data can be integrated over a time which can be varied from 1-99s. In normal operation the specifications were for a scan range of over 3 FSR, a step size of 8 and an integration time of 1 or 2 seconds for increment. The total time of a scan for 1 second integration time is ~ 4 minutes.

(4) Photon detector:

The detection system incorporates a photon counting photomultiplier tube (EMI 9863B/350 type) whose characteristics are given in table 2.7. The photomultiplier is housed in a thermoelectrically cooled enclosure (FACT-50 MK chamber) which can reach a temperature of -20°C .

The output photoelectron pulses from the photomultiplier tube are amplified and subsequently discriminated against the background noise by an integrated hybrid charge sensitive preamplifier, discriminator and pulse shaper (Model A-101 PAD, Amptek Inc). The TTL output of the PAD circuit is compatible with any photon counter input.

TABLE 2.7

Photomultiplier tube

Type	: EMI- 9863/350 photon counting type
Surface	: S-20, 14 stages
Quantum Efficiency	: (6300 Å) ~ 7%
Effective aperture	: 9 mm
Dark counts	: 450 count/s (25°C)
	: < 10 count/s (-15°C)
Photomultiplier gain	: 2.7×10^7

(5) Recording

The photon counts and the step numbers which are proportional to the optical gap and hence the scan wavelength are continuously displayed on a computer terminal and also recorded through an interface on a dot matrix printer for hard copy. An X-Y plotter provides, a useful analog version for visual check of the data being recorded.

2.4.5 Performance

The instrument has been fully assembled in the laboratory and tested. Fig. 2.10 shows the Laboratory assembly of the instruments for testing. The instrument was used with 1 m telescope at Vainu Bappu Observatory, Kavalur for observing Comet Halley for 5 nights in April 1986.

Finesse: Figure 2.12 shows the profile of 5 basic functions described in 2.2 and their convolved resultant synthetic profile, superimposed with He-Ne laser profile at 6328 \AA . The free spectral range of 4.04 \AA is scanned in 76.1 steps. One resolution element (1 FWHM) is therefore 0.144 \AA giving an effective finesse of 28. The effective finesse deduced theoretically is ~ 30 which shows that the system performance is optimum.

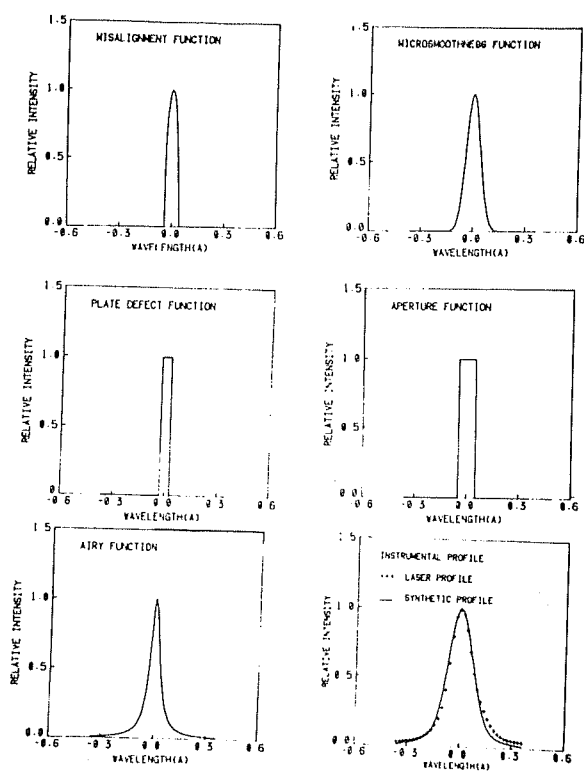


Figure 2.19. Instrumental profile of scanning Fabry-Perot spectrometer. Five basic functions contributing to the instrumental profile and the convoluted resultant function along with the laser profile.

Stability: The stability of the etalon and associated electronics was determined by taking laser calibration scans of the system several times during a night of observation. The departure of the laser peak from its original value is a measure of the stability. It was found that in a typical 6 hour period the maximum departure corresponds to ~ 2.5 elementary steps or 0.016 \AA° in wavelength at 6328 \AA° or a relative velocity resolution of 0.76 km/s . The line profiles of several standard astronomical objects such as Orion nebula, M8 and NGC 2440 were taken in order to check the instrumental performance. Fig. 2.13 gives the line profiles of Orion nebula and M8. The line widths are consistent with the published results.

Owing to the limited time, (5 nights allotted) on the 1 meter telescope for observations and tests observations on Halley with the above spectrometer were somewhat limited. The $[\text{OI}]$ and NH_2 profiles derived from these observations are discussed in detail in Chapter 4.

2.5. The Telescope at Gurushikhar

For most of the period, Halley observations were carried out with a 35 cm telescope from Gurushikhar Mt. Abu. Main features of the telescope and site are described below.

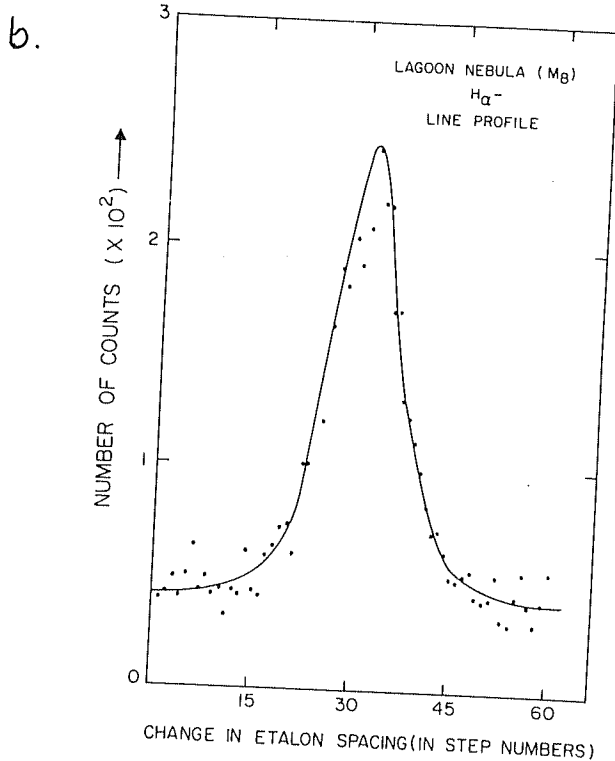
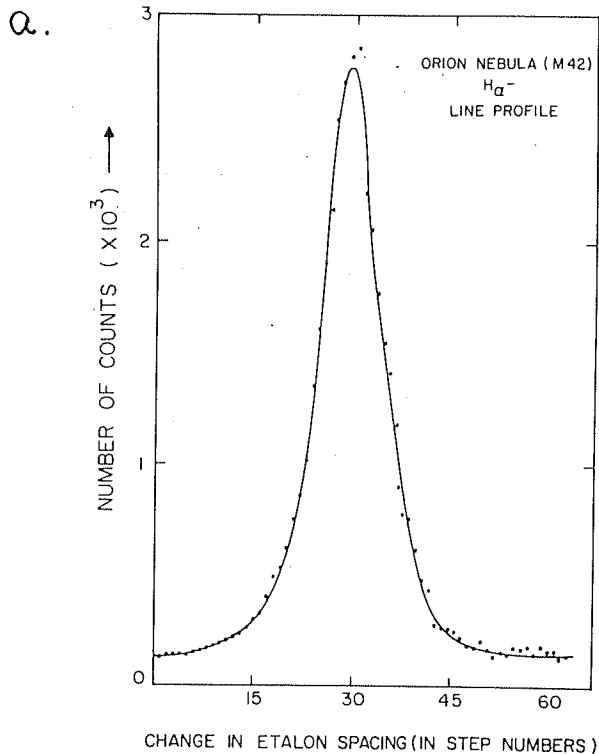


Figure 2.13. Line profile of the standard astronomical objects obtained with the piezo-electrically scanning Fabry-Perot spectrometer.

a. Orion Nebula

b. M8.

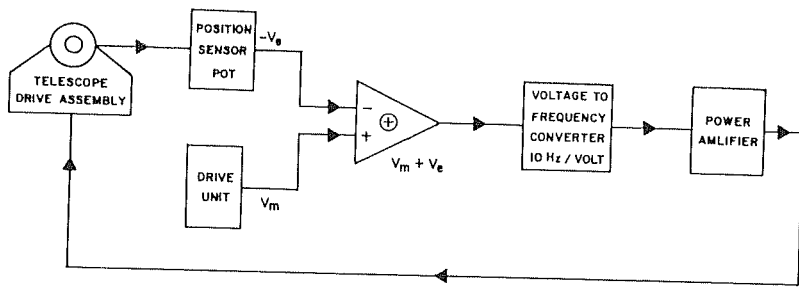
2.5.1 The Drive Corrector

The 35 mm aperture telescope was mounted on a special Gaussian equatorial mount (Byers Co Ltd) and housed in a makeshift enclosure during the 8 month period of Halley observations. Special care was taken to achieve the polar alignment precisely and balance the telescope with counter weights against the instrument. However the most serious problem with the commercial drive used on C-14 was gear periodic error which amounted to several tens of arcseconds in peak to peak amplitude.

We devised a special corrector mechanism to overcome these errors. Employing a specially developed drive corrector (Ashok et al., 1987) the drive stability of the telescope was achieved to a level ~ 5" or better.

In principle the drive corrector senses the periodic error in phase by a suitably coupled four-quadrant potentiometer to the shaft of the erroring gear. The error voltage, so obtained is frequency converted and fed in antiphase to the drive motor. Fig. 2.14 schematically shows this method of error correction.

In practice a four-quadrant potentiometer has a continuous value of resistance from 0- to 5 K and back to 0- varying linearly with the rotation of 360° . By suitably biasing the potentiometer a triangular shaped error voltage V_e was generated, the amplitude of which was



SCHEMATIC LAYOUT OF THE DRIVE CORRECTOR

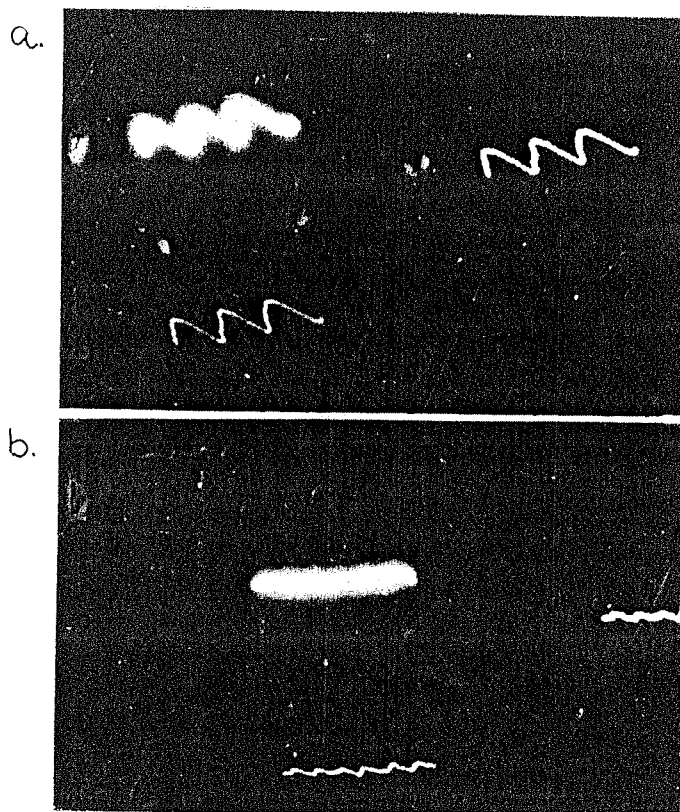
Figure 2.14. Schematic diagram of the drive corrector.

determined by the magnitude of the error. The amplitude V_e formed one input to the summing amplifier while the mean tracking voltage V_m derived from a potential divider network formed the other. The summing voltage was frequency converted at a rate of 10 KHZ/v. The varying output of V/F converter was suitably amplified to give 30 W power for the telescope's drive motor.

The observed peak-to-peak deviation from mean tracking rate was around 50" which was successfully brought down to about 5" (Fig. 2.15 a,b). However for comet observations, the error was slightly more, as long integration times were used. The average error, however, does not exceed $\sim 20''$. Nevertheless, for analysis only those images were chosen, which had minimum tracking error (Judged from the star trails). Since for interferograms no spatial information can be obtained in the inter fringe gap, the spatial resolution is not stringent. Error due to these sources will be discussed in detail in the following chapters.

2.6. The Observing Sites

The observations were made mainly from Gurushikhar, Mt. Abu, India and for five nights at Vainu Bappu Observatory, Kavalur. Table 2.8 gives the geographical co-ordinates of these sites. In general the sky conditions were excellent at both places during the observations. On several occasions at Mt. Abu the Fabry-Perot interferograms were recorded in



Star trails with (bottom) and without (top) the drive corrector.

Figure 2.15 Star trailing before (a) and after (b) the use of drive corrector.

TABLE 2.8

Observing site details

	Kavalur	Gurushikhar (Mt.Abu)
Latitude	+12° 34' 35"	+24° 39'
Longitude	78° 49' 45"E	72° 43' E
Altitude	725 m	1700 m

Na D_1 D_2 (5890,5896) lines with varied intensity as shown in Fig. 2.16. These fringes are associated with night airglow due to their extent and not with the comet.

2.7. The Observations and Data

The Comet P/Halley 1982i was first recorded by us on 16 Oct. 1985, when the comet was at 2.14 AU, with an estimated magnitude of ~ 11 . Comparing the star field of Oct 15 and 16 the comet was unambiguously identified. Figure 2.17 a,b show the comet field on three successive days. Soon after recovering the comet the IHW filter photograph in C_2 (5140/90 \AA^0) and blue continuum (4845/65 \AA^0) were successively taken on Oct. 20, 1985 (Fig. 2.18 a,b). A complete set of photographs of Comet Halley in all the IHW filters on a single day is given in Fig. 2.19. The observations were continued upto 15 Jan. 1986 ($r = 0.8$ AU) in the pre-perihelion period. In the post perihelion the observations were taken from 8 March 1986 ($r = 0.82$ AU) till 7 May 1986 ($r = 1.72$ AU).

Around 200 frames of good quality including 100 frames of white light images of the inner coma have been obtained. Six interferograms have been recorded. The statistics of the data is given in table 2.9.

Appendix 2.1

Construction of Instrumental Profile

The instrumental profile of a Fabry-Perot spectrometer is the convolution of five basic functions given in table 2.2. In order to construct the instrumental profile for the instruments used in the present work the individual functions were generated by a FORTRAN programme through the computer with the manufacturer's specified data on the etalon. Since the parallelism between the two plates was achieved by adjusting the voltages in piezo-electric transducers and minimizing the "breathing effect" of the laser fringes, the half width of the profile due to misalignment was kept variable. Varying misalignment was function several convoluted instrumental functions were generated and the best fit with the observed laser profile was chosen. The resultant instrumental width was found to be $\approx 0.14 \text{ A}^\circ$ and the finesse 20. The effective finesse deduced theoretically for the scanning Fabry-Perot spectrometers is ~ 30 which shows that the system performance is optimum. Similar exercise was carried out for the imaging Fabry-Perot spectrometer.

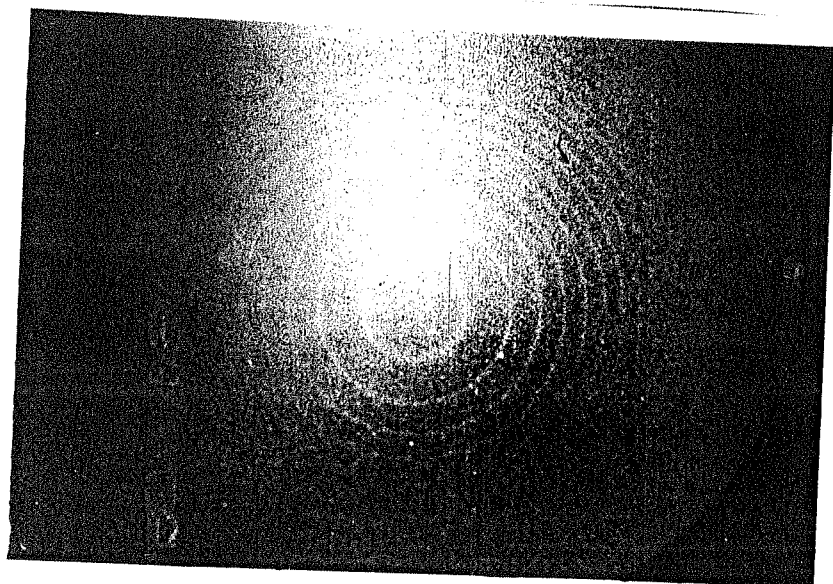
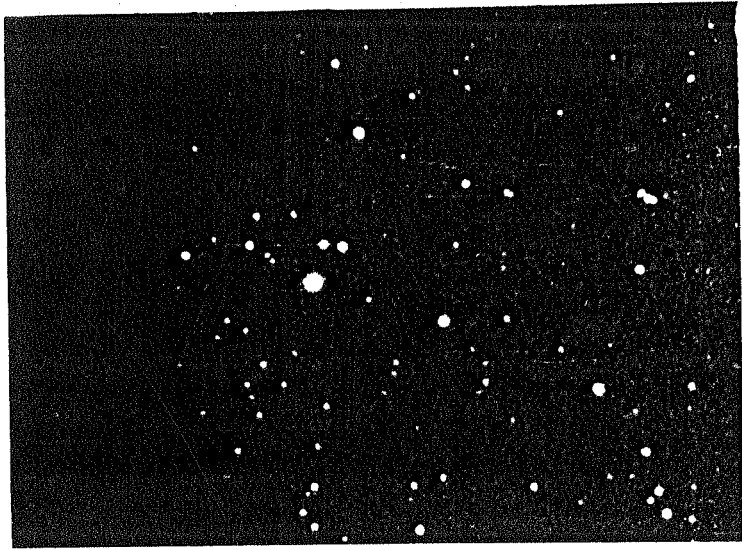


Figure 2.16. Atmospheric Na line fringes.

a.



b.

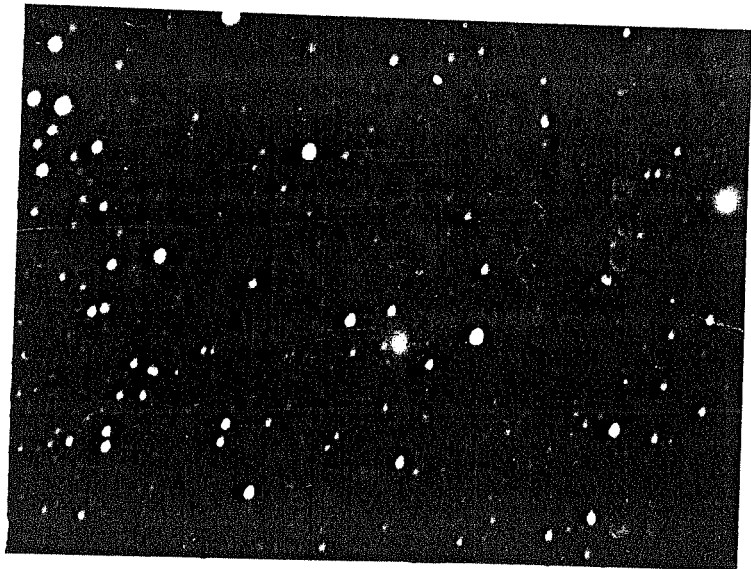
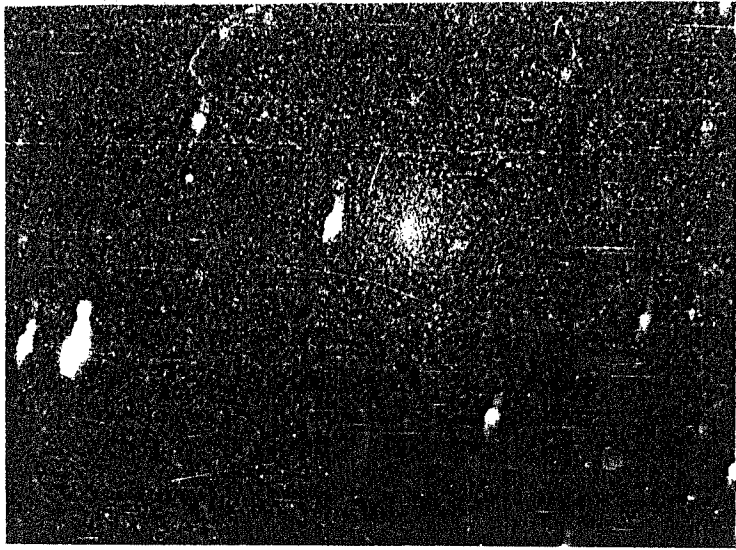


Figure 2.17. Comet field in successive days i.e. (a) 16 Oct. 1986, (b) 18 Oct. 1986. Note the changing position of the comet with respect to the star field.

a.

C₂



b.

Cont.

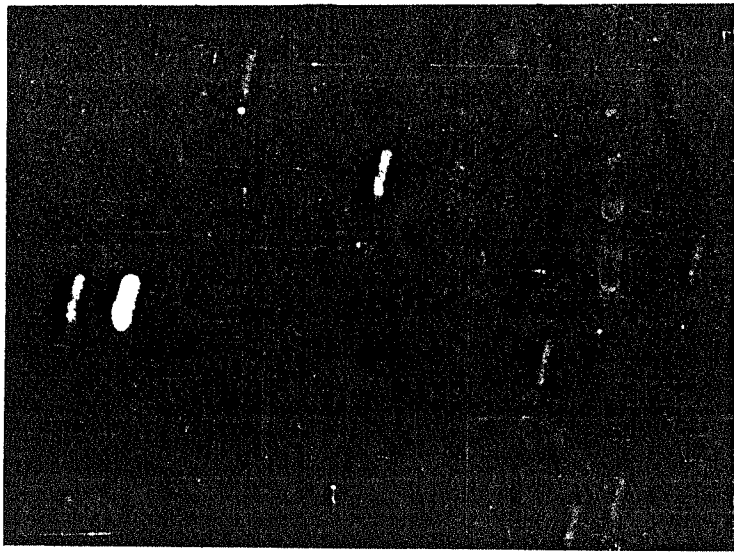
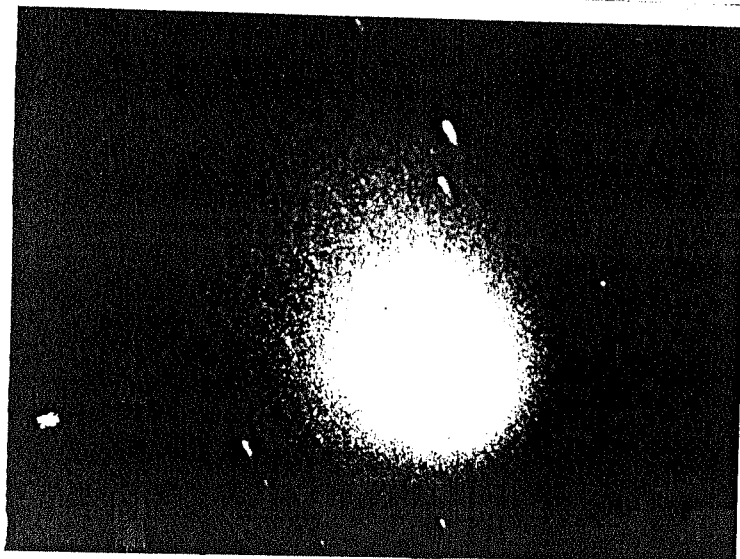
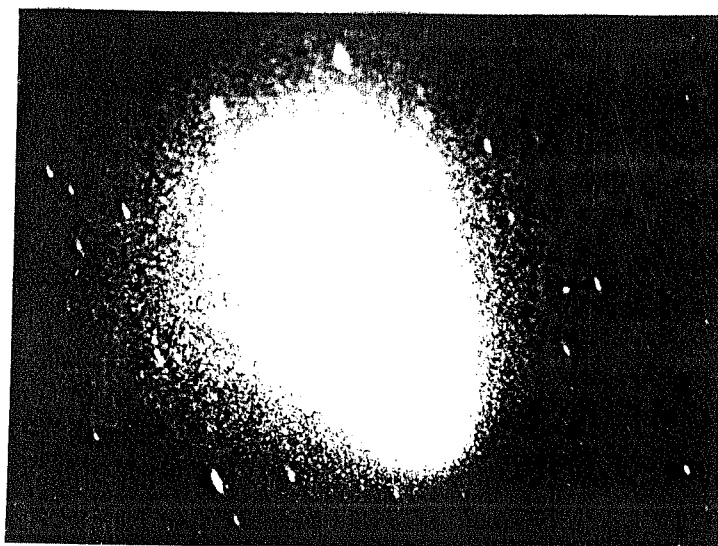


Figure 2.18. Image of comet Halley in C₂ and continuum emission bands taken on Oct 10, 1985.

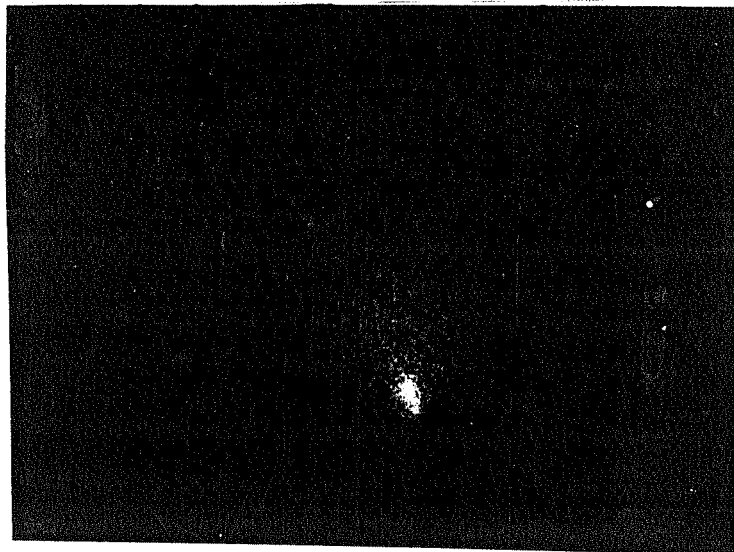


14W C_2 filter, 30^s exposure.

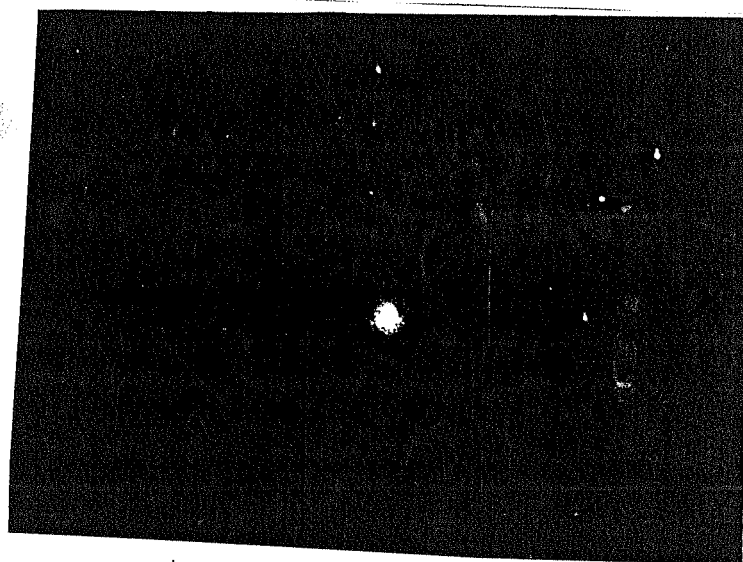


4845/65 \AA , 30^s exposure.

Figure 2.19. IHW filter photographs taken on 23 March 1986.



IHW CN 240^s exposure.



Co⁺ 4260 1165⁻ 60^s exposure.

Figure 2.19. IHW filter photographs taken on 23 March 1986.

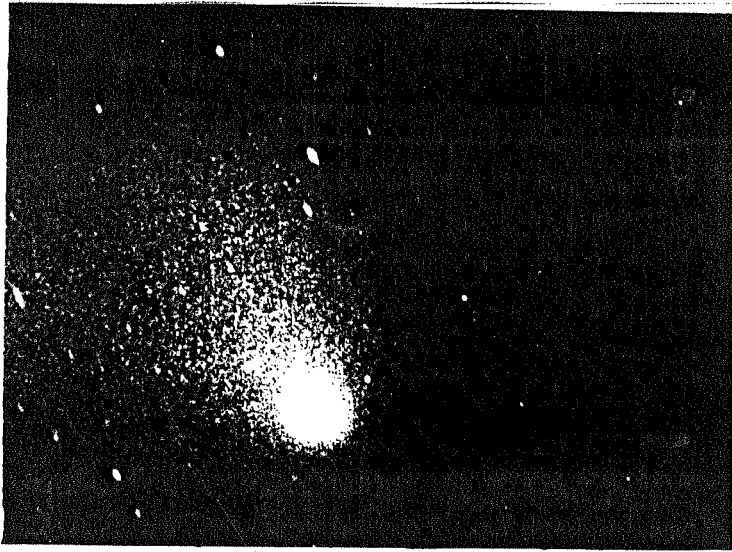


E3 4060/70 240^s exposure.



NO filter, < 1^s exposure.

Figure 2.19. IHW filter photographs taken on 23 March 1986.



H_2O^+ 7000/175 Å 30^s exposure.



6840/90 Å 30^s exposure.

Figure 2.19. IHW filter photographs taken on 23 March 1986.

Table 2.9

Gurushikhar Observations Statistics of Data

Mode 1 (Filter Imagery)

<u>Emission</u>	<u>No. of frames</u>
C ₂	46
CO ⁺	30
H ₂ O ⁺	25
CN	2
White light	111
Comet + laser	27

Mode 2 (Interferograms)

<u>Emission</u>	<u>Date</u> <u>U.T</u>	<u>Heliocentric</u> <u>Distance</u> <u>in AU</u>	<u>Exposure</u> <u>time</u> <u>(minutes)</u>
C ₂	1986 Jan 12.604	0.84	10
	1986 Mar 22.985	1.04	10
	1986 May 1.965	1.63	30
H _α (6563 Å)	1986 Mar 13.0	0.89	11
Na(5890/5896 Å)	1986 Mar 22.999	1.04	10
[OI] (6300 Å)	1986 Mar 15.994	0.92	15

Note : Comet + laser frames were taken to determine the position of the centre of the fringe pattern in the interferograms.

CHAPTER 3

THE TIME VARYING PLASMA PROCESSES IN THE COMA

During the perihelion passage of a comet strong interaction between the cometary plasma and solar wind occur within 2 AU from Sun. Apart from producing large ionic tails, these interactions give rise to a number of time varying plasma features such as Disconnection Events (DE), helical waves, kinks and condensations. The life time of these features vary from less than an hour to few days. In 1985-86 apparition of Comet Halley a number of such events were observed. On 13th March 1986, one such feature was observed by us. The event featured as an enhanced intensity region in the southern part of the coma in the images taken with λ 7000/175 \AA° filter (H_2O^+ emission). A $\text{H}\alpha$ interferogram was obtained following these imagery observations. Using the interferogram a velocity map was constructed, which indicated a rapid dispersal of the feature.

Near Nucleus image of Jan 8, 1986 obtained by us and from the Nainital Observatory show the evolution of a condensation region within the coma. The condensation is distinctly observed in the blue enhanced images. From two images taken 1 hour apart, the velocity of the condensation

was found to be ~ 37 km/s in the anti-solar direction. Such features are conjectured to be the precursors of the ionic structures in the tail. Wide field photographs of 9th Jan 1986 show the tail rays evolving from a condensation region in the ionic tail. Such features called the "tail rays" can lead to DEs. The photographs of Jan 10th, 1986 show a major DE. Hence the condensation observed by us can be regarded as a potential precursor of the 10th Jan DE.

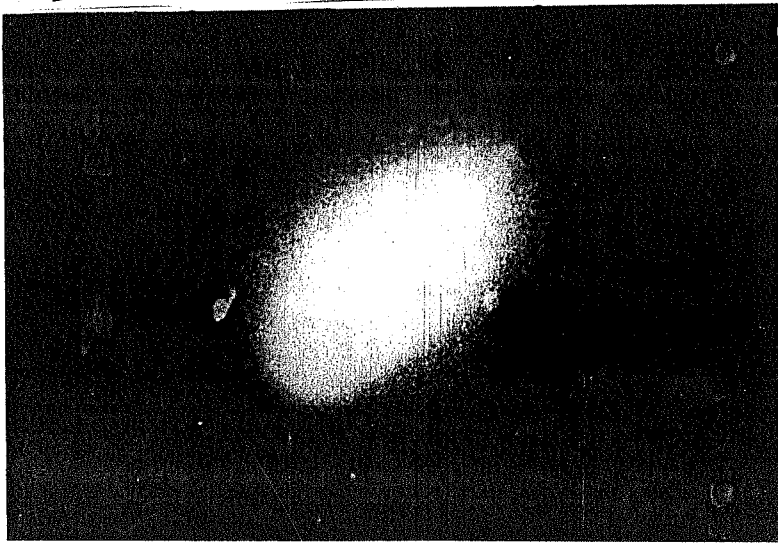
In this chapter a brief account of our observations related to the Near Nucleus plasma activity of Comet Halley is followed by a detailed discussion of the two events discussed above.

3.1 An Overview of the Near Nucleus Plasma Activity of Comet P/Halley in 1985-86

On several occasions, during Oct. 1985 to May 1986, A number of Comet Halley images were obtained in the emissions of H_2O^+ , CO^+ and their nearby continuum. Figure 3.1 shows the selected images. Table 3.1 summarizes the observations.

On 9th and 10th Nov 1985, we had the first exposure in ionic emission lines. The emissions were found too weak to be properly recorded. However, the 9th Nov white light image shows a faint straight jet like structure extending to $\sim 10^5$ km from the nucleus, which is not seen in 10th

H_2O^+



CO^+

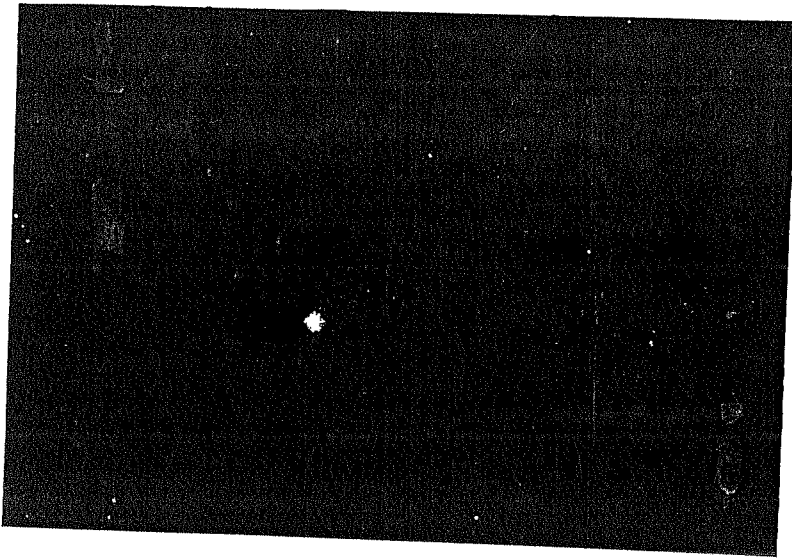


Fig 3.1 Comet images in H_2O^+ & CO^+ emission taken on 9 March 1986.

TABLE 3.1

Selected images for an overview study of the near nucleus
plasma activity of Comet P/Halley in 1985-86

<u>Date</u>	<u>Filter</u>	<u>Remark</u>
1985 Nov 9	Nil	10^5 km long jet like structure
1985 Nov 10	Nil	No jet
1985 Dec 4	CO^+ , H_2O^+ , Blue Cont, red cont	No structure
1985 Dec 5	"	No structure
1985 Dec 27	"	Tail visible in ionic emission
1986 Jan 13	"	Tail length is more in ionic emission
1986 Mar 8	"	HO^+ emission is stronger than CO^+ , signature of DE is discernible
1986 Mar 23	"	Fan like tail is seen
1986 April 28	"	Tail not clearly seen
1986 May 8	"	A kink is observable in the ionic tail at a distance of $\sim 10^5$ km from the nucleus.

photograph. On 12th and 15 Nov 1985, clear strong jet activities were observed. Signature of these jets are also seen on 17th Nov and the coma asymmetries on 20th Nov. The photographs earlier than 9th Nov do not show appreciably the signature of the jet. From the sequence of photographs during this time, it can be concluded that the activity started around 9th Nov 1985 and repeated at an interval of ~ 2 days. The photographs taken in CO^+ emission (Jockers, 1985) and UBR bands (Liu, 1987) show the abundance of CO^+ ion in the jets. The cause of this event is not yet well established. As the solar activity was quite low during Nov 1985 (solar Geophysical data prompt report, 1985), the solar related cause is probably ruled out.

The photographs taken during Dec 1985 do not show any unusual feature. In early Dec (4/5) photographs the tailward elongation is discernible, whereas in late Dec (27th) photographs such elongation is not seen, even though the coma appeared to be brighter in later photographs. In the sequence of photographs, the neutral C_2 emission was brighter than the corresponding blue continuum whereas the ionic emission was found to be comparatively weaker.

Following a number of outbursts during the first week of Jan 1986 the cometary activity was enhanced. The white light photographs of 13th Jan 1986 show a clear tail feature. H_2O^+ and CO^+ images show long tails compared to their corresponding continuum images.

In the post perihelion period, we have obtained good quality photographs during the first fortnight of March, when a number of space craft encounters with the comet were taking place. In H_2O^+ and CO^+ images taken on 1986 March 8th, the tail could be seen upto 5×10^5 km from the nucleus. H_2O^+ emission was seen to be stronger than CO^+ emission. A dramatic DE has been observed during this time, originating at 8.8 UT at a distance of 1.3×10^6 km from the nucleus (Wu et al 1987). From a series of photographs (from various sources) it can be estimated that the DE front was moving in the plane of sky at a velocity of ~ 35 km/s, which increased to 60-130 km/s during the following days. In the 8.8 UT the feature is expected to be seen in our photographs. Also if the sector boundary crossing at 7.64 UT is responsible for this DE (Niedner et al 1986) and it moved at a typical velocity of ~ 20 km/s, then its signature might be present in our photographs. Our photographs clearly show the branching of the tail. The DE front is not readily seen, which might have been buried in the coma brightness.

Our 23/24 March 1986 data show a fan shaped tail feature with H_2O^+ brighter than CO^+ . At this time the Comet was showing strong outburst and jet activity. The photometric observations by Gong et al (1987) at 22.9 UT show a clear enhancement of ~ 4 magnitudes in several emission bands. A detailed study of the image obtained by us

would provide useful information for understanding the influence of outburst on the structures of the tail.

In April 28/29 images, the tail features were not clearly seen, whereas the coma was brighter. The 8/9 May 1986 images of coma show a narrow straight and long tail with a number of short scale structures. A helical structure within $\sim 10^5$ km is clearly seen.

The H_2O^+ images were taken with IHW filter at λ 7000/175. Hence the contribution due to the continuum is significant. However, the inferences drawn above are in comparison with the continuum images taken at λ 6840/60. Therefore the conclusions are not expected to change drastically.

3.2 The Optical Interferometric Observations of a Transient Plasma Structure in the Coma of Comet Halley - The 1986 March 13 event.

In this section the detailed account of the observations and data analysis of the imagery and the $\text{H } \alpha$ interferogram obtained on 13th March 1986 event is presented following a brief review of such event on other comets. At the end, a detail discussion of the event is followed by outlining a possible theoretical model.

3.2.1 Introduction

During the perihelion passage of a comet, apart from the normal development of an extended coma, dust and ion tails, a number of less predictable events occur which provide clues about its composition and about the interaction of the cometary plasma with the solar wind. Dust jets occurring from the localized regions in the 'afternoon side' of the rotating nucleus produce non-gravitational accelerations or decelerations depending on the sense of rotation (Whipple 1950, 1951). Brightness flares of 1 to 2 magnitudes or more have been frequently reported in many comets like P/Schwassman-Wachmann 1, Morehouse 1908 III, Humason 1962 VIII (Wyckoff 1982), P/Tuttle - Giacobini - Kresak (Kresak 1974) and West 1975 n (Cosmovici 1978). Suggestions have been made that outbursts in the cometary nuclei may be caused by chemical heating, by the presence of ices more volatile than H_2O^+ or by the exothermic crystallization of amorphous ice (Donn and Urey 1957, Whipple 1980). Comets during outbursts have shown enhanced CO^+ emission (Greenstein 1962, Festou 1986) and it has been suggested that if a sudden phase change in H_2O^+ ice is the outburst source then strong H_2O^+ emission might be observed (Wyckoff 1982).

The cometary ion tail exhibits a variety of dynamically active structures like streamers, kinks, helices and condensations resulting from the complex interaction of the

cometary plasma with the fast moving solar wind (Brandt 1982). At times dense clouds of plasma emanate from the coma, propagate down the tail and the sequence of events can be followed for several hours (Wolf 1909). The correlations of the ionization rate with solar wind behaviour (Jockers 1985) establishes the importance of ion exchange reactions between cometary neutrals and solar wind plasma. The dramatic tail disruptions or disconnection events (DE) have been extensively observed (Bobrovnikoff 1937, Jockers and Lust 1973, Jockers 1985, Burlaga 1973, Niedner et al. 1978a, 1980, Ip 1980 and Niedner IHW Newsletter No.9 p.2). The occurrence of DEs have been correlated with sector boundary of the interplanetary magnetic field crossing the comet tails and a mechanism for DEs has been suggested (Brandt 1968).

3.2.2 Transient events

Apart from disconnection events which can be followed for several days, there have been reports of events even more transient. Bernard (1893) in his visual observations of the great comet of 1882 had noted transient features. Photographs of Comet Kohoutek taken on 19 January 1974 showed transient plasma features 10° away from the nucleus (Roosen 1976). Transient features lasting ~ 1 hour have been reported at ~ 50 arc sec from the nucleus along the sun-comet line of Giacobini-Zinner on several occasions (Telesco et al. 1986). The spectrophotometric observations of

Comet IRAS-ARAKI-ALCOCK 1983d between 4000 \AA and 4900 \AA obtained on the night of 1983 May 9/10 revealed an abrupt and dramatic brightening of the inner coma during a 20 minutes interval, preceded and followed by periods of normal stability (Lutz et al 1986). Figure 3.2 show the temporal variability of continuum, C_2 emission and CN brightness of the comet during this time. Several possible mechanisms such as the outburst of ices from the nucleus and a compression wave in the solar wind enhancing the gas and dust density of the coma were invoked to explain these observations. Russell et al., (1987) have pointed out that due to the alignment of the interplanetary magnetic field with the solar wind flow, the coma could not have been shielded from the solar wind as a result of weak mass loading. This could have given rise to a Venus like interaction (Alexander et al., 1986) producing a large ionization deep inside the coma.

In its recent apparition, Comet Halley has also exhibited some transient features. Elongated jet like structures moving rapidly have been seen on blue and red images during November 1985 (Grun 1986, Jockers 1985). These observations show a large, curved, jet like structure extending 21 arc min to the south of the cometary nucleus nearly perpendicular to the projected antisolar direction. An image taken ~ 3.5 hours later shows that the direction of strongest emission had shifted by 10° . Study of the Giotto observations and the corresponding ground based

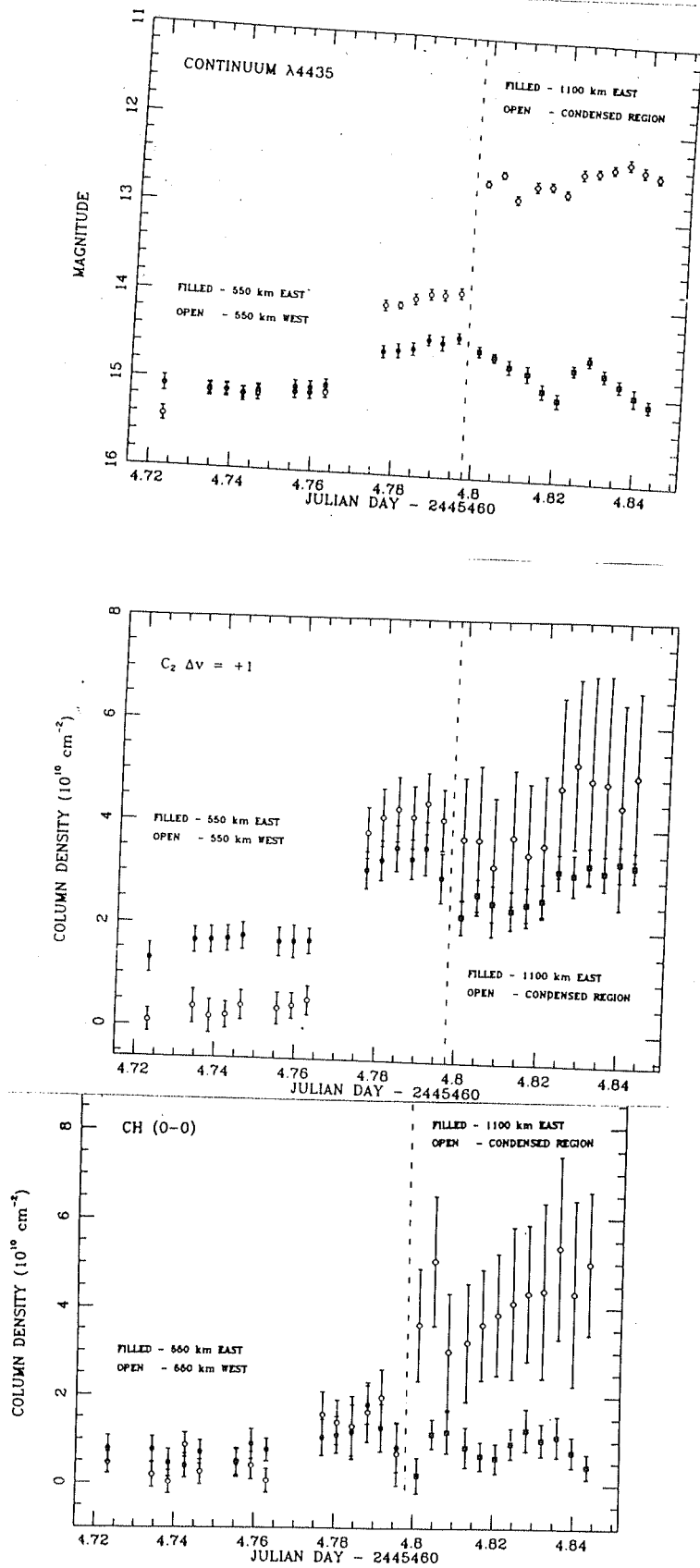


Figure 3.2. Temporal variability of comet IRAS-Araki-Alcock 1983d. It shows enhancement of continuum, C_2 and for only 30 minutes (Lutz et al 1986).

observations have also yielded short lived plasma phenomena lasting less than an hour (Ip et al 1986). Vega I and Vega II observations of Comet Halley also show several such transient processes of short time scale. The Comet Halley observations will be discussed in detail in section: 3.2.5 (A).

The digital spectra and images of Comet Halley obtained from Naismith focus of the 2.3 meter telescope at Siding Spring Observatory, Australia with a fast CCD and custom built video data acquisition system reveals a number of very rapidly time varying phenomena in terms of rapid variation ($< 1^s$) molecular emission bands. These variations belong to the inner coma region, from the core out to several minutes of arc (Ritting et al., 1986). However, these data await final analysis and interpretation.

3.2.3 Methods of observation and analysis

The observations were taken from Gurushikhar, Mt. Abu, using the imaging Fabry-Perot Spectrometer in spectrometric mode described in the section 2 of chapter II. Table 3.2 gives the comet parameters during the observations.

(A) Observations

Table 3.3 gives the journal of the observations on 13 March 1986. It was only while selecting the frames for the

TABLE 3.2

Comet parameters during observations
13.3.1986.

Date UT	AU	Km/s	AU	Km/s	V orbi- tal Km/s	Parker's spiral Angle
	Δ	$\dot{\Delta}$	γ	$\dot{\gamma}$		
13 March 0 ^h UT	0.98	-43.18	.89	25.47	45	42°

TABLE 3.3

Journal of Observations

S.No.	UT of exposure	Exposure	Filter
1.	March 12 23:26:55	1 ^s	White light
2.	March 12 23:29:30	5 ^s +Laser (flash)	White light + Laser
3.	March 13 00:06:34 00:09:34	3m	7000Å ^o /175Å ^o H ₂ O ⁺ filter
4.	March 13 00:10:17 00:15:17	5m	"
5.	March 13 00:18:54 00:30:00	11 ^m 06 ^s	6563/5Å ^o H _α interferogram

digitization was it noticed that the frames of March 13 1986 show additional features and that the $H\alpha$ interferogram had been recorded on the same day Figure 3.3 is the white light frame wherein a projection in one direction is readily seen. Figure 3.4 and Figure 3.5 are H_2O^+ ($7000 \text{ \AA} / 175 \text{ \AA}$) imageries of the coma taken ~ 40 minutes after the white light frame and distinctly feature the blob. The blob is at a projected distance of $2 \times 10^5 \text{ km}$ from the nucleus and occupies an extent $30,000 \text{ km} \times 20,000 \text{ km}$ in the plane of the sky. The blob is seen at a position angle 160° measured North through East relative to the nucleus. In the interferogram frame at least three fringes are clearly seen. In the microdensitometric tracing fainter fringes and structures in the fringe profile can be recognised. The blob feature was shown to be definitely associated with the comet after a careful considerations of various possibilities which are detailed in Section A.1.

The details of digitisation of the $H\alpha$ interferogram, H_2O^+ and white light pictures and processing of the digitized images are given in section A.2. Figure 3.6 shows the interferogram in $H\alpha$ taken with a 5 \AA bandwidth filter with an exposure of 11 minutes.

Section A.1

Association of the blob with the comet: \rightarrow

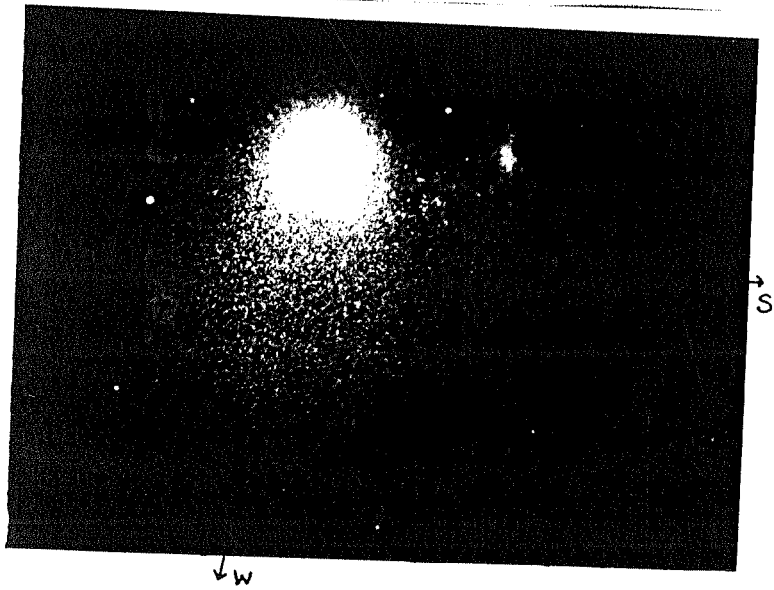


Figure 3.4. H_2O^+ (7000/175 Å) frame taken at 1986 March 13.006 UT (180^s exposure). 1 mm = 8000 km.

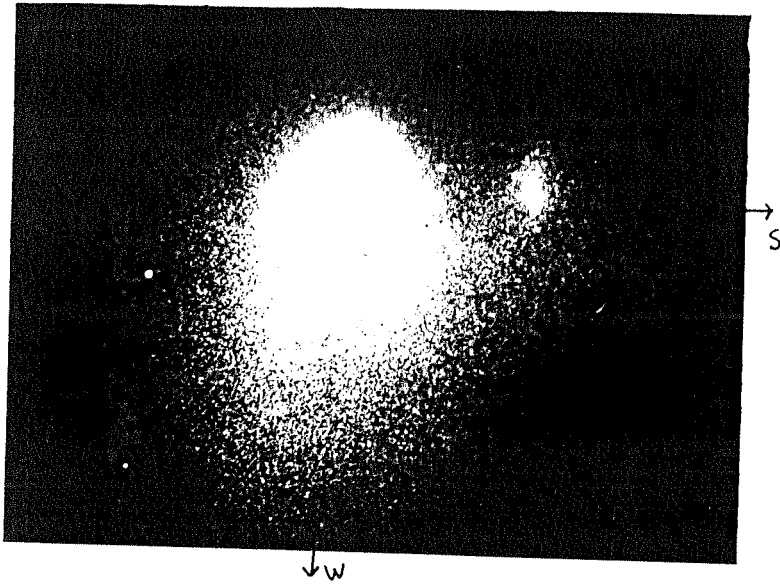


Figure 3.5. H_2O^+ (7000/175 Å) frame taken at 1986 March 13.0089 UT (300^S exposure). 1 mm = 8000 km.

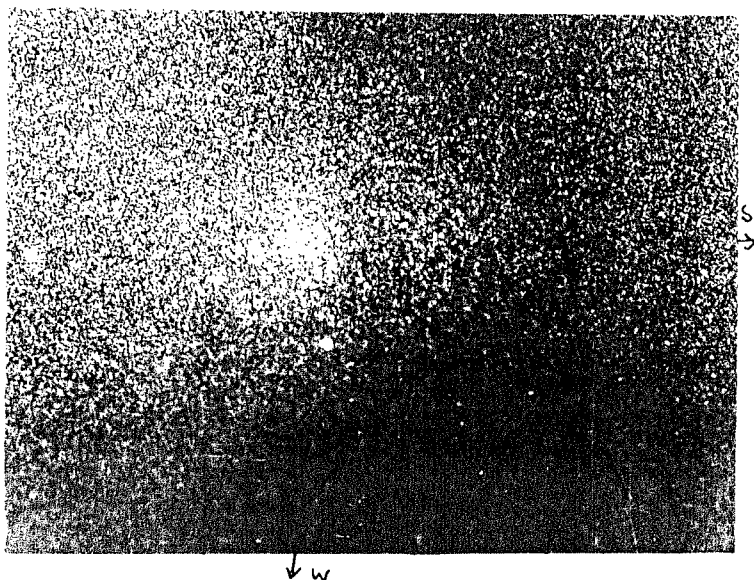


Figure 3.6. H-alpha (6563/5 A) frame taken at 1986 March 13.02 UT (660^S exposure).

A detailed careful study has been made to establish the reality of the blob and to associate it with the comet.

1) An extensive search of star catalogues by us and by Dr. David Rees of University College, London (Private communication, 1987) was carried out. The star map in the path of Comet Halley, during the period March - 12 March 15, 1986 is given in fig.3.7. Fig 3.8 show the identification of several stars in the comet frames taken on 13th March 1986. It can be readily noted that no stellar object brighter than 11th magnitude corresponds to the blob position seen in H_2O^+ images. It is concluded that the feature is definitely brighter than this limit and is not a compact object. Hence no stellar association with the blob is possible.

2) Search for a nebular object in the vicinity of the blob in the NGC catalogue of nonstellar objects (Sulentic and Tifft, 1973) also led to a negative result, thereby ruling out nonstellar astronomical objects down to the magnitude 16.

That the feature is not an instrumental artefact due to a possible reflection in the filters is confirmed by repeated checks of the instrument. Further

1) Out of about 200 photographs taken with similar filters, only on this occasion is such a blob feature

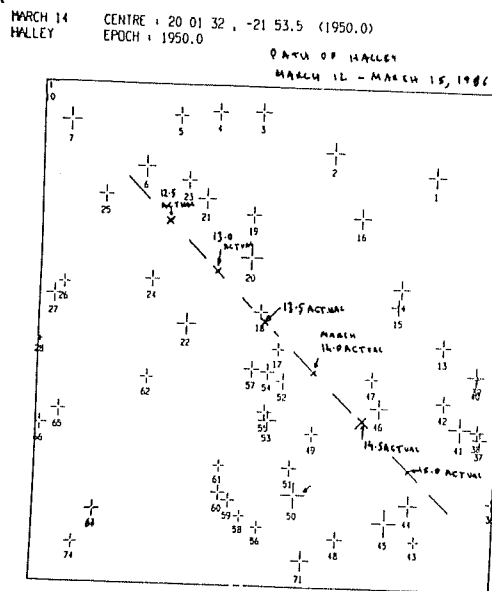


Figure 3.7. The star field in the path of comet Halley, during March 12-15, 1986. (Courtesy: Dr. David Rees, University College, London).

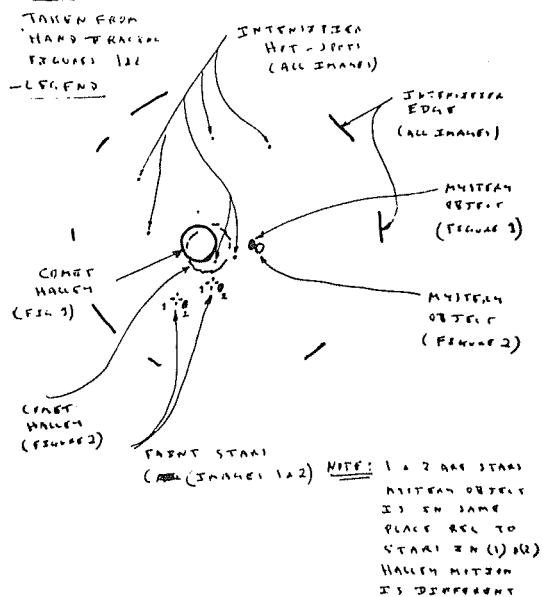
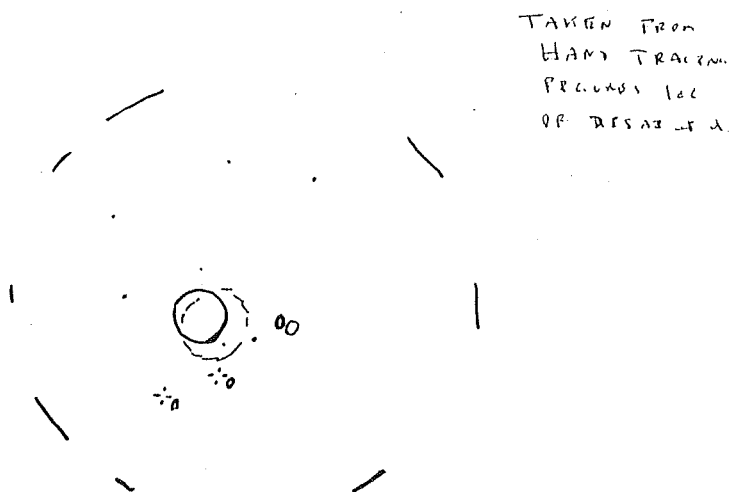


Figure 3.8. Identification of the field stars in the H_2O^+ frame of comet image. (Courtesy: Dr. David Rees, University College, London).

noticed.

2) The region of enhanced brightness in H_2O^+ correlates with a feature in the white light frame where no filter was used.

3) During Dec 1985 to March 1986, at least 11 exposures were taken to obtain the $H \alpha$ interferogram of the comet. The exposure durations vary from 5 m to 60 m. No occasion except on 13th March 1986, was a $H \alpha$ interferogram obtained.

In order to identify the region of the comet to which the interferogram belongs, frame matching was carried out, using the image intensifier hot spots as the control points. After applying appropriate correction for the cometary motion, it was established that the interferogram is centred on the blob region of H_2O^+ image and is hence clearly associated physically with the blob emission.

As our instrument cannot record airglow [OI] 6300 emission which is ~ 100 R during our observations, the threshold can be set to > 100 R. Since the instrumental sensitivity remains same between 6300 \AA to 6563 \AA the similar threshold can be used to estimate the $H \alpha$ flux. This consideration implies that the strength of $H \alpha$ emission record as interferogram is > 100 R. The $H \alpha$ flux measurement in Kerr et al (1987) given in Fig. 3.9 show that the $H \alpha$ flux at the central coma of the comet was \sim

60 R.

Section A.2

Digitisation and image analysis

The H_2O^+ images and the $\text{H}\alpha$ interferogram taken on photographic film were digitized with a 1010M (Perkin-Elmer) PDS microdensitometer system. The digital images have a pixel size of $20\mu\text{m}$ which is comparable with the intensifier resolution to produce the continuous tone image of the film. The gray level in each pixel is represented by 8 bit binary numbers and stored in a standard format (Pub No: TM 16913250, Perkin-Elmer corporation). Each horizontal scan of the image is stored as one record of the image file. An image file contains about 1000 such records corresponding to the number of horizontal scans required to complete the image. The digital images were computer processed to enhance the faint features. In order to obtain the sharp intensity gradients the local background was removed from the digital image. The median-filter algorithm with a 10×10 pixel window was used to generate a lowpass "model" of the image, representing all the largest structural information in the image. This low pass model was then subtracted from the unprocessed image to produce a highpass filtered picture. Fig. 3.10 shows the isodensity contours of the H_2O^+ image. A distinct blob is clearly seen at position angle 160° (measured from north

through east) with respect to the nucleus. The blob is at a projected distance of 2×10^5 km in the plane of the sky from the nucleus. The isodensity contours of the white light image in Fig. 3.11 also show a distinctive projection (in terms of contour asymmetry) in the same region as the blob in the H_2O^+ frame. The contrast enhanced image shows that the extent of the blob in the plane of the sky is 30,000 km x 20,000 km and the peak brightness ratio of the blob to the comet nucleus is < 0.12 .

(B) Velocity determination

Careful microdensitometric measurements of the fringe diameter have been made and the instrumental parameters precisely defined using He-Ne laser interferogram. A careful comparison was made with an earlier $H\alpha$ interferogram on the Orion trapezium region, which served as a celestial spectral reference of known radial velocity relative to the earth. From the measurements of the fringe shift, we obtain for the blob a recession radial velocity of 30 ± 10 km/s relative to the comet (as seen from the earth). The interfringe separation and hence the relative velocity distribution can be better determined than the net absolute radial velocity. A procedure for determining the relative velocity distribution is detailed in section B.1. The relative velocity values are given in Table 3.4 and their spatial distribution is featured in Figure 3.13.

TABLE 3.4

Relative Radial velocity determination
from line shifts

S.No.	Position angle in degrees	Distance $\times 10^4$ km	Internal velocity km/s	Comments
1.	203	31.3	20 ± 2	
2.	200	28.7	23 ± 2	
3.	192	23.3	9 ± 2	
4.	187	36.7	10 ± 9	
5.	185	30.7	23 ± 6	
6.	181	24.7	-1 ± 2	
7.	178	38	5 ± 10	
8.	178	36.7	21 ± 8	
9.	178	34	-21 ± 8	
10.	178	31.3	-27 ± 6	
11.	178	24.7	0.0	
12.	175	24.7	11 ± 1	
13.	174	31.3	-4 ± 2	
14.	171	33.3	-15 ± 2 -36 ± 2	split fringe
15.	171	23.3	2 ± 5	
16.	170	23.3	1 ± 3	
17.	168	30	18 ± 8	
18.	167	32.7	1 ± 10	
19.	166	22.7	4 ± 2	
20.	166	33.3	1 ± 10	
21.	165	30	-6 ± 8	

22.	164	33.3	26 ± 11	
23.	163	22	9 ± 2	
24.	163	29.3	5 ± 3	
25.	160	32	37 ± 6	
26.	160	20.7	-6 ± 1	
27.	160	14	4 ± 1	
28.	158	15.3	-18 ± 1	
29.	158	16.7	-16 ± 1	
30.	158	17.3	5 ± 1	
31.	158	18.4	11 ± 1 1 ± 1	split fringe
32.	158	19.7	16 ± 1	
33.	157	28	2 ± 1 -25 ± 1	split fringe
34.	154	30.7	-43 ± 9	
35.	153	26.7	-9 ± 6	
36.	150	25.3	1 ± 2	
37.	148	28.7	4 ± 8	
38.	145	27.3	10 ± 2	
39.	145	24	32 ± 1 19 ± 2	split fringe
40.	145	30.8	15 ± 9	
41.	145	32.7	1.1 ± 10	
42.	144	29.3	0 ± 2	
43.	143	22.7	21 ± 2	
44.	142	28	6 ± 2	
45.	140	20.7	5 ± 1 -3 ± 2	split fringe
46.	137	18.7	32 ± 1 -10 ± 2	split fringe

47.	135	22.3	1 ± 2	
48.	135	16.7	-9 ± 2	
49.	135	15.3	18 ± 2	
50.	133	12.7	12 ± 2 33 ± 2	split fringe
51.	138	18	8 ± 2	
52.	135	16	27 ± 2	

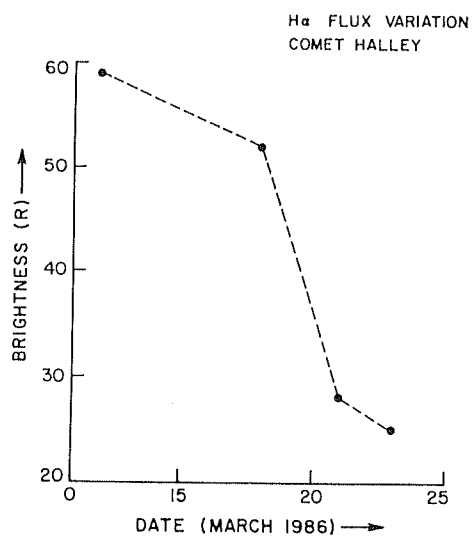


Figure 3.9. Variation of cometary H-alpha flux intensity during mid-March 1986. (Kerr et al. 1987).

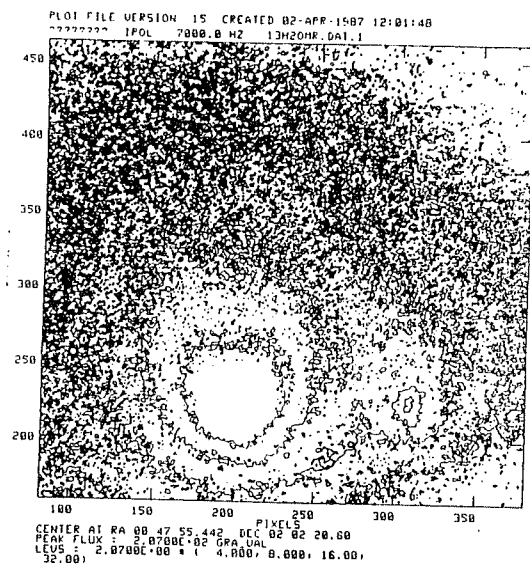


Figure 3.10. Isophoto for H_2O^+ image of comet Halley at 1986 March 13.0089 UT. Contour levels are at 4, 8, 12, 32 per-cent of the peak photographic density.

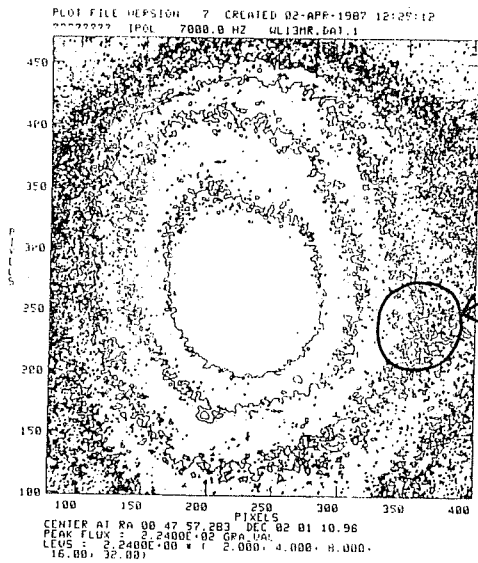
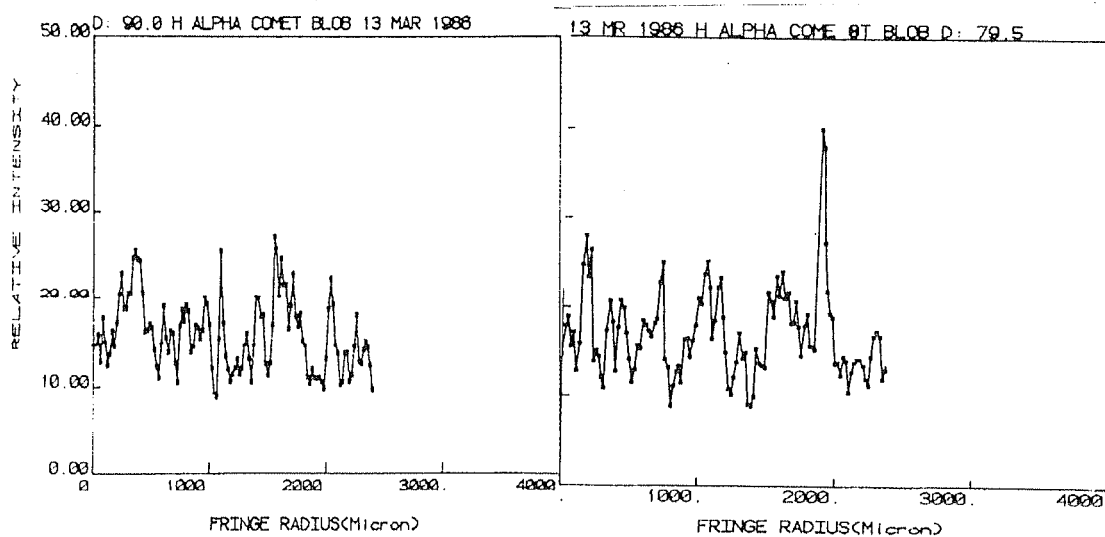
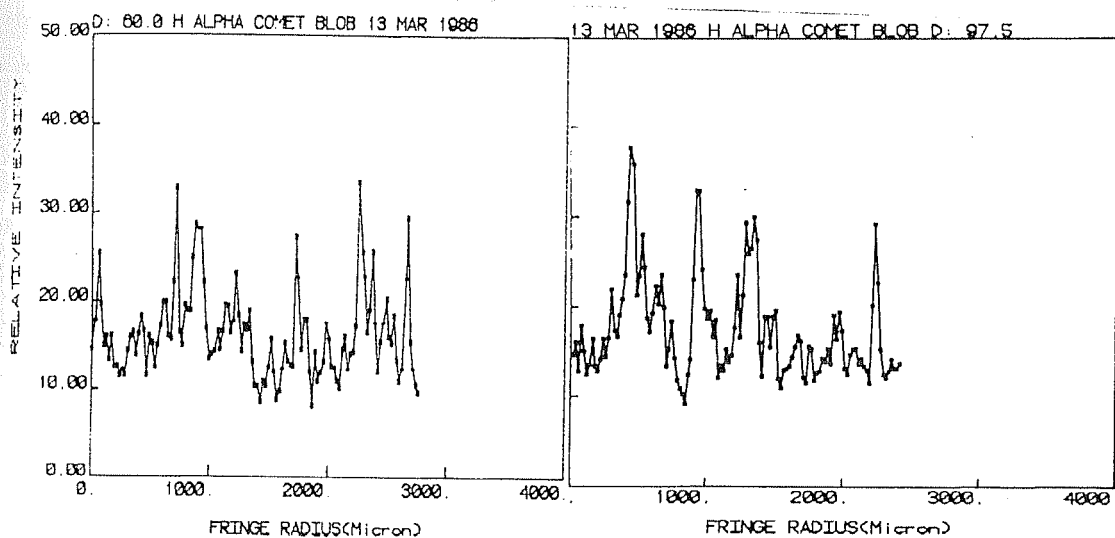
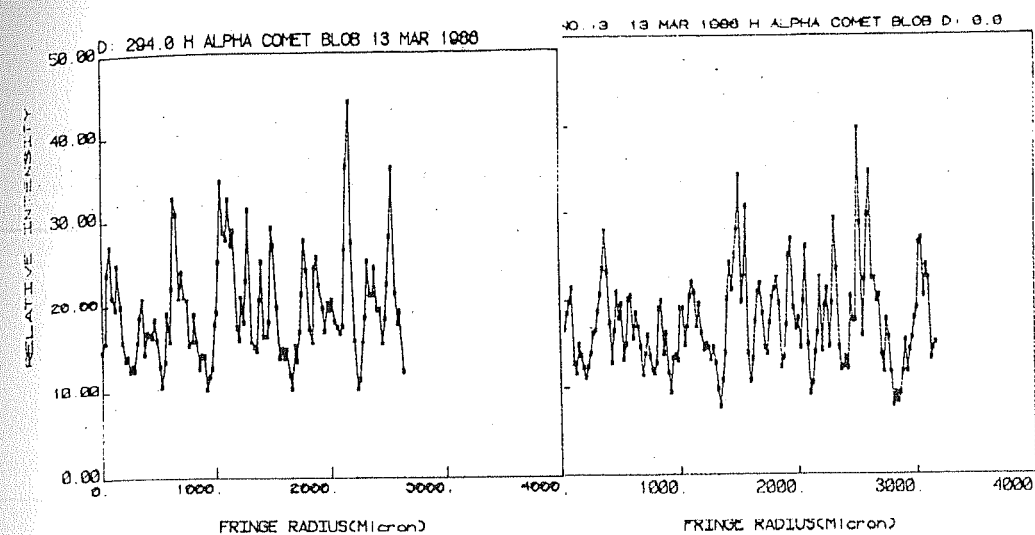


Figure 3.11. Isophotos for whitelight image of comet Halley on 1986 March 12.977 UT. The contour levels are at 4, 8, 16 and 32 percent of the peak photographic density. The contour assymetry corresponding to the position of the H_2O^+ blob in figure 10 is shown with an arrow marked circle.



3.12. Radial scans in the Halpha interferogram at angles = (a) $294^{\circ}.0$, (b) $0^{\circ}.0$, (c) $60^{\circ}.0$. (d) 79.5° , (e) 90.0° , (f) 97.5° , where is the angle measured at the centre of the interferogram with respect to the comet blob line extended in southern direction as $0^{\circ}.0$.

EVENT OF 13 MARCH 1986
DIFFERENTIAL VELOCITY MAP OF THE BLOB REGION IN THE PLANE OF THE SKY IN km/s

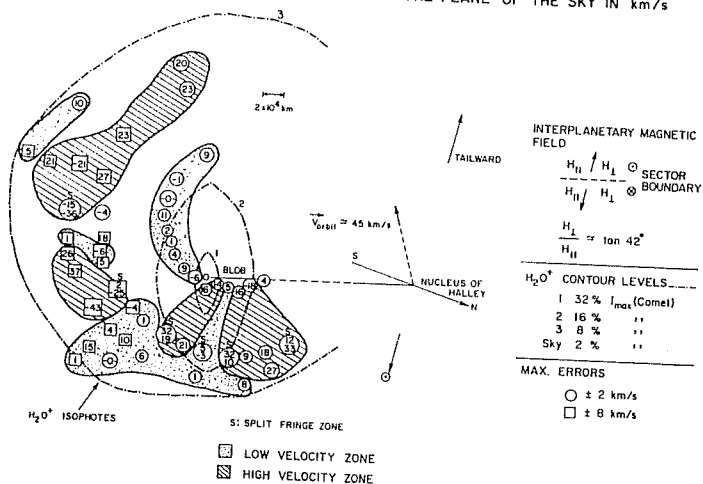


Figure 3.13. Doppler shift dispersion velocity distribution in the H₂O⁺ blob region. H₂O⁺ isophotes contour levels are drawn approximately from figure 10.

Section B.1

Radial scan analysis and determination of differential velocity map

In order to obtain the relative velocities of different parts of the H_2O^+ blob, a number of radial scans were taken from the centre of the interferogram and fringe shifts were measured. It is first necessary to very precisely locate the fringe centre.

Determination of interferogram fringe centre:

The digital interferogram was displayed on the image monitor and the approximate position of the fringe centre was determined by a visual inspection. Its precise location was then obtained by using a task 'IRING' of the Astronomical Image Processing System (AIPS) environment. In this task the approximate centre obtained by visual inspection, the diameter and width of the 2nd ring are given as inputs to obtain the integrated gray value of the annuli. Shifting the position of the centre to its neighbouring pixels the procedure was repeated. The pixel giving the maximum value of integrated flux of annular ring was taken as the pixel defining the centre of the FP fringe system. With this procedure the fringe centre could be determined to an accuracy of two pixels ($\sim 40 \mu\text{m}$ on the film).

Retrieval of the radial scan:

The interferogram was sampled along radial directions at various angles with respect to the horizontal reference scan. Fig 3.12 shows the example of few such scans. The record number (Y-coordinate) containing the centre of the interferogram can be directly used as one radial scan of the interferogram. Since the pixel sizes of the digital interferogram image is $20\mu\text{m}$ the sampling error in this case is also $20\mu\text{m}$. However, while obtaining the radial scan along other directions the sampling error depends on the angle of the scan direction with respect to the horizontal scan. In this case the record numbers were incremented or decremented with respect to the record number of the horizontal scan and the corresponding position of the data point was calculated by specifying the desired angle. The sampling error is given by (for non zero values of θ):

$$\Delta X' = \frac{\Delta X}{\sin \theta}$$

..3.1

Where, $\Delta X = 20\text{ m}$ and X' is the sampling step in the direction defined by θ .

Velocity determination:

To obtain the wavelength corresponding to the observed radius of the fringe in the interferogram a search grid was generated to obtain a number of sets of possible radii values within the filter bandwidth.

The basic equation of the Fabry-Perot etalon is given by:

$$2\mu t \cos\theta = n\lambda$$

..3.2

where μt is the optical spacing of the etalon and θ the angle of incidence. For integral values of n the constructive interference condition is satisfied and bright fringes are seen.

For a camera lens of focal length F , the above equation (for small θ) simplifies to:

$$2\mu t (1 - R^2 / 2F^2) = n\lambda$$

..3.3

where R is the radius of a particular fringe. Using

calibration interferogram μ t is estimated. A grid of radii values for the first fringe is generated using the above spacer value for slightly different wavelength around $H\alpha$ and the value for the best match with the observed radius is noted. The radius for the lower order (outer) fringes were then calculated with respect to the first fringe. From equation 2 it follows that

$$R \, dR / F^2 = \frac{8\lambda}{\lambda} = V/C$$

where $dR = R_{cal} - R_{obs}$

Knowing the calculated and observed radius of the interference fringe pattern the relative velocity (V) of the observed $H\alpha$ emission at various positions can be calculated.

Error estimation:

There are two sources of error.

(i) The effective instrumental width of 0.11 \AA for the red Fabry-Perot etalon results an error in velocity estimation to 5 km/s.

(ii) The error due to sampling depends upon the

radius at which the velocity is estimated and on the direction of the scan as defined by θ . This error is generally more than the error due to the instrumental limiting resolution. The errors are classified into two zones with high and low values and indicated appropriately in Fig.3.13.

In addition to the determination of the velocity structure in the blob, line profile analysis of a few bright portion of the $H\alpha$ interferogram have also been carried out in order to study the local dynamics of the hydrogen gas in the blob. Figure 3.14 shows some line profiles which can be seen to be asymmetric, indicating nonisotropic flow of the gas in the blob. The profiles close to the blob centre are highly structured. Least square Gaussian profiles were fitted to the data to obtain the equivalent widths and hence internal expansion velocities. The line profile analysis indicates the relative velocity spread of 5 to 22 km/s in reasonable agreement with the doppler shift velocities measured in the blob. Table 3.5 summarizes the internal velocities obtained from the line profile analysis. There is evidence for fringe splitting at several places in the interferogram, which unambiguously establishes the existence of large differential velocities in the blob.

3.2.4 Discussions

The differential velocity field derived from the $H\alpha$ interferogram and the line profile measurements show a complex structure. The exact mechanism of the event is not quite clear at present. However, here we discuss the broad characteristics of the data and their implications to the understanding of the transient events in the cometary atmosphere.

(A) State of the coma activity on 13th March 1986
from other observations

As the event took place only 24 hours before the Giotto encounter with Halley the cometary coma was under close observation. Unfortunately Giotto cameras were not on at the time of the event to provide confirmation of our event. The white light images taken at South African Astrophysical Observatory at $2^h 32^m 05^s$ UT (~ 2.5 hours after our observations) do not show a blob. Three different jet like structures at 65.5° , 87.5° and 102.5° (angle with respect to sun) appearing in the E - S direction, confined to the inner coma region 20, 000 to 35, 000 km from the nucleus are however seen. A comparison of red filter pictures of 13th and 14th March 86 shows that the dust activity was more on 13th compared to 14th March by a factor of ~ 2 (Cosmovici et. al, 1986). Evidence of such activity is also observable in the images taken at 0415 UT on 13 March at Catania observatory in Italy (Formisano V. et al. 1986). Dust concentration in the vicinity of the nucleus was also

TABLE 3.5

Doppler Line width velocity from line profile

S.No.	Position angle in degrees	Distance *10 ⁴ km	Internal velocity Km/s	Comments
1.	174	24.7	11 10	split ~ 7.5 km/s.
2.	140	20.7	10 6	split ~ 6.6 km/s.
3.	160	17.3	8 <5	split ~12.8 Km/s.
4.	135	22.7	22	
5.	127	18.0	13	
6.	180	23.3	10 16	
7.	200	28.7	10	
8.	204	30.7	21	

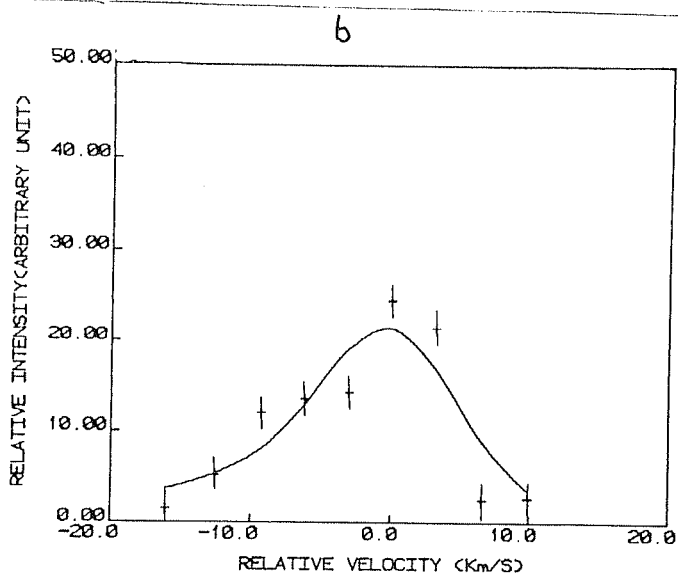
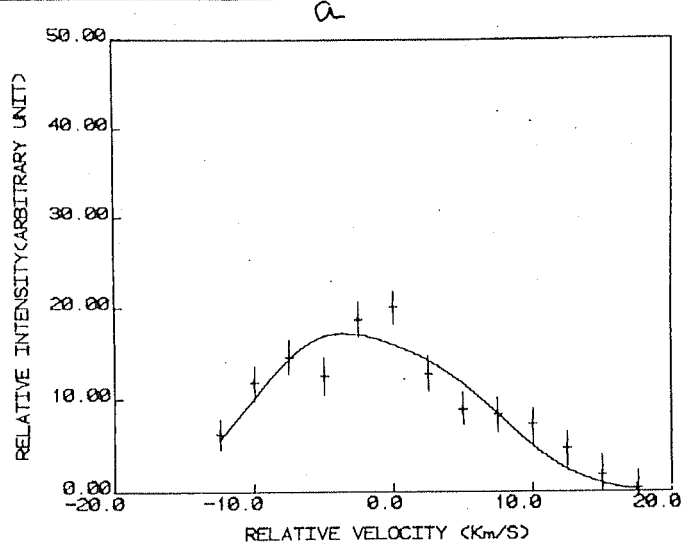


Figure 3.14. Line profiles from selected regions of the interferogram at,

(a) PA : 174° , d : 24.7 (b) PA : 140° , d : 20.7

where PA : position angle and d = cometocentric distance in ($\times 10^4$) km.

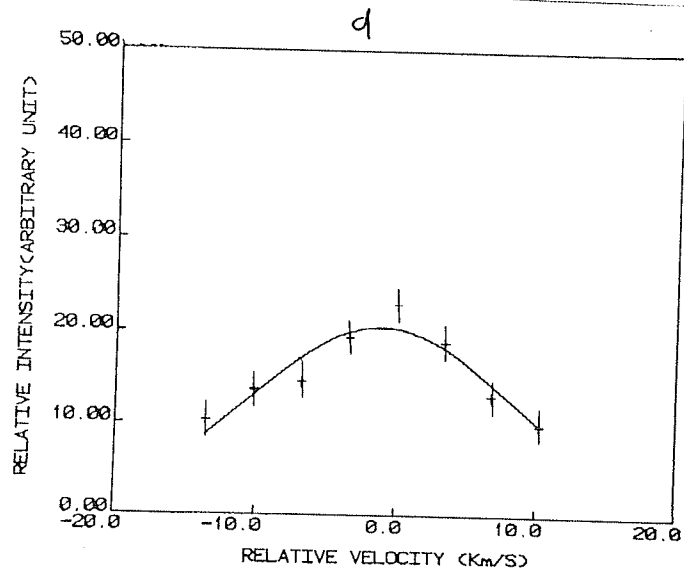
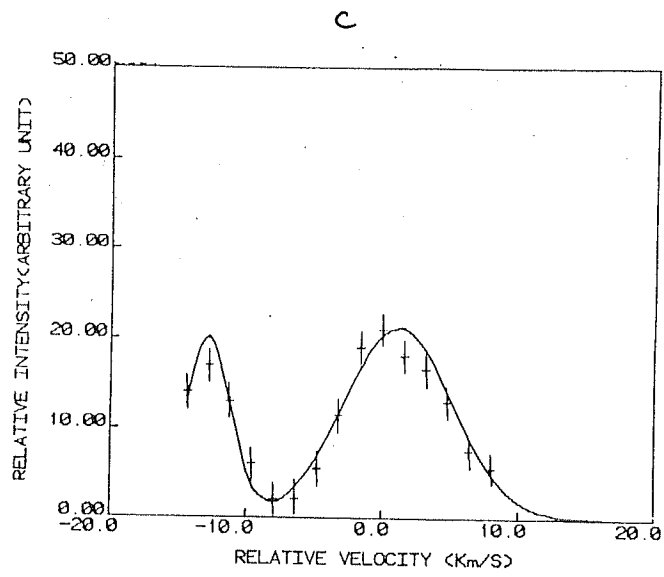


Figure 3.14. Line profiles from selected regions of the interferogram at,

(c) PA : 160° , d : 17.3 (d) PA : 135° , d : 22.7

where PA : position angle and d = cometocentric distance in ($\times 10^4$) km.

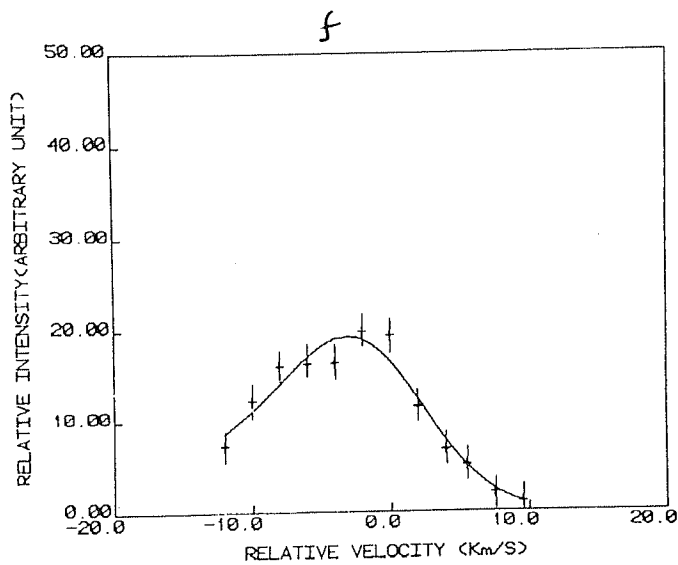
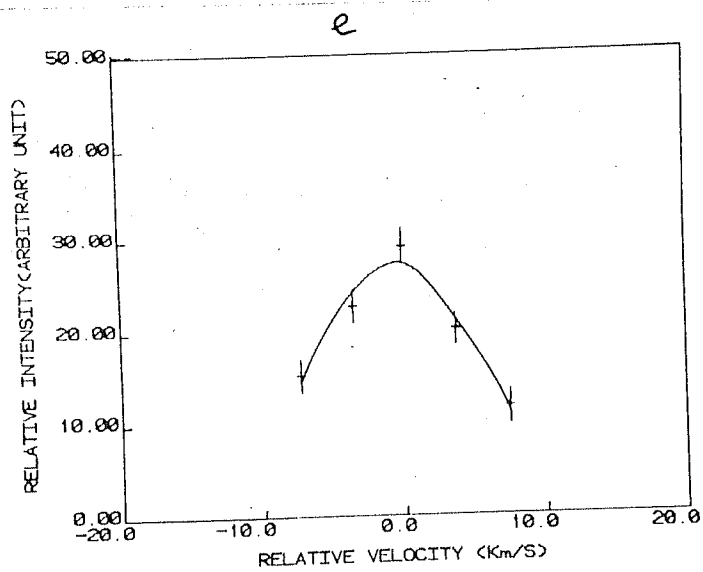


Figure 3.14. Line profiles from selected regions of the interferogram at,

(e) PA : 127° , d : 18.0 (f) PA : 180° , d : 23.3

where PA : position angle and d = cometocentric distance in $(\times 10^4)$ km.

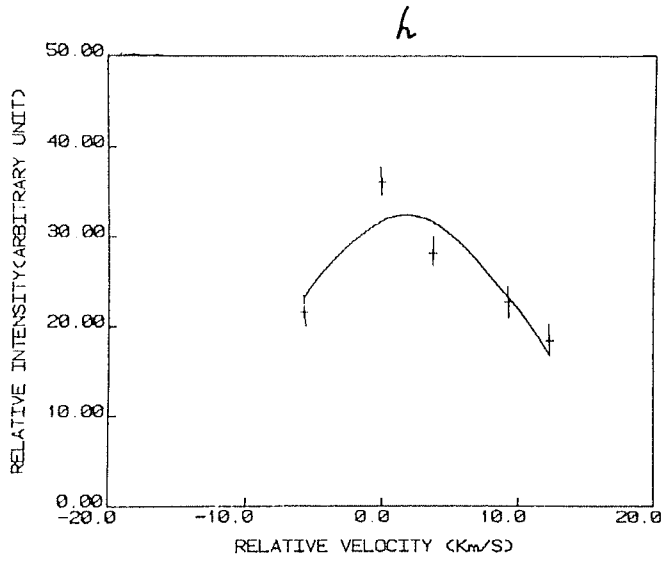
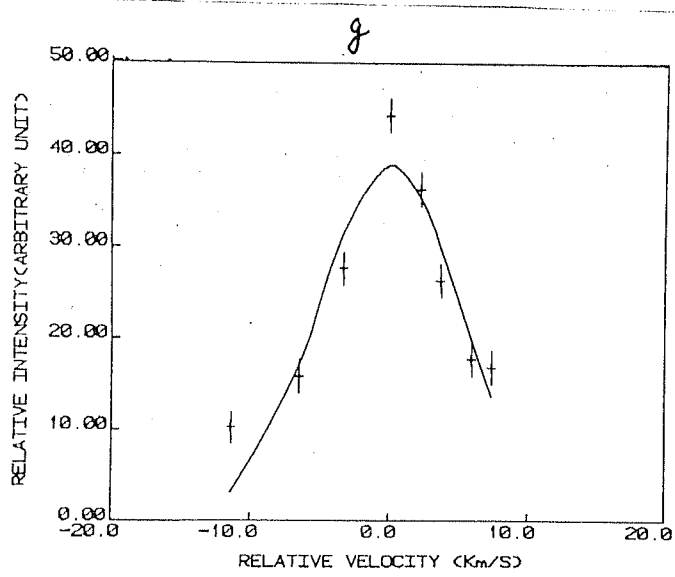


Figure 3.14. Line profiles from selected regions of the interferogram at,

(g) PA : 200° , d : 28.7 (*h*) PA : 204° , d : 30.7

where PA : position angle and d = cometocentric distance in $(\times 10^4)$ km.

monitored at the 3.9 m Anglo-Australian telescope on 11th, 12th and 13th March 1986. Development of the jets over a period of 3 days could be traced in the photographs but again there is no evidence for a blob structure (Chakaveh et al. 1986).

The Ly α images taken at 10^h 54^m UT on 13 March do not show any asymmetry beyond $\sim 10^5$ km from the nucleus indicating the hydrogen gas flow to be unaffected by the cometary activity (Mc Coy, 1986). Photometric observations during the period 5th to 17th March 1986 show a day to day variation of intensities in several emission bands. The data show an enhancement by a factor of about two in the production rate of all observed species on 13th March compared to the neighbouring days but there are several days during the observations period when such enhancements occurred. (Schleicher et al. 1986).

Festou et al (1986) have reported an enhanced count rate in IUE fine error sensor in 12 x 12 arc second aperture at 19^h UT on 13 March indicating an increase in the cometary visual brightness. The spectra indicate enhanced H₂O and CS production rates. Observations with spectral resolution at the wavelength of Hydrogen (6563 Å⁰) have been carried out by Kerr et al (1987) from Arecibo-Observatory. Observations in March 86 are characterised by highly structured H α profiles implying nonisotropic outflow of H atoms. Velocities relative to the

comet of 35 km/s have been noted from the position of the fringe peaks. The observations for 13th March give a $H\alpha$ surface brightness of 59 ± 13 Rayleighs for a 5.9 arc minute field of view. The profile analysis show that $H\alpha$ emission was confined to highly directional flow indicating the association of jet activities. From the observations discussed above we are led to the conclusion that while 13 March 1986 was a day of enhanced dust activity it was not an unusual one. The absence of the blob at other longitudes suggests that the ionic event observed by us is a transient one lasting a few hours only and that the cause is likely to be external to the comet. The few images of the comet reported over Indian longitudes on this day are on a scale too coarse for the blob to be discerned (A.Desai et al.1987, A.K.Bhatnagar 1987 - Private communications).

However, there appears to be some evidence for transient ionic features lasting ~ 1 hour in the inner coma of Comet Halley. A comparison of ground based SAAO CCD H_2O^+ observations with the Giotto NMSE and IMSE measurements of Comet Halley reveals such an activity in the comet. These instruments on Giotto had recorded a plasma pile up region at $\sim 10^4$ km from the nucleus which should have showed up in the ground based CCD images as inhomogeneous structures. The clear absence of such structures in the CCD images suggests their rapid time variability ~ 1 hour (Ip et al,1986).

In the case of Vega-1 encounter, the SDA sensor observed

a burst of ions with energies $\sim 100-1000$ eV near the closest approach to comet Halley lasting ~ 5 minutes. Based on the magnetic field observations in the path of the spacecraft (Verigin et al, 1987) it was concluded that the burst was produced by the motion of cometary ions of water-group accelerated upto supersonic speeds \sim few tens of km/s. Further they point out that the acceleration could be caused by merging of interplanetary magnetic field lines of opposite polarity retarded by the presence of cometary plasma and neutrals. Figure 3.15 describes the topology of the magnetic field around closest approach as deduced from the measurements of the magnetic field direction (the arrows) along the Vega-1 trajectory. The dotted area in the figure represents the region in which the bursts of accelerated ions was observed. Such observations of well-defined intensity enhancement of ions with energies > 40 keV are reported from Tunde-M experiment on board Vega-1 (Somogyi et al 1986).

The theoretical studies have shown several possible explanations for such outbursts in the cometary ionosphere (Delsemme 1979). The rapid ionization of the gaseous material in the coma can be achieved by the discharge of cross tail electric current. Such ionization surge, well within the coma, can also be caused by electron jetting in the reconnection current sheet which is produced by the passage of an interplanetary sector boundary through the comet (Niedner 1980).

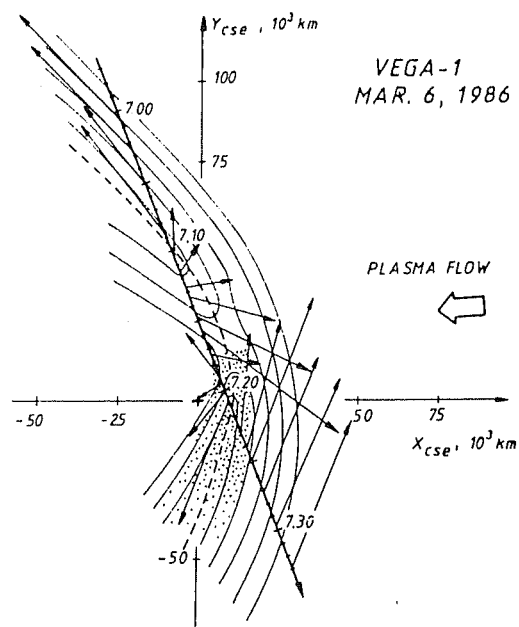


Figure 3.15. Topology of the magnetic field around the closest approach as deduced from the measurement of the magnetic field direction (the arrows) along the Vega-1 trajectory. The burst of accelerated ions was observed in the dotted area (Vergini et al 1987).

(B) State of the interplanetary magnetic field

Since it is conjectured that the observed event could be a special type of disconnection event caused by the passage of an interplanetary Magnetic field boundary through the comet it is pertinent to enquire about the state of the interplanetary magnetic field at the time of the event.

Comet Halley was predicted to enter a current sheet warp at about the time of the Japanese cometary space probe Sakigake's encounter on March 11, 1986 and to exit from it two days later (Niedner 1986). The observations from Sakigake and Giotto show that it was indeed the case (Saito et al., 1986, Neubauer et al., 1986). The multiple crossing of the current sheet by the comet during March 11-14, 1986 was clearly evident from Sakigake's measurements, which located the sector boundary at 7×10^6 km upstream of Comet Halley. It is known that only if comet penetrates the sector boundary perpendicularly can major ionic tail disconnection events take place (Niedner et al., 1978). However, since no major DE was observed during this period, Saito et al (1986) proposed that the crossing of the sector boundary by the comet was quasi-parallel as shown in figure 3.16. The Sun-Comet-Earth geometry and the Parker's spiral at the time of our observation is given in Fig. 3.17. Since the comet was

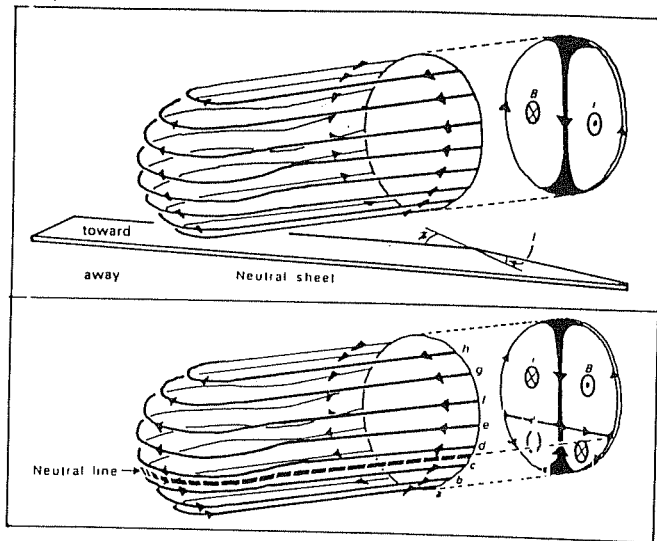


Figure 3.16. The quasi-parallel crossing of the sector boundary by comet Halley (Saito et al 1986).

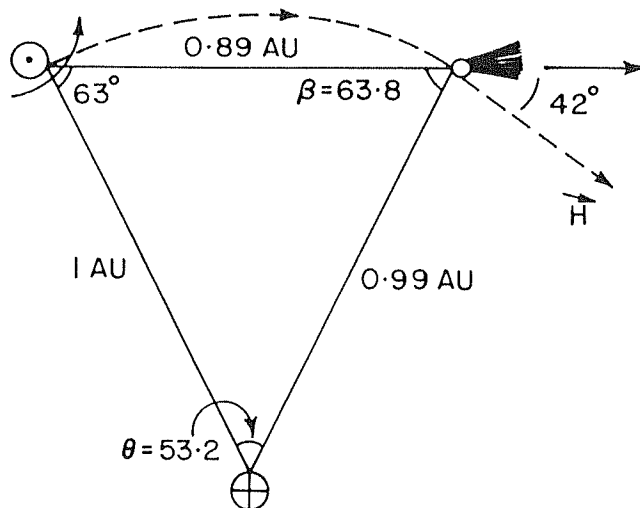


Figure 3.17. Sun-Comet-Earth Geometry and the interplanetary magnetic field structure during observations.

crossing the ecliptic plane at this time, sun, comet and earth can be considered to be in the same plane. According to Saito et al (1986) the comet crossed the neutral sheet at a small attack angle. Considering the motion of the comet, they pointed out that, the southern part of Halley dipped first into the away sector, changing the polarity of the field line from towards to away polarity. Though the authors argue that the gradual reconnections of field lines may not lead to a drastic DE, no quantitative picture is outlined.

Further if the radial alignment of the field occurred at that time the inner region of the coma could not have been shielded from the solar wind flux, which could have led to an enhanced ionization as in the case of Venus and Comet IRAS-ARAKI-alcock (Russell et al., 1987). The time scale of ionization by these processes are found to be very short $\sim 10^3 - 10^4$ s.

Qualitatively the geometry of the reconnecting magnetic fields can be represented in Fig. 3.18. Here, the magnetic field lines of reversed polarity flow towards each other at a relative velocity in the Z-direction, are cut in the diffusion region (the hatched area) and the reconnected field lines flow out of the diffusion region in +x-direction. The $\vec{J} \times \vec{B}$ driven electron jets in the reconnection current sheet would then produce sufficient energy to create a rapid ionization region.

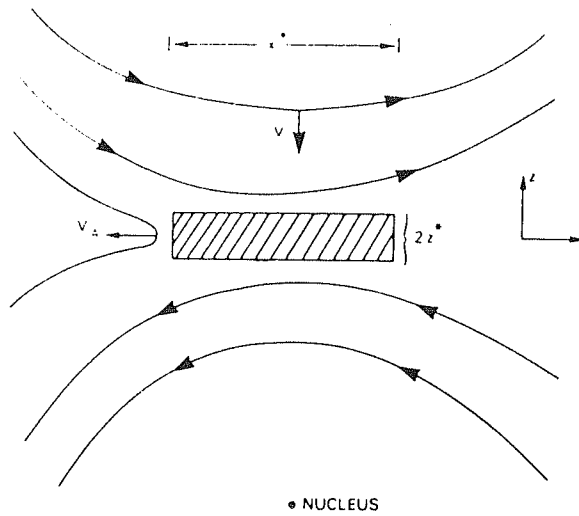


Figure 3.18. Geometry of reconnecting fields just before a disconnection event (DE). The direction of plasma outflow from the diffusion region (shaded) is given by v_A .

(C) Kinematics of the blob:

The relative radial velocity measurements show a complicated velocity field as represented in fig.3.13. However, dividing the map into high and low velocity zones, it can be noticed that the velocities are clustered into compact regions. There are some zones of high relative velocity. A number of split fringes are also seen especially on the Sunward side. The velocity distribution around the blob is also not symmetrical, indicating thereby that the expansion of the blob is not simply governed by the diffusion process.

(i) Estimate of time of dispersal

Assuming the surface brightness of a spherical blob to vary as $1/r^2$ and an isotropic constant expansion velocity of 30 km/s it is possible to estimate crudely the time taken (τ) by the blob intensity (I_0) to reach the blackground sky level (I). The time of dispersal of the blob is given by:

$$\tau \approx \frac{R_0}{V} \sqrt{I_0/I}$$

..3.5

For $I_0/I \sim 8.1$ and $2 R_0 \sim 3 \times 10^4$ km and $V \sim 30$ Km/s, $\tau \sim 23$ minutes.

A slowing down of the dispersal velocity would result in a longer period of visibility. However, it is unlikely that the blob will survive for more than a few hours. The short life span can explain the lack of sightings of the blob by groups located at other longitudes.

(ii) Mass:

Assuming the blob to be spherically symmetric to a first approximation, with a $2 \times 10^{22}/r^2$ (cm) dependence of H_2O^+ number density we estimate the mass of the blob to be

$$\int_{\text{Extent of the blob}} 4 \pi n(H_2O^+) r^2 dr = 10^{10} \text{ g}$$

..3.6

3.2.5 A theoretical model for the event

Based on the knowledge that a sector boundary crossing had taken place during the time of the event, a theoretical model for the formation and movement of the blob is suggested below.

The plasma tail disconnection events in Comets are believed to be caused by magnetic reconnection which occurs due to the passage of a sector boundary through the

cometary head (Niedner and Brandt 1978,1979,1980). One of the consequences of the magnetic reconnection is that plasma flows out of both sides of the reconnection region at the Alfven speed as shown in fig.3.18. We propose that the ejection of H_2O^+ blob observed by us on 13th March is caused by magnetic reconnection in a way as described in fig.3.15. The blob during its outflow in the solar wind is constrained by the pressure balance equation:

$$\frac{B_c^2}{4\pi} \left(\frac{R_o}{R_s} \right)^2 + \rho_c \left(\frac{R_o}{R_s} \right)^2 V_c^2 = \rho_s V_s^2 \quad \dots 3.7$$

Where ρ_c is the blob density at R_o and is assumed to vary as r^{-2} ; B_c is the magnetic field at R_o and is assumed to vary as r^{-1} ; V_c is the outflow velocity which is close to Alfven velocity V_A in the Cometary head and is assumed to remain constant; R_o is the initial position of the blob, measured from the nucleus. ρ_s and V_s are the density and velocity of solar wind and R_s is the observed separation of the blob from the comet head in the H_2O^+ frames. Magnetic field of the solar wind is taken to be much smaller than the Cometary magnetic field and is neglected.

From equation (1), one finds:

$$\left(\frac{R_s}{R_o}\right)^2 = \frac{2 V_A^2 \mathcal{I}_c}{V^2 \mathcal{I}_s} \quad \dots 3.8$$

The time τ taken for the blob to reach R_s is given by:

$$\tau = \frac{R_s - R_o}{V_A} \quad \dots 3.9$$

From the measurements made by Vega space missions to Comet Halley it follows that the number density of H_2O^+ ions at a distance of $\sim 10^4$ km from the nucleus has a value $\sim 3 \times 10^3$ /cc. and varies approximately as $1/R^2$ where R is the distance to the comet nucleus. The plasma convective velocity estimates imply a velocity 2-3 km/s at $\sim 10^4$ km which rises to ~ 20 km/s at $\sim 2 \times 10^5$ km, the distance from the nucleus at which the H_2O^+ blob is seen (R_s). (Vaisberg et al., 1987).

Putting in the values $V_A \sim V_c \sim 20$ km/s,
 $V_s \sim 450$ km/s $\mathcal{I}_s \sim 1.7 \times 10^{-25}$ g/cc (10 solarwind protons/cc)
 $\mathcal{I}_c \sim 10^{-19}$ g/cc.

$$\text{We get } R_o/R_S = \left(\frac{f_s}{2f_c} \right)^{1/2} \frac{v_s}{v_A} \sim 1/5$$

..3.10

Therefore the initial position of the blob should be 4×10^4 km from the nucleus. The time taken by the blob to reach the position $R_S \sim 2 \times 10^5$ km is given by

$$\tau = \sqrt{\frac{R_S - R_o}{v_A}} \sim 2.2 \text{ hours}$$

..3.11

The cometary magnetic field at the initial position R_o is $\sqrt{4\pi P_c} v_A \sim 200 \gamma$ and at R_S is $\sim 10 \gamma$.

The Cometary magnetic field B_c may appear to be rather high but is not unacceptable especially when the field is expected to undergo compression in the cometary head. Thus plasma outflow caused by magnetic reconnection provides a reasonable description of the H_2O^+ blob.

3.2.6 Summary and Conclusion

Fabry-Perot interferometric observations along with the H_2O^+ emission imagery data taken at $\sim 0^h$ UT on 13th March

1986 reveal a transient ionic activity in the coma of Comet Halley.

1) A distinct extended brightness region (blob) in the H_2O^+ image is clearly seen at position angle 160° relative to the nucleus at 2×10^5 km projected distance in the plane of sky.

2) A $H\alpha$ interferogram is recorded in the region of H_2O^+ blob. Interferogram analysis shows:

(i) The blob has a recession radial velocity of $\sim 30 \pm 10$ km/s relative to the comet (as seen from the earth).

(ii) Gaussian analysis of the line yields Doppler line width velocities from 5 to 22 km/s (Fig. 3.14)

(iii) The relative differential velocity map exhibits a structured distribution. High velocity and low velocity regions are clustered. Fringe splitting is observed at many places on the Sunward side.

(iv) The dispersal time at the blob is estimated to be approximately ~ 30 minutes. The event is definitely a transient one.

3) An upper limit to mass of the blob should be $\sim 10^{10}$ g.

4) Comet was crossing the interplanetary sector boundary at about the time of the observations. An explanation of the event has been attempted from the state of the interplanetary magnetic field geometry in the vicinity of the comet. Our event appears at a time when disconnection events are most expected. However, it occurs in a region of the coma and not in the ionic tail wherein are triggered the normal disconnection events. The direction of the blob movement and its duration are unlike a typical disconnection event. This event appears to be triggered by nuclear activity in combination with the current sheet crossing.

In conclusion, we would like to stress on the need for close monitoring of a comet, particularly in the ionic emissions like H_2O^+ or CO^+ during its period of maximum activity to ensure that the transient events like the one reported here are not missed out. Such events by many observers can provide valuable insights into this intriguing aspect of cometary behaviour and the interrelationship with the interplanetary medium.

3.3 The Plasma Condensation Region in the Coma of Comet Halley Observed on 8th Jan 1986.

The recent observations of Comet Halley and the advent

of Image Processing techniques have shown that the coma is far from homogenous and isotropic. Straight plasma jets and spiral dust jets are often seen in the near nucleus region. The processed images of the comet in molecular and atomic emissions have clearly shown that these species follow the spiral trajectory in the inner coma region (A' Hearn et al 1986, Cosmovici et al 1988). The collimated flow of atomic hydrogen is inferred from Fabry-Perot observations (Kerr et al., 1987). Several plasma structures, in terms of enhanced brightness in the coma region (Ip et al 1987) in the ground based imaging observations and enhanced electron or ion density (Ip et al 1987) from the in-situ measurements have been inferred in Comet Halley.

Some of these ionic features observed in the near nucleus of the coma region are expected as the precursor of several fine features observed in the ion tail of comets. For example Wurm et al (1967) could successfully trace the ray structures within 10^3 km from the nucleus. One of the most distinguished features, widely observed in the tail are the condensation regions, which appear as the confined enhanced bright clouds moving in the down stream of the tail. Extensive work on Comet Kohoutek by Jockers (1985) showed that these features move at an average speed of $\sim 69 \pm 27$ km/s within 5×10^6 km and 90 ± 29 km/s outside. Further he pointed out the evidence that at least some tail condensations originate in and or expelled from the coma region with a speed of $\sim 20-40$ km/s. These numbers agree

qualitatively with the velocities obtained for other comets (Vsyekhsyatskii and Demenko 1976, Jockers et al. 1972, Miller 1969, Lust 1967, Ahnert 1943). However the motion of such features depend on specific situation in which they are produced and controlled by magnetic field configuration. The mechanism of formation of such features are expected to be at a relatively shorter time scale as deduced from the observations (Eddington 1910, Wurm 1963).

Our short exposure, high spatial resolution imaging data of Comet Halley taken on 1986 January 8.59 and 8.632 UT show such a feature at a distance of 2.4×10^5 km from the nucleus, moving at a mean speed of ~ 36.5 km/s. A similar image taken from Nainital Observatory also shows the signature of the feature. CCD images taken in CO^+ and H_2O^+ emission by Michael A'Hearn show long jet like structures in the coma and in the tail region. The sequence of wide angle photographs taken on 10th January 1986 show a "dramatic" DE starting at 10.375 UT, whose roots can easily be traced on to the 9th January images.

In this section the observation and analysis of the data apparently related to 10th January DE obtained by us, is presented. A possible mechanism of its formation is outlined. The relation of the observed condensation with the tail activity is discussed in detail.

3.3.2 Methods of observation and Analysis of Jan 8 →

→ 1986 event.

The observations were taken from Gurushikhar, Mt. Abu, using the imaging Fabry-Perot instrument in imaging camera mode described in section of the chapter II. Table 3.6 gives the comet parameters during the observations.

(A) Observations:

Table 3.7 gives the Journal of observations on 8 January 1986. The data obtained by us consists of two white light images taken through a Fabry-Perot etalon having high reflection coatings for the wavelength region 5700 \AA to 6700 \AA . Consequently the transmission is high in the blue region. The blue enhanced white light images are therefore expected to be sensitive to CO^+ emission at 4260 \AA . One image was taken through the above etalon with a Kodak Wratten filter No. 25 which is characterised by transmission longward of $\lambda \ 5900 \text{ \AA}$. A white light image taken with a 102 cm telescope was procured from U.P State Observatory, Nainital. The CCD images of the comet in ionic emission lines have been kindly provided by Micheal F A'Hearn. Table 3.8 summarizes the data base.

The blue enhanced images distinctly show the condensation region of size $\sim 10^4 \text{ km}$ at a distance of $\sim 10^5 \text{ km}$ from the nucleus.

TABLE 3.6

Comet parameters at the time of observations

Date UT	RA	Dec	δ RA	δ Dec	Δ AU	$\dot{\Delta}$ Km/s	R AU	\dot{R} Km/s
JAN 8 590	2158.553	-411.891	-1.3'/hr	0.53'/hr	1.29	30.43	0.9	-25.64

TABLE 3.7

Journal of Observations

UT		Exposure time	Filter	Film
JAN	8.590	10^S	Blank	2415
JAN	8.595	120^S	25	2415
JAN	8.638	10^S	Blank	2485
				Kodak emul- sion.

TABLE 3.8

The data base for the study of 8th Jan 1986 event

<u>Date (UT)</u>	<u>Exposure time</u>	<u>Filter</u>	<u>Film</u>	<u>Remarks</u>	<u>Source</u>
January 8.124	-	CO ⁺	CCD	Strong ray structure	UPSO Nainital.
January 8.582	5 m	-	IIa-o	Tracking not good	
January 8.590	10 ^s	Blank	2415	Condensation seen	
January 8.595	120 ^s	Kodak 25	2415	No condensation seen	Physical Research Laboratory
January 8.638	10 ^s	Blank	2485	Condensation moved in the antisolar direction	"
January 8.94	-	Blank	IIa-o	A strong kink is seen in the antisolar direction	Yunan Observatory China

The blob is absent in the red enhanced image taken with Kodak Wratten filter 25. The white light image obtained from UPSO, though not of good quality, shows the signature of the condensation in terms of asymmetric distribution of enhanced brightness in the outer coma region. The CCD images of A'Hearn, taken in CO^+ emission show strong rays in the direction of the condensation. Fig. 3.19 show the images mentioned above.

(B) Identification of the condensation

A careful study has been made in order to establish the reality of the condensation and its association with the comet. The investigation in this case is relatively straight forward since the bright stars are registered in all the cometary images obtained with various instruments. Comparing the star field of the comet frame obtained by us and from UPSO, Nainital (Fig. 3.19), it is clear that 6 bright stars are common to both the frames and these 6 stars are not the artifact of the instruments used. Therefore if we consider the condensation recorded by us is a ghost image of the Cometary Nucleus (because of the internal reflection), we must get similar reflected ghost images of the bright field stars (as the star brightness are more than that of cometary nucleus). Since in our comet frames we do not see the ghost images of the stars, we do not consider that the observed condensation is a ghost of the Cometary Nucleus. Extensive search of star catalogue and the NGC catalogue of

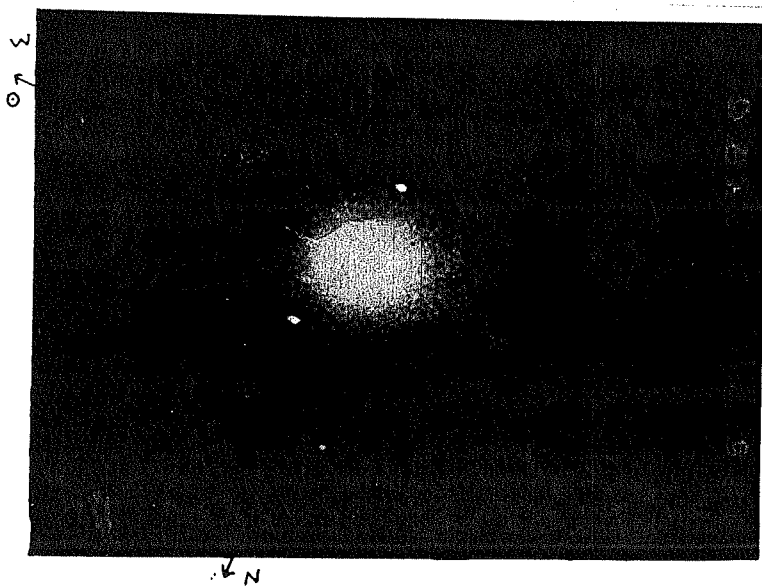


Figure 3.19a. White light photograph of comet Halley taken on 1986 Jan 8.590 UT. (2415 Kodak film). Scale $1 \text{ mm} = 1.5 \times 10^4 \text{ km}$.

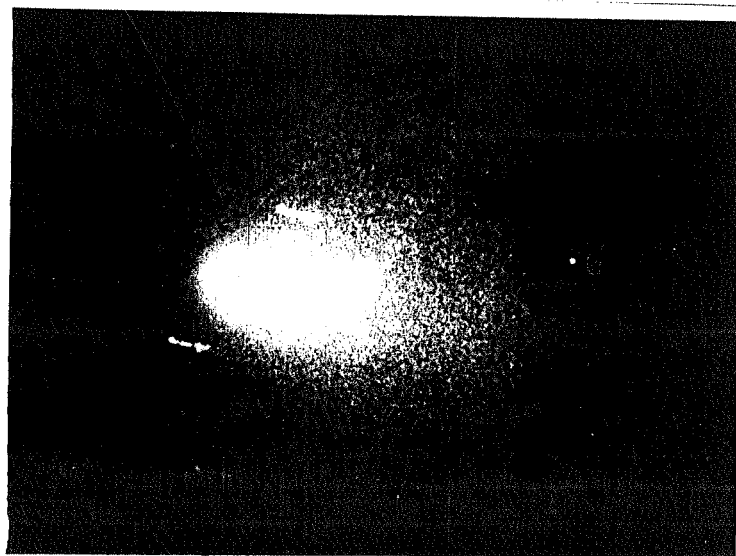


Figure 3.19b. Photograph of comet Halley taken with a Kodak 2.5 Wratten filter on 1986 Jan 8.595 UT (2415 Kodak film). Scale $\underline{1}$ mm = 1.5×10^4 km.

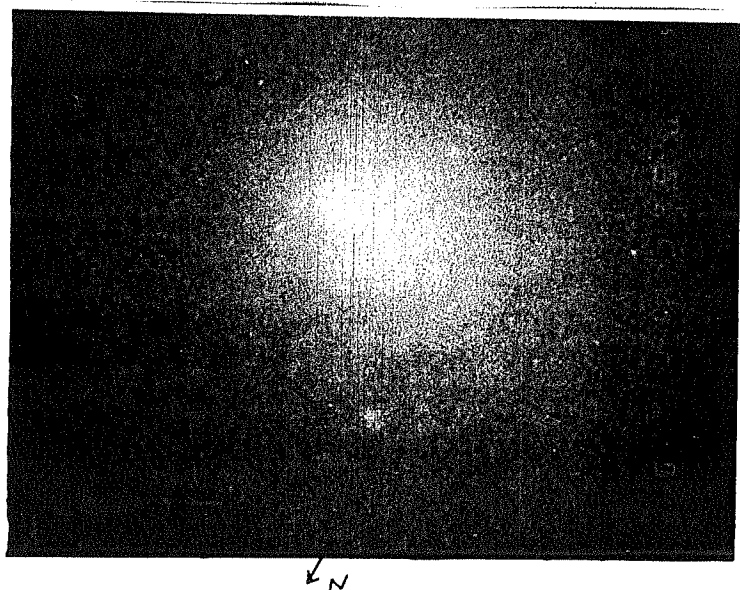


Figure 3.19c. White light photograph of comet Halley taken on 1986 Jan 8.638 UT (2485 Kodak film). Scale 1 mm = 1.5×10^4 km.



Figure 3.19d. White light photograph of comet Halley taken on
1986 Jan 8 ⁵⁴² UT at UP State Observatory, Nainital.
Scale 1 mm = 3 x 10⁴ km.

non stellar objects was made in order to assure that the feature is not due to any other astronomical object in the plane of sky with the observed field of view. Thus we are lead to the inescapable conclusion that the condensation region belongs to the Comet Halley.

(C) The velocity determination:

As a first step, the relative coordinates of the stars in the frame, Comet Nucleus and the centre of the condensation region were measured with a Zeiss film reader. Finally the accurate positions were determined using a microdensitometer with an uncertainty of 3" (~ 3000 km). The frames taken at an interval of 1^h, showing the condensation, were matched taking the field stars as control points. The comet was moving in the plane of sky at a rate of $-1.3'/\text{hr}$ in RA and $+0.53'/\text{hr}$ in Dec. The resultant displacement of the comet in one hour is 1.4' in the North-West direction making an angle 21° to the West. This is represented in Fig. 3.20. The second image of the comet with respect to the stars was indeed found to show the displacement relative to the first image by 1.4 and in the North-West direction. The superimposed (with respect to star field) frame is illustrated in Fig. 3.21. In order to find the net velocity of the condensation with respect to the comet, the Cometary motion has to be corrected. Hence the comet position in the 2nd frame was displaced so as to match with the position in the 1st frame. The position of the condensation was also

Comet motion on 8.1.86

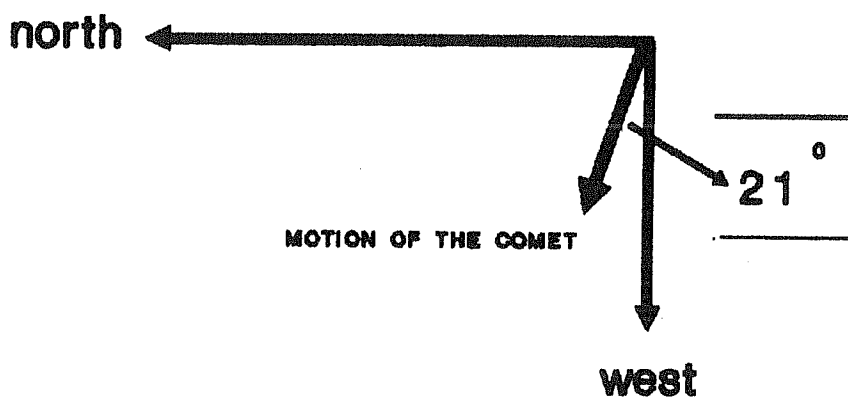


Figure 3.20. The motion of the comet in the plane of sky at the time of our observations on 1986 Jan 8.

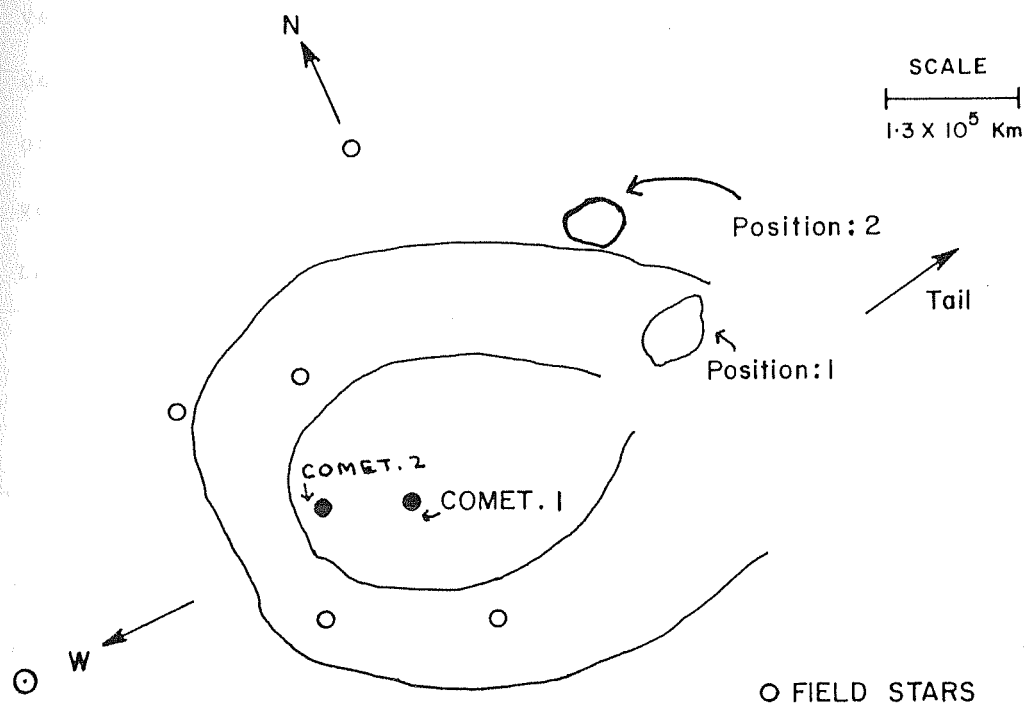


Figure 3.21. The sketch of superimposed comet frames taken at 8.590 UT and 8.638 UT. Only stars are matched.

displaced by same amount in the same direction. Fig. 3.22 show the superimposed comet images. A similar exercise was also carried out with the UPSO photograph. The distance of the condensation region at different times with respect to the Nucleus was determined as given in table 3.9. The velocity determined from the displacement of the condensation in the plane of sky was corrected for the orientation of the anti-solar direction in the sky. The velocities (corrected or uncorrected) are also given in table 3.9.

(D) Determination of the size of the condensation:

The brightness profiles of the comet and the condensation in different directions from the nucleus were obtained by taking microdensitometry scans, using a slit of height 5700 km and width 1400 km at the comet. Fig. 3.23 shows two brightness profile of the comet are along the direction of condensation and the second in the direction from the nucleus. The average width of the condensation region (10% above the background) is ~ 0.7 mm on the film, corresponding to $\sim 4 \times 10^4$ km at the comet. The intensity ratio of the peak brightness of the condensation to the neighbouring coma region is ~ 1.8 .

(E) The emission from the condensation:

The condensation region was seen only in those images

TABLE 3.9

Velocity of the condensation

	Projected distance of the blob in sky	Distance between the blob at two times	Velocity of the condensation region (in the plane of sky)
UT	$\times 10^5$ km	km	km/s
JAN 8.590	2.4		
JAN 8.638	3.0	12×10^4	28 ± 3 km/s
JAN 8.940	6.8	38×10^4	17 ± 5 km/s

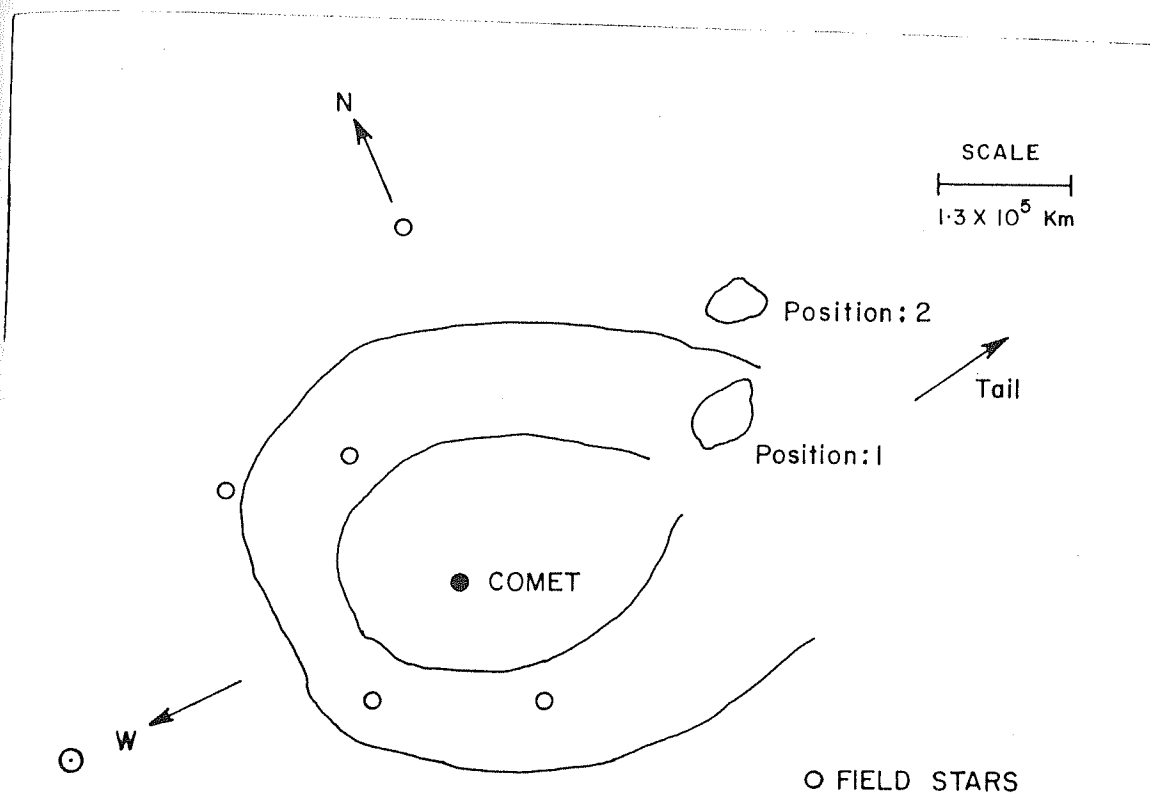


Figure 3.22. The sketch of the superimposed comet images. In the diagram the centre of the comet in two frames taken at 8.590 UT and 8.638 UT are made coincident. The net displacement of the condensation is evident.

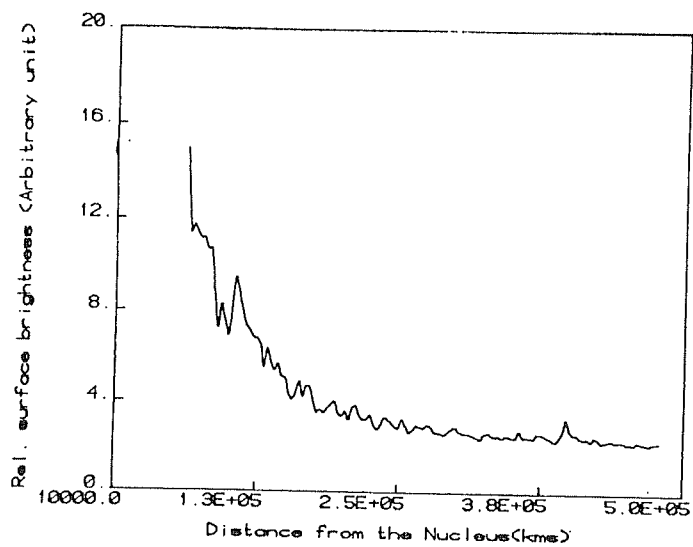
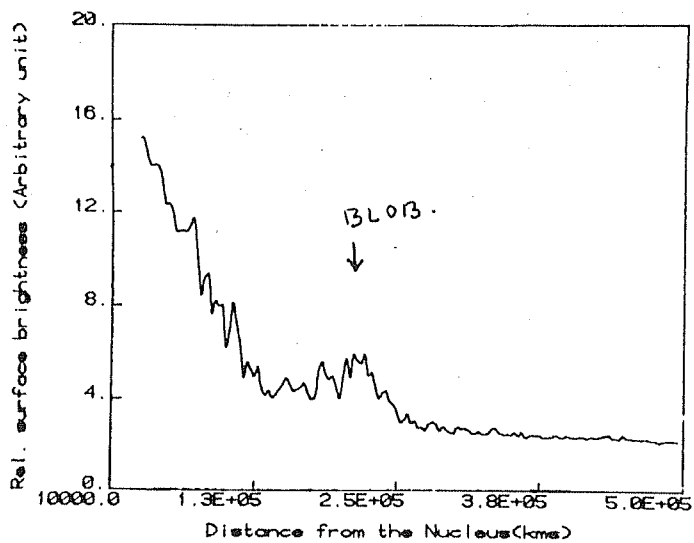


Figure 3.23. The brightness profiles of the comet along the condensation and in the opposite direction.

of the comet, which were blue enhanced by using a red FP etalon. The images taken with a Kodak wrattern filter-25 which is a high pass filter at 5900 \AA^0 do not show the feature. Though the signature of the condensation is evident in the white light image, it is not distinctly seen. This suggests that the brightness of the feature was mostly in blue region.

The velocity determination show that the condensation was moving at $\sim 37+5 \text{ km/s}$. It is difficult to conceive the motion of the neutrals at such high speed.

It is observed on other occasions that such features are bright in ionic emission lines. For example the photographs of Comet Halley taken with a focal reducer instrument in CO^+ and CO_2^+ emission lines on 1986 April 11.11 UT clearly show a confined plasma cloud moving in the anti-solar direction (Jockers et al 1987). These observations preceed the outstanding DE at 11.33 UT. The plasma cloud was seen at a distance of $\sim 5 \times 10^4 \text{ km}$ from the nucleus. Several narrow rays were seen to originate from this cloud. The multislit spectra taken by the same author on 10th April show that in blue region CO^+ is the prominent ionic emission. CO_2^+ and OH^+ also emit in the wavelength region below 3700 \AA^0 .

The condensation observed by us is followed by an outstanding DE of 10th Jan. The CO^+ images taken with a CCD

by Dr. A'Hearn show the long straight ray structures in the same direction as the motion of the condensation region observed by us. Hence the rays can be regarded as having originated from this condensation. Hence the event observed by us appears to be similar to that of 11 April observations. It can therefore be inferred that the condensation mostly consists of ionic material. CO_2^+ and OH^+ emissions fall beyond the spectral sensitivity of the image intensifier used by us but not CO^+ (4260 \AA). These considerations lead to the conclusion that the emission from the condensation is mostly due to CO^+ ions.

(F) Ionization time scale

The excess ions in the condensation region must have been formed due to an anomalous ionization mechanism operating on a short time scale. If the time scale of the ionization mechanism is T and if the velocity of the ions produced is V then the maximum extent of the ionization region d can be expressed as;

$$d = VT$$

...3.12

Hence the upper limit of the ionization time scale can be expressed as $T < d/V$.

Assuming that the particles of the condensation region have the same velocity as determined from the motion of the feature i.e. ~ 37 km/s, the ionization time scale can be estimated as $\sim 1.1 \times 10^3$ s. However, even if the thermal velocities of the ions i.e. $\sim 5-7$ km/s are considered as the ion velocity within the condensation, the ionization time scale cannot exceed 10^4 s. Therefore it is concluded that the condensation region is the resultant of a rapid ionization process lasting for $\sim 10^3 - 10^4$ s.

3.3.3 Discussion

(A) The nuclear Activity of Comet Halley in early January 1986.

In early January 1986 Comet Halley was active and showed complex jet features almost every day including some northward jets and antisunward jets as shown in Fig. 3.24 (Larson et al 1987). Watanabe et al (1987) have reported the major jet activity in the coma of the comet particularly on 8th Jan 1986. Due to the jet activity the near nucleus contours are expected to be distorted. The ratio of the semimajor axis to the semiminor axis i.e. R_{AB} would then represent the degree of jet activity. Watanabe et al have plotted R_{AB} as a function of days in Dec. 1985 and Jan. 86, which is reproduced in Fig. 3.25. The maximum activity on

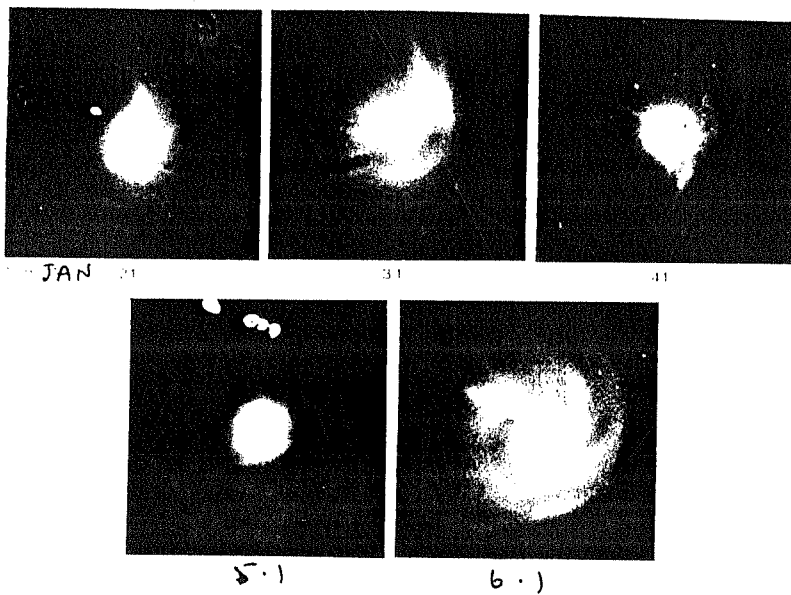


Figure 3.24. The jet activity of the inner coma of comet Halley in the early January 1986 (Larson et al 1986).

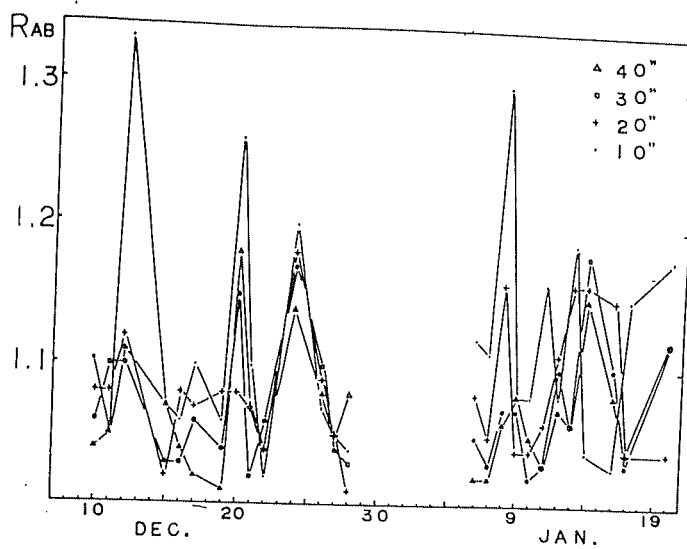
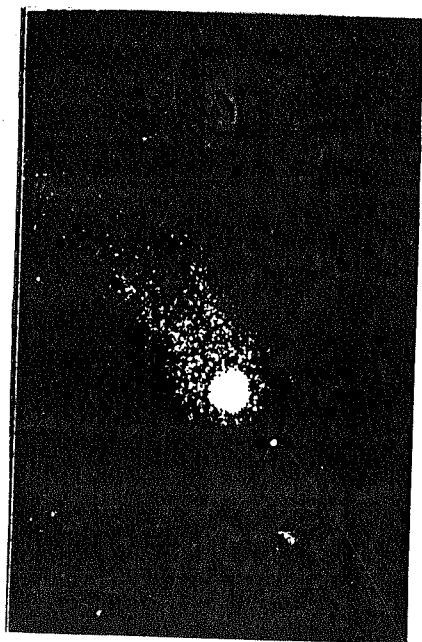


Figure 3.25. Day to day variation of the axial ratio R_{AB} which indicates the activity of jets (Watanabe et al 1987).

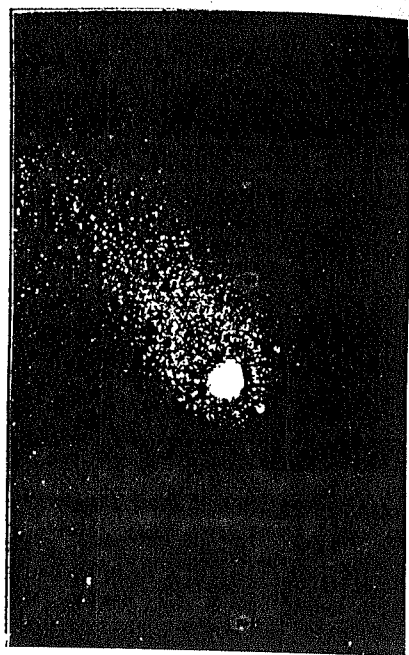
8th Jan 1986 can be clearly noticed from this diagram. In the first week of Jan 1986, the nuclear activity in the Comet Halley was episodic with cycles of roughly two days (Larson, 1986). The outburst recorded in optical CCD images on January 6.1 UT at Catalina Observatory show complex curved sunward jets and a bright linear antisolar jet. The IR observations on January 8.1 UT (Tokunaga 1986) show the brightness excess of $\sim 30\%$ compared to the neighbouring days. During these events an excess amount of the gas alongwith the dust must have been released. In order to estimate the production rate of CO released on 8.1 UT, Q_{CO} was plotted as a function of heliocentric distance. Assuming that during the outburst observed in IR, a similar amount of excess gas must have released, the production rate can be estimated as $Q_{CO} \sim 2.3 \times 10^{29}/s$.

The anisotropy created due to these outbursts, however cannot propagate to the outer coma region to a distance of $\sim 10^5$ km from the nucleus (Kolem et al 1986). Hence though the above discussion show that the comet was active during our observation, the observed condensation seems to be distinctly different from the jet activities or the nuclear outbursts. The ray structures observed in the ionic tail during this time are very strong. Fig. 3.26 show the strong ray structure in the CCD images of the comet taken in CO^+ emission. It is possible that the root of the ionic ray structure seen in Fig. 3.26 is the condensation region observed in the images obtained by us.

a.



b.



c.

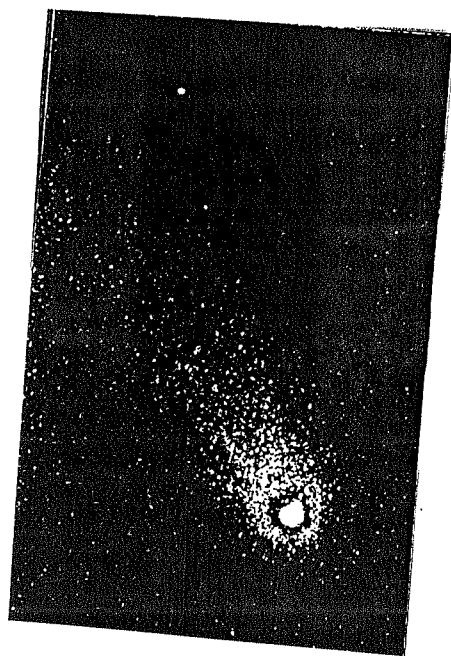


Figure 3.26. Strong ray structures in the wide field photographs of comet Halley taken in CO^+ emission band (Courtesy M.A'Hearn, University of Maryland, USA).
(a) Taken on 1986 Jan 8, $02^{\text{h}}:05^{\text{m}}$ UT
(b) Taken on 1986 Jan 8, $02^{\text{h}}:29^{\text{m}}$ UT
(c) Taken on 1986 Jan 8, $03^{\text{h}}:03^{\text{m}}$ UT.

(B) The source of ionization:

Identification of the correct ionization mechanism of the short time scale required (10^3 - 10^4 s) is a difficult task and often it is not uniquely determined for a single observation. For example the photoionization, solar wind charge exchange reactions, "internal" mechanisms (eg. Ip and Mendis 1975, 76) and gas phase reactions (Oppenheimer 1975) have been proposed and all are more or less still under consideration today, as possible ionization sources. Perhaps they all occur but in different regions of the coma. Table 3.10 gives various possible ionization mechanism for CO and their time scale. In this section the short time scale ionization mechanisms is discussed in order to investigate an appropriate ionization source producing the observed condensation.

B.1 Alfven mechanism:

It was proposed by Alfven (1954,60) that if the neutral gas and magnetized plasma are in a relative motion with a velocity exceeding a critical value V_c than an anomalous ionization mechanism only can reduce the speed of relative motion. In such cases, some hypothetical collisionless interaction between the plasma species triggers the energy flow to electrons via plasma waves, thereby ionizing the

TABLE 3.10

Time Scale of Possible Ionization Mechanism

<u>Mechanism</u>	<u>Time scale (sec)</u>	<u>Reference</u>
1. Photo ionization	$\sim 8 \times 10^5$	Fernandez et al (1983)
2. Charge exchange	$\sim 1.6 \times 10^6$	Ip (1985)
3. Electron impact	$\sim 4.5 \times 10^7 / n_e - 6.0 \times 10^7 / n_e$	Ip (1985)
4. Alfven Mechanism	$\sim 10^4 - 10^5$	Formisano et al (1982)
5. Discharge of crosstail current	$\sim 10^3 - 10^4$	Ip and Mendis (1975, 1976)
6. Magnetic field reconnection mechanism	$\sim 10^4$	Niedner Jr. (1980)
7. Gasphase reactions	$\sim 10^4$	Openheimer (1975)

$n_e \rightarrow$ Electron number density.

Fernandez J.A., Jockers K., 1983, Rep.Prog.Phys., 46, 665.

Ip W.H., 1985, Adv.Spac.Res., 5, 47.

Formisano V. et al., 1982, Planet.Space Sci., 30, 491.

Ip W.H. and Mendis D.A., 1975, Icarus, 26, 457.

Ip W.H. and Mendis D.A., 1976, Icarus, 29, 147.

Niedner Jr, 1980, Ap.J., 241, 1980

Openheimer, M., 1975, Ap.J., 196, 251.

neutrals. The critical velocity is given by,

$$v_c = \sqrt{\frac{Ze\phi}{m}}$$

$$= 12.6 \text{ km/s for CO}$$

...3.13

where m = mass of the neutrals, ϕ = ionization potential of the species under consideration. The detailed theory of critical velocity ionization (CVI) mechanism in the cometary atmosphere was developed by Formisano et al (1982). The collisionless transfer of the fraction of the particles kinetic energy for ionization of the neutrals is the crucial part of CVI process. The efficiency η is defined as,

$$v_c = \eta^{1/2} \sqrt{\frac{Ze\phi}{m}}$$

...3.14

Formisano et al (1982) have also shown that the efficiency of energy transfer in a varified gas turns out to be very low i.e. $\eta = 0.025$ and reaches a relative high value $\eta = 0.67$ only in a sufficiently dense gas. The Townsend condition for avalanch ionization of the gas, restricts the region of anamolous ionization of cometary gas to the inner part of the coma. The same authors have

also shown that for the production rate of $\sim 2 \times 10^{29}$ molecules/s the ionisation efficiency smoothly changes from 0.025 at a distance $> 3 \times 10^4$ km to the value 0.67 at $r < 1.5 \times 10^3$ km, where the approximation of dense gas is valid. As discussed earlier, the gas production rate for CO i.e. Q_{CO} during the time of our observations was $\sim 2.3 \times 10^{29}/s$.

Hence assuming that the ionization might have taken place within $\sim 10^4$ km from the nucleus, it is required that the relative velocity between the neutral and plasma component in this zone must exceed the critical velocity. The spacecraft measurements show that the plasma velocity within 4×10^4 km from the nucleus is mostly $\sim 3-7$ km/s (Schwenn R 1987) which is much lower than the critical velocity. Therefore it is unlikely that the mechanism can produce ionization in condensation region discussed here.

However, Galeev et al (1986) have shown that in the presence of the plasma instabilities of high growth rate, CIV mechanism can be effective, giving rise to some features observed by vega-2. A detailed analysis of the electron energy, magnetic field and the particle velocity data from several spacecrafts is still awaited for reaching a firm conclusion.

B.2 Current disruption:

It was proposed for the case of earth's magnetotail

that, a cross tail current system with a current sheet separating two tail regions of opposite magnetization should be present (Nees 1965). This process was also observed in the simulation experiments performed by Podgorny et al (1979). In the case of comet, if the structure of the magnetic field and the electric current in the cometary tail type I can be represented by an electric current circuit, the disruption of the cross-tail current system may lead to a current discharging through the cometary ionosphere and the dissipation of the magnetic energy stored in the tail. These are called the "cometary aurora" events, which might be the source of hypothetical internal ionization sources as advocated by Wurm (1963). It is also pointed out that even if only 25% of the cross tail current of energetic electrons ($\sim 1-10$ Kev) were to close through the cometary head it could cause rapid ionization in the inner coma with a time scale of, as small as $\sim 5 \times 10^3$ s.

As proposed by Ip et al (1976), the model cross-tail current system with an electric field E acting across the tail aligned magnetic field \vec{B}_t , can be represented as in Fig. 3.27. If the tail-aligned field is \vec{B}_t , the current density j in the current sheet is given by the Maxwellian relation

$$\vec{\nabla} \times \vec{B}_t = \frac{4 \pi}{c} j$$

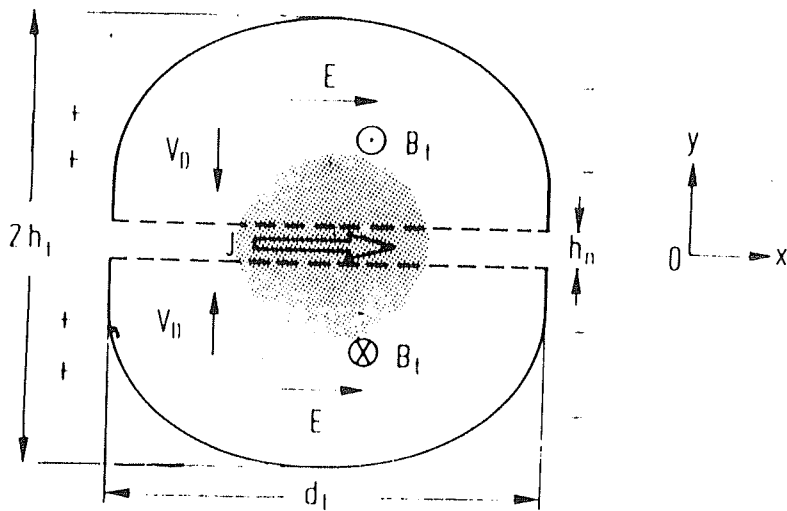


Figure 3.27. The model of cross tail current system with an electric field E acting across the tail aligned magnetic field. The resulting $\vec{J} \times \vec{B}$ force will act in such a way that the ion tail plasma are accelerated tail wards B_t . (Ip et al 1982).

under steady conditions. The sheet current density integrated through the thickness of the current sheet 'Ln' then will be,

$$j_s = \frac{CBt}{4}$$

...3.16

and the total cross tail current flowing through the central current sheet may be estimated to be,

$$I_t = \frac{C}{4\pi} B_t L_t$$

...3.17a

where L_t is the length of the ion tail. If the total cross tail current I_t is expressed in Amperes, the tail-aligned magnetic field B_t in gamma (1 gamma = 10^{-8} Gauss) and the total length of the tail carrying the current L_t in km, then

$$I_t = 1.6 B_t L_t$$

...3.17b

The total length of the plasma tail on 8th Jan 1986 estimated from Fig. 2.28 in $L_t \sim 10^7$ km. Taking $B_t \sim 80$ V, which is a typical value obtained from spacecraft measurements, the total current is $\sim 1.3 \times 10^9$ A.

When the disruption of the tail current estimated above takes place, there could be field aligned current discharging through the cometary head as shown in Fig. 3.29. Such transient effects are expected to accelerate the charged particles and consequently energize them to Alfvén energy of a few Kev. Under these circumstances the effective (anomalous) resistivity will increase well above the classical value as shown experimentally by Hamberger et al (1970). This would lead to instabilities in a finite resistivity current sheet pinch. The detailed calculations of this process is quite uncertain, owing to the unavailability of the precise measurement of magnetic field, temperature of electrons and ions and number density at the place of the formation of these structures. However, Morison and Mendis (1978) have shown with the typical values, that these processes can lead to the observable condensation structures.

The time scale of ionization due to such disruption can be estimated as described by Ip (1975). If the ionization took place within a region of 10^3 km in the inner coma region, the relevant ionization time scale can be expressed as,

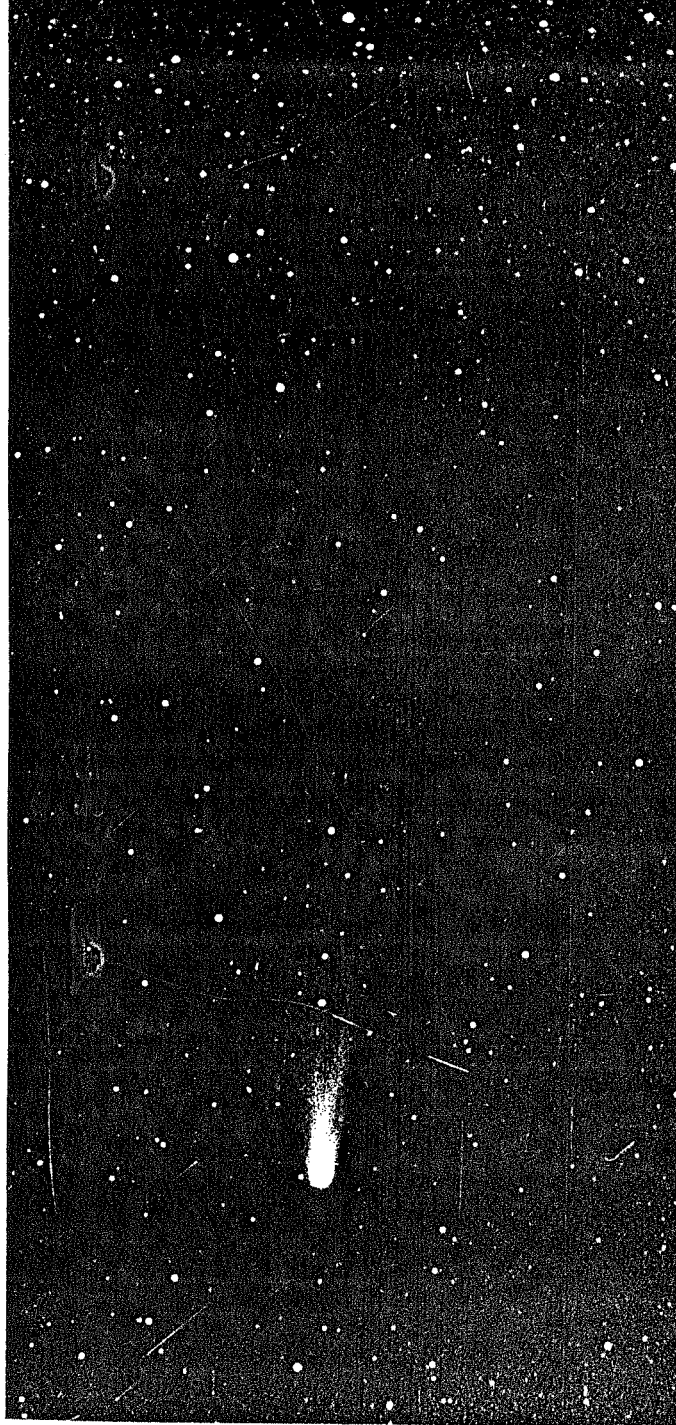


Figure 3.28. Wide field photograph of comet Halley taken on 1986 Jan 8. The length of the tail estimated is $\sim 10^7$ km.

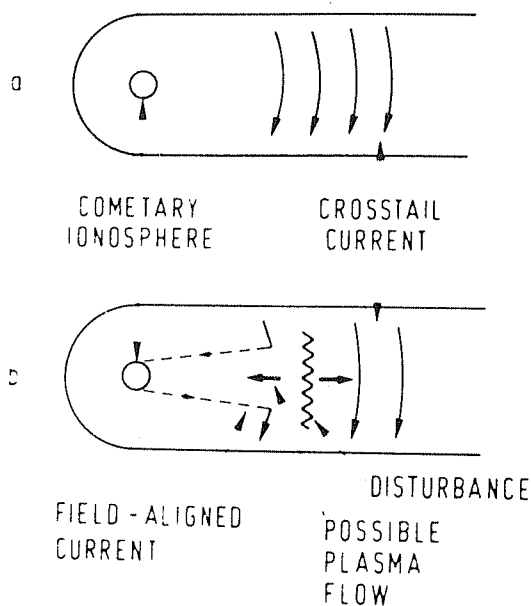


Figure 3.29. Schematic drawing of the cometary sub "storm" circuit (a) Flowing of the cross tail current across the current sheet is steady. (b) partial interruption of the cross tail current produces a tail aligned current discharging through the cometary ionosphere. It has been suggested that dissipation of the magnetic energy stored in the ion tail in this way may provide the ionization source for the internal ionization mechanism advocated by Wurm (1963).

$$t_i \approx \frac{1.6 \times 10^7}{I_c x f_i x \sigma_i}$$

Where f_i = factor for multiple ionization $\sim 10-20$...3.18

σ_i = electron ionization crosssection = 5×10^{-17}
cm²

I_c = fraction of the total current I_t , which
is discharged for the tail disruption.

Theoretically, Ip and Axford (1982) has shown that for the magnetic field configuration given in Fig. 3.30, the $\vec{J} \times \vec{B}$ force in the 'o' type loop would tend to focus the cometary plasma in this region, whereas the cometary ion in the vicinity of the x-point would be dispersed. This would lead to the growth of condensation of ionized material in the ion tail.

However, the discussion so far, clearly show the status of a complete understanding of the formation mechanism of such structures. There exist several potential physical mechanisms which can give rise to the observed ionic condensation regions at several parts of the comet, yet the measurements are not adequate to point to a particular physical processes for a given feature. Using the in-situ probes, the chance of obtaining the relevant parameters of these features is low. Hence ground based and well

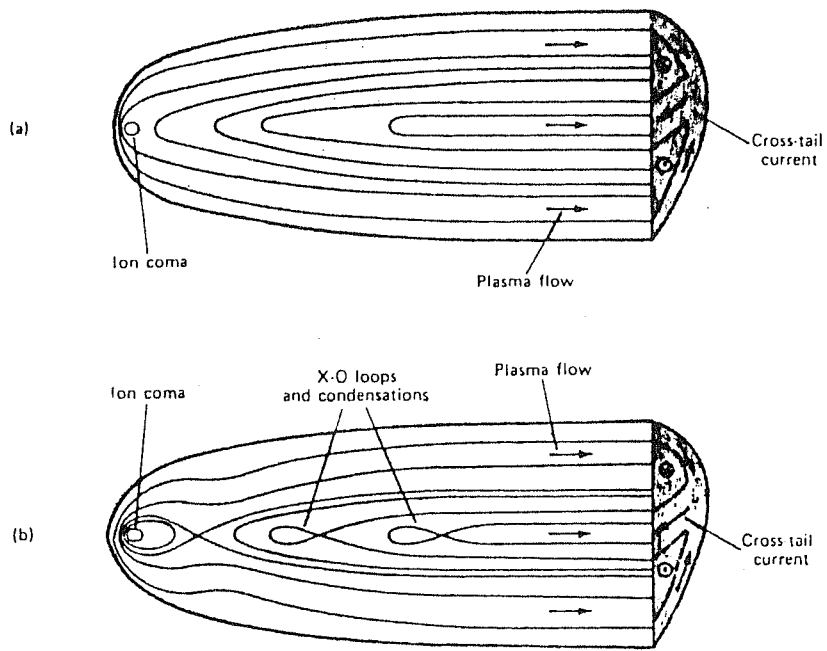


Figure 3.30. Possible effect of the reconfiguration of the magnetic fields in the ion tail. (a) The quiet time structure is shown with the cross tail current without inhomogeneities in the cross tail current sheet. (b) Break up of the current sheet which on one hand would lead to a field aligned current discharging into the ionosphere and on the other, to the formation of X and O type loops would perhaps result in the enhancement of plasma density in the vicinity of the O type loops (Ip et al 1982).

coordinated specialized experiments, mostly with high resolution spectroscopy are of vital importance in this case. The author, therefore, strongly feels the need for such a study in a future active comet.

(C) The acceleration of the condensation:

It is conjectured that the condensation was created nearer to the nucleus as a result of the discharge of cross tail current system followed by the nuclear outburst at 8.1 UT. Assuming that the plasma condensation region has moved in the downstream direction with least lateral diffusion, it is possible to determine the acceleration of the condensation. To determine the mean acceleration 'a' of the plasma in the condensation, we assume that it had an initial velocity $V_0 \sim 1 \text{ km/s}$ at $t_0 \sim 8.1 \text{ UT}$. The condensation reached at $S = 2.5 \times 10^5 \text{ km}$ after 12.365 hours. In this case the average acceleration needed for the transport of the plasma in the condensation region, from the near nucleus region to the region of observation is,

$$a = \frac{2 (S - V_0(t_1 - t_2))}{(t_1 - t_2)^2} \sim 25 \text{ cm/s}^2 \quad \dots 3.19$$

where $t_1 - t_2 = 12.365 \text{ hours}$ (the time taken for the plasma to move from near nucleus region to the region of

observation).

The accelerations of this magnitude are commonly encountered in cometary plasma and several theoretical mechanisms are developed to explain them as discussed in chapter 1. The exact mechanism which might have given rise to the observed acceleration in the present case is not known. However, in what follows, we will outline a simple mechanism accounting for the observed acceleration.

Ip (1980) suggested $\vec{J} \times \vec{B}$ force in the comets due to the field lines towards the anti-sun direction may produce an acceleration of about $\sim 10\text{-}20 \text{ cms}^{-2}$. In his model, it is assumed that ion-tail system is two-dimensional with Z, pointing in the axial direction and the magnetic field B can be described by having a constant X-component,

$$B_x = \text{Cont}$$

...3.20

and a Z-component

$$B_z = B_z(\infty) \tanh \left(x/L_n \right)$$

...3.21

where L_n is the width of the current sheet. These equations satisfies the conditions that $B_z \rightarrow 0$ as $x \rightarrow 0$ and that $B_z \rightarrow B_z(\infty)$ as $x \rightarrow \infty$ (Tandberg-Hanssen 1924).

If the cometary plasma is further assumed to be isothermal and if there is pressure equilibrium in the x -direction, then,

$$\frac{dp}{dx} = - \frac{B_z}{4\pi KT} \left[\frac{dB_z}{dx} - \frac{dB_x}{dz} \right] \quad \dots 3.22$$

$$\text{and } f = \frac{m_i B_z (\infty)^2}{8\pi KT} \left[1 - \tanh^2 \left(\frac{x}{L_n} \right) \right] \quad \dots 3.23$$

where K is the Boltzmann constant, T the plasma temperature, and m_i the ion mass. Hence the Lorentz force $\vec{J} \times \vec{B}$ can be written as,

$$\begin{aligned} \vec{J} \times \vec{B} &= \frac{1}{4\pi} B_x \frac{d}{dx} (B_z) \\ &= \frac{B_x B_z (\infty)}{4\pi L_n} \left[1 - \tanh^2 \left(\frac{x}{L_n} \right) \right] \quad \dots 3.24 \end{aligned}$$

and the acceleration due to the curvature force would be,

$$a = 2 \left(\frac{B_x}{B_z (\infty)} \right) \left(\frac{KT}{m_i} \right) \left(\frac{1}{L_n} \right) \quad \dots 3.25$$

The Lorentz acceleration is therefore dependent on the ratio of the magnetic field component normal to and parallel to the current sheet, as well as the thermal pressure KT and the width of the cross tail current sheet. In the present case we use the values for B_x from spacecraft measurement data i.e. ~ 10 , and $B_z \sim 10$. The same measurements show $L_x \sim 10^4$ and $T \sim 4 \times 10^2$ K (Galeev A. 1987). Taking these values from eqn (3.25) it follows that

$$a = 24 \text{ cm/s}^2$$

Since this value is close to the observed value, such a mechanism can be responsible for the acceleration of the plasma in the condensation region.

However, once the condensation region reaches the outer coma region, its motion would no longer be governed by the mechanism described above. At this region the solar wind conditions in the vicinity of comet would mostly control its motion, which is discussed in the following section.

3.3.4 Relation of the observed condensation region with the tail activity

As discussed earlier, several of the ionic features in the tail are thought to be generated within the coma region.

Hence an investigation was carried out to identify the potential tail features (in the wide field photographs taken following our observations) which might be the resultant of the condensation region.

A dramatic disconnection event was observed at a distance of 2×10^6 km from the nucleus on January 10.375 UT ^(Fig. 3.31). The front edge of the disconnected tail was seen to move in the north side of the tail in which the condensation was observed. Table 3.11 summarizes the observations of the Comet Halley showing the DE. The observed distance of the front edge of the DE was plotted against the time of the observation. The front between two observations was determined taking a pair of data points at a time. Fig. 3.32 and 3.33 show respectively the position of DE front and its velocity as a function of time. From Fig. 3.33 it is clear that the motion of the DE front was not smooth. Such motions of the plasma feature leading to March 20 and April 11 DE are also deduced (Brosius et al. 1987). These observed variability in velocity and hence in acceleration are due to the manifestation of different forces (e.g. Lorentz force, solar wind dynamic pressure force) dominating the disconnected tail motions at different distances from the nucleus. It is also expected that these individual forces vary with position and/or time. The velocity of the condensation region observed by us is 37 ± 3 km/s in the antisolar direction. If it had moved with the same velocity

TABLE 3.11

Summary of the observations on the motion of the front edge of
the disconnected tail on 10 January 1986

<u>S.No.</u>	<u>Time (UT)</u>	<u>Separation of the DE front ($\times 10^6$ km)</u>	<u>Average velocity (Km/s)</u>
1.	10.375	1.8	
2.	10.434	1.9	19.6
3.	10.645	3.0	60.3
4.	10.688	3.4	107.7
5.	10.740	3.5	22.3
6.	10.802	4.0	93.3
7.	11.052	5.3	60.2
8.	11.416	7.6	73.1

These measurements have been taken from various published wide
angle comet photograph taken on the time given in column 1.

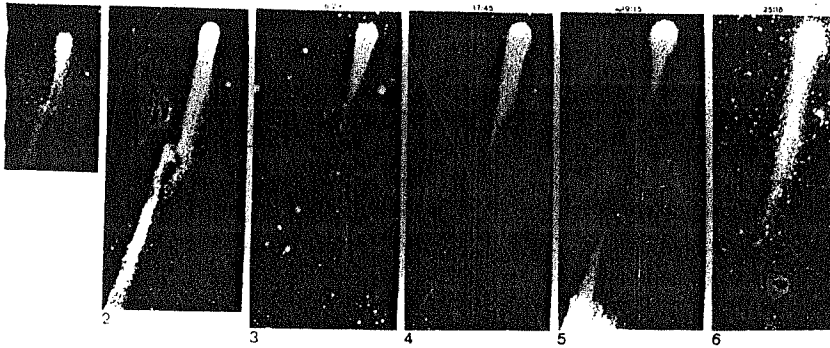


Figure 3.31. The wide field photographs of comet Halley taken on 10th Jan 1986, showing a dramatic DE.

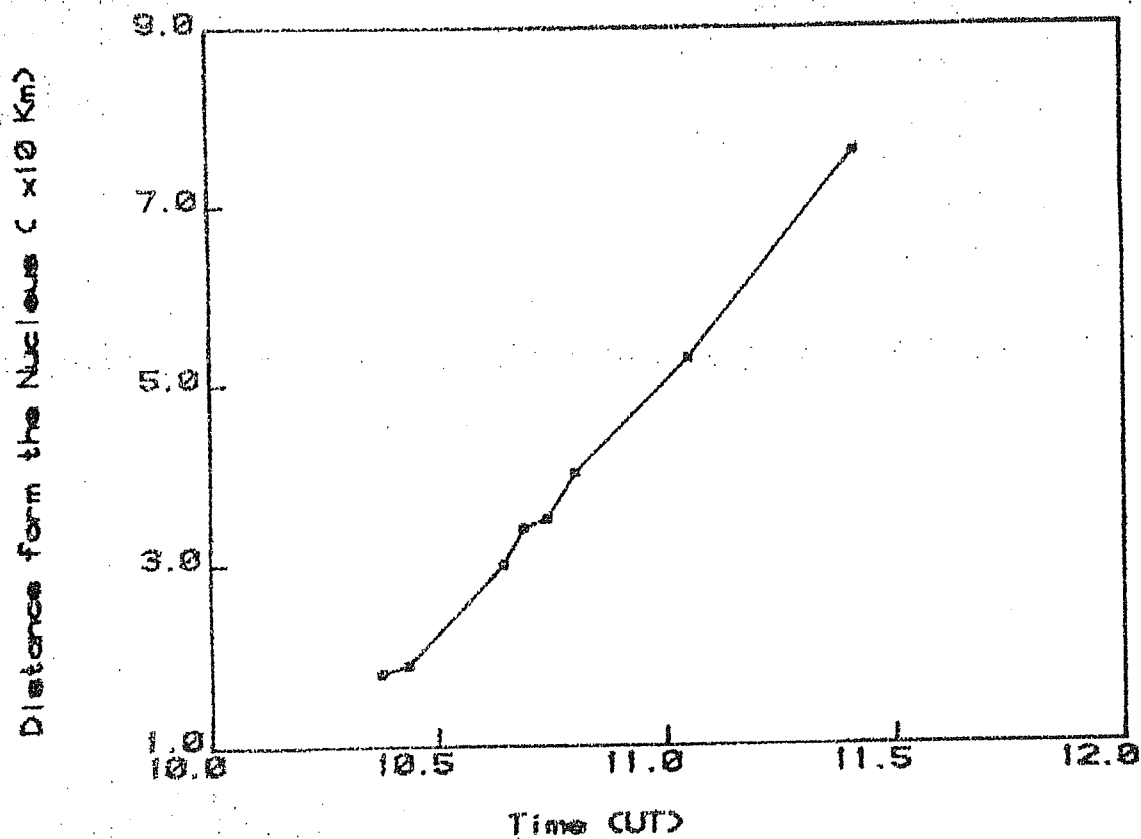


Figure 3.32. Plot of position of DE front as a function of time on 10th Jan 1986.

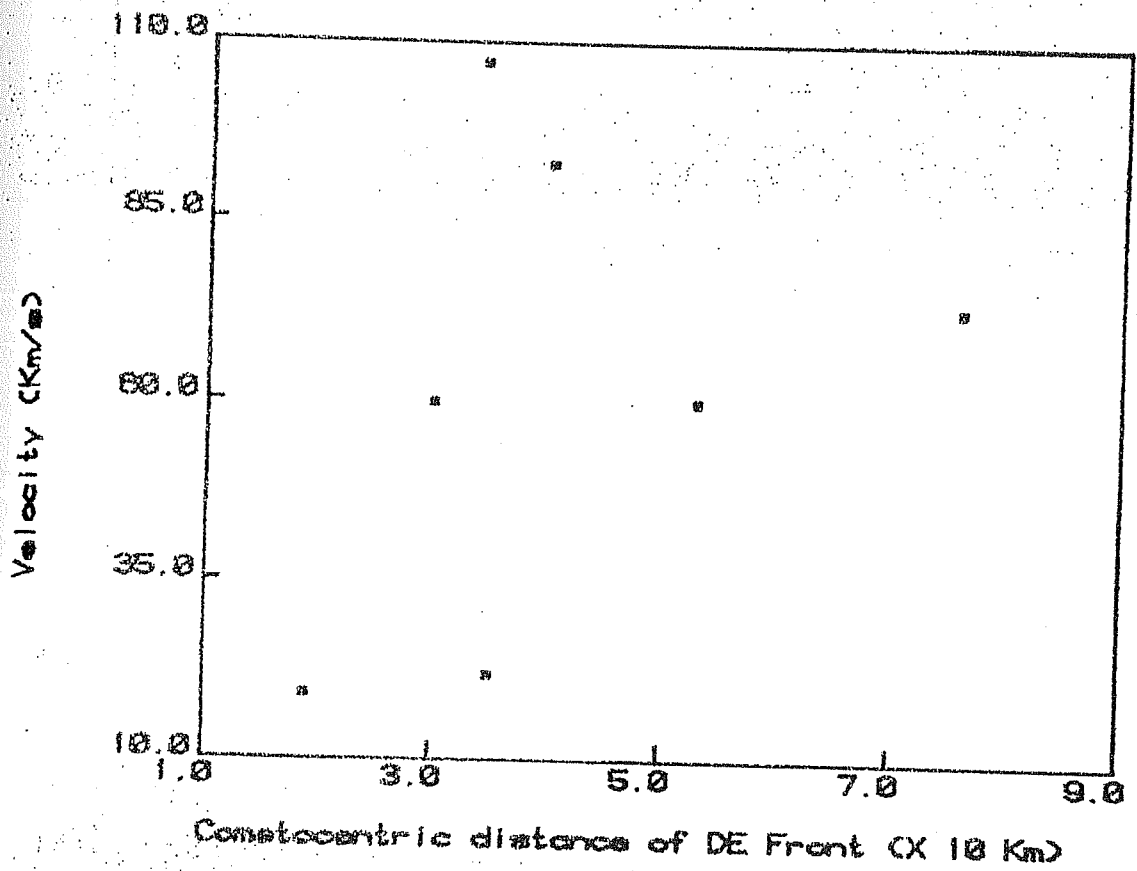


Figure 3.33. Plot of velocity of DE front as a function of time on 10th Jan 1986.

in the anti-sun direction, it would have reached a distance of $\sim 5.6 \times 10^6$ km on January 10.375 UT. This is much larger than the distance at which the DE front was observed. However, the preceding discussion shows that the motion of such features is not smooth in the anti-solar direction (Fig. 3.33). Therefore if we assume that such a random motion did exist during the period January 8.632 to 10.375 UT, it would have caused an effective deceleration in the anti-solar directions. The observations taken at Yunna Observatory, China following our observations at January 8.93800 has been kindly supplied by Dr. Qin. The wide field photographs taken by them show a Z-shaped thurst at the place about 0.2° away from the nucleus, which moved further to the place 1.3° on January 9.92407. The velocity required for the condensation observed at 8.638 to reach the position of the Z-shaped thurst region at 8.938 UT is ~ 16 km/s. In a simple model called "ink model" Jockers (1985) has described such features emerging as a result of the interaction of solar wind with the slow moving tail features such as condensations. Therefore it is reasonable to expect that the condensation observed by us has led to the dramatic DE of 9-10th January 1986. Hence our observation supports the scenario that the dramatic disconnection events in the ionic tail originate deep inside the coma with velocities of $\sim 20-40$ km/s.

3.3.5 Summary and Conclusions:

1) The imaging observations of Comet Halley on 8th January 1980, show a condensation region to the north of the tailward direction of the coma. The analysis shows that the condensation was moving at a velocity of $\sim 37 \pm 4$ km/s in the down stream direction. The investigation on wavelength of the emission shows that the condensation was strong in CO^+ ionic emission.

2) From the estimation of the time scale of ionization it is concluded that the ionization of the material in the condensation region was rapid, in a time scale of $\sim 10^3 - 10^4$ s.

3) Investigation of several processes of ionization mechanism shows that the discharge of crosstail electric currents, passing through the neutral sheet in the near nucleus region is the most probable mechanism for producing the condensation. Hence it is suggested that the condensation was produced at 8.1 UT following a major outburst and accelerated in the down stream direction with an acceleration of $\sim 25 \text{ cm/s}^2$ by the $\vec{J} \times \vec{B}$ force due to the cometary magnetic field.

4) This feature, most probably is the precursor of the dramatic DE observed on 10th January 1986.

5) These observations therefore support the contention that most of the plasma features observed in the tail have originated in the coma with a initial velocity of $\sim 20-40$ km/s.

CHAPTER 4

STUDY OF THE NEUTRALS

4.1 Introduction

Study of the neutral gaseous component in the coma of a comet is a very important aspect of cometary physics. Observationally this comprises of carefully measuring the emission line intensities of various neutral species and their outflow velocities at various positions in the coma and thence the scale lengths, life times of the species etc. This leads to the understanding the nature of the parent molecule, which might have originated from the nucleus during evaporation process. Knowledge of nuclear constituent in turn, has vital implications for the mechanism of formation of solar system.

The ground based and space craft observations of Comet Halley (1982i) clearly established that H_2O is the most abundant molecule. Observations by Fourier Transform spectrometer on Comet Halley from Kuiper Airborne Observatory (KAO) by Mumma et al (1986) showed sharp emission lines of H_2O in ν_3 band. Using a standard outflow model they derived a large water production rate $Q(H_2O) \sim$

1.7×10^{29} mol/s for their 24 December 1985 spectra. Post perihelion observations by Larson et al (1986) and Weaver et al (1986) also support this finding. The insitu measurements by Vega and Giotto spacecraft have also established the dominance of H_2O molecule in the coma. Vega results lead to $Q(H_2O) \sim 1.3 \times 10^{30}$ mol/s (Sagdeev et al 1986) and Giotto results showed $Q_{H_2O} \sim 5.5 \times 10^{29}$ mol/s. Further the $Ly \alpha$ measurements from rockets inferred the production rates of $\sim 3.6 \times 10^{29}$ and 1.9×10^{30} on 1 and 29 Jan 1986 (Craven et al 1986). Similar inferences are also derived by other authors (Kaneda et al 1986, McCoy et al (1986). Earlier the $Ly \alpha$ study of several other comets such as Comet Kohoutek, Bennett and West showed that H_2O is a major constituent of comets.

While the advances in the cometary physics due to space probes and aircraft based instrumentation have been impressive, from the point of view of sustained observations with a large heliocentric distance coverage, ground based spectroscopic observations have been equally important. The ground based measurements of $H \alpha$ and [OI] 6300 emission can be of great importance. However, the strength of $H \alpha$ emission is several times weaker in the coma compared to [OI] emission. Further, in the following discussion it will be clear that H_2O is the only parent molecule for [OI] 6300 emission. High resolution measurements of [OI] 6300 emission from Comet Halley 1982i were carried out by several authors (Magee et al 1987, Roseler et al 1986, Kerr et al 1987, Debi

Prasad et al 1988) by using sophisticated Fabry-Perot spectrometers. Similar measurements were earlier carried out for the comet Kohoutek (Huppler et al., 1975). However, [OI] 6300 measurements were also carried out using other techniques. These are extensively discussed by Spinrad (1982). The main difficulty in the measurement of neutral oxygen 6300 Å emission is the contamination due to NH_2 emission lines. High resolution spectroscopy permits to separate spectrally the NH_2 lines from [OI] thereby providing uncontaminated [OI] for qualitative studies.

The first section of this chapter describes the line strength and outflow velocity measurement of [OI] carried out by the author during 1985-86 apparition of Comet Halley. The correlation study of [OI] 6300 emission line with other characteristic cometary parameters is also presented in this section.

Another major neutral component in the cometary atmosphere is the carbon bearing species. In situ measurements of Comet Halley established CO_2 as the next most abundant molecule after water (Reinhard 1986). Apart from the continuum, the visible part of the cometary spectrum is dominated by emissions from carbon bearing compounds such as C_2 , C_3 , CH_4 , etc (Festao 1986). C_2 band emission is the strongest in the cometary visible spectrum. The three bands of C_2 emission in visible spectrum were also the first identified emissions in cometary atmosphere

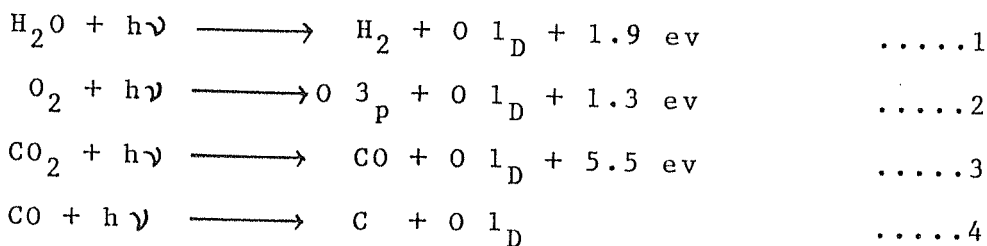
in 1864 by Donati. Eventhough this is the oldest identified spectrum, several important aspects of its formation still remain to be understood even today. For example eventhough the intensity distribution among various vibrational levels are explained by Krishnaswami and O' Dell (1977), by statistical equilibrium calculations, the recent insitu measurements of the spatial variation in the triplet/singlet ratios (Vasynek 1988) show that the statistical equilibrium may not be valid in the inner coma region where the collisions are high. The spatial variation of C_2 (Swan band) intensity was used to determine the C_2 scale length with simple Haser model (Combi 1978, Bappu et al., 1979). Several recent observations indicated that this may not be the fact. The central deficiency of C_2 observed in the case of IRAS-ARAKI-ALCOCK during 10th May 1983 (Oliveresen et al., 1985) is an example of such deviation. In summary, it can be stated that the problem of C_2 is yet to be understood completely. In this contest therefore it is useful to determine several physical parameters such as outflow velocity, temperature and density etc.

In the present work the interferograms in the C_2 (0-0) Swan band were obtained on three occasions during the pre and post perihelion period of Comet Halley. In section 2 of this chapter the analysis of the interferogram efforts to deduce velocity information is presented.

4.2 [OI] 6300 Emission Line Study

The forbidden transition of [OI] at 6300 Å line in cometary spectra was first established by Swings and Greenstein (1958) from the high resolution spectra of Comet Mrkos and later in Comet Seki. Subsequently the re-examination of several low dispersion spectra of comets by Swings (1962) established the presence of cometary [OI] line on many occasions.

The metastable energy state configuration giving rise to the 6300 Å emission is shown in Fig. 4.1. Table 4.1a summarizes the transition probabilities and lifetime of several transitions. Since the transition probability is low, these lines cannot be produced by the fluorescence mechanism. The collisional excitation is also inadequate for explaining the observed line emissions. Therefore it is presumed that these lines arise due to the photodissociation of some parent molecules in an excited singlet state 1_D from which it decays to the ground state 3_P . 1_D states can be generated by the following processes,



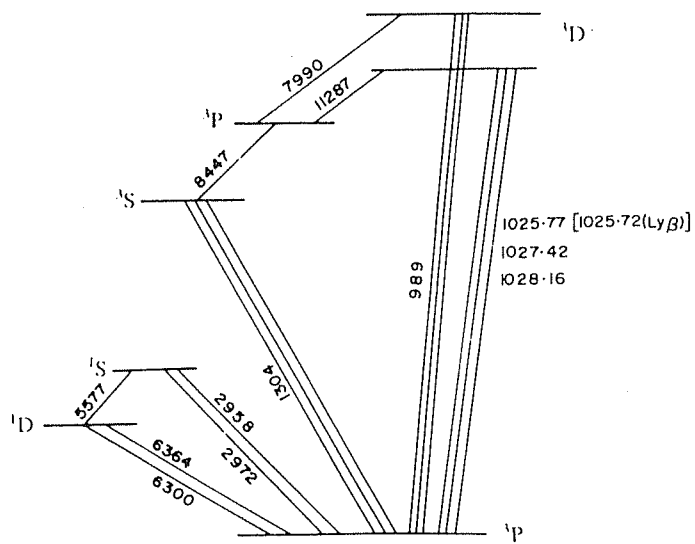


Figure 4.1. Energy level diagram of oxygen atom showing various transitions.

TABLE 41 α .

FORBIDDEN TRANSITIONS OF O(I)

Transition	Wavelength	Probability (sec ⁻¹)	Lifetime (sec)
$^3P_2 - ^1S_0$	2958.4 Å	3.7×10^{-4}	2.70×10^3
$^3P_1 - ^1S_0$	2972.3 Å	6.7×10^{-4}	14.9
$^1D_2 - ^1S_0$	5577.35 Å	1.34	0.75
$^3P_2 - ^1D_2$	6300.2 Å	5.10×10^{-3}	1.96×10^2
$^3P_1 - ^1D_1$	6363.9 Å	1.64×10^{-3}	6.10×10^2
$^3P_1 - ^3P_2$	63 μ m	8.95×10^{-3}	1.1×10^4
$^3P_0 - ^3P_1$	147 μ m	1.70×10^{-2}	5.9×10^4

The dominant contribution for producing $O\ 1_D$ state comes from the photodissociation of water, about 10% of the water molecule become excited oxygen atoms. 90% of these [OI] atoms decay down to the 1_D state (Festou and Feldman 1981, Feldman 1983), which then radiates the red lines at $\lambda\ 6300, 6363\ \text{\AA}$. The contribution due to the other parent molecules are found to be negligible. For example CO_2 and CO, have also been considered as the source for extended [OI] 6300 emission through the photodissociation reactions 3 and 4. The theoretical branching ratio for reaction 3 is 46% and reaction 4 is 5% (Levine 1985). Using the measured relative abundances of CO (Woods et al 1986) and CO_2 (Krankowsky D et al 1986) and assuming the scale lengths $CO = 1.3 \times 10^6$ km (1 AU) and $CO_2 = 5 \times 10^5$ km (1 AU) (Levine 1985) Roesler et al (1987) found that within the range of $\sim 10^5$ km from the nucleus [OI] 6300 emission from photodissociation of CO and/or CO_2 is negligible. The Giotto and rocket measurements of CO yields an even smaller relative abundance (Woods et al 1986; Eberhardt et al 1986). Fig. 4.2 show a model calculation for the relative importance of each $O\ 1_D$ source as a function of distance from the nucleus at $R_u = 1.7$ AU. It is clear from the figure that the dominant source of $O\ 1_D$ atoms in the inner coma region (where the 6300 emission is strong enough to be detected above the continuum) is H_2O .

The $O\ 1_D$ doublet state emits $6300\ \text{\AA}$ and $6363\ \text{\AA}$ with

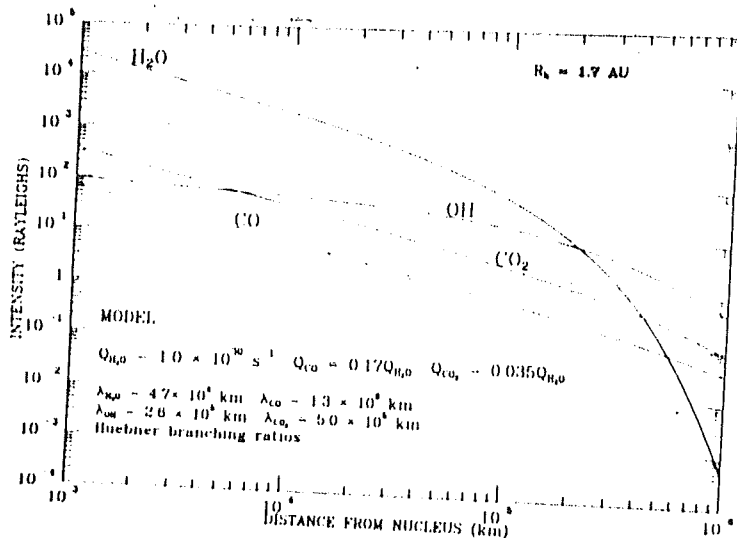
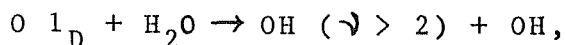


Figure 4.2. Model calculation of relative intensities of [OI] 6300 Å emission from H_2O , OH, CO, CO_2 source molecules. λ = Scale length of various parent molecules used in the model. Scale lengths are the values at 1 AU. R_h = comet's heliocentric distance. Q = production rates (Roesler et al 1987).

the transition probabilities of $5 \times 10^{-3}/s$ and $1.64 \times 10^{-3}/s$ respectively. It is observed that the strength of 6363.87 Å⁰ line is ~ 30% of 6300 Å⁰ line because of the quenching processes involved in the cometary atmosphere. However, the details of the quenching processes are not known. One way in which O 1_D may be collisionally quenched in the inner coma is,



$$\alpha = 2.1 \times 10^{-10} \text{ cm}^3/s$$

However, the quenching scale radius given by $N\alpha\tau = 1$ is ~ 600-1000 km for a typical Halley like comet.

At low resolution spectra [OI] emission is always limited by NH₂ blending. Arpigny et al (1987a,b) have shown that, there exist appreciable variations not only in the NH₂/[OI] ratio, but also in the relative intensities of the various NH₂ emissions themselves. They have therefore concluded that the abundance of excited oxygen atoms evaluated from the forbidden red lines applying the corrections for NH₂ blend measured from other lines, are liable to errors of 50 to 100% in some cases, even if other sources of considerable uncertainties (solar ultraviolet flux, photodissociation coefficients, branching ratios) are known to exist in the same context.

The use of high-resolution spectroscopic techniques in

the recent days could overcome the blending problem and also separate the emission from terrestrial airglow effects. The high-resolution [OI] observations made earlier with Fabry-Perot spectrometers are summarized in table 4.1b. Fig. 3 shows the variation of [OI] 6300 \AA^0 emission as a function of heliocentric distance for several comets.

4.2.1 Observation of [OI] 6300 emission of comet Halley with scanning Fabry-Perot spectrometer

(A) Observations

At the time of closest approach to earth of Comet Halley in April 1986, a high resolution piezoelectrically controlled scanning Fabry-Perot spectrometer was coupled with a 1 m telescope to observe some of the optical emission lines of the coma. The experiment was initially aimed at studying the spatial distribution of oxygen and hydrogen atoms and their velocity fields through high spatial and spectral resolution observations of [OI] 6300 \AA^0 and $\text{H}\alpha$ 6563 \AA^0 emissions and hence the formation and dynamics of these atoms in the cometary atmosphere. However, the faintness of the line emissions did not permit the study of spatial distributions. Even in the inner coma $\text{H}\alpha$ was barely detectable, [OI] 6300 \AA^0 emission however was well observed and spectrally well separated from its NH_2 blending at the resolution of $\lambda/\delta\lambda \sim 6 \times 10^4$.

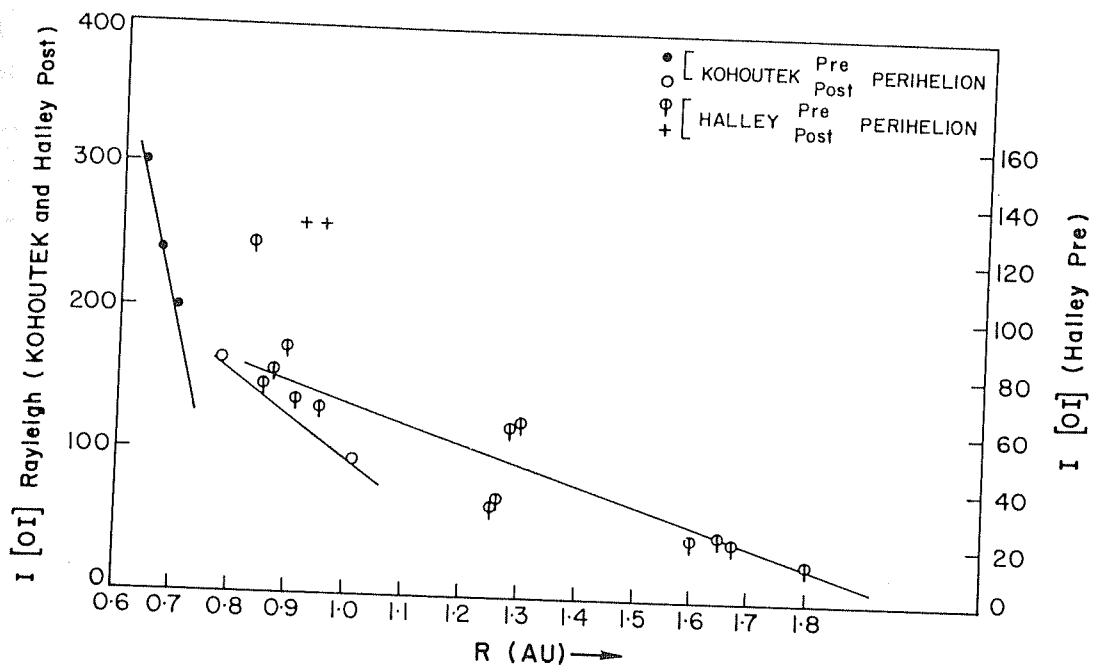


Figure 4.3. Variation of [OI] 6300 Å emission as a function of heliocentric distance for several comets.

TABLE 4.1 b.

[OI] 6300 Å observations of comets with Fabry-Perot

Comet	Heliocentric distance (R) in AU	Instrument	Comments	Reference
Kohoutek	0.65-1.08	Field of view = 4" Resolution = 40,000	<ol style="list-style-type: none"> 1. Flux = $200 \pm 100 R$ at 0.7 AU 2. Flux decreases as $R^{-4.2}$ (Fig.3) 3. Line width 2.7 km/s, wider than telluric emission. 4. Surface brightness of the coma follows a power law τ (τ = cometo-centric distance) 	Huppler et al. (1975)
Halley	1.98	Field of view = 14" Resolution = 30,000-200,000	<p>Cometary line width 3.05 ± 0.11 km/s. Telluric line width 1.6 ± 0.1 km/s.</p>	Roesler et al. (1985)
	0.83-2	Field of view $\approx 7'$	Flux varies as $R^{-0.4}$ (Fig.3)	Scherb et al. (1985)
	0.89	Field of view $\approx 5.9'$ Resolution: 30,000	<ol style="list-style-type: none"> 1. Flux $\approx 260 R$ 2. The surface brightness show a decrease of flux by a factor of 2 at 6' away from the head. 3. Line widths 3.9 ± 1.5 km/s at 0.92 AU 7.4 ± 2.2 km/s at 0.94 AU 	Keer et al. (1987)
	1.35	Field of view $\approx 50''$ Resolution: 45,000	<ol style="list-style-type: none"> 1. Flux = $150 \pm 40 R$ 2. Line width: 3.5 km/s. 	Present work

The spectrometer used for the present work is described in detail in section 4 of chapter 2. The aperture used at the focal plane of the telescope corresponds to 50 arcsec in the sky (~ 1500 km at comet). The free spectral range of the spectrometer was 4.342 \AA at 6563 \AA and 4.001 \AA at 6300 \AA corresponding to $496 \mu\text{m}$ spacer value. This large FSR played a crucial role in avoiding the interorder mixing of the spectral features. In other words, if the free spectral range had been 1.684 \AA less than the present value, than n th order of $[\text{OI}] 6300 \text{ \AA}$ would have overlapped with the $(n+1)$ th order of NH_2 at $\lambda = 6298.62$ emission, A careful choice of free spectral range is therefore essential for the experiments of this kind. The guiding errors during these observations were well within the seeing limit $\sim 2''\text{--}3''$. The flux calibration at $\text{H}\alpha$ was obtained by observing the trapezium region of Orion nebula (M 42) with the same aperture. Table 4.2 gives the cometary parameters during our observations. The journal of observations is given in table 4.3.

(B) $[\text{OI}]$ results

The Fig. 4.4 is the spectral scan of about one free spectral range taken at 6300 \AA with field of view centered on the nucleus. Since the red airglow 6300 emission was not clearly recorded in our scan, the identification of the spectral features was not straightforward. Assuming that the two well defined principal features separated by the free

TABLE 4.2

Cometary parameters during observations

Date	Δ AU	$\dot{\Delta}$ km/s	R AU	\dot{R} Km/s
10.4.86	0.42	0.03	1.32	26.51
13.4.86	0.42	13.35	1.36	26.47
14.4.86	0.43	17.59	1.38	26.43
15.4.86	0.44	21.94	1.39	26.38

Δ and R are geocentric and heliocentric distances respectively.

TABLE 4.3

Journal of scanning Fabry-Perot observations

<u>Date UT</u>	<u>Object</u>	<u>Filter</u>	<u>Remarks</u>
10.554	Orion	6563/3 Å	
10.600	Comet Halley	6563/3A°	(Several scans in each filter were taken)
		6300/5A°	
		5890/30A°	
13.800	Orion		
	NGC 2440	6563/3A°	
	M8		
13.833	Comet Halley	6300/5A°	
to 13.880			
14.855	Comet Halley	6300/5A°	
15.850	Comet Halley	6300/5A°	
		6563/3A°	

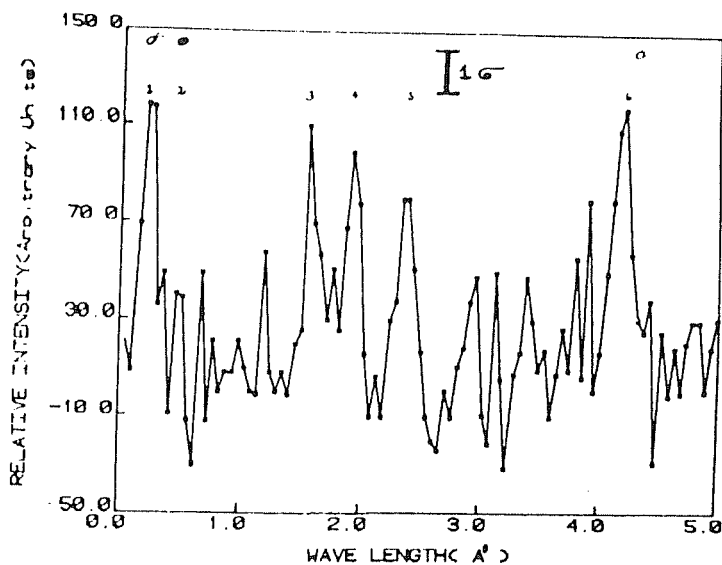


Figure 4.4. Cometary [OI] 6300 Å and NH₂ lines obtained using the piezo-electrically scanning spectrometer on 13 April 1986. Features (1) cometary [OI] 6300 Å (2) Expected position of airglow [OI] emission, (3) NH₂ 6299.004 Å (4) NH₂ 6298.6 Å, (5) unidentified (6) Next order of cometary [OI] 6300 Å.

spectral range of the spectrometer (i.e. 4.004 \AA) are two adjacent orders of cometary [OI] emission, the additional feature appearing between them could readily be determined as NH_2 emission of cometary origin. The position of airglow emission is identified. Since the prefilter used in the instrument was of 5 \AA band width, no other wavelength is expected to appear in the spectra. The principal features marked 1 and 6 separated by 4.001 \AA (one free spectral range at 6300 \AA) are identified as the two adjacent orders of 6300.304 \AA cometary emission in the cometocentric reference frame. The features 3 and 4 are attributed to NH_2 (0, 8, 0) band emission. Fig. 4.5 shows the $0 \text{ } 1_D$ line profile observed and a best fit gaussian superposed. The gaussian line width after correction for instrumental broadening (0.13 \AA) corresponds to 3.5 km/s . The result is in agreement with those of Huppler et al (1975) who had studied comet Kohoutek a double etalon system and had derived a half width $\sim 3 \text{ km/s}$ for the [OI] line, suggesting a systematic coma expansion rate of $\sim 1.5 \text{ km/s}$. The symmetric profile indicates the isotropic flow of the oxygen atoms.

The airglow emission at 6300 \AA was barely detected above the noise level of the detector within our 50 arcsec field of view. Since our observations were taken near local midnight when the telluric emission is minimum (V.R. Rao 1971), assuming the airglow flux to be $\sim 40 \text{ R}$, we estimate the cometary $0 \text{ } 1_D$ flux to be $> 150 + 40 \text{ R}$. This estimation

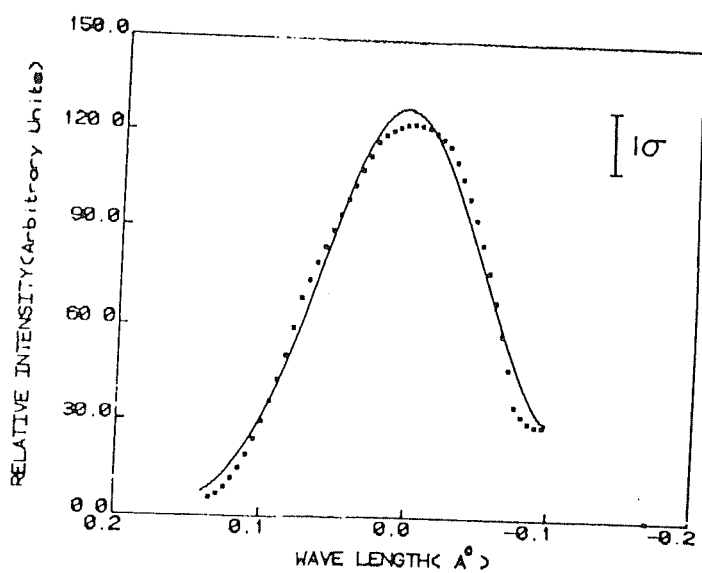


Figure 4.5. [OI] line profile. The solid line is a least square fit Gaussian.

agrees with the instrumental flux calibration on Orion Nebula on the same day. This value is also consistent with the value expected at a heliocentric distance of ~ 1.35 AU by extrapolating the results of Kerr et al (1987).

(C) Study of NH_2 emission

The NH_2 spectrum arises due to excitation from the asymmetric ground state to a linear state, followed by the de-excitation to the ground state through "vibronic" transitions. The absorption spectra of NH_2 free radical was first observed in the laboratory during flash photolysis experiments with ammonia (Herzberg et al., 1952). The laboratory spectrum is extremely rich and has been rather thoroughly studied by Dressler (1959). Table 4.4 gives details of the NH_2 band emission near 6300 \AA .

In the cometary atmosphere these molecules are supposed to be formed by fragmentation of ammonia molecules NH_3 or hydrazine N_2H_4 (Greenstein 1962). However, Robinson et al (1959) have noted that NH_2 can easily be synthesized from N and H in low pressure discharges and they point out that this might provide another possible interpretation of the production of NH_2 in even a rarefied gas cloud like a comet. The detection of this molecule in comets was originally interesting as an evidence of the presence of the triatomic molecule in the comets.

TABLE 4.4

Theoretical and observed NH_2 (0,8,0) Transition

Transition ¹	λ (Å) Theoretical	λ (Å) ² Observed	Intensity ³ in Rayleigh	$\text{NH}_2/[\text{OI}]$
$1_{11} - 1_{01}$	6294.45 6295.83			
$2_{12} - 2_{02}$	6297.32 6298.62	6298.604	75 ± 50	0.5
$3_{13} - 3_{03}$	6298.98 6300.91	6299.004	78 ± 50	0.52
$4_{14} - 4_{04}$	6300.78 6301.96			
$5_{15} - 5_{05}$	6300.91 6300.85			
$6_{16} - 6_{06}$	6299.52 6300.08			
[OI]	6300.304			

1. Notation from Dressler and Ramsay (1959).

2. Observed wavelengths are in agreement with Arpigny et al. (1986).

3. Intensity is corrected for filter transmission.

The NH_2 spectrum in comets show a series of bands over the entire optical spectrum corresponding to successive levels of bending vibration decaying to the ground vibrational states. The relative strength of different vibrational bands appear qualitatively to be controlled by the solar flux available for fluorescence. It is also noted as the general fact that the comets with the highest oxygen (and thus the highest total volatile) production rates are quite dusty and usually have rather strong NH_2 lines in the red. The direct correlation between $\text{Q}[\text{OI}]$ and the $\text{NH}_2/[\text{OI}]$ flux ratio suggests a decrease in this ratio of a factor of two or so for a hundred fold decrease in the absolute gas production (Spinrad 1987). It is now, however, not clear whether this spectroscopic correlation implies a true composition difference or a change in the "weathering" of surface of "worn-out" short period comets. The NH_2 observations made earlier are summarized in table 4.5.

From the 6300 spectral scan of the coma we extracted the NH_2 emission features. The wavelengths calculated for the features marked 3 and 4 in Fig. 4. With reference to the feature 1 (i. e. 6300.304) agrees well with two of the rotational lines of NH_2 (0-8-0) band. However, feature 5 remains unidentified within the errors of estimation, as it cannot be attributed to any of the NH_2 lines of the (0-8-0) band. Table 4.4 lists the observed NH_2 lines and expected lines if all rotational levels were populated (Dressler and Ramsay 1959). The observed relative intensities were

corrected for the varying transmission of the filter across its 5 \AA band width. We obtain the ratio $\text{NH}_2 \text{ 6298.62 [OI] 6300.304}$ of ~ 0.5 + the value obtained by Arpigny et al (1987) at about the same period is ~ 0.3 . Considering the variation this ratio with the filter transmission characteristics induced by temperature changes, we do not consider the difference in the values to be significant. As pointed out by Arpigny et al (1986) a careful study of spatial variation of NH_2 (0-8-0) lines, well resolved from the [OI] 6300.304 \AA over the extent of the emission coma remains to be carried out.

The profiles were also fitted with equivalent gaussian profiles. Fig. 4.6 (a,b) show the NH_2 line profiles observed and the best fit Gaussian line width after correction instrumental broadening (0.13 \AA) corresponding to $\sim 3 \text{ km/s}$ which is in good agreement with the results of Roesler et al (1986). Table 4.6 gives the ratio of $\text{NH}_2 \text{ 6298.6/[OI]}$ of several comets.

4.2.2 Observations of [OI] 6300 emission of Comet Halley with Imaging Fabry-Perot spectrometer

(A) Observations

The observations of Comet Halley with the imaging Fabry-Perot spectrometer was carried out in order to obtain the spatially resolved spectral feature of [OI] 6300

TABLE 4.5

NH₂ observations of comets

Comet	Heliocentric distance R (AU)	Comments	Reference
Kohoutek	0.37	<ol style="list-style-type: none"> 1. NH₂ cloud extends to 0.74×10^4 km in coma. 2. NH₂ is concentrated more towards the nucleus compared to C₂. 3. NH₂ emission increases markedly with C₂ as R increases. 	A'Hearn (1975)
Halley	0.87 - 1.04	<ol style="list-style-type: none"> 1. Flux on head with 5.6' aperture ≈ 110 R, 6' sunward ≈ 175 R, 6' antisunward ≈ 175 R. 	Kerr et al. (1975)
	0.77	<ol style="list-style-type: none"> 1. line width 2.4 ± 0.2 km/s 	Roesler et al. (1985)

TABLE 4.6

The ratio of NH_2 ($2_{12} - 2_{02}$) of comets

Comet	Field of view	R AU	R km/s	NH_2 6298.62/[OI] ($2_{12} - 2_{02}$)	Authors
Halley	0.9'	1.28	-26.66	0.53	F.I.Roesler
	7'	0.77	-23.06	0.3	"
	2"x20"	1.25	+26.7	0.3	Arpigny C.
	50"	1.35	+26.51	0.5	Present work
Mrkos	3"	0.58	+12.00	0.1	Greenstein
Kohoutek	3"	0.34-0.63		0.2	Kohoutek
Wilson	2"x20"	1.22	-5	0.28	Arpigny C.

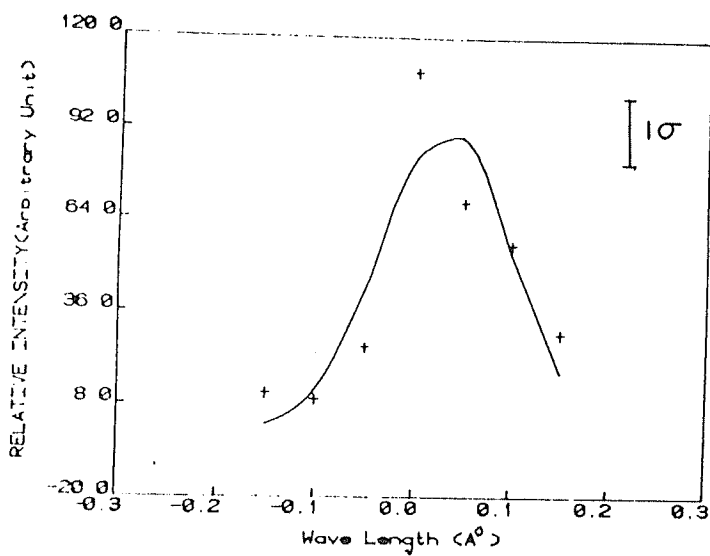


Figure 4.6a. NH_2 ($3_{13}-3_{03}$) 6299.004 Å line profile. The solid line is a least square fit gaussian.

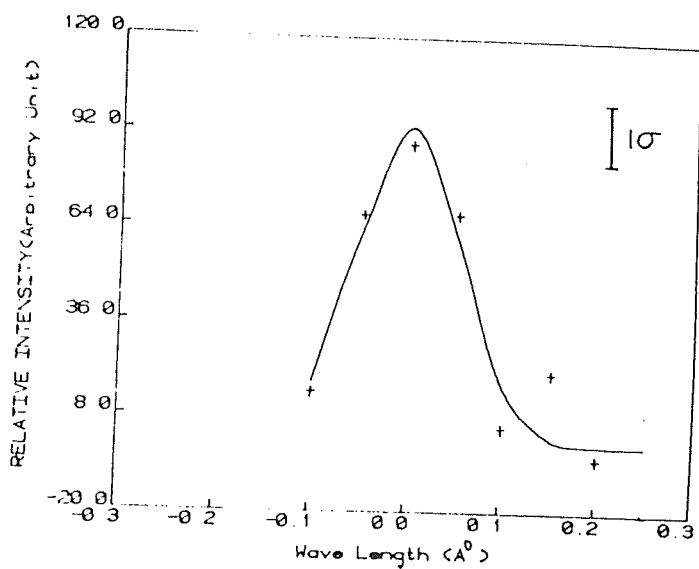


Figure 4.6b. NH_2 ($2_{12}-2_{02}$) 6298.6 Å line profile. The solid line is a least square fit gaussian.

Gurushikhar, Mt. Abu, with the instrument described in the section 3 of chapter 2. A well defined interferogram in [OI] 6300 emission was obtained on 15 Mar. 1986 during the post perihelion period, when the cometary emission was at its peak. Table 4.7 gives the journal of observations and table 4.8 the cometary parameters at the time of observations.

Fig. 4.7 show the white light comet image taken before the interferogram frame. The coma (visual) size was $\sim 10^6$ km. The [OI] 6300 emission interferogram, shown in Fig. 4.8 belongs to the central coma region, 10^5 km in size. The interferogram is attributed to purely cometary emission of [OI] and not the terrestrial airglow emission of [OI] because

(1) The interferogram is anisotropic and confined to the coma region - Airglow would have given a wide field, isotropic interferogram.

(2) Only on one day does this interferogram appear - when the cometary activity was at its highest. An airglow interferogram should have shown up every night.

Further from extensive trial runs on the instrumental sensitivity it is clear that normal airglow emission at 6300 \AA is too faint to generate an interferogram with the 2415 film used. It requires high speed special filters like 2485 and fairly long integration times to record airglow

(Fig.4.9).

(B) Analysis and Results

In the interferogram five Fabry-Perot fringes are clearly seen. As a first step, coordinates of several points on the interferogram fringes were determined by using a Zeiss microdensitometer. The equation of circle was fitted to these points in order to determine the radius of various fringes. Table 4.9 gives the fringe number and the measured radius. As discussed in chapter 2, the fringe radius and the order number of a given follows the relation,

$$2 \mu t \left(1 - \frac{R^2}{2F^2} \right) = n \lambda$$

$$\text{i.e. } R^2 = \left[1 - \left(\frac{\lambda}{2 \mu t} \right) n \right] 2 F^2$$

...(1)

This shows that R^2 vs n is a straight line for a fixed λ .

Therefore, in the cometary atmosphere, within the region of interferogram, if there does not exist any relative motion of oxygen atom in the line of sight, then the plot of R^2 vs n derived from the interferogram would follow a straight line. In order to find out the possible existence of such relative motion, R^2 vs n along with the best fit straight line was plotted as shown Fig. 4.10. The deviation

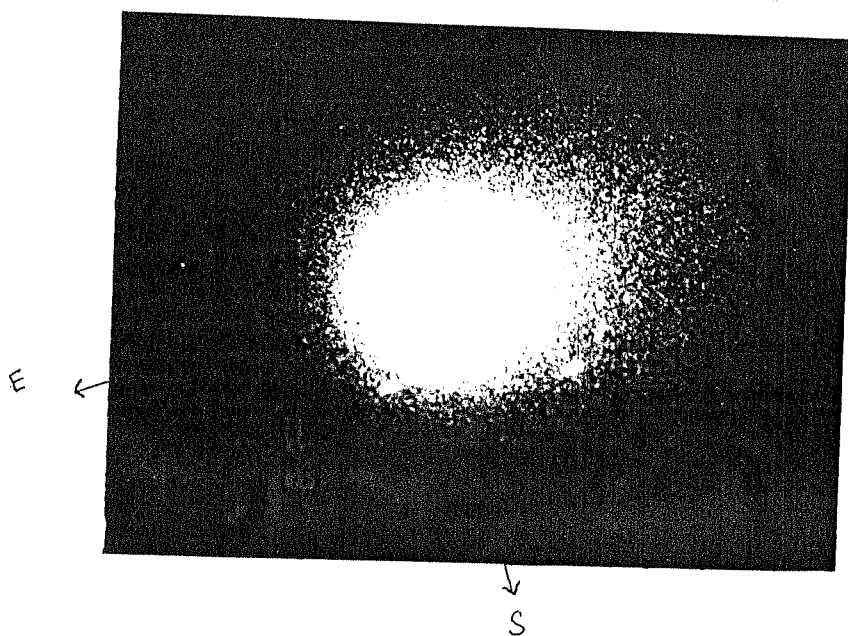


Figure 4.7. The white light image of comet Halley taken on 1986 March 14.97 UT.

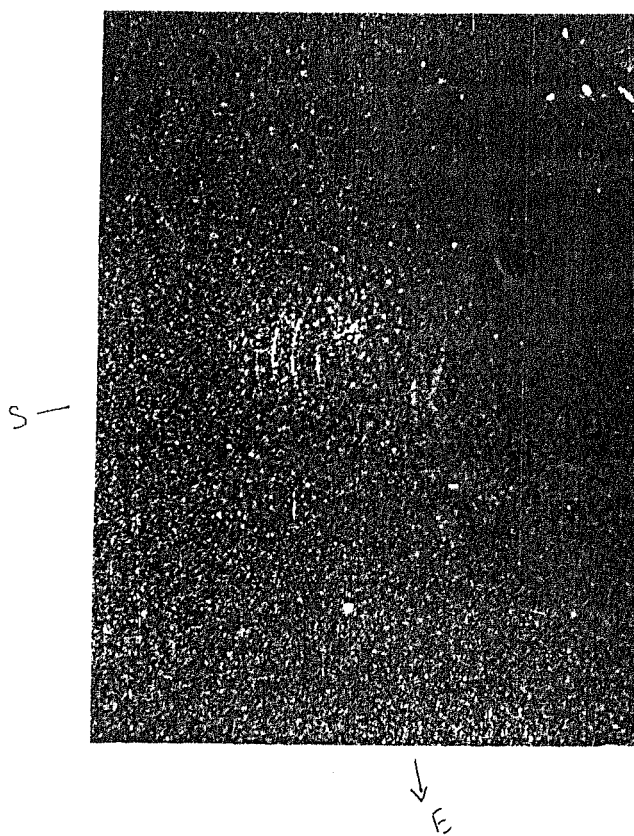


Figure 4.8. The Fabry-Perot interferogram of comet Halley in [OI] 6300 Å emission taken on 1986 March 15.0 U.T.

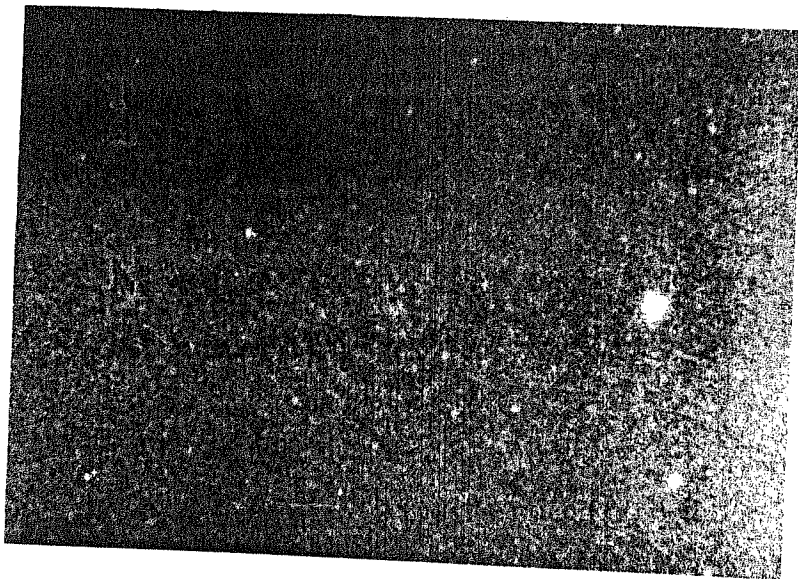


Figure 4.9. The red airglow [OI] 6300 \AA interferogram taken on 1986 Jan 11.597 UT.

[OI] 6300 EMISSION

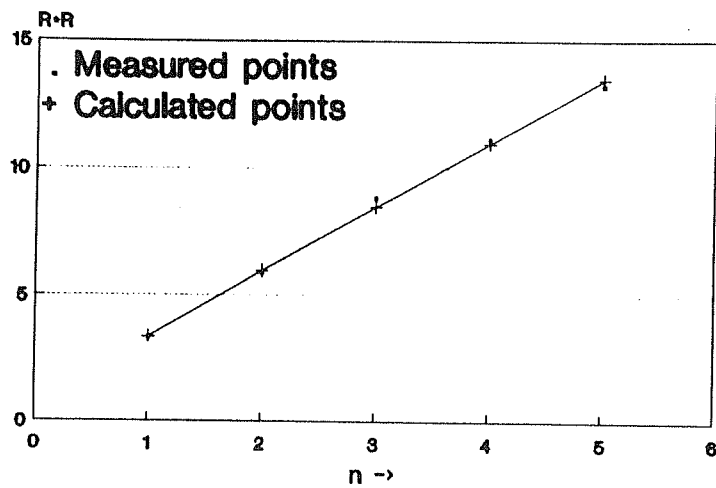


Figure 4.10. Plot of the n Vs R^2 in [OI] 6300 interferogram where n = order of interferogram fringes. R = radius of interferogram fringes.

TABLE 4.7

Comet parameters during the Imaging Fabry-Perot
observations in [OI] 6300 emission

Date UT	RA (1950)	Dec	(AU)	Km/s	RR (AU)	R Km/s
March 14.0	20 0.404	-22 1.64	0.93	-43.44	0.9	25.66

TABLE 4.8

Journal of imaging Fabry-Perot [OI] 6300 A° emission
observations on 13/14.3.86

S.No.	Date (UT)	Filter	Exposure	Film
1.	March 13.97	White light	5 ^s	Kodak 2415
2.	6300/5A°	6300/5A°	900 ^s	Kodak 2415

TABLE 4.9

Radius of the [OI] 6300 fringes of different
order recorded in the interferograms

Order number	Radius R(mm)	R ²
n	1.818	3.306
n-1	2.426	5.877
n-2	2.970	8.819
n-3	3.333	11.111
n-4	3.636	13.223

of individual points from the fitted straight line were calculated. The velocity corresponding to these deviations in radius were estimated. The mean deviation was found to be

≈ 5 km/s. However, the error in the measurements of fringe radius is ~ 4 km/s. Hence it is concluded that there does not exist any significant differential velocity of oxygen atoms within 10^5 km of the nucleus in the coma of Halley's Comet. To be more precise, the velocity dispersion does not exceed ~ 5 km/s in the coma within 10^5 km of the nucleus at the time of our observations.

This result is in consistent with the outflow velocity derived from the line profile measurements. Kerr et al (1987) have measured the width of the line profile of [OI] 6300 emission on Jan 15.363 UT. They have obtained the width of 3.9 ± 1.5 km/s using an aperture of 354 arcsec in size, which corresponds to 2×10^5 km of the comet. These results are due to the integrated effect of the velocity field in the field of view. Our spatially resolved data in the interferogram indicates the absence of outflow velocities > 5 km/s anywhere in the emission coma. Further, our results do not suggest any outflow of oxygen atoms into narrow field angle since we do not see any sharp gradient above the measurement limits.

The theoretical outflow velocity of oxygen atom due to the photodissociation process of H_2 is ~ 1 km/s. The insitu measurements of the H_2O velocity is 0.90 ± 0.2 km/s

(Krankowski et al 1986) to ~ 1.2 km/s at $\sim 10^5$ km (Lammerzahl et al 1987) and the IR measurements show a value of 0.9 ± 0.2 and 1.4 ± 0.2 km/s for pre and post perihelion spectra respectively (Larson et al 1986). Hence if H_2O is the parent molecule for oxygen atom, it is not expected to exceed the upper limit to the velocities inferred by us. Therefore our results are not inconsistent with the conjecture of H_2O as the parent for oxygen atoms.

4.2.3 Comparative study of [OI] 6300 emission among comets

In the preceding discussions we have pointed out that among the potential parent species of $O\ I_D$, the dominant one is H_2O . This would mean that production rate $Q\ [OI]$ is related to QH_2O . Therefore it is useful to study the correlation of $Q[OI]$ with the other characteristic cometary parameters which are apparently related to the cometary age.

The aging of comets is evidenced by a number of observable phenomena: production of gas, dust and meteor particles, splitting of cometary nuclei, non gravitational effects in the comet's motion, sudden and progressive absolute brightness variations and ultimate disappearance. Kresak (1985) has discussed in detail different sources of information on aging process and their implication for the mean life time of comets. It is evident, however, that no single index can be used to precisely define the life time

of a comet in the solar system.

The reciprocal semi-major axis was chosen as an aging index, in the manner generally used in studies of Oort cloud and orbital evolution of comets. It is shown by various authors (Everhard 1976, Marsden and et al., 1978) that subsequent planetary perturbations gradually reduce the aphelion distance, increasing $1/a$. Consequently $1/a$ increases with time after a comet first makes a sufficiently close approach to the sun to come under the gravitational influence of planetary system. In a rough statistical sense, therefore, the age of a comet varies as $1/a$. Using such considerations Yeomans (1986) successfully modeled the orbital evolution of Comet Halley and derived a dynamical age of $\sim 200,000$ years.

The size of a comet can also be regarded as the index of its age. As the comet makes multiple revolutions around the sun, its size decreases due to the continuous mass loss. Hence the age of a comet can be regarded as varying inversely with its size. It is difficult to measure the cometary size directly from earth due to the presence of a diffused coma around it. However the size of a comet can be assessed statistically by assuming that its absolute brightness is in proportion to the surface area of the vapourizing nucleus (Delsemme 1979). i.e. the total intensity of the cometary coma 'I' must be proportional to the nuclear radius squared, $I = \pi \cdot K r_N^2$. This is also the

basic assumption of the vaporization theory of comets (Delsemme and Miller 1971). Here one point to be noted is that the initial size distribution of the "new" comets while entering into the solar system is taken to be constant. This certainly would not be true in practice. The author is not aware of any size distribution function of the "new" comets. However, from the physical considerations the uniformity of the initial size distribution of comets appears possible i.e. Delsemme (1979) pointed out that the mere accumulation of orbits below $1/a = 100$ implies that comets decay fast. Therefore, the comets of smaller size would become extinct soon and would not effect the present study. The number of large size cometary bodies would be too small. Therefore the present conclusions are unlikely to be effected by such objects. Therefore the initial size distribution of the newly entering comets for the present study is taken to be uniform. It is however felt that the final conclusions will be stronger if an appropriate distribution function is used. Another reason of studying the variability of absolute brightness with production rate is to understand the composition and structure as a function of depth in the cometary nucleus with the assumption that all the comets are similar objects.

In the present discussion the inverse of semimajor axis is taken as the index of dynamical age of a comet and the absolute brightness is taken as the index of its physical evolution. The production rate of [OI] inferred from [OI]

6300 emission measurements is plotted against the age index.

(A) Source of Data

The oxygen production rate of several comets have been published recently from the reliable 0.1_D 6300 \AA observations (Spinrad 1987). To compare these production rates these values are extrapolated for a standard heliocentric distance of 1.5 AU. For the purpose of extrapolation of the cometary production rates, generally a power law is fitted. The difficulty in this procedure is to determine an unique power law exponent. Even for the numerous production rates now being published for Comet Halley, authors disagree about the power law exponent for H_2O production (Schreb et al 1986, Feldman et al 1986). The exponent n varies between -2 to -5. However for the present data set $n = -3.5$ is used for all the comets. This "compromise" in exponent selection would introduce a scatter in the final analysis.

The absolute total magnitude H_0 of periodic comets is difficult to determine from the available photometric data, owing to strong bias by instrumental effects and their random internal brightness fluctuations. Recently there have been attempts for producing the internally consistent list of H_0 values (Kresak et al 1987, Hughes 1987). In computing the mean value of H_0 , weighting factors must be taken into account so as to reduce the effect of any departures from

the brightness law and for the instrumental corrections. Carefully applying such corrections to the light curve of various comets on their several return, Kresak et al (1987) have produced H_0 values of all known periodic comets ($P < 200$ years). These values are used to represent their aging index in the present work.

The $1/a$ parameter is calculated by adopting the values (perihelion distance) from the catalog of short period comets published by Belyaer et al (1987). Table 4.10 summarizes the data base for the present discussion.

(B) Results and Discussions

The results are shown in Fig. 4.11. The Fig. 4.11a shows the variation of the oxygen production rate with respect to the total absolute brightness B_0 of the comets. The straight line determined by the method of least squares is given by:

$$\log Q_0[OI] = 30.41 - 0.404 m_0$$

where $m_0 = -2.5 \log_{10} B_0$.

The oxygen production rate is well correlated to the absolute brightness with the correlation coefficient of 0.95. A few important comets i.e. P/Halley, Kohoutek, P/Wild 3,

TABLE 4.10

The Data Base for correlation study

Comet	q AU	\overline{H}	Q[OI]	A^{-1}	$\log B_o$	atoms/s $\log Q[OI]$	Q/B
Panther 1980u	1.6573	5.2	260	6.1098×10^{-4}	-2.0809	2.415	4.496
Meier 1980q	1.522077	6.2	220	∞	-2.4815	2.342	4.824
Kohoutek 1973f	0.1424249	2.51	130	-ve	-1.0039	2.114	3.118
P/Halley 1982i	0.5871	2.8	120	0.0557	-1.118	2.070	3.199
P/Stephen-Oterma	1.5744	6.3	49	0.0889	-2.5229	1.690	4.213
P/Borrelly	1.3192	7.6	45	0.2793	-3.0458	1.653	4.699
P/Wild 2	1.4940	6.6	23	0.2971	-2.6383	1.362	4
Bradfield 1979I	0.545294	7.5	15	∞	-3	1.176	4.176
P/Swift-Gehrels	1.3611	7.7	14	0.2269	-3.0969	1.146	4.243
P/Tuttle	1.0149	7.5	12	0.1748	-3	1.079	4.079
P/Giacobini-Zinner	0.9960	9.2	12	0.2864	-3.699	1.079	4.778
P/Wild 3	2.2875	7.0	5	0.2763	-2.7959	0.699	3.495

P/Ecke	0.3410	8.8	4.5	0.4507	-3.5229	0.653	4.176
P/Kearns-Kwee	2.2235	6.6	4.0	0.2314	-2.6383	0.602	3.240
P/Crommelin	0.7345	8.9	4.0	0.1100	-3.5229	0.602	4.125
IRAS-ARAKI-ALCOCK 1983d	0.991372	9.7	3.0	0.0202	-4	0.477	4.477
P/Brooks	1.8497	7.3	1.2	0.2758	-2.9208	0.079	3
P/Grigg-Skjellerup	0.9892	11.7	0.5	0.3379	-4.68	- 0.301	4.398
Sugano-Siagusa- Fujikawa 1983e	0.471127	11.5	0.4	0.0002	-4.6	- 0.398	4.125

Brightness vs Q[OI]

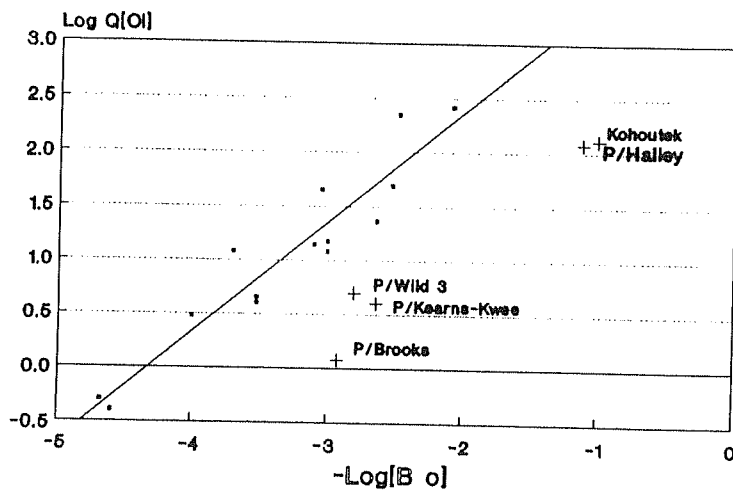


Figure 4.11a. Variation of oxygen production rate $Q[\text{OI}]$ with respect to the total absolute brightness B_o .

P/Kearus-Kwee and P/Brooks do not follow the sf line. Fig. 4.11b show the normalized $Q[OI]$ i.e. $Q[OI]/B_o$ the absolute brightness. From this figure also it is evident that normalized production rate remains constant with respect to the absolute brightness. Comet Halley along with other comets show a lower ratio implying a lower oxygen production rate than expected from the general trend. This means the Comet Halley produces less oxygen by a factor of ~ 15 than expected from its absolute brightness. Similarly other five comets in the plot also have a lower production rate than expected. It was initially thought that using an averaged power law of -3.5 to interpolate the oxygen production rate might have given rise to the apparent low production rate of oxygen. However, taking the actual production rate, measured at ~ 1.58 AU is much lower than the value used here. Moreover as can be seen from Fig. 4.12 the oxygen production rate falls rapidly with a power law $\gamma^{-4.7}$ than the index -3.5 . Therefore in any case the production rate of oxygen in Comet Halley is lower than expected.

This behaviour could possibly be due to the one more of the three following reasons. 1) In bright comets due to the excess production rate, the collision in the inner coma region may be dominant to quench the $O\ 1_D$ state leading to a decrease in the 6300 \AA^0 flux. 2) The gas/dust may be low, so that the dust component can dominantly contribute to the total absolute brightness, leading to an apparent decrease

Brightness vs Relative $Q[OI]$

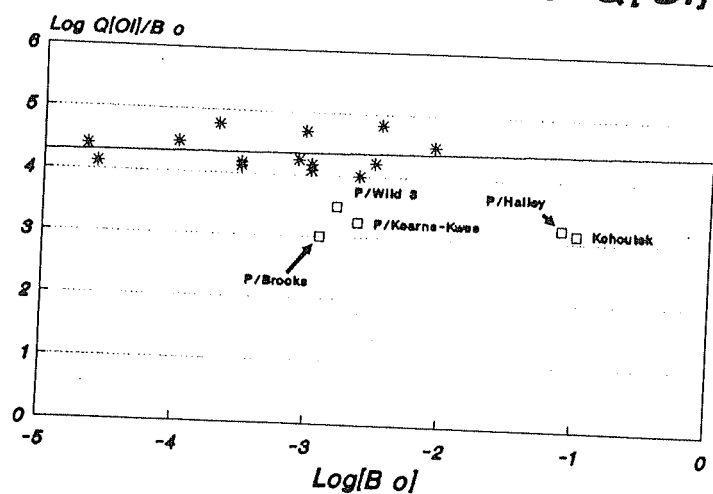


Figure 4.11b. Variation of normalized oxygen production rate i.e. $Q [OI]/B_o$ with respect to the total absolute brightness B_o .

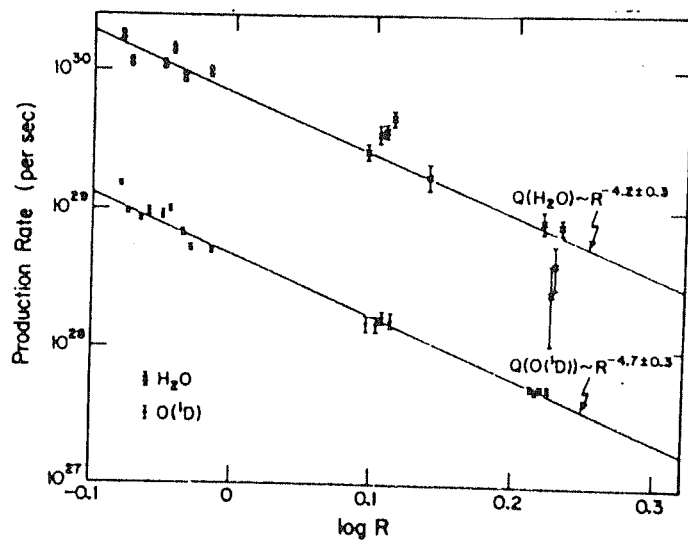


Figure 4.12. Preperihelion values of $Q(\text{H}_2\text{O})$ and $Q(\text{O}^1\text{D})$ versus R (AU) (Scherb et al 1986).

in the [OI] production rate.³) The total brightness might be contributed by other dominating gaseous components such as C_2 or CN leading to an apparent underestimation of [OI]. As mentioned earlier quenching scale length for the typical production rate of Comet Halley is only 600-1000 km, which is a very small fraction, compared to the range of projected distance from comet nucleus contributing to the [OI] emission in the coma of Comet Halley (Magee-Sauer et al 1988). Hence the quenching mechanism cannot be regarded for lowering the [OI] production rate in Halley's Comet. The estimation of gas/dust ratio shows that Comet Halley has a value of 10^{-4} (Sagdeev et al 1986) and Kohoutek 9.2 (Ney et al 1982) which similar to the values for the comets following the general trend, such as P/Encke showing 9.6 (Ney et al 1982). Hence it is unlikely that the dust component is responsible for the apparent decrement of [OI] production rate. To explore the third possibility we have considered the production of C_2 and CN. A'Hearn et al., (1981) have produced a similar plot with the production rate of C_2 and CN with absolute magnitude for several comets. Since around 50% of the comets are common between A'Hearn's plot and ours, we can use this to see the position of Comet Halley. Adding the data for Comet Halley and G-Z the same plot is reproduced in Fig. 4.13. The C_2 and CN production rates for Comet Halley is taken from Catalano et al (1987) and G-Z from Sterken et al (1987). It can be readily seen that whereas the CN production rate follows

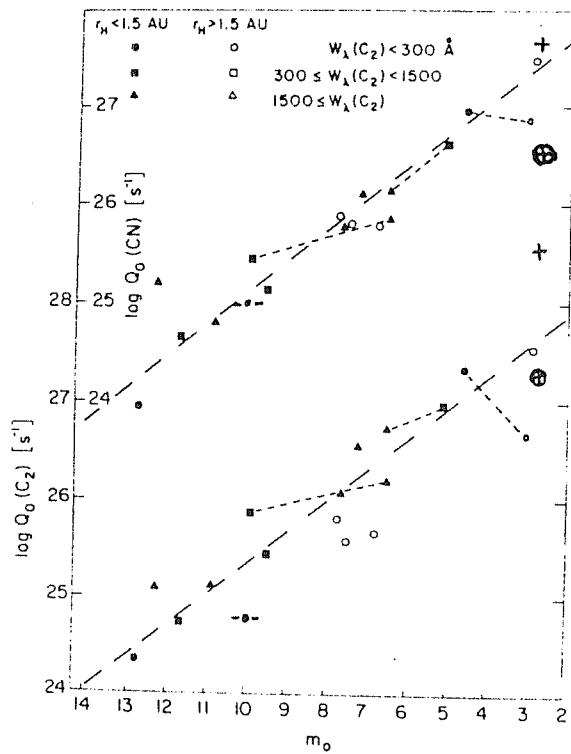


Figure 4.13. Correlation between intrinsic production rates and absolute visual magnitude for several comets. The location of P/Giacobini - Zinner is indicated by \oplus and comet Halley preperihelion by + and post perihelion by \oplus .

the same trend within errors, the C_2 production rate in post perihelion period is higher by several orders. C_2 being a prominent emission in the visible region of cometary spectra, it is quite possible that the apparent enhancement in the absolute brightness of Comet Halley is due to the enhanced C_2 emission. Therefore it can be conjectured that the $Q(C_2)/Q[OI]$ is more in Comet Halley than in other comets falling on the straight line in our plot, therefore P/Halley is a carbon rich Comet.

The $[OI]$ production rate does not seem to have any correlation with the index of dynamical age i.e. $1/a$. This is quite apparent from the Fig. 4.14. The chemical evolution of comets does not appear to have any systematic relation with its dynamical evolution.

4.3.4 Conclusions

(A) The scanning Fabry-Perot spectrometer profiles show

(1) The cometary $[OI]$ emission at 6300.304 \AA was readily detected and NH_2 emission of (0-8-0) band was spectrally well separated from it.

(2) The estimated intensity of $[OI]$ on 13 April 1986 ($r = 1.30 \text{ AU}$, $\Delta = 0.42 \text{ AU}$) was 150 ± 4^0 Rayleighs.

1/a VS RELATIVE Q[OI]

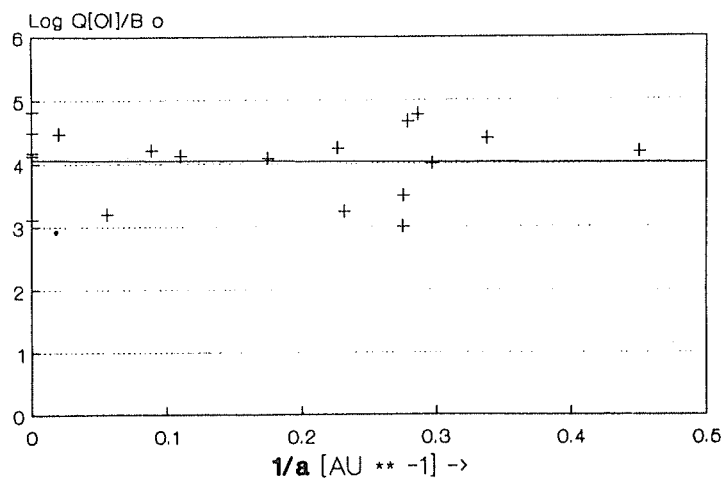


Figure 4.14. Plot of $Q[\text{OI}]/B_o$ versus $1/a_o$, where a_o is the semi-major axis of the comet.

$$(3) \quad \frac{\text{The ratio } (0-8-0) \text{ NH}_2 (2_{12}-20_{02})}{[\text{OI}] 6300 \text{ \AA}^0}$$

integrated over 50" aperture was found to be 0.5. The NH_2 line profile widths are ~ 3 km/s.

(B) During the imaging Fabry-Perot observation we recorded the interferogram in $[\text{OI}] 6300 \text{ \AA}^0$ emission on 15 March 1986 ($r = .91$ AU, $\Delta = .94$ AU). The interferogram belongs to the coma of size $\sim 10^5$ km. The intensity estimation show a value > 200 R, consistent with other observations. The fringe analysis show that the differential outflow velocity does not exceed ~ 5 km/s within $\sim 10^5$ km in the coma.

(C) The correlation studies of $Q[\text{OI}]$ with the absolute brightness and $1/a$ show that most of the comets follow a tight correlation of $[\text{OI}]$ with their absolute brightness. There are some important exception to this trend, including Comet Halley. No correlation exists between $Q[\text{OI}]$ with $1/a$. The same study shows that Comet Halley has less $Q[\text{OI}]$ than expected from its absolute brightness. Consideration of several possibilities led to the conclusion that Comet Halley has also higher C_2 production rate. It is conjectured that Halley's Comet is a carbon rich comet.

4.3 Study of C_2 Interferogram

(1) Aim

As pointed out earlier the outflow velocity is an important parameter in modeling the C_2 emission brightness distribution in the coma. Particularly if the parents of these molecules are ions as pointed out by Cosmovici (1988) than their velocity would vary within the coma. As we have pointed out in chapter 3 section 3.3 the ionic features in the coma move with velocities of ~ 37 km/s. This fact was also observed by Huppler's H_2O^+ observations (Huppler et al., 1975) and from the studies of Jockers (1985). Therefore if the parents of C_2 is connected to some ionic species we must get the relative velocities of C_2 molecules in the coma of the order of $\sim 15-30$ km/s, which are the typical ionic velocities in the coma. Therefore this study aims at finding out the relative velocities of C_2 molecules in the coma of Comet Halley.

(2) The observations

These observations were taken from Gurushikhar, Mt. Abu with the C-14 telescope and the Imaging Fabry-Perot spectrometer as described in chapter 2, section 2.3. Table 4.11 gives the cometary parameter during our observations. Two of these observations were in pre perihelion period and the one in post perihelion period. Table 4.12 gives the Journal of observations. The white light cometary images and the interferograms are given in Fig. 4.15, 4.16, 4.17.

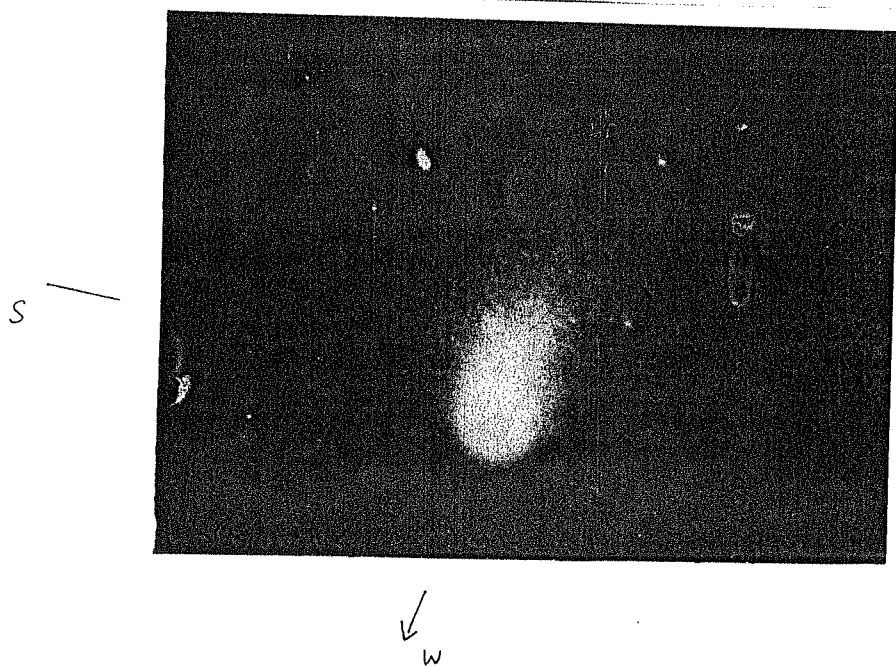


Figure 4.15a. White light image of the comet Halley taken on 1986
Jan 9.6 UT ($R = 1.31 \text{ AU}$ $\Delta = 0.89 \text{ AU}$).
(10 seconds exposure).



Figure 4.15b. Interferogram in C_2 taken on 1986 Jan 9.62 UT.
(120 seconds exposure).

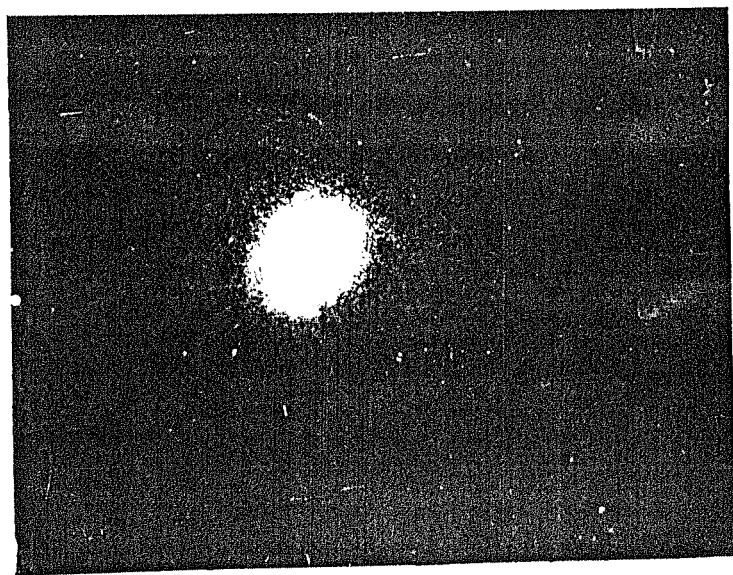


Figure 4.16b. Interferogram in C_2 taken on 1986 Jan 12.604 UT.
(600 seconds exposure).

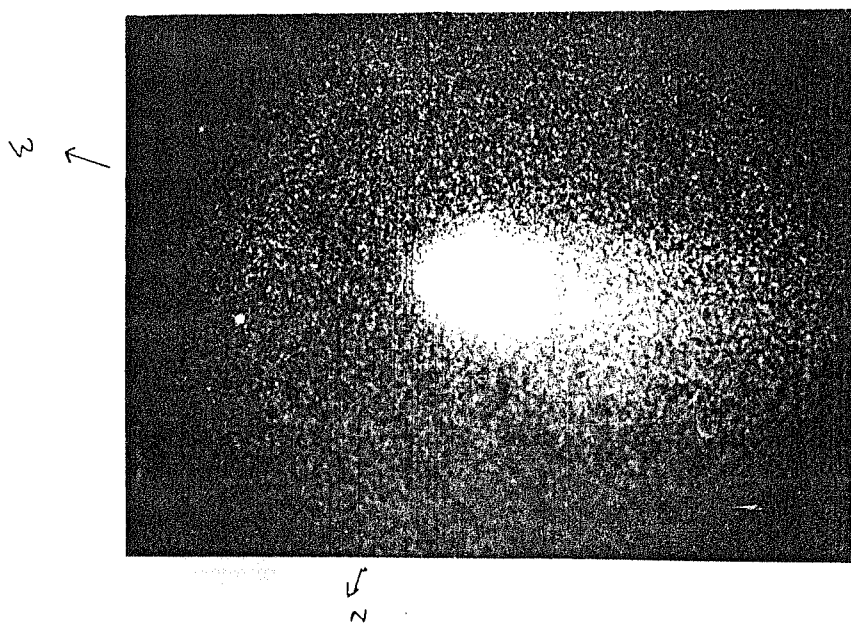


Figure 4.1a. White light image of the comet Halley taken on 1986 Jan 12.6 UT. ($R = 0.84 \text{ AU}$ $\Delta = 1.36 \text{ AU}$) (30^{S} exposure).

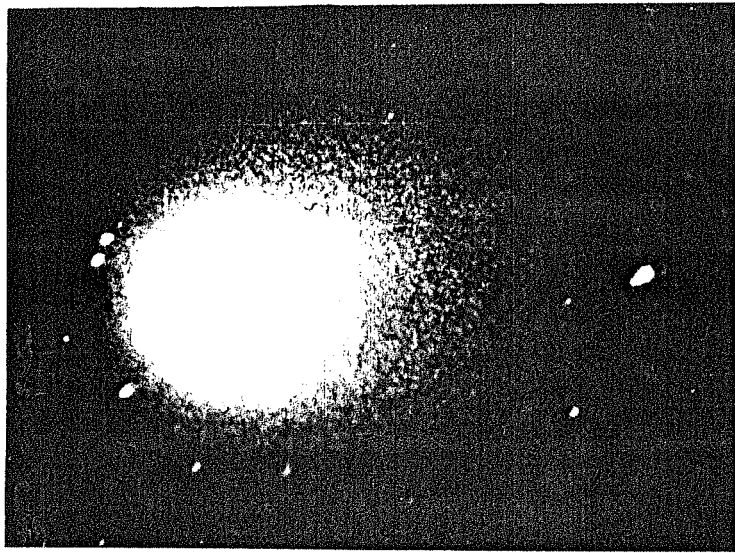


Figure 4.17~~0~~ White light image of the comet Halley taken on 1986 March 22.992 UT (10 seconds exposure).

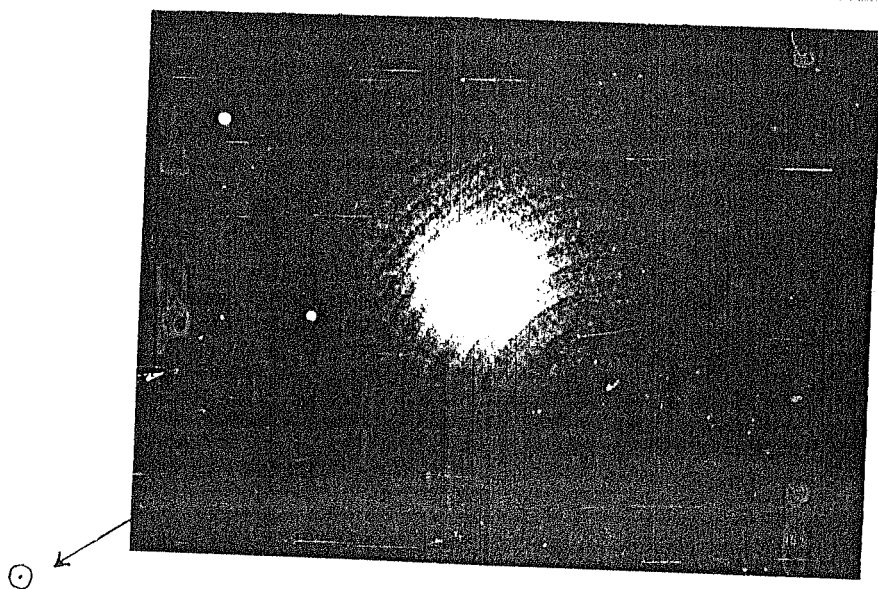


Figure 4.17b. Interferogram in C_2 taken on 1986 March 22.985 UT (600 seconds exposure).

The interferograms are taken with C_2 IHW filter at $5140/90 \text{ \AA}$. Within this band width number of rotational lines appear. The strongest line in this band is the band head at 5165 \AA , which is illustrated in Fig.4.18. Considering the filter transmission and the detector response we find that the band head would appear as the strongest line in our interferogram.

(3) The dispersion velocity measurement:

In order to find out the region of the cometary coma associated with the recorded Fabry-Perot fringe pattern, the white light and interferogram frames were matched with respect to the image intensifier spots. It was then inferred that the interferogram belongs to the inner part of the coma. Taking the brightest region of the coma as the centre of the comet, the distribution of C_2 molecule was found to be symmetric around the central coma region. The extend of the coma on which interferogram was registered was found to be $\sim 10^6 \text{ km}$.

The Fabry-Perot fringe pattern observed in the comet have a number of fringes with varying intensity. A complete analysis of the interferogram involves, producing a synthetic spectra with known instrumental parameters and intensity distribution in various rotational lines and

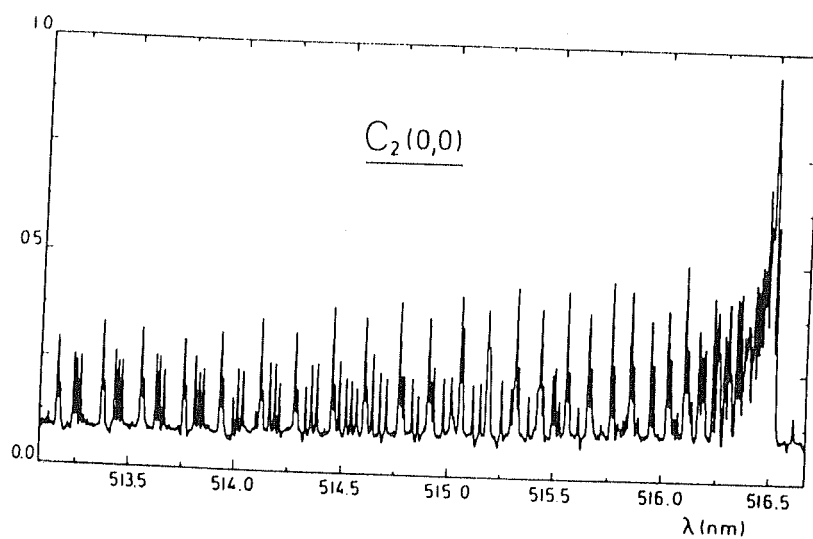


Figure 4. 18. The rotational intensity distribution in the $C_2(0,0)$ band of P/Halley ($r = 0.85$ UT) at 100,000 resolution (Arpigny et al 1986).

matching with the observed spectra in order to derive the useful physical parameters. However, in the present analysis, we have taken only the band head at 5165 \AA in order to determine the differential motion of the C_2 molecules in the coma. The intense line on the interferogram was identified as 5165 \AA . To confirm the identification, the radius of various orders of the Fabry-Perot fringe for 5165 \AA were calculated. It was seen that the radius of bright fringes of the interferogram on the average agree with the calculated radius after applying the correction for the cometary motion. This exercise gives the confidence that all the fringes of higher intensity having a sharp edge are due to the same line.

In order to determine the differential velocity of C_2 molecules the same method as described in 4.2.2 was applied. The radius of the fringes were approximately measured with the help of a Zeiss film reader. For a precise determination of the radius, a microdensitometric scan with PDS 1010G (Perkin-Elmer) was taken along the centre of the interferogram. This scan belongs to the direction perpendicular to the Sun-Comet vector in the plane of comet. Fig. 4. 29. shows the scan. The distance of each peak from the fringe centre were determined, with the knowledge of the fringe centre, which was determined precisely for a single fringe. Table 4.13 summarizes the measurements. Since the pixel size used for scanning the interferogram was $20 \mu \text{ m}$ we consider this as our measuring error, which corresponds

RELATIVE INTENSITY (in Arbitrary Unit)

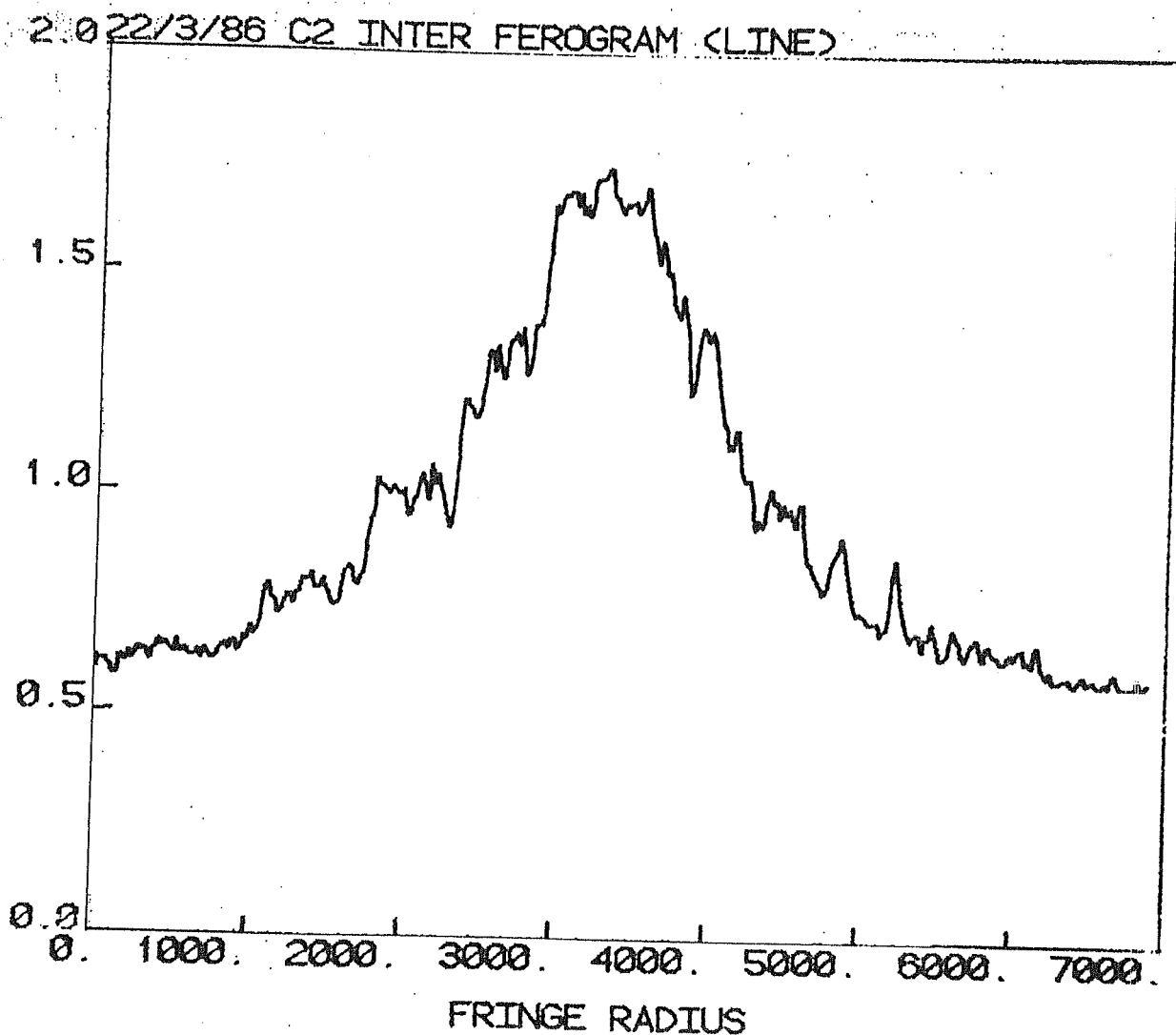


Figure 4. 19. The microdensitometry scan from the central part of the C_2 interferogram taken on March 22.992 UT.

to the error in velocity as ~ 7 km/s. After determining the radius of individual fringe peaks the R^2 vs n diagram was plotted, where R =radius of the fringe and n =order. A straight line was fitted to the points and the deviation of each individual points ΔR from the fitted straight line was calculated. Fig. 4.20, 4.21, and 4.22 show the R^2 vs n plot. The velocity deviation ΔV was calculated as,

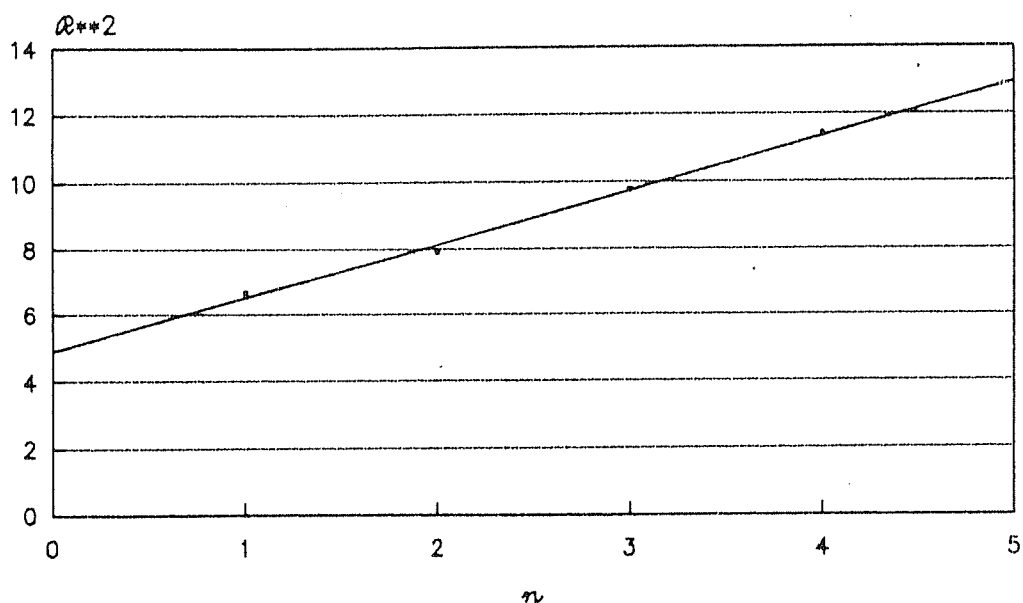
$$\Delta V = \frac{R \Delta R}{F^2}$$

where F =focal length of the imaging lens, used in the Fabry-Perott interferometer =50 mm. The root mean square value of ΔV is ~ 4 km/s.

Therefore we conclude that there does not exist the differential motion of C_2 molecules in the line of sight within 10^6 km/s from the nucleus above 7 km/s, in the direction perpendicular to the Sun-comet vector on 22/23 March 1986.

Our results indicate that accelerated ionic molecules cannot be the parent of C_2 . However, from the spacecraft measurements it is found that the velocity of heavy ions of mass group $\sim 39-49$ AMU increase steadily from ~ 0 km/s at the centre to ~ 6 km/s at 4×10^4 km/s from the nucleus (Korth et al., 1987). The measurements of the velocity of

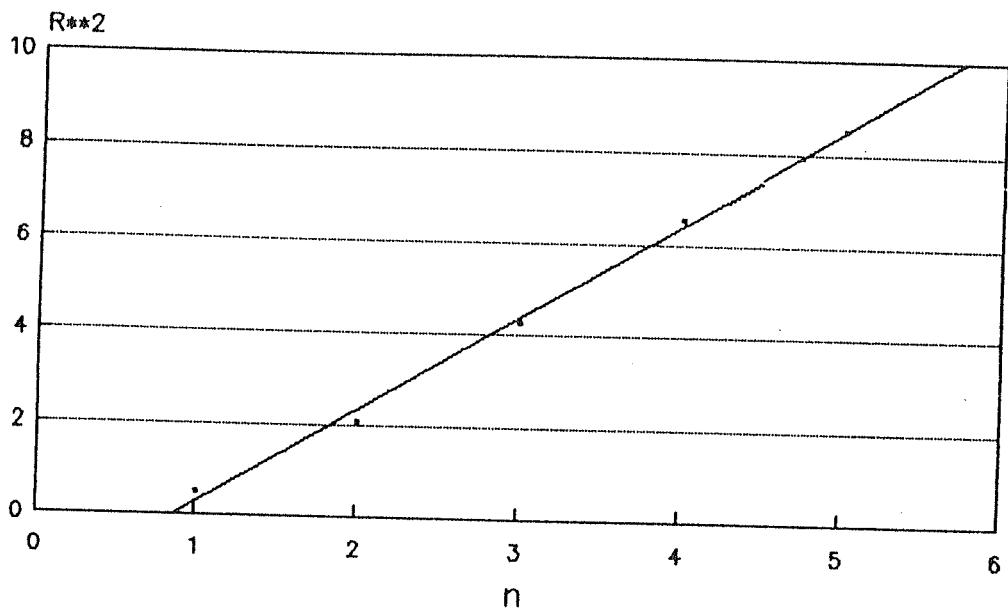
n Vs R^{**2}
 C2 interferogram 9/1/86



X axis indicates $n, n+1, n+2$ etc

Figure 4.20. Plot of the n Vs R^2 for the C_2 interferogram taken on 1986 Jan 9.62 UT where n = order of interferogram fringes and R = fringe radius.

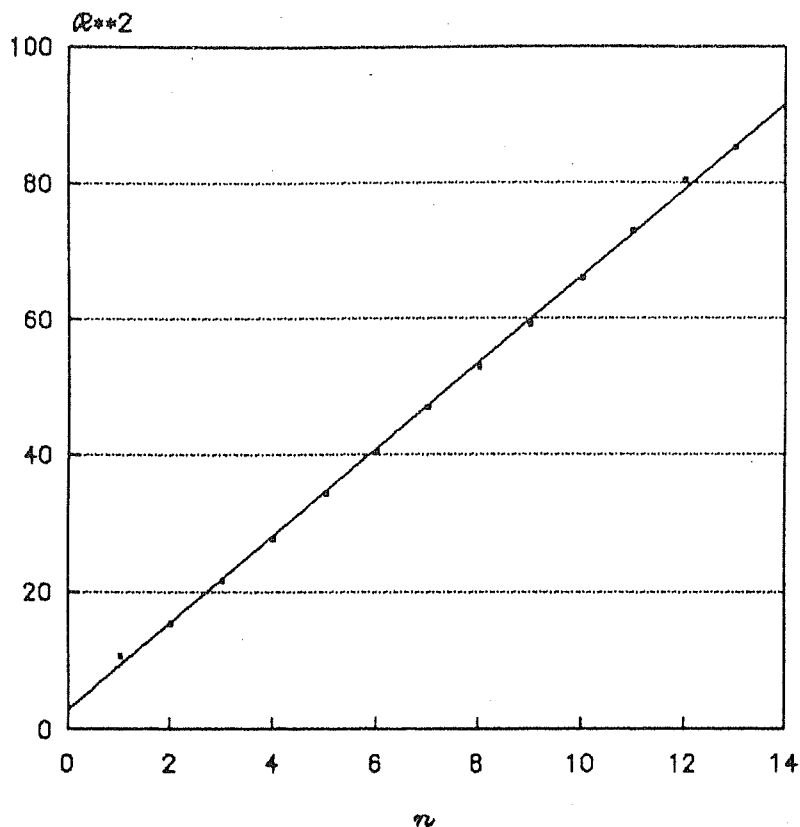
n Vs R^{**2} C2 interferogram 12/1/86



X axis indicates n,n+1,n+2 etc

Figure 4.21. Plot of the n vs R^2 for the C_2 interferogram taken on 1986 Jan 12.604 UT, where n = order of interferogram fringes and R = fringe radius.

n Vs R^{**2}
 C2 interferogram 22/3/1986



If axis indicates $n, n-1, n-2$ etc.

Figure 4.29. Plot of the n vs R^2 for the C_2 interferogram taken on 1986 March 22.985 UT where n = order of the interferogram fringes and R = fringe radius.

TABLE 4.11

Comet parameters during the Imaging
Fabry-Perot observations in C₂ emission

Date UT	RA (1950)	Dec	(AU)	Km/s	R (AU)	R Km/s
January 9.0	21 57.154	-4 16.66	1.31	29.81	.89	-25.46
January 12.0	21 52.072	-4 50.64	1.36	27.75	.84	-25.76
March 22.0	19 34.308	-27 32.30	.76	-43.47	1.02	26.57

TABLE 4.12

Journal of imaging Fabry-Perot C₂ emission observations

S.No.	Date UT	Filter	Exposure	Film
1.	January 9.597	White light	10 ³	Kodak 2415
2.	January 9.624	5140/90A°	120 ^S	Kodak 2415
3.	January 12.603	White light	30 ^S	Kodak 2415
4.	January 12.604	5140/90 A°	600	Kodak 2415
5.	March (~)22.0	5140/90 A°	600	Kodak 2415
6.	March (~)22.0	White light	10 ^S	Kodak 2415

TABLE 4.13

Radius of the C_2 fringes of different order
recorded in the interferograms

<u>Order number</u>	<u>Radius R (mm)</u>	<u>R²</u>
(9/10 January 1986)		
n	2.6	6.25
n-1	2.8	7.91
n-2	3.13	9.76
n-3	3.38	11.39
(12/13 January 1986)		
n	1.06	1.13
n-1	1.44	2.07
n-2	2.06	4.25
n-3	2.56	6.57
n-4	3.13	9.77
(22/23 March 1986)		
n	3.25	10.56
n-1	3.92	15.37
n-2	4.65	21.62
n-3	5.27	27.77
n-4	5.85	34.22
n-5	6.35	40.32
n-6	6.85	46.92
n-7	7.27	52.85
n-8	7.69	59.14

n-9	8.12	65.93
n-10	8.54	72.93
n-11	8.96	80.28
n-12	9.23	85.19

such ions are not available after this distance. However, the extrapolation of these results would indicate a velocity > 10 km/s for the heavy ions in the region beyond 10^5 km/s from the nucleus. Since this lies above the measurement error of our observations, we conclude that it is unlikely that the complex heavy ions are the parent molecules of C_2 beyond 10^5 km from the nucleus.

(4) Conclusions

The following conclusions are drawn from the present work on C_2 (0-0) swan band emission study.

(1) The C_2 emission around the nucleus does not show the asymmetry in the Sun-antisun direction or perpendicular to Sun-antisun direction. It is almost symmetrically distributed around the central coma region - up a distance of $\sim 10^6$ km/s.

(2) There does not exist any differential motion of C_2 molecules above 7 km/s, within 10^6 km/s from the nucleus.

(3) It is unlikely that the complex ions are the parent species of C_2 molecules in the region of the coma beyond 10^5 km/s from the nucleus.

(4) Perhaps the strongest conclusion can be made from the present study is that with amateur class telescope and

simple but powerful back-end instrumentation, it is possible to obtain the valuable data in cometary astronomy, which are extremely valuable for several aspects of cometary physics.

CHAPTER 5

SUMMARY

The well predicted apparition of the periodic Comet Halley (1982i) provided a unique opportunity for the astronomers to participate in the world wide coordinated observational programmes organized by the International Halley Watch (IHW). Observations were also carried out by earth orbiting satellites, high flying aircraft and by the space missions. One of the important aspects of the ground based investigation was to use modern instrumentation and sophisticated methods of data analysis to achieve high resolution in spatial, spectral and temporal domains leading to new scientific results. The present work is concerned with high-resolution spectroscopic study of selected cometary emission lines by using the Fabry-Perot Spectrometers, and the study of filter images of the coma obtained in the different broad band cometary emissions using an image intensifier. Specifically the objectives were:

- 1) To obtain two dimensional spectra of cometary emissions in the form of Fabry-Perot interferograms in order to study the dynamics of several species in the cometary atmosphere.

2) To obtain short exposure imageries of the coma in selected wavebands of cometary emission to study the time evolution of short lived features.

3) To study the doppler shift of the ionic emission lines as a function of cometocentric distance in the tail so as to distinguish between the "hydromagnetic wave" and "particle" motion concept for explaining the observed acceleration of plasma tail features.

To achieve the above stated objectives two different types of Fabry-Perot systems were developed. One was an imaging Fabry-Perot system coupled with an image intensifier to a 35 mm camera. The system covered the entire visible region with two optically contacted Fabry-Perot etalons having spectral resolutions $\sim 0.3 \text{ \AA}^0$ (4500 - 5500 \AA^0) and 0.1 \AA^0 (5700 - 7000 \AA^0). There was provision in this instrument for removing the Fabry-Perots and introducing a telecompressor lens for obtaining direct imageries in the various cometary emissions over the entire extent of the coma. This Fabry-Perot system was coupled to a dedicated 14 inch (C-14) telescope with a special drive corrector. The bulk of the observations were carried out by this telescope - Fabry-Perot system over a period of eight months from Oct 1985 to May 1986. The observations were greatly facilitated by the use of the image intensifier with an average gain of

3×10^4 which permitted short exposures of a few seconds in white light and of a few minutes in the filters. Step wedge calibration impressed on the films (Kodak 2415) permitted relative intensities to be derived.

The second Fabry-Perot system was a sophisticated central aperture scanning photoelectric Fabry-Perot with piezoelectric controls having a finesse of 28 at 6328 \AA . This complicated system could be used only at the 1 m telescopes. Observations of Comet Halley using the piezoelectric Fabry-Perot system were carried out for a few nights in April 1986 when the comet was making its closest passage with respect to earth. Observations were carried out in [OI] 6300 \AA , $H\alpha$ 6563 \AA , Na D lines (5890 \AA and 5896 \AA).

The data set from the imaging Fabry-Perot system consisted of over 200 imageries of which ~ 100 were white light pictures. Six interferograms 3 in C_2 , one each in $H\alpha$ (6563 \AA), OI (6300 \AA) and Na D ($5890, 5896 \text{ \AA}$) were obtained.

The photographic data on 35 mm films were digitized with a high precision micro-densitometer (Perkin-Elmer 1010 G) with a spatial resolution of $\sim 20 \mu\text{m}$ compatible with the image intensifier resolution. Some of the digital images were processed in Astronomical Image Processing System (AIPS) environment. The interferograms were also

processed by specially developed software.

Results

I. Transient Plasma Events

a) Event of 13 March 1986

A transient plasma event in the coma of Comet Halley was recorded by the filter imagery and the imaging Fabry-Perot system on 1986 March 13.0 UT when the comet was crossing the sector boundary of the interplanetary magnetic field. The feature was observed in the form of a blob in H_2O^+ (7000 \AA) at position angle 160° relative to the nucleus (NESW) at a projected distance of $2 \times 10^5 \text{ km}$ in the plane of sky. An interferogram in the $H \alpha$ centred on the blob was also recorded. The detailed analysis of the $H \alpha$ interferogram shows that the dispersion velocity of the blob material was $\sim 30 \pm 10 \text{ km/s}$ leading to a rapid dispersal in about an hour. It is suggested that the crossing of the interplanetary magnetic field boundary with the attendant field reconnections has resulted in the observed feature.

b) Event of 8 January 1986

The blue enhanced near nucleus images of 8th January 1986 recorded an ionic condensation region of size $\sim 4 \times 10^4 \text{ km}$ in the tailward direction at a distance of $\sim 2.3 \times 10^5 \text{ km}$

from the nucleus. It is shown that this excess ionization region is formed as a result of a rapid ionization process, most probably the discharge of cross tail electric current in the inner coma region, with time scale of 10^3 - 10^4 seconds. The condensation was moving with a velocity of $\sim 37 \pm 3$ km/s in the antisunward direction. From the study of wide field photographs of Comet Halley on 9th and 10th January, it appears that most probably this condensation is the precursor of the dramatic Disconnection Event of 10th January 1986.

II High-resolution spectroscopic study in [OI], NH_2 and C_2 wan band

The [OI] 6300 \AA emission, spectrally well separated from NH_2 (0-8-0) band was observed on 1986 April 13th with the piezo-electrically controlled Fabry-Perot spectrometer. The intensity of [OI] 6300 \AA emission within 50" of the inner coma was estimated as 150 ± 40 R at $r = 1.36$ AU and the ratio NH_2 ($2_{12} - 2_{02}$)/[OI] was 0.5. The [OI] and NH_2 line profiles are symmetric with Gaussian widths of ~ 3 km/s. A Fabry-Perot interferogram in [OI] 6300 \AA emission was taken earlier 1986 March 15th, with the imaging interferometer. It is inferred from this observation that the intensity of the 6300 flux within 10^5 km in the inner coma was > 200 R. The interferogram is characterised by low dispersion velocities and small fringe width suggesting an outflow speed of < 5 km/s.

A general correlation study of [OI] 6300 intensity with the Comet's aging parameters was carried out for ~ 23 comets. It is shown that [OI] 6300 intensity has a strong correlation with comet's absolute brightness and no correlation with the inverse of semimajor axis which is an index for dynamical age. Comet Halley is found to have production rate reduced by factor of ~15 than what is expected from its absolute brightness. On the other hand C_2 production rate is found to be higher.

Three Fabry-Perot interferograms in C_2 (0-0) Swan band have been recorded. The fringe analysis show that the differential outflow velocity within 10^6 km from the nucleus does not exceed ~ 7 km/s. Therefore it is unlikely that C_2 has ionic sources.

Suggestions for Future Work:

In this section a few suggestions are made on the basis of the present work which would help in improved Fabry-Perot observations of future comets.

- 1) One of the projected aims of the present work was to measure the Doppler shifts of the emission of ionized species as a function of the distance from the nucleus. Large Doppler shifts if detected could prove conclusively

that the rapidly varying structure in the ion tail are due to particle motion and not wave motion. However the main ionic emission CO^+ at 4260 \AA^0 was beyond the operating spectral range of our Fabry-Perot system. Further this instrument has a spatial extent of ~ 20 arc minutes and could not be used to cover events in the tail. Hence as a logical continuation of the present work it would be most appropriate to observe doppler velocities in CO^+ over the entire extent of the ion tail of a future bright comet.

2) In employing the single Fabry-Perot systems for obtaining emission line profiles in comets by central aperture scanning, future experiments should aim at improving the signal to noise by removing the scintillation noise in the continuum arising due to the existence of large spatial variation of brightness in the coma. We have suggested a scheme (Debi Prasad et al., 1988) for such an improvement. Briefly this involves using a modulating mask placed in the Fabry-Perot fringe plane allowing the photo detector to look alternatively at the flux at the wavelength of the line and then the adjacent continuum with same band width and from the same portion of the sky and record the difference. This method was successfully used to measure the line emission from lithium vapour trail released in the upper atmosphere during day time (Desai et al., 1979). Employing this technique a group of scientists of this laboratory have successfully detected the day airglow emission at 6300 \AA^0 .

3) The instruments having multiple functions like camera mode spectroscopic mode etc, with an easy switching between the modes are likely to play an increasingly important role in the future observation of comets. Such an instrumentation was used in the the present work. Larson (private communication) have also developed such an instrument called "a coronagraphic CCD camera/spectrograph". This instrument has several optical interfaces between the telescope and CCD to function as a camera, a spectrograph and a two dimensional photometer and polarimeter. By combining all these easily variable functions in the instrument, the observer has a great flexibility to choose the type of observation best suited to the observing conditions. The author advocates such instruments for cometary studies in the future.

4) One of the main conclusions of the present study is that it is important to study the transient events in the cometary coma. This objective requires stations closely spaced in geographic longitudes. Even for Comet Halley observations the longitudinal coverage was not complete particularly in the Eastern longitudes. Therefore it is useful to think of a coordinated team, having similar low cost but sophisticated instruments (of the type used for the present work by the author) for taking observations from several parts of the world at the time of the

apparition of a bright comet. The observations of main concern pertain to the images of coma and the tail in narrow band filters and Fabry-Perot interferograms.

5) Several theoretical problems in the cometary science have not been studied in great detail. The longevity of the condensation regions for ~ 150 hours while moving in the coma is not clearly understood. On the other hand even though several ideas exist to explain the anomalous ionization processes in the cometary coma the short life time of some cometary plasma features are not well understood. It is therefore important to study the theoretical aspect of these problems taking into account the large data obtained during the Halley campaign.

6) Though, by and large, comets are found to exhibit more of similarity than diversity in their chemical composition of the nucleus, some comets show excess in some particular species. A systematic study is needed to establish origin of the observed chemical heterogeneity among the cometary nucleus.

Future space mission to comets would undoubtedly involve insitu sampling of the cometary nucleus to solve the age old question "What is a comet really made of?" several space missions are already on the pipe line e.g. Comet Rendervous Asteroid Flyby. It is interesting to note that all these space missions can be aimed at only the

known comets with well defined orbits confined mainly to the inner solar system.

A bright new comet containing in its pristine nucleus the key to many of the questions concerning the origin and evolution of our solar system would be probed not by space missions but, by and large, by ground based instrumentation and a few earth orbiting satellites. Hence, even in the space age, ground based observations of comets with sophisticated instrumentation will continue, in a decisive way, to enrich and advance the physics of comets.

REFERENCES

CHAPTER 1

- A'Hearn M.F., Feldman P.D., Schleicher, D.G., 1983, Ap. J. Lettt., 279, L 99.
- A'Hearn M.F., Feldman, P.D., 1985, Ice in the Solar System, (D.Reidel Pub. Co.) 463.
- A'Hearn M.F., 1986, Asteroids, Comets, Meteors II, Uppasala, Uppsala University, 187.
- A'Hearn, M.F., 1988, ann. Rev. Earth Planet Sci., 16, 273.
- Alfven, H., 1954, On the origin of the Solar System, Oxford University Press, New York.
- Alfven H., 1957, Tellus, 9, 92.
- Alfven, H., Carliquist, P., 1967, Solar Phys., 1, 220.
- Alurkar, S.K., Bhonsle, R.V., Sharma, A.K., 1986, Nature, 322, 439.
- Alvarez, L.W., Alvarez, W., Asaro, F., Michael, H.V., 1980, Science 208, 1095.
- Alvarez, W., Muller, R.A., 1984, Nature, 308, 718.
- Anantharikrishnan, S., Bandhari, S.M., Rao, A, P., 1975, Astrophys. Space.Sci., 37, 275.
- Ananthakrishnan, S., Manoharan, P.K., Venugopal, V.R., 1987, Nature, 329, 698.
- Anders, E., Owen, T., 1977, Science, 198, 453.
- Antrack, D., Biermann, L., Lust, Rh, 1964, Ann. Rev. Astron. Astrophys., 2, 327.
- Arpigny, G., Dossin, F., Manfroid, J., Magain, P., Danks, A.C., Lambert, D.L., Sterken, C., 1986, The ESO Messenger

No. 45, 8.

- Arpigny, C., Maganin, P., Manfroid, J., Dossin, F.,
Danks, A.C, Lambert, D.L., 1987, *Astron.. Astrophys.*,
1-4.
- Arpigny, C., Zeippen, C.J., Klutz, M., Magain, P.,
Autsemekers, D., 1987, *Diversity and Similarity,
of Comets*, 607.
- Aumann, H.H., Beichman, C.A., Jong, T.D., Houck, J.R.,
Low, F.J., Neugebauer, G., Walker, R.G., Wesselins,
P.R., 1984, *Ap. J.*, 278, L23.
- Aumann, H.H., 1985, *Pub. Astr. Soc. Paci*, 97, 885.
- Barker, E.S., Lambert, D.L., Tomkin, J., Africano, J.,
1978, *Pub. Astr. Soc. Paci*, 90, 514.
- Battrick, B., Rolfe, E.J., Reinhard, R.R., 1986,
20th ESLAB Symposium Vol II, ESA SP-250, P.397.
- Bhatt, H.C., 1985, *Astron. Astrophys.* 146, 363.
- Biermann, L., 1951, *Z. Astrophys.*, 29, 274.
- Biermann, L., Brosowski, B., Schmidt, H.U., 1987,
Solar Phys., 1, 254.
- Biermann, P., Tinsley, B.M., 1974, *Astron.Astrophys.*,
30, 1.
- Buffon, G.L.L., 1745, *De la formation des
planetes* Paris.
- Buti B., 1982, *Ap. J.*, 252, L43.
- Buti B., 1983, *Ap. J.*, 268, 420.
- Buti B., Lakhina, G.S., 1987, *Geo. Res.*, let.
14, 107.
- Buti B., 1988, *Cometary and Solar plasma
Physics*, World Scientific, Singapore.
- Cameron, A.G.W., 1973, *Icarus*, 1, 13.
- Cameron, A.G.W., 1973, *Icarus*, 18, 407.
- Celnik, W.E., Kaler, T.S., 1987, *Astron.
Astrophys.* 187, 233.
- Chernikov, A.A., 1975, *Soviet Astron.*, 18, 505.
- Chopra, P.C., 1985 (January) *Jain Journal*, 67.

- Chyba, C., Sagan, C., 1987, *Nature*, 329, 208.
- Chyba, C. F., 1987, *Nature*, 330, 632.
- Club, S.V.M. and Napier, W.M., 1982, *Qr.J.Roy Astron. Soc.* 23, 45.
- Club, S.V.M. and Napier, W.M., 1984, *Mon. Not. Roy. Astr. Soc.*, 208, 575.
- Cole, W., 1823, *On the theory of comets*, London.
- Cosmovici, C.B., Ortolani, S., 1984, *Ices in the solar system*, Proc. NATO workshop.
- Cosmovici, C.B., Ortolani, S., 1984, *Nature*, 310, 122.
- Danks, A.C., Lambert, D.L., Arpigny, C., 1974, *Ap. J.*, 194, 745.
- Davies, R.E., Delluva, A.M., Koch, R.H., 1984, *Nature*, 311, 748.
- Debi Prasad, C., Chandrasekhar, T., Desai, J.N., Ashok, N.M., Krishan, V., 1988, *J. Astron. Astrophys* (In press).
- Debi Prasad C., Desai, J.N., 1988, *Mon. Not. Roy. Astr. Soc.*(submitted).
- Delseme A.H., 1977, *The Pristine nature of Comets*, In *Comets., Asteroids, Meteorites*, ed A.H.Delseme (Toledo, Ohio: Univ. of Toledo), pp.3.
- Devine, N., Fechtig, H., Gombosi, T.I., Hanner, M.S., Keller, H.U., Larson, S.M., Mendis, D.A., Newburn Jr., Reinhard R., Sekanina, Z., Veomans, D.K., 1985, *Space Sci. Rev.*, 43, 1.
- Donn, B., 1976, *The Study of Comets*, NASA SP-393, 663.
- Eberhardt, P. et al., 1986, in *20th ESLAB symp. (ESA Sp 250)*, Vol I, 539.
- Everhart, E., 1972, *Astrophys. Letters*, 10, 131.
- Feldman P.D., A'Hearn, M.F., Millis, R.F., 1984 *Ap. J.*, 282, 799.
- Fernandez, J.A. and Ip W. -H, 1983, *Asteroids Comets, Meteors*, Uppsala University, p387.

- Fernandez, J.A., Jockers, K., 1983, Rep. Prog. Phys., 46, 665.
- Finson, M.L., Probst, R.F., 1968, Ap.J., 154, 353.
- Galeev, A.A., 1987, Astron. Astrophys., 187, 12.
- Goraya, P.S., Singh, M., 1983, Inf. Bull. Var. Stars No.2455.
- Goswami, J.N., Lal D., 1978, The Moon and the Planets, 18, 371.
- Greenberg, J.M., 2490 N., 1988, Nature, 331, 124.
- Greenstein, J.L., 1962, Ap. J., 136, 688.
- Griffin, R., 1978, Pub. Astr. Soc. Pac., 90, 518.
- Guigay, G., 1960, J. Observateurs, 43, 101.
- Hajivassiliou, C.A., Duffett-Smith, P. J., 1987, Mon. Not. R. Astr. Soc., 229, 485.
- Hallam, A., 1979, Nature, 281, 430.
- Halley, E., 1705, A synopsis of the astronomy of comets, London : John Senex.
- Harwit, M., Salpeter, E.E., 1973, Ap. J., 186, L37.
- Hasegawa, I., 1980, Vistas in Astronomy, 24, 59.
- Havneso, 1970, Icarus, 12, 331.
- Huebner, W.F., Gigueve, P.T., 1980, Ap.J. 238, 753.
- Hearnshaw, J.B., 1972, Mem. Roy. Astron. Soc., 77, 55.
- Herschel, W., 1783, Phil. Trans. R. Soc. London. 73, 213.
- Hill, J.R., Mendis, D.A., 1980, The Moon and the Planets, 23, 53.
- Hopnis, H.L.F., Gombosi, T.I., 1986, 20th ESLAB Symp., ESA SP-250 II, 397.

- Horanyi, M., Mendis, D.A., 1985,
Ap. J., 294, 357.
- Hoyle, F., Wickramasinghe C., 1978,
Astrophys & Sp̄sc., 53, 523.
- Hoyle, F., 1980, Vistas in Astronomy,
24, 123.
- Hoyle, F., Wickramasinghe, N.C, 1986,
Nature, 322, 509.
- Hoyle, F., Wickramasinghe, N.C., 1987,
Nature, 328, 117.
- Hughes, D.W., 1983, Mon. Not. R. Astr.Soc.,
204, 1291.
- Hughes, D.W., 1987, Phil. Trans. R.Soc.
London, A. 323, 349.
- Huppler, D., Reynolds, R.J., Roesler F.L.,
Scherb f, Trauger, J., 1975, Ap.J., 202, 276.
- Hut, P., Alarez, W., Elder, W.P., Itansen, T.,
Kauffman, E.G., Keller, G., Shoemaker, E.M.,
Wissman, P.R., 1987, Nature, 329, 118.
- Hyder, C.L., Bandt, J.C., Roosen, R.G., 1974,
1974, Icarus, 23, 601.
- Intriligator, D.S., 1985, Geo. Res. Let., 12, 187.
- Ip. W.-H., Mendis, D.A., 1978, Ap. J. 223, 671.
- Ip. W.-H., Mendis, D.A., 1976, 1976, Icarus, 29, 147.
- Ip. W.-H., 1979, Cometary atmospheres : Observations
and theoretical models, in Cometary Missions,
Proc. workshop on cometary missions, Bamberg,
Feb. 1979, Axford et al (Eds.), P.69.
- Ip. W.-H., 1980, Astron. Astrophys., 81, 260.
- Ip. W.-H., Cosmovici, C.B., Mack, P., 1986,
20th ESLAB Symp., ESA SP-250 I, 507.
- Irvine, W.M., Leschine, S.B., Scholerb, F.P.,
1980, Nature, 283, 748.
- Jacquinet, J., 1954, J. Soc. Amer., 44, 761.
- Jockers, K., Lust, R., 1973, Astron. Astrophys.

- 26, 113.
- Jockers, K., 1981, *Icarus*, 47, 397.
- Jockers, K., 1985, *Astron. Astrophys. Suppl. Ser.*, 62, 791.
- Jockers, K., Geyer, E.H., Rosenbauer, H., Hanel, A., 1987, *Astron. Astrophys.* 187, 256.
- Kant, I., 1755, *Universal Natural Histons of theory of Heavens*.
- Kerr, R.B., Tepley, C.A., Cageao, R.P., Atreya, S.K., Donahue, S.K., Chechneff, I.M., 1987, *Geophys. Res. Lett.*, 14, 53.
- Kevin, A.M., David, J.S., 1988, *Nature*, 331, 612.
- Klebesadel, R.W., Strong, I.B., Olson, R.A., 1973, *Ap. J., Leh.*, 185, L85.
- Kokuba, N., Mayedes, T., Grey, H., 1961, *Geochim Cosmochim. Acta*, 21, 247.
- Kotra, R., 1981, *Organic Analysis of Antartic Carbonaceous Chondrites*, Ph. D., Dissertation., University of Maryland.
- Krishna, V., 1980, *Solar Phys.*, 68, 343.
- Lagrange, J.L., 1814, *Sur l'origine des Cometes Additions a la Connaissance des Temps*, 211.
- Lambert, D.L., Danks, A.C., 1983, *Ap. J.*, 268, 428.
- Laplace, P.S., 1805, *Teorie des Cometes Mechanique Celeste*, 4, 193.
- Larson, R.B., 1972, *Nature, Phys. Sci.*, 236, 7.
- Larson, H.P., Davis, D.S., Mumma, M.J., Weaver, H.A., 1986, *Ap. J.*, 309, L95.
- Larson, S., Sekaninia Z., Levy, D., Tapia, S., Senay M. 1986, 20th ESLAB Symp., ESA SP-250 II, 145.
- Larson, H.P., Davis, D.S., Michael, J., Mumma, J., Weaver, H.A., 1987, 20th ESLAB Symp., ESA-SP-250 I, 335.
- Lee, T., Papanatassion, D.A., Wasserburg, G.J., 1976, *Geophys. Res. Lett.*, 3, 109.
- Lee, T., Papanastassion, D.A., Wasserburg, G.J., 1977,

- Ap. J., Lett., 211, L107.
- Lee, L.C., Wu C.S., 1979, Ap.J., 228, 935.
- Lutz, B.L., Wagner, R.M., 1986, Ap. J., 308, 993.
- Lyttleton, R.A., 'The comets and their origin',
1953, Cambridge University Press.
- Maddox, J., Nature, 321, 723.
- Marsden, B.G., Sekanina, Z., Everhart, E., 1978,
Astron. J., 83, 64.
- McFadden L.A., Gaffey, M.J., Mccord, T.B., 1984,
Icarus, 59, 25.
- Mendis, D.A., 1978, The Moon and Planets, 18, 361.
- Miller, S.L., 1953, Science, 117, 15.
- Minami, S., White, R.S., 1986, Geophys. Res. Lett.,
13, 849.
- Mumma, M.J., Weaver, H.A., Larson, H.P., Davis, D.S.,
Williams, M., 1986, Science, 232, p. 1523.
- Napier, W.M., Clube, S.V.M., 1979, Nature, 282, 455.
- Niedner, M.B., Brandt, J.C., 1978, Ap. J., 223, 655.
- Niedner, M.B., Brandt, J.C., 1979, Ap. J., 234, 723.
- Ness, N.F., Donn, B., 1966, Nature et origine des
Cometes, 13th Liege Symp., p.343.
- Oliversen, R.J., Hollis, J.M., Brown, L.W., 1985,
Icarus, 63, 339.
- Oort, J.H., 1950, Bull. Astron. Inst. neth, 11, 91.
- Opik, E.J., 1971, Irish Astron. J., 10, 35.
- Owen, T., 1973, Ap. J., 184, 33.
- Paul, J.W.M., et al, 1965, Nature, 208, 133.
- Preston, G.W., 1967, Ap. J., 147, 718.
- Quirk, W.J., Tinsley, B.M., 1973, Ap. J., 179, 69.
- Rao, N.N., Rao, U.N., Das, A.C., 1988, Astrophys.
Sp. Sci., (submitted).
- Raup, D.M., Sepkoski, J.J., Jr., 1984, Proc. Natl.,

- Acad. Sci., USA, 81, 801.
- Rickman, H., 1986, ESA Workshop on "Comet sample Nucleus Return mission, ESA SP-249, 185.
- Roosen, R.G., Bandt, J.C., 1976, The Study of Comets, Part I, NASA Sp-393, p.378.
- Russell, H.N., 1920, Astron. J., 33, 49.
- Sagdeev, R.Z., Blamont, J., Galeev, A.A., Morz, V.I., Shapira, V.D., Shevehenko, V.I., Szego, K., 1986, Nature, 321, 259.
- Sarkar, A., 1986, Ind. J.E.S., 13, 14.
- Schmidt, H.V., Wegmann, R., 1982, Comets, Tucson, Arizona, University of Arizona Press, p.538.
- Sekanina, Z., 1973, Astrophys. Letts., 14, 175.
- Shih, P., Scherb, F., Roesler, F.L., 1984, Ap. J., 279, 453.
- Shimoyama, A., Ponnampereuma, C., Vanai K., 1979, Nature, 282, 394.
- Shklovskii, I.S., 1974, Sov. Astron., 18, 390.
- Smith, B.A, Terrile, R.J., 1984, Science, 226, 1421.
- Spinrad, H., Stauffer, J., Neuburn, R.L., 1979, Publ. Astron. Soc. pac., 91, 707.
- Stawikowsky, A., Greenstein, J.L., 1964, Ap. J., 140, 1280.
- Steven, J.S., Chaluner, C.P., Peter, J.C., Andrew, J.C. David, S.H., Alan, D.J., Gough, M.P., Andrew, J.N., Richard, P.R., David, J.S., Les, J.C.W., 1985, Nature, 318, 269.
- Talbot, J.R., Arnett, W.D., 1973, Ap. J., 186, 51,69.
- Telesco, C.M., Decher, R., Baugher, C., Campins, H., Mozurkewich, D., Thronson, H.A., Cruikshank, D.I., Hammel, H.B., Larson, S., Sekanina, Z., 1986, Ap. J., 310, L61.
- Tinsley, B.M., Cameron, A.G.W., 1974, Astrophys. Space Science., 31, 31.
- Truran, J.W., Cameron, A.G.W., 1971, Astrophys. Space Sci., 14, 179.

- Terasawa, T., et al., 1986, 20th ESLAB Symp., ESA SP-250, part I, p.281.
- Verigin, M.I., Axford, W.I., Gringauz, K.I., Richter, A.K., 1987, Geophys. Res. lett. 19, 987.
- Wallis, M.K., 1973, Planet, Space Sci., 21, 1647.
- Wallis, M.K., Ong, R.S.B., 1976, The Study of Comets, NASA SP-393, p.856.
- Wallis, M.K., Hassan, M.H.A., 1982, in Cometary Exploration, Vol. 2., Ed., T.I., Gombosi (Budapest: Hungarian Acad. Sci. Pub). p. 57.
- Weaver, H.A., Mumma, M.J., Larson, H.P., Davis, D.S., 1986, Nature, 324, 441.
- Weber, P., Greenberg, J.M., 1985, Nature, 316, 403.
- Weissman, P.R., 1980, Astron. & Astrophys. 85, 191.
- Whipple, F.L., 1977, Icarus, 30, 736.
- Weissman, P.R., 1987, "Diversity and Similarity of Comets", ESA SP-278, 31.
- Wescott, E.M., Stenbeck-Nielson, H.C., Halliman, T.J., Davis, T.N., Peek, H.M., 1976, J. Geophys. Res. 81, 4495.
- Whipple, F.L., 1950, Ap. J., 111, 779.
- Whipple, F.L., 1964, Proc. Natl. Acad. Sci., 51, 711.
- Whipple, F.L., 1975, Astron. J., 80, 525.
- Whipple, F.L., 1987, Phil. Trans. R.Soc. London., p 323, 339.
- Wurm, K., Mammano, A., 1967, Icarus, 6, 281.
- Wyckoff, S., et al., 1986, 20th ESLAB Symp. ESA SP-250, part I, p.311.

CHAPTER 2

- Ashok, N.M., Chandrasekhar, T., Manian, K.S.B.,
J. Phys. E : Sci. Instrum. 20, 469 (1987).
- Chandrasekhar, T., Desai, J.N., Angreji P.D.,
Appl. Optics, 20, 2172 (1981).
- Chandrasekhar, T., 1982, Ph.D.Thesis
Gujarat University, (1982).
- Deharveng, L., Astron. Astrophys. 29, 341 (1973).
- Desai, J.N., Proc. Indian, Acad. Sci., (Earth
Planet Sci), 93, 189 (1984).
- Gupta, R., Ph. D. Thesis, Gujarat University, (1985).
- Hernandez, G., Fabry-Perot interferometers
Cambridge University Press, Cambridge (1986).
- Hicks, T.R., Reay, N.K., Scaddan, R.J., J. Phys.
E : Sci. Instrum. I., 27 (1974).
- Hicks, T.R., Reay, N.K., Atherton, P.D.,
J. Phys., E. Sci. Instrum. 17, 49 (1984).
- Huppler, F.L., Scherb, F., Trauger, J., 1975
Ap. J., 202, 276.
- Jacquinet, J. Opt. Soc. Amer. 44, 761 (1954).
- Jacquinet, P., Rep. Prog. Phys., 24, 267 (1960).
- Jones, R.V., Richards, J.C.S., J. Phys., E : Sci.
Instrum. 6, 589 (1973).
- Meaburn, J., Detection and Spectrometry of faint
lights, D. Reidel, Hingham.
- Ramsey, J.V., Appl. Opt. 1, 411 (1962).
- Ramsey, J.V., Appl. Opt., 5, 1297 (1966).
- Vancouleurs, G.De., Pence, W.D., Ap. J., 242, 18
(1980).
- Vaughan, A.H., 1967, Ann. Rev. Astron. Astrophys.
5, 139.

CHAPTER 3

- A'Hearn M.F.S., Hoban, P.V., Birch, Bowers, R.,
Martin, R., Klinglesmith, D.A., III, 1986, Nature,
324, 649.
- Ahnert, P., 1943, Z. Astrophys. 22, 286.
- Alexander, C.J., Luhmann, J.G. and Russel, C.T., 1986,
Geophys. Res. Lett. 13, 917-920.
- Alfven, H., 1954, On the origin of the solar system,
Oxford University Press, Oxford.
- Alfven, H., 1960, Rev. Mod. Phys. 32, 710.
- Barnard, E.E., 1893, Astron. Assoc. J. 9:59-63.
- Bobrovnikoff, N.T., 1931, Publ. Lick Obs. 17,
Part II, 309.
- Brandt, J.C., 1968, Ann. Rev. Astron. Astrophys.
6, 267-86.
- Brandt, J.E., 1982, Comets, The University of Arizona
press, Tucson, Arizona, 519-537.
- Brosius, J.W., Holman, G.D., Niedner, M.B.,
Brandt, J.C., Slavin, J.A., Smith, E.J., Zwicky, R.D.,
Bame, S.J., 1987, Astron. Astrophys., 187, 267.
- Burlaga, L.F., Rahe, N., Donn. B., Neugebauer, M.,
1973, Solar Physics, 30, 211.
- Chakaveh, S.C., Green, S.F., Ridley, J.H., McDonnell,
J.A.M. and Hughes, D.W., 1986, Proc. 20th ESLAB
Symp. on Exploration of Halley's Comet, Heidelberg,
ESA SP-250, p.163-165.
- Chandrasekhar, T., Debi Prasad C., Desai, J.N.,
Ashok, N.M., and Gupta, Ranjan, 1987, 1987,
ESA. SP-278, "Diversity and Similarity of Comets",
567-570.
- Chandrasekhar, T., Ashok, N.M., Debi Prasad, C. and
Desai, J.N., 1987, Opt.Engg. 27, 67-70.
- Cosmovici, C.B., 1987, Astron. Astrophys. 63, 83-86.
- Cosmovici, C.B., Mack, P., Craubner, H., and Schwarz,
G., 1986, Proc. 20th ESLAB symposium on the exploration
of Halley's Comet, Heidelberg, ESA SP-250, 151-555.

- Cosmovici, C.B., Schwarz, G., Ip, W.H., Mack, P.,
1988, Nature, 332, 705.
- Delsemme, A.H., 1979, (NASA conf. pub.2089) p.136-166.
- Donn, B. and Urey, H., 1957, Ap. J., 123, 339-342.
- Eddington, A.S., 1910, Mon. Not. Roy. Astron. Soc.
70, 442-458.
- Festou, M.C., Feldmann, P.D., A'Hearn, M.F., Arpigny,
C., Cosmovici, C.B., Danks, A.C., Mcfadden, L.A.,
Gilmozzi, R., Patriarchi, P., tozzi, G.P., Wallis,
M.K., Weaver, H.A., 1986, Nature, 321, 361-365.
- Formisano, V., Galeev, A.A., Sagdeev, R.Z., 1982,
Planet, Space Sci., 30, 491.
- Formisano, V., Amata, E., Agnelli, G., Bellucci, G.,
Cristaldi, S., 1986, Proc. 20th ESLAB Symposium
on the Exploration of Halley's Comet., Heidelberg,
ESA SP-250, 127-132.
- Galeev, A.A. 1967, J. Plasma Phys. 1, 104.
- Galeev, A.A., Gringauz, K.I., Klimov, S.I.,
Remizov, A.P., Sagdeev, R.Z., Savin, S.P.,
Sokolov, a.Y., Vergin, M.I., 1986, Geophys. Res. Lett.
13, 845.
- Gong (Kung) S.M., Wu G.J., Chen, P.S., Zhang, X.F.,
Sun, S.S., 1987, Astron. Astrophys., 187, 594.
- Greenstein, J.L., 1962, Ap.J., 136, 686-690.
- Grun. E., Graser, V., Kohoutek, L., Thick, U.,
Massonne, L., and Schwehm, G., 1986, Nature,
Vol. 321, 144-147.
- Hamberger, S.M., Jancarik, J., 1970, Phy. Rev. Lett.
25, 999.
- Ip. W.H., Mendis, D.A., 1975, ICARUS, 26, 459.
- Ip. W.H., Mendis, D.A., 1976, ICARUS 29, 147.
- Ip. W.H., 1980, Astron. Astrophys. 81, 260.
- Ip. W.H., 1980, Astron. Astrophys., 92, 95-100.
- Ip. W.H., Cosmovici, C.B., Mack, P., 1986,
Proc. 20th ESLAB Symp., on Exploration of Halley's
Comet., Heidelberg, ESA SP-250, 507-510.

- Ip. W.H., Axford, W.I., 1982, Comets, Ed. L.Wilkening,
The University of Arizona press, Tucson, Arizona,
p.588.
- Ip. W.H., Cosmovici, C.B., Mack, P., 1986, proc.
20th ESLAB SYMP., ESA SP-250, I, PP.507.
- Ip. W.H., Schwenn, R., Rosenbauer H., Balsiger, H.,
Neugebauer, M., Shelley, E.G., 1987, Astron.
Astrophys., 187, 132.
- Jockers, K., Lust Rh, Nowak, Th. 1972, Astron.
Astrophys., 21, 199.
- Jockers, K., and Lust, R., 1973, Astron. Astrophys.
26, 113-121.
- Jockers, K., 1978, Astron. Astrophys. Suppl.
Ser. 62, 791-838.
- Jockers, K., and Geyer, E.H., 1985,
The ESO Messenger, No.42, 9.
- Jockers, K., Geyer, E.H., Rosenbauer, H., Hanel, A.,
1987, Astron. Astrophys., 187, 256.
- Kerr, R.B., Tepley, C.A., Cageao, R.P., Atreaya, S.K.,
Donahue, T.M., and Cherchnneff, I.M., 1987,
Geophys. Res. Lett., 14, 53-56.
- Kresak, L., 1974, Bull.Astron. Inst. Czeh. 25,
393-304.
- Komle, N.I., W.H., Ip., 1987, Astron. Astrophys.
187, 405-410.
- Larson, S.M., 1986, IAU Telegrams, Circular No.4159,
9, Jan. 1986.
- Larson, S., Sekanina, Z., Leves, D., Tapias, Senay,M.,
1987, Astron. Astrophys. 187, 639.
- Liu Z. L., 1987, Astron. Astrophys., 187, 225.
- Lust, Rh., 1967, Z. Astrophys. 65, 236.
- Lutz., B.L., and Wagner, R.M., 1986, Ap. J.,
308, 993-1000.
- Mc Coy, R.P., Opal, C.B., and Carruthers,G.R.,1986,
Nature, 324, 439-441.
- Miller, F.D., 1969, Astron. J., 74, 248.

- Morrison, P.J., Mendis, D.A., 1978, Ap. J., 226, 350.
- Ness. N.F., 1965, J. Geo. Res. 70, 2989.
- Niedner, M.B., and Brandt., J.C., 1978,
Ap. J., 223, 723-732.
- Niedner, M.B., and Brandt, J.C., 1979,
Ap. J., 234, 723-732.
- Niedner, M.B., and Brandt, J.C., 1980,
Icarus 92, 257-270.
- Niedner, M.B., 1980, Ap. J., 241, 820-829.
- Niedner, M.B., 1986, IHW Newsletter, No.9, 2-6.
- Niedner, M.B., Schwingenschuh K., 20th ESLAB Symp.
on Exploration of Halley's Comet. ESA SP-250,
Vol III, p.419.
- Oppenheimer, 1975, Ap. J., 196, 251.
- Podgorny, I.M., Dubinin, E.M., Potanin Yu N.,
Shkolnikova, S.I., 1979, Astrophys.Space. Sci., 61,
369.
- Rettig Z.T., Ruchti, R., Baumbaugh, B., Baumbaugh, A.,
Knickerbocker, K., Dawe, j., (1986), 20th ESLAB Symp.
ESA SP-250, p.93 Vol.III.
- Roosen, R.G., and Brandt, J.C., 1976, The study of
Comets Part I., NASA Sp. 393, pp. 378-379.
- Russel, C.T. and Luhmann, J.G., 1987,
Geophys. Res. Lett. 14, 991-994.
- Schleicher, D.G., Millis, R.L., Tholen, D., Lark, N.,
Birch P.V., Martin, R., and A'Hearn M.F., 1986,
Proc. 20th ESLAB Symp. on Exploration of Halley's
Comet, Heidelberg, ESA Sp-2501, 565-567.
- Schwenn, R. et al, 1987, Astron. Astrophys., 187, 160.
- Somogyi, A.J., et al (34 authors) 1986,
Nature 321, 285-288.
- Sulentic, J.W. and Tifft, W.G., 1973,
The Revised New General Catalogue of astronomical
objects, The University of Arizona Press, Tucson.
- Takao Saito, Kiyohumi yumoto, Kunio Hirao, Towoko
Nakagawa and Keiji Saito, 1986,

- Nature, 321, 303-307.
- Tokunaga, A.T., Golisch, W.F., Griep, D.M.,
Kaminski, C.D, Hanner, M.S., 1986, Astron. J.
92, 1183.
- Vaisberg, O.L., Zastenker, G., Smirnov, V.,
Khazanov, B., Omelchenko, A., Fedorov, A, and
Zakharov, D., 1987, Astron. Astrophys. 187, 183-190.
- Verigin, M.I., Axford, W.I., Gringauz, K.I. and
Richter, A.K., 1987, Geophys. Res. Lett., 14, 987-990.
- Vsyekhsvyatskii, S.K., Demenko, A.A., 1976,
Problemy Kosm. Fiz., 11, 111.
- Watanbe, J. et al., 1987,
Diversity and Similarity of Comets
ESA SP-278, 657.
- Whipple, F.L., 1950, Ap. J., 111, 375-394.
- Whipple, F.L., 1951, Ap. J., 113, 464-474.
- Whipple, F.L., 1980, Astron. J., 85, 305-313.
- Wolf, M., 1909, Astron. Nachrichten,
180, No. 4297, 1-12.
- Wu M.C., Qin, P.Z., 1987, Astron. Astrophys.
187, 264.
- Wurm K., 1963, The Physics of Comets, In the
Moon Meteorites and Comets (B.M. Middelhurst
and G.P. Kuiper, Eds), pp. 573-617. University of
Chicago Press, Chicago.
- Wurm, K., and Mammano, A., 1967, ICARUS 6, 281.
- Wurm, K. and Mammano, A., 1972, Astrophys and Space
Science, 18, 273.
- Wyckoff, S., 1982, Comets,
(Ed. Wilkening), the University of Arizona Press,
Tucson, Arizona, 3-55.

CHAPTER 4

- A'Hearn M.F., Millis, R.L., Birch, P.V., 1981, Astron. J., 86, 1559.
- Arpigny, C. et al., 1987, Diversity and Similarity of Comets, ESA SP-278, p.571.
- Arpigny, C., magain, P., Manfroid, J., Dossin, F., Danks, A.C., Lambert, D.L., 1987, Astron. Astrophys. 187, 485.
- Bappu, M.K.V., Parthasarathy, M., Sivaraman, K.R., Babu, G.S.D., 1979, Mon. Not. Roy. Astron. Soc., 189, 897.
- Belyaev, N.A., Kresak, L., Pittich, E.M., Pushkarev, A.N., 1986, Catalogue of short-period comets, (Astronomical Institute Slovak Academy of Sciences, Bratislava).
- Catalano, F.A., Baratta, G.A., Strazzulla, G., 1987, Diversity and Similarity of Comets, ESA SP-278, p.181.
- Combi, M.R., 1978, Astron. J., 83, 1459.
- Cosmovici, C.B., Schwarz, G., Ip W.H., Mack, P., 1988, Nature, 332, 705.
- Craven, J.D., Frank, L.A., Rairden, R.L., Dvorsky, M.R., 1986, Geophys. Res. Lett., 13, 873.
- Debi Prasad, C., Chandrasekhar, T., Desai, J.N., Ashok, N.M., 1988, J. Astrophys. Astron.(submitted).
- Delsemme, A.H., and Miller D., 1971, Planet, Space. Sci., 19, 1229.
- Delsemme, A.H., 1979, Dynamics of the solar system, (D.Reidel Dordecht), p.265.
- Dresser, K., Ramsay, D.A., 1959, Phil. Trans. R.Soc. Lond. A., 251, 553.
- Everhart, E., Raghavan, N., 1970, Astron. J., 75, 258.
- Feldman, P.D., 1983, Science, 219, 347.
- Feldman, P.D. et al., 1986, 20th ESLAB Symp., ESA SP-250, 325.
- Festou, M.C., Feldman, P.D., 1981, Astrophys.,

103, 154.

Greenstein, J. L., Arpigny, C., 1962, Ap. J., 135, 892.

Hertzberg, G., Ramsay, D.A., 1952, J.Chem.Phys., 20, 347.

Huppler, F.L., Scherb, F., Tranger, J., 1985, Ap. J., 202, 276.

Hughes, D.W., 1987, Diversity and Similarity of Comets, ESA SP-278, p.43.

Jockers, K., 1985, Astron. Astrophys. Supl. Ser.62, 791.

Kerr, R.B., Tepley, C.A., Cageao, R.P., Atreya, S.k., Donahue, T.M., Charchneff, I.M., 1987, Geophys. Res. Lett. 14, 53.

Krishnawami, K.S., O'Dell, C.R., 1977, Ap.J., 216, 158.

Krankowsky, D., Lammerzah1, P., Herrwerth, I., Woweries, J., Eberhardt, P. et al., 1986, Nature, 321, 326.

Kresak, L and Kresakova, M., 1987, Diversity and Similarity of Comets, ESA SP-278, p.37.

Kresak, L., 1985, The origin & evolution, ed. A. Caursi et al., (D.Reidel, Dordrecht) p.279.

Kaneda, E., Hirao, K., Shimizu, M., Ashihara, O., 1986, Geophys. Res. Lett., 13, 833.

Korth, A et al., 1987, Astron.Astrophys. 187, 149.

Lammerzahl, et al., 1987, Astron. Astrophys., 187, 169.

Larson et al., 1986, 20th ESALAB Symp., ESA SP-250 II, p.145.

Larson, H.P., Davis, D.S., Mumma, M.J., Weaver, H.A., 1986, A.P., 309, L98.

Levine, J.S., (Ed) 1985, The photochemistry of the atmosphere, Academic Press, New York.

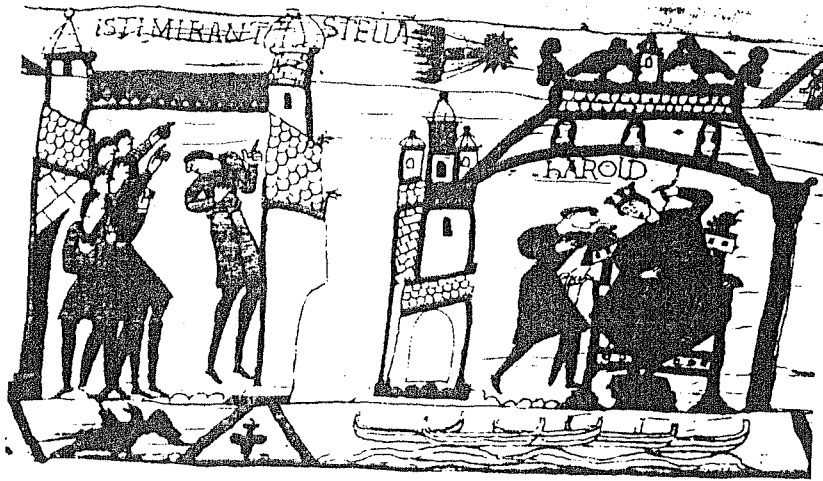
Magee-Sauev K., Roesler, F.L., Scherb, F., Harlander, J. 1988, Icarus (submitted).

Marsden, B.G., Sekanina, Z., Everhart, E., 1978,

- Astron. J., 83, 64.
- McCoy R.P., Opal, C.B., Carruthers, G.R., 1986,
Nature, 324, 439.
- Mumma, M.J., Weaver, H.A., Larson, H.P., Davis, D.S.,
Williams, M., 1986, Science, 232, 1523.
- Ney, E.p., 1982, Comets, Ed. Wilkening, L., (The
University of Arizona Press, Tucson, Arizona) p.323.
- Oliversen, R.J., Hollis, J.M., Brown, L.W., 1985,
ICARUS, 63, 339.
- Reinhard, R., 1986, Nature, 321, 313.
- Robinson, G.W., McCarty, M., 1959, J.Chem. Phys.
30, 999.
- Roesler, F.L., Scherb, F., magee, K., Harlander, J.,
Reynolds, R.J., Yelle, R.V., 1985, Adv. Sp.Res.
5, 274.
- Roesler et al., 1987, Diversity and Similarity of
Comets, ESA SP-278, p.217.
- Ramachandra Rao, V., 1971, Ph.D.Thesis, Gujarat
University, India.
- Sagdeev, R.Z., Blamont, J.B., Galeev, A.A., Moroz,
V.I., Shapiro, V.D., Shevchenko, V.I., Szego, K.,
1986, Nature, 321, 259.
- Spinrad, H., 1982, Pub. Astron. Soc. Paci., 94, 1008.
- Spinrad, H., 1987, Ann. Rev. Astron. Astrophys.,
25, 231.
- Sterken, C., Manfroid, J., 1987, Diversity and
Similarity of Comets, ESA SP-278, 191.
- Schreb, F., Roesler, F.L., Magee, K., Harlander, J.,
Reynolds, R.J., 1985, Adv. Space. Res., 5, p.275.
- Swing, P., 1962, Ann. d' Astrophys., 25, 165.
- Swings, P., Greenstein, J.L., 1959, Compt. Rend.,
246, 511.
- Vanysek, V., Valnicek, B., Sudova, J., 1988,
Nature, 333, 435.
- Weaver, A., Mumma, M.J., Larson, H.P., Davis, D.S.,
1986, Nature, 324, 441.

Woods, T.N., Feldman, P.D., Dymond, K.F., Sahnou, D.J.,
1986, Nature, 324, 436.

Yeomans, D.K., 1986, 20th ESLAB Symp., ESA SP-250,
419.



Typical cartoons in 1857 (above) and in 1988 (below).

